Modulation of New Delhi Metallo-β-Lactamase-1 activity using Affimers

Lia Emma De Faveri

Submitted in accordance with the requirements for the degree of

Doctor of Philosophy

The University of Leeds

Faculty of Biological Sciences

School of Molecular and Cellular Biology

December 2018

The candidate confirms that the work submitted is her own and that appropriate credit has been given where reference has been made to the work of others.

Acknowledgements

Although this thesis is an individual work, I could never have reached the heights or explored the depths without the help, support and guidance of a number of people. First of all I'd like to thank Dr Darren Tomlinson for giving me this opportunity and for his expertise and guidance throughout the project. Also to my co-supervisors Professor Mike McPherson, Dr Alex O'Neill and Dr Christian Tiede for their excellent advice, humour, and for making it to my 9am monthly meetings (most of the time). I am also very grateful to BBSRC for funding this project.

Thank you to everyone (past and present) in the Tomlinson and McPherson groups for their friendship, support and for making every day in the lab more enjoyable and fun. In particular to Sophie Saunders for her contributions to this project and the endless kinetic assay repeats (sorry!). To Tom, for your patience in teaching me all the protocols at the start and for the many many laughs (and not telling Christian when I messed up!). To Hannah, for our shared love of gossip, cats and gin. And of course to Sophie, Rob and Danah, who I've been lucky enough to share this journey with. Thank you for all the wonderful memories, the banter, the shared commiserations when experiments failed, the many drinking sessions and general camaraderie. It's been a blast and wouldn't have been the same without you.

I am so grateful to my friends and family. To my Mum and Dad for their encouragement and belief, and for providing, without question or hesitation, emotional (and financial!) support. To my sister Amy, brother-in-law Matt and my new niece Imogen - for being inspirations of strength these past few months, for bribing me with baby cuddles and for the thesis SOS rescue box! You are heroes. To my friends for understanding my lack of free time and for their encouragement, despite having no idea what I do.

Finally, to Jon. For your continuous support and not murdering me in my sleep these past few months. I know you've been holding on to the hope these past four years that as soon as I finish my PhD we'll be rich, I should probably tell you now that that's not going to happen.

Abstract

Metallo-β-lactamases (MBLs) are a class of Zn^{2+} containing enzymes that hydrolyse the β-lactam bond in β-lactam antibiotics and render them inactive. New Delhi metallo-β-lactamase 1 (NDM-1) is particularly troubling as the gene bla_{NDM-1} is plasmid borne resulting in rapid widespread dissemination. With few effective antibiotics against NDM-1 expressing bacteria, and resistance developing to those which remain, there is an urgent need to find new MBL inhibitors.

Combining β-lactam antibiotics with β-lactamase inhibitors is considered amongst the most reliable of strategies for tackling resistant pathogens. However, the development of effective β-lactamase inhibitors has proved challenging. MBLs share a conserved active site with a number of human proteins and therefore orthosteric inhibitors often result in adverse side effects.

Affimers may represent an alternative for the selection of novel MBL inhibitors. An Affimer that binds NDM-1 and inhibits it in a dose dependent manner was isolated, as confirmed in β-lactamase activity assays and cell based assays in clinical strains. Initial results indicated that Affimer 21 is an allosteric inhibitor, suggesting that it may be highly specific for NDM-1, reducing the possibility of off-target effects. To elucidate the binding interaction, attempts were made at obtaining a co-crystal structure and alanine scanning mutagenesis of the two variable regions was performed. The functional effects of the alanine substitutions on efficacy of NDM-1 inhibition were measured and the data used to guide the generation of sub-libraries to select for improved inhibitors. However, despite stringent screening approaches, the original Affimer has so far proven to be the the most effective inhibitor, with an estimated IC_{50} of 0.37 μM.

Further investigation into the use of Affimers as a platform for identifying novel inhibitors effective against metallo-β-lactamases could represent a useful tool in the ongoing battle against antibiotic resistant pathogens.

Table of Contents

Acknowledgements ..... **iii**

Abstract ..... **iv**

Table of Contents ..... **iv**

List of Tables ..... **xi**

List of Figures ..... **xiii**

Abbreviations ..... **xvii**

Chapter 1 Introduction **2**

1.1 Background 2

1.2 History of antibiotics 3

1.3 Gram-negative bacteria and infections 4

1.4 Emergence of antibiotic resistance 6

1.4.1 Overuse and misuse 7

1.4.2 Agricultural use 8

1.4.3 Failure of discovery 9

1.5 Mechanisms of resistance 9

1.5.1 Plasmid encoded resistance 10

1.5.2 Modified cell wall 11

1.5.3 Porins 12

1.5.4 Efflux pumps 12

1.5.5 Biofilms 14

1.5.6 Outer membrane vesicles 16

1.5.7 Modification of the target 17

1.5.8 Inactivating enzymes 18

1.5.9 Penicillin binding protein mutations 19

1.5.10 β lactamases 21

1.6 Metallo β-lactamases 22

1.7 New Delhi Metallo β-lactamase 1 (NDM-1) 23

1.8 Reversing resistance 27

1.8.1 β-lactamase inhibitors currently in clinical development 27

1.8.2 Metallo-β-lactamase inhibitors in clinical development 29

1.8.3 Zinc binding and zinc chelating metallo-β-lactamase inhibitors 29

1.8.4 Covalent metallo-β-lactamase inhibitors 31

1.8.5 Other metallo-β-lactamase inhibitors 31
1.8.6 Novel biologics as metallo-β-lactamase inhibitors.....32
1.9 Affimer reagents 33
1.10 Phage display and library generation.....35
1.10.1 Library generation.....35
1.10.2 M13 bacteriophage.....36
1.10.3 M13 phage infection and life cycle.....37
1.10.4 Phage display.....39
1.10.5 Phage display screening 41
1.11 Objectives 43
Chapter 2 Materials and Methods 44
2.1 Materials.....45
2.1.1 Bacterial strains and cloning vectors 45
2.1.2 Growth media and buffer recipes 46
2.1.2.1 Growth media 46
2.1.2.2 Buffer recipes.....47
2.1.3 Antibiotics.....47
2.2 Methods.....48
2.2.1 DNA manipulation 48
2.2.1.1 Polymerase chain reaction (PCR) 48
2.2.1.2 Splice overlap extension (SOE) 49
2.2.1.3 Final amplification of the SOE product 50
2.2.1.4 BAP tag cloning 50
2.2.1.5 Construction of Aff21ΔVR1 and Aff21ΔVR2 mutants 52
2.2.1.6 Alanine scanning mutagenesis.....53
2.2.1.7 Agarose gel electrophoresis 54
2.2.1.8 Restriction digests.....55
2.2.1.9 Dephosphorylation.....55
2.2.1.10 Ligations.....55
2.2.1.11 Transformation of *E. coli* by heat shock 55
2.2.1.12 Transformation of *E. coli* by electroporation 56
2.2.1.13 Purification of DNA from *E. coli* by mini or maxiprep 57
2.2.1.14 Purification of DNA from an agarose gel.....57
2.2.1.15 Purification of PCR products.....57

2.2.1.16 Measuring DNA concentration 57
2.2.1.17 DNA sequencing 58
2.2.2 Phage display techniques 58
2.2.2.1 Biotinylation of target proteins with EZ-Link® NHS-SS-Biotin 58
2.2.2.2 ELISA to confirm biotinylation 58
2.2.2.3 Phage display for biotinylated targets 59
2.2.2.3.1 First panning round 59
2.2.2.3.2 Second panning round 61
2.2.2.3.3 Third panning round 63
2.2.2.4 Phage display for non-biotinylated targets 64
2.2.2.4.1 Isolation of Affimer proteins against individual strains of *S. aureus* biofilm 64
2.2.2.4.2 Isolation of Affimer proteins that bind *S. aureus* biofilm but not planktonic cells of the same strain 65
2.2.2.5 Phage display with competition 66
2.2.2.6 Phage ELISA 67
2.2.3 Protein production and purification 68
2.2.3.1 Subcloning into pET11a plasmid 68
2.2.3.2 Protein production 69
2.2.3.2.1 Production in BL21 Star (DE3) cells 69
2.2.3.2.2 Production of biotinylated NDM-1 in AVB101 cells 70
2.2.3.3 Protein purification 70
2.2.3.3.1 Purification of Affimer proteins 70
2.2.3.3.2 Purification of NDM-1 71
2.2.3.3.3 Dialysis of purified protein 72
2.2.3.4 Protein analysis 72
2.2.3.4.1 Protein concentration 72
2.2.3.4.2 SDS PAGE gel electrophoresis 73
2.2.3.4.3 Coomassie Blue staining of SDS PAGE gels 73
2.2.3.4.4 Western blot analysis of SDS PAGE gels 73
2.2.3.4.5 Competition ELISA 74
2.2.4 Library generation 75
2.2.4.1 Generation of focused phage libraries 75

2.2.4.2 Estimation of phage titre by spectrophotometer 77
2.2.4.3 Estimation of phage titre by plating out 77
2.2.5 Enzyme assays 78
2.2.5.1 β-Lactamase activity assays 78
2.2.5.2 Kinetic analysis 79
2.2.6 Cell assays.....79
2.2.6.1 Minimum inhibitory concentration (MIC) 79
2.2.6.2 Cell growth assay 80
2.2.6.3 U-2 OS cell toxicity assay 80
2.2.7 Complex formation and crystallization trials 81
2.2.7.1 Complex formation 81
2.2.7.2 Size exclsuion chromatography 81
2.2.7.3 Concentration of protein 81
2.2.7.4 Crystallization trials 81
2.2.7.5 Crystallization optimisation 82
Chapter 3 Hitting difficult targets: proof of concept 83
3.1 Isolation of Affimer reagents against individual fluorescent proteins for imaging applications 85
3.1.1 Results 88
3.2 Identifying Affimer reagents that bind small molecules 92
3.2.1 Results 95
3.3 Affimers against prokaryotic biofilms as potential diagnostic tools for infective endocarditis.....101
3.3.1 Results 103
3.4 Chapter summary and future work.....107
Chapter 4 Isolation & characterisation of NDM-1 specific Affimer reagents.....111
4.1 Introduction 112
4.2 Results.....115
4.2.1 Investigating the effects of isolated Affimer reagents on NDM-1 activity.....115
4.2.2 Characterisation of Affimer 21 119
4.2.2.1 IC_{50} of Affimer 21.....119
4.2.2.2 Kinetic analysis of Affimer 21 120
4.2.2.3 Binding epitope 122

4.2.2.4 Effect of Affimer 21 on meropenem activity in *Klebsiella pneumoniae* 123
4.2.2.5 Tolerance of Affimer 21 in mammalian cells 124
4.2.2.6 Structural characterisation by crystallography 125
4.2.2.6.1 Crystallization screen 1 128
4.2.2.6.2 Crystallization screen 2 131
4.2.2.6.3 Crystallization screen 3 133
4.2.2.6.4 Crystallization screen 4 136
4.2.2.6.5 Crystallization optimisation 140
4.3 Chapter summary and future work 140
Chapter 5 Identification of critical residues in the Affimer 21:NDM-1 interaction 145
5.1 Introduction 146
5.2 Results 148
5.2.1 Construction and characterisation of Aff21ΔVR1 & Aff21ΔVR2 mutants 148
5.2.2 Site-directed mutagenesis of Affimer 21 151
5.2.2.1 IC_{50} of Affimer 21 D2.4A and G.19A 161
5.2.2.2 Combining alanine mutations 163
5.3 Chapter summary and future work 165
Chapter 6. Affinity maturation of Affimer 21 168
6.1 Introduction 169
6.2 Results 170
6.2.1 Generation of library 1 170
6.2.2 Isolation of Affimers against NDM-1 from library 1 176
6.2.2.1 Insertion of an N-terminal biotin acceptor peptide to NDM-1 constructs 176
6.2.2.2 Phage display screening of library 1 183
6.2.3 Generation of library 2 194
6.2.4 Isolation of Affimers against NDM-1 from library 2 197
6.3 Chapter summary and future work 203
Chapter 7 Discussion and future perspectives 207
7.1 Affimer 21 as an allosteric inhibitor of NDM-1 208
7.2 Affinity maturation of Affimer 21 210
7.3 Comparison to other NDM-1 inhibitors 212

7.4 Continuation of the project and future applications 214
7.4.1 Structural characterisation 214
7.4.2 Assessing the likelihood of development of resistance 216
7.4.3 Affimer inhibitors as therapeutics 217
7.5 Conclusions 219
References 221

List of Tables

Table 1.1 Common gram-negative bacteria and their associated infections.....6

Table 1.2 β-lactam-β-lactamase inhibitor combinations that have reached the stage of clinical development.....28

Table 2.1 Stock and working concentrations of antibiotics.....47

Table 2.2 Reaction components for PCRs using Phusion High-Fidelity (HF) DNA polymerase (ThermoFisher).....48

Table 2.3 Reaction conditions for PCRs carried out using Phusion HF DNA polymerase.....48

Table 2.4 Reaction components for PCRs using KOD Hot Start DNA polymerase.....48

Table 2.5 Reaction conditions for PCRs carried out using KOD Hot Start DNA polymerase.....49

Table 2.6 Reaction components for SOE using Phusion HF DNA polymerase.....49

Table 2.7 Reaction conditions for SOE carried out using Phusion HF DNA polymerase.....49

Table 2.8 Reaction components for final amplification reaction carried out using KOD Hot Start DNA polymerase (Millipore).....50

Table 2.9 Reaction conditions for final amplification reactions carried out using KOD Hot Start DNA polymerase.....50

Table 2.10 Primers for construction of Aff21ΔVR1 and Aff21ΔVR2 mutants.....53

Table 2.11 Complementary primer pairs (F and R) for generation of site-directed mutants.....54

Table 2.12 Sequencing primers.....58

Table 2.13 KingFisher Flex 'Phage_display_pH_elution' protocol.....62

Table 2.14 PCR primer sequences.....69

Table 2.15 Library generation primers.....76

Table 3.1 Variable region sequences for Affimer reagents selected against FPs.....91

Table 3.2 Variable region sequences for Affimer reagents selected against FPs.....96

Table 3.3 *Staphylococcus aureus* strains used in this study.....103

Table 4.1 Variable region sequences for Affimer reagents selected against NDM-1.....114

Table 4.2 Kinetic parameters for NDM-1 with and without Affimer 21.....121

Table 4.3 Summary of apo and complex crystal structures of NDM-1.....127

Table 4.4 Examples of some of the parameters affecting crystallisation.....142

Table 5.1 Amino acid sequences of Aff21ΔVR1 and Aff21ΔVR2.....148

Table 5.2 Amino acid sequences of the 18 alanine scanning mutants of Affimer 21 157

Table 6.1 Variable region amino acid sequences of 8 clones from Library 1 173

Table 6.2 Estimation of library size from total infected cells.....174

Table 6.3 Variable region sequences for Affimer reagents selected against NDM-1 from library 1 184

Table 6.4 Variable region amino acid sequences for Affimers selected against NDM-1 from library 1 by competitive screening 187

Table 6.5 Variable region amino acid sequences of 10 clones from Library 2 196

Table 6.6 Estimation of library size from total infected cells.....196

Table 6.7 Variable region sequences for Affimers selected for NDM-1 from library 2 199

Table 6.8 Amino acid groups for isolated Affimers from library 1.....204

Table 6.9 Amino acid groups for isolated Affimers from library 2.....206

Table 7.1 Reported IC_{50} values of other NDM-1 inhibitors 213

List of Figures

Figure 1.1 Deaths attributable to anti-microbial resistance (AMR) in 2014 and deaths predicted in 2050 compared to other major causes of death 2

Figure 1.2 Differences in the cell wall structure of gram-positive and gram-negative bacteria 5

Figure 1.3 Contribution of factors driving antibiotic resistance 7

Figure 1.4 Innate and acquired antibiotic-resistance mechanisms in Gram-negative bacteria 10

Figure 1.5 Challenges in treating biofilm associated bacterial infections 15

Figure 1.6 Mechanism of action of β-lactam antibiotics 19

Figure 1.7 Chemical structures of the β-lactam antibiotics 20

Figure 1.8 Hypothesised mechanism of carbapenem hydrolysis by metallo β-lactamases 22

Figure 1.9 Structure of apo-NDM-1 25

Figure 1.10 Crystal structure of the Affimer scaffold 34

Figure 1.11 The M13 bacteriophage particle 37

Figure 1.12 Schematic of the M13 bacteriophage life cycle from cell entry to release of progeny phage 38

Figure 1.13 Schematic representation of the pBSTG1-Aff phagemid vector 40

Figure 1.14 Phage display protocol 42

Figure 2.1 Design of primers for BAP tag insertion using the inverse PCR mutagenesis method 51

Figure 2.2 Generation of Aff21ΔVR1 and Aff21ΔVR2 DNA 52

Figure 2.3 Generation of library insert DNA 75

Figure 3.1 Alignment of protein sequences for eGFP, CFP and YFP 88

Figure 3.2 Phage ELISA results for Affimer reagents selected against individual fluorescent proteins (FPs) 90

Figure 3.3 Purification of isolated Affimers that bind to FPs 91

Figure 3.4 Chemical structure of Diclofenac 93

Figure 3.5 Phage ELISA results for Affimer reagents selected against Diclofenac (DCF) 95

Figure 3.6 Purification of isolated Affimer that binds to Diclofenac 96

Figure 3.7 Direct ELISA using a gradient of concentrations of DCF Affimer 98

Figure 3.8 Direct ELISA using a gradient of concentrations of DCF Affimer 99

Figure 3.9 Competition Diclofenac (DCF)-Affimer ELISA.....100

Figure 3.10 Numbers of phage infected colonies after panning to isolate Affimers that bind specifically to individual strains of *S. aureus* 104

Figure 3.11 ELISA screen to confirm Affimer binding to *S. aureus* strains 105

Figure 3.12 Numbers of phage infected colonies after panning to isolate Affimers that bind specifically to S. aureus cells grown as biofilms 106

Figure 4.1 Phage ELISA results for Affimer reagents selected against NDM-1....113

Figure 4.2 Sequence logo 115

Figure 4.3 Purification of isolated Affimers that bind to NDM-1.....116

Figure 4.4 Effects of Affimer reagents on rate of nitrocefin hydrolysis by NDM-1 118

Figure 4.5 IC_{50} of Affimer 21 119

Figure 4.6 Kinetic analysis of inhibition of NDM-1 by Affimer 21.....120

Figure 4.7 Mechanism of inhibition of NDM-1 by Affimer 21.....121

Figure 4.8 Assessment of the binding epitope of NDM-1 required for Affimer 21 binding.....122

Figure 4.9 Restoration of meropenem potency by Affimer 21 in a clinical strain of K. pneumoniae expressing NDM-1 124

Figure 4.10 Affimer 21 is well tolerated in mammalian cells.....125

Figure 4.11 Phase diagram for crystallisation of macromolecules 126

Figure 4.12 SDS-PAGE analysis of Affimer 21 production and purification 128

Figure 4.13 Purification of Affimer 21 by size exclusion chromatography (SEC) 130

Figure 4.14 Purification of Affimer 21:NDM-1 complex by size exclusion chromatography.....132

Figure 4.15 SDS-PAGE analysis of Affimer 21:NDM-1 complex production and purification 134

Figure 4.16 Purification of Affimer 21:NDM-1 complex by SEC 135

Figure 4.17 SDS-PAGE analysis of Affimer 21:NDM-1 complex production and purification 137

Figure 4.18 Purification of Affimer 21:NDM-1 complex by SEC 138

Figure 4.19 Crystallisation drop images for Affimer 21:NDM-1 protein complex.....139

Figure 4.20 Alignment of protein sequences for reported crystal structures of NDM-1.....139

Figure 5.1 Production and purification of Aff21ΔVR1 and Aff21ΔVR2 mutants 149

Figure 5.2 Effects of Aff21ΔVR1 and Aff21ΔVR2 on rate of nitrocefin hydrolysis by NDM-1 150

Figure 5.3 Production of Affimer 21 alanine scanning mutants 152

Figure 5.4 Repeat linear amplifications of Affimer 21 alanine scanning mutants 153

Figure 5.5 Gradient linear amplifications of Affimer 21 alanine scanning mutants G2.7A and P1.7A 154

Figure 5.6 Gradient linear amplifications of Affimer 21 alanine scanning mutants G1.1A, Y1.2A and G2.6A 155

Figure 5.7 Repeat linear amplification of Affimer 21 alanine scanning mutant Y1.2A 156

Figure 5.8 Production and purification of Affimer 21 mutants 158

Figure 5.9 Effects of alanine substitutions in Affimer 21 on rate of nitrocefin hydrolysis by NDM-1 160

Figure 5.10 IC_{50} of Affimer 21 G1.9A and D2.4A 162

Figure 5.11 Production and purification of Affimer 21 mutants G1.9A + D2.4A and G1.9A + N2.5A 164

Figure 5.12 Effects of double alanine substitutions in Affimer 21 on rate of nitrocefin hydrolysis by NDM-1 165

Figure 6.1 Fragment 1 and 2 171

Figure 6.2 Construction of Library 1 insert DNA by splice overlap extension 172

Figure 6.3 Number of colonies on ligation test plates 173

Figure 6.4 Inclusion rates (%) of amino acids in the 5 randomised positions of library 1 175

Figure 6.5 Structure of apo-NDM-1 (PDB: 3SPU) 177

Figure 6.6 Insertion of an N-terminal biotin acceptor peptide to NDM-1 constructs 178

Figure 6.7 SDS-PAGE analysis of NDM-1 (+BAP) production and purification in AVB101 and BL21 StarTM (DE3) cells, with and without additional biotin 179

Figure 6.8 Biotinylation checks for NDM-1 (+ BAP) 180

Figure 6.9 Phage ELISA results to confirm Affimer 21 phage binds to NDM-1 (+BAP) 181

Figure 6.10 Rate of nitrocefin hydrolysis by NDM-1 182

Figure 6.11 Phage ELISA results for Affimer reagents selected from library 1 against NDM-1 (+BAP) 183

Figure 6.12 Sequencing results of ten library 1 clones 184

Figure 6.13 Sequencing trace of variable region 1 for eluted phage pool 185

Figure 6.14 Phage ELISA results for Affimer binders selected from a competitive screen of library 1 against NDM-1 (+BAP) 186

Figure 6.15 Heat map showing amino acid enrichment at the randomised positions of Affimer 21 188

Figure 6.16: SDS-PAGE analysis of Affimer production and purification in BL21 StarTM (DE3) cell 188

Figure 6.17 Effects of Affimer reagents on rate of nitrocefin hydrolysis by NDM-1 192

Figure 6.18 Construction of Library 2 insert DNA by splice overlap extension ... 194

Figure 6.19 Number of colonies on ligation plates 195

Figure 6.20 Inclusion rates (%) of amino acids in the 4 randomised positions of library 2 197

Figure 6.21 Phage ELISA results for Affimer binders selected from a competitive screen of library 2 against NDM-1 (+BAP) 198

Figure 6.22 Heat map showing amino acid enrichment at the randomised positions of Affimer 21 199

Figure 6.23 SDS-PAGE analysis of Affimer production and purification in BL21 StarTM (DE3) cells 200

Figure 6.24 Effects of Affimer reagents on rate of nitrocefin hydrolysis by NDM-1 202

Abbreviations

2TY	2x tryptone and yeast
Aff	Affimer
AME	Aminoglycoside-modifying enzymes
AMR	Antimicrobial resistance
BSTG	BioScreening Technology Group
CRE	Carbapenem-resistant *Enterobacteriaceae*
CFP	Cyan fluorescent protein
DARPin	Designed Ankyrin Repeat proteins
DCF	Diclofenac
DNA-PAINT	DNA-points accumulation in nanoscale topography
E. coli	Escherichia coli
ECDC	European Centre for Disease Prevention and Control
FP	Fluorescent protein
FPBA	Fluorescent protein-binding aptamers
GFP	Green fluorescent protein
GT	Glycosyltransferase
IMP	Imipenemase
IPTG	Isopropyl β-D-1 thiogalactopyranoside
KPC	*Klebsiella pneumoniae* carbapenemase
LA-MRSA	Livestock-associated Methicillin-resistant *Staphylococcus aureus*
MBL	Metallo beta-lactamase
MDR	Multi-drug resistant

MGE	Mobile genetic element
MRSA	Methicillin-resistant *Staphylococcus aureus*
NAG	N-acetylglucosamine
NAM	N-acetylmuramic acid
NDM-1	New Delhi metallo-beta-lactamase 1
OMP	Outer membrane protein
OMV	Outer membrane vesicle
OPPF	Oxford protein production facility
OXA	Oxacillinase
PALM	Photoactivation localization microscopy
PBP	Penicillin binding protein
PCP	Personal care product
PPI	Protein-protein interaction
SBL	Serine beta-lactamase
SEC	Size exclusion chromatography
SMLM	Single molecule localisation microscopy
SOC	Super Optimal broth with Catabolite repression
STORM	Stochastic optical reconstruction microscopy
SUMO	Small ubiquitin-like modifier
TBS	Tris buffer saline
TMB	Tetramethylbenzidine
VEGFR	Vascular endothelial growth factor receptor
VIM	Verona integron encoded metallo-β-lactamase
VR	Variable region
YFP	Yellow fluorescent protein

Chapter 1

Introduction

1. Introduction

1.1 Background

Over the past seventy years the antibiotics era has been hampered by emergence of resistance. The incidence of multi-drug resistant infections has dramatically increased worldwide. Methicillin-resistant *Staphylococcus aureus* (MRSA) and more recently, New Delhi Metallo β-lactamase 1 (NDM-1) expressing *Enterobacteriaceae* feature regularly and prominently in the media. However, despite this increase in bacterial resistance, development of new antimicrobial agents is declining (Wise et al., 2011).

The emergence and spread of antibiotic-resistant bacteria is now considered to be one of the biggest threats to human health (World Health Organisation., 2016). Multi-drug resistant infections currently claim at least 700,000 lives each year; and this is predicted to rise to 10 million by 2050, taking the expected mortality rate higher than that caused by cancer (O'Neill, 2014) (Figure 1.1).

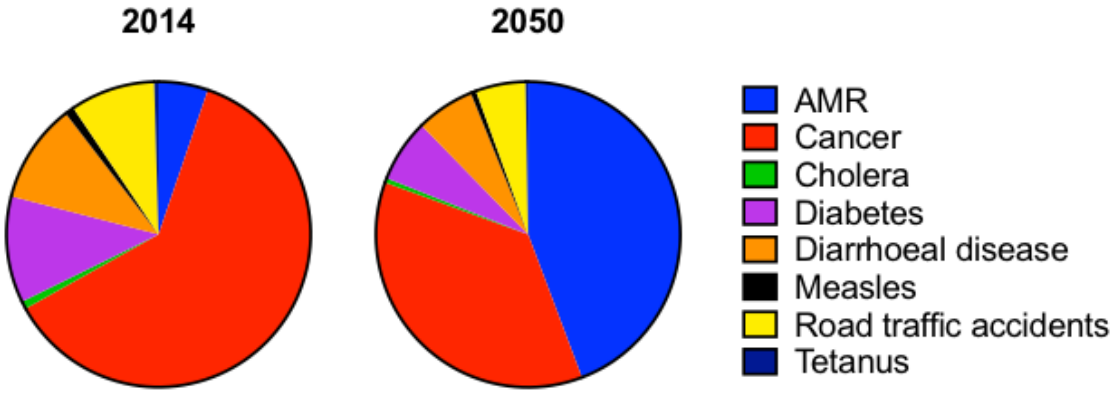

Figure 1.1: Deaths attributable to anti-microbial resistance (AMR) in 2014 and deaths predicted in 2050 compared to other major causes of death. Data sourced from AMR review paper (O'Neill, 2014).

Antibiotic resistance also encompasses an extensive economic cost, which is expected to grow if resistance is not tackled. The World Bank has estimated it could cost the world economy $1 trillion annually after 2030 (World Bank Group, 2017) and a reduction of 2-3.5 % in Gross Domestic Product (GDP). If antimicrobial drug resistance

is not tackled, between now and 2050 the world could expect to see a loss of between 60 and 100 trillion dollars worth of economic output - equivalent to the loss of around one years total global output. Furthermore, in the short term it is predicted that the world's GDP will be 0.5 % lower by 2020 and 1.4 % by 2030, with a death-toll of more than 100 million people (O'Neill, 2014).

In 2013, Britain's Chief Medical Officer Dame Sally Davies issued a public warning regarding the overuse of antibiotics and the subsequent emergence of resistance (Walsh, 2013). She stated 'If we don't take action, then we may all be back in an almost 19th Century environment where infections kill us as a result of routine operations. We won't be able to do a lot of cancer treatments or organ transplants.' This warning triggered a number of scientific reports, action plans, and pledges to reduce the use of antibiotics by the World Health Organisation (WHO), the Farm and Agricultural Organisation (FAO), and the G20 (Kirchelle, 2018). Despite this, international reduction plans have been slow to translate and a robust way of tackling the problem has yet to be realised.

1.2 History of antibiotics

Although antibiotics are often viewed predominately as a modern discovery, there is evidence to suggest that they have been used in some capacity for millennia. Historical reports suggest that ancient civilizations used naturally available treatments such as honey, herbs, animal faeces and even the topical application of mouldy bread to treat infections (Gould, 2016). Traces of tetracycline have been found in the bones and enamel of skeletons from ancient Sudanese Nubia from the years 350-550 AD as well as in femoral bones from Egypt dating back to the late Roman period (Aminov, 2010).

Although plants and other natural substances were historically used as antibiotics, the actual "antibiotic era" did not begin until the 19th century when Paul Ehrlich, a German physician, discovered that certain chemicals dyes selectively stained bacterial cells (Ehrlich, 1877). He concluded that it must be possible to find substances that kill bacteria without harming other cells, effectively founding the concept of chemotherapy. In 1909 he discovered that a chemical called arsphenamine was an effective treatment for syphilis (Ehrlich, 1910). Shortly after this, in 1928, came the

serendipitous discovery of penicillin by Alexander Fleming. Despite researchers before him having reported similar observations regarding the antimicrobial activity of penicillin, it was Fleming's remarkable persistency and conviction that led to its eventual success. He spent 12 years trying to resolve problems with purification and stability before Oxford-based scientists Florey and Chain published work describing a purification technique that eventually led to its commercial availability (The Nobel Prize in Physiology or Medicine, 1945). Fleming was also one of the first people to warn about the dangers of antibiotic resistance (New York Times, 1945).

The following 20 years became known as the 'Golden Age' of antibiotic discovery. Within 10 years of the end of World War 2, a number of important antibiotics had been discovered and developed. They became the foundation for the treatment of infectious disease and along with the introduction of better hygiene, led to a dramatic reduction in worldwide morbidity and mortality due to bacterial infections (Davies, 2006).

Today, antibiotics not only play a vital role in human health, they underpin the practice of modern medicine and have played a pivotal role in achieving major advances in medicine and surgery (Gould et al. 2013). They are critical for the prevention and treatment of infections in patients who are receiving chemotherapy; who have chronic diseases such as diabetes, end-stage renal disease, or rheumatoid arthritis; or who have had complex surgeries such as organ transplants, joint replacements, or cardiac surgery. Additionally, in less-developed countries, antibiotics dramatically reduce the morbidity and mortality rates from infections caused by poor sanitation and living conditions (Rossolini et al., 2014).

1.3 Gram-negative bacteria and infections

Bacteria can be broadly classified as either Gram-positive or Gram-negative, according to their cell wall structure (Figure 1.2).

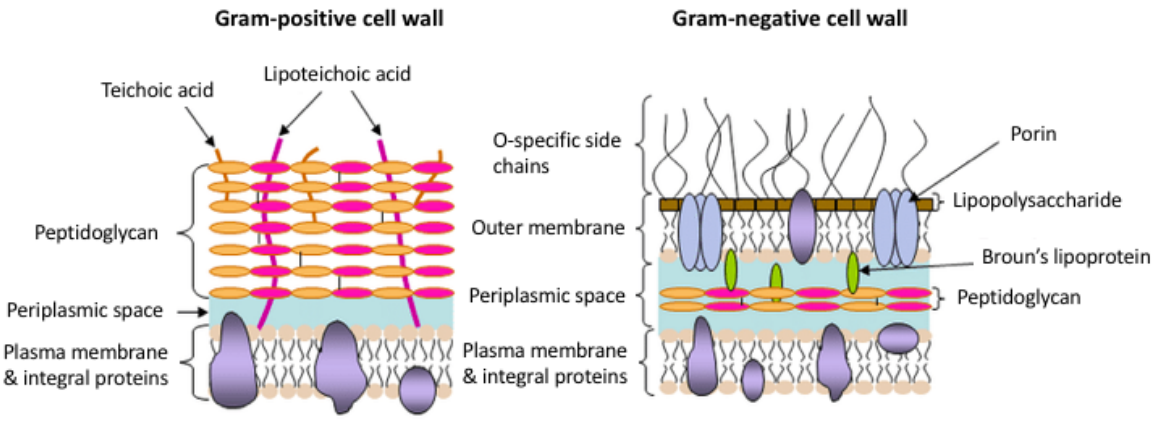

Figure 1.2: Differences in the cell wall structure of Gram-positive and Gram-negative bacteria. Gram-positive cell walls contain one lipid plasma membrane and a thick peptidoglycan layer interlinked with teichoic and lipoteichoic acids. Gram-negative bacteria have an inner and an outer membrane and only a thin layer of peptidoglycan in the periplasmic space. The outer membrane of Gram-negative bacteria is also rich in lipopolysaccharide (exotoxin). (Atanosova, 2010).

Gram-negative bacteria are notoriously more difficult to treat than Gram-positive bacteria due to the low permeability barrier of a double-membrane cell envelope and a lipopolysaccharide-rich (endotoxin) outer membrane (Zgurskaya et al, 2015). Bacteria are genetically very versatile and are able to incorporate DNA from different species and genera into their own genome. They evolve very quickly and are able to multiply rapidly (Hamilton-Miller, 1990). Additionally, both Gram-positive and negative bacteria are able to exchange genetic material via horizontal gene transfer, allowing easy dissemination of mutations and resistant genes.

Gram-negative bacteria are responsible for a wide range of acute infections (Table 1.1). The most common species *Enterobacteriaceae* and *Pseudomonaceae* are normally located in the digestive tract and have relatively low virulence. However, in patients with weakened immune systems these bacteria are capable of entering the bloodstream and without effective treatment can lead to circulatory shock, acute respiratory distress and multiple organ failure (Schellekens et al, 1989).

Table 1.1: Common Gram-negative bacteria and their associated infections. Data sourced from Peleg et al., 2010.

Gram-negative bacteria	Associated infections
Escherichia coli	Pneumonia, urinary tract infections, blood stream infections, diarrhoea
Klebsiella pneumoniae	Pneumonia, urinary tract infections, blood stream infections, diarrhoea, endocarditis, meningitis
Acinetobacter baumanii	Wound infections, pneumonia, urinary tract infections, blood stream infections, meningitis
Pseudomonas aeruginosa	Pneumonia, blood stream infections, urinary tract infections, cellulitis
Neisseria gonorrhoeae	Gonorrhoea

All of the Gram-negative species reported in Table 1.1 have demonstrated antibiotic resistance (National Institute of Allergy and Infectious Diseases, 2016). One of the most troubling is the rapid international spread of carbapenem resistant *Klebsiella pneumoniae* which has mortality rates of up to 53 % (Munoz-Price, 2013).

1.4 Emergence of antibiotic resistance

Antibiotics have saved billions of lives. However, there is no doubt that the overuse and misuse of antibiotics have had the largest impact on the evolution of resistance by increasing selection pressure (Ventola, 2015) (Figure 1.3). By 1960 antibiotics were being routinely used for treatment of both human and animal infections and for growth promotion in livestock, and resistance was beginning to become apparent (Davies, 2006).

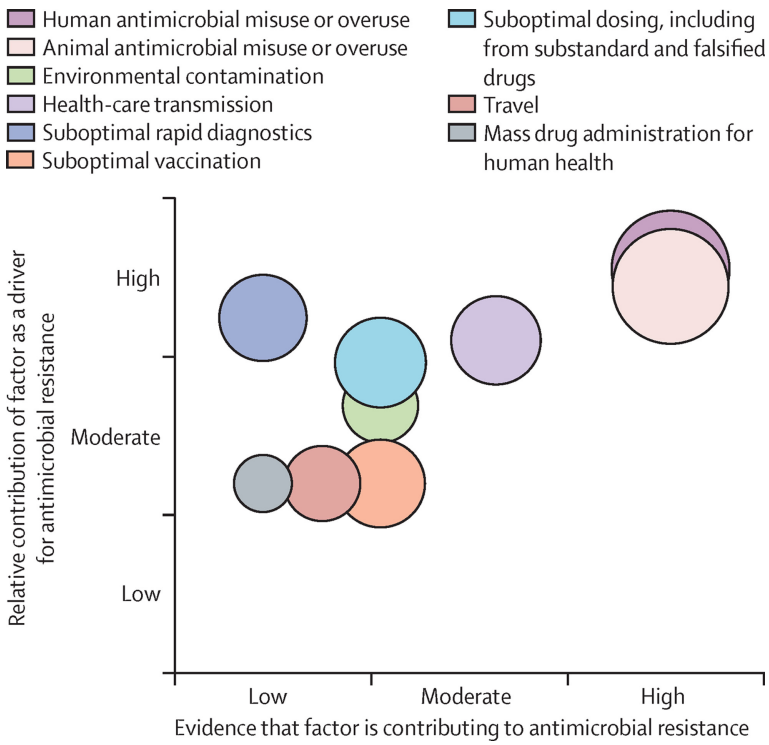

Figure 1.3: Contribution of factors driving antibiotic resistance. A representation of the potential contribution of factors that are thought to drive antibiotic resistance. Evidence suggests that the misuse and overuse of antimicrobials in human and animals has the biggest contribution to antibiotic resistance (Holmes et al, 2015).

1.4.1 Overuse and Misuse

Despite warnings about increasing resistance, antibiotics are still overprescribed globally. In many countries, the production and prescription of antibiotics is unregulated and results in drugs that are of variable quality, easily accessible and cheap; promoting overuse. Increased online access has also led to a surge in the unregulated purchasing of antibiotics, even in countries where antibiotics are currently regulated (Michael et al, 2014).

Antibiotics are effective only against bacteria but it is often difficult to differentiate between a bacterial and a viral infection without expensive and lengthy testing. In the past, this has led to antibiotics being pre-emptively prescribed for infections that will not respond to these treatments. Additionally, antibiotic dosages are designed to eradicate an entire bacterial population and yet prescribed courses of antibiotics are

often not completed. This can promote the incidence of surviving bacteria adapting to low level doses of antibiotics and developing resistance (Read et al, 2014). A review by Davies et al (2006) reported on the effects of sub-inhibitory concentrations of antibiotics on the transcriptional profiles and phenotypes of *Salmonella typhimurium, Escherichia coli*, *Pseudomonas aeruginosa* and *Staphylococcus aureus.* A wide range of effects were observed including increased adhesion, increased mutational frequency and enhanced horizontal gene transfer. Additionally, another study revealed that sub-inhibitory concentrations of imipenem in *Pseudomonas aeruginosa* induces both *ampC,* a gene that codes for β-lactamase; and increases the production of alginate to form thicker and more robust biofilms (Bagge et al, 2004).

1.4.2 Agricultural use

In 1948, the scientist Thomas Jukes discovered that the addition of low levels of tetracycline to the diets of chickens and pigs increased their growth rate, even when they were perfectly healthy (Carpenter, 2000). Subsequently, antibiotic use in food production began to increase and was introduced on farms, fishing fleets and processing plants to treat and prevent disease, increase feed production, and preserve food. Resistant bacteria and bacterial plasmids are transported on animal skin, in faeces and contaminated water and by various mechanisms, can be transferred to humans (Kruse et al, 1994). By 1965 the association between antibiotic use in cows and transmission of resistant bacteria to humans, had begun to be recognised (Anderson et al, 1965). Evidence suggests a food-borne transmission route for extended-spectrum β-lactamase and Ambler class C β-lactamase genes via handling or consumption of contaminated meat (Voets et al, 2013). Infections with the superbug MRSA are normally community or clinically associated. However, in 2014 the European Centre for Disease Prevention and Control (ECDC) initiated a survey to collect data on the incidence of livestock-associated MRSA (LA-MRSA) in humans. Although overall occurrence amongst all types of MRSA was low (3.9 %), 17 out of 19 countries reported confirmed cases of LA-MRSA (ECDC survey, 2017). Despite this amassing evidence, a ban on the use of antibiotics for growth promotion in livestock in the European Union did not occur until 2006, and outside Europe such use still occurs widely (Antibiotic Research UK, 2018).

1.4.3 Failure of discovery

There have been no new classes of antibiotics discovered for treatment of Gram-negative bacterial infections in the past 40 years. Pharmaceutical companies are no longer investing in the discovery of new antibiotics and many major pharmaceutical companies have abandoned the antibiotic field (Nature editorial, 2018). Increasingly stringent regulations in clinical trials and the high costs associated with drug discovery have meant that antibiotics are simply no longer a good economic investment for many companies. The recruitment of patients for clinical trials can be challenging as hospitals move quickly to contain resistant outbreaks. Antibiotics are normally used for relatively short periods and are often curative, making them less profitable than drugs which can be used for chronic, long-term conditions (Ventola, 2015). Additionally, there are now many campaigns advising restraint regarding the use of antibiotics. As a result, clinicians will often withhold new antibiotics as a reserve for more serious and difficult to treat infections and this adds to the lack of return on investment for pharmaceutical companies (Davies, 2006).

1.5 Mechanisms of resistance

Bacteria are remarkable in the diversity of their mechanisms for response to environmental threats. The bacterial response to antibiotics is a prime example of bacterial defence and adaptation. Bacteria often carry innate resistance to certain antibiotics but are also capable of acquiring resistance through mutations and horizontal gene transfer. Resistance to one class of antibiotics is often obtained through multiple pathways and a single bacterial cell is able to exploit a variety of mechanisms to survive the effect of an antibiotic. Some of these mechanisms are outlined in Figure 1.4.

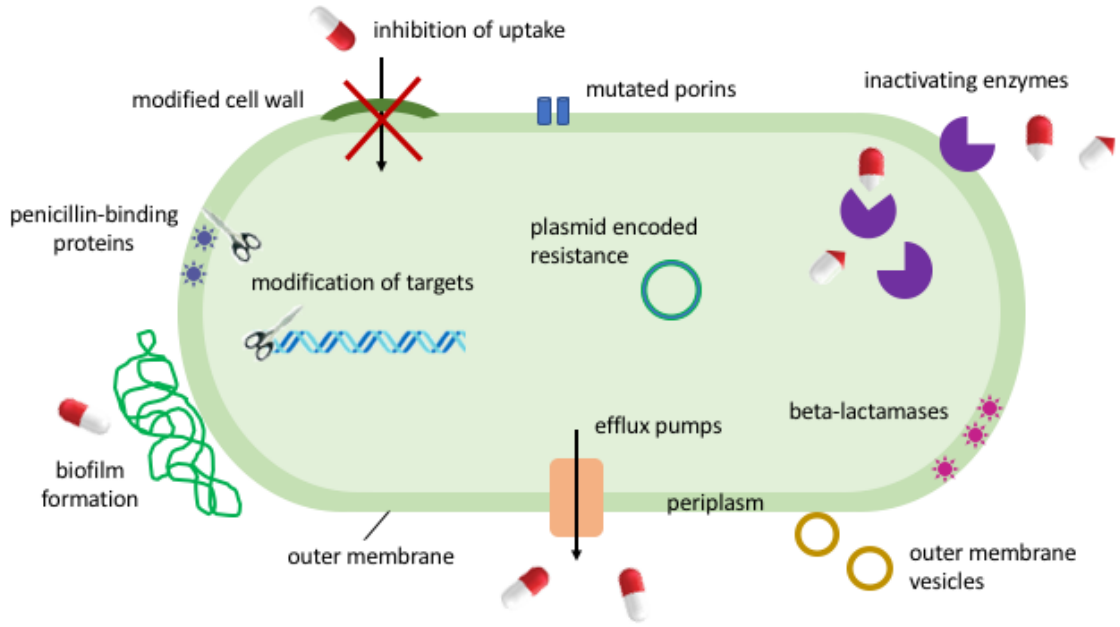

Figure 1.4: Innate and acquired antibiotic-resistance mechanisms in Gram-negative bacteria. There are various mechanisms by which bacteria can resist antibiotics. Many of these are mediated by genes encoded on a mobile plasmid. These mechanisms include a modified cell wall, which inhibits antibiotic uptake; mutated porins, which reduces the movement of drug through the cell membrane; the presence of β-lactamases in the periplasmic space, which degrades the β-lactam; increased expression of transmembrane efflux pumps, which expels the drug from the bacterium before it can have an effect; modification of targets, which prevent the antibiotic from binding to its site of action and outer membrane vesicles, which provide a first line of defence and protect neighbouring communities of bacteria. The use of antibiotics creates a selective pressure that encourages the honing and specification of these mechanisms. Adapted from (Sriramulu, 2013).

1.5.1 Plasmid encoded resistance

Plasmids are mobile double-stranded DNA molecules that have broad diversity due to their ability to collect mobile genetic elements (MGEs) such as insertion sequences, integrons and transposons which can provide selectable advantages to their hosts. Many of the resistant mechanisms found in Gram-negative bacteria can be mediated by plasmid encoded genes. These resistance genes can be horizontally transferred between cells by conjugation, a very efficient method of gene transfer that has been shown to occur most frequently in patients undergoing antibiotic treatment (Huddleston, 2014). Plasmids that carry a number of resistance genes enable bacteria to become resistant to multiple drugs in a single event, and can spread widely through susceptible populations.

New resistance elements are often acquired by mutations. Once a resistant mutant evolves, treatment with the equivalent antibiotic will eradicate the non-mutant population and bacteria containing the new resistance gene will predominate. Often, the mutational change can result in decreased fitness of the cell and therefore the mutation will only be successfully selected for in the presence of the antibiotic where it provides a survival advantage (Munita et al, 2016). Most mutations that result in antibiotic resistance alter antibiotic action by one of the following mechanisms, i) modification of the target, ii) inhibition of drug uptake, iii) activation of efflux pumps or iv) modulation of regulatory networks. Often, these mutations are expressed alongside other resistance factors such as modifying enzymes and β-lactamases, making them extremely difficult to treat.

In addition to these acquired resistance genes, many bacteria are naturally or intrinsically resistant to certain classes of antimicrobials. Bacteria naturally present in soil contain intrinsic novel antibiotic resistant elements. Research has shown that some of these resistant genes predate the antibiotic era suggesting that antibiotic resistance is a naturally occurring and ancient phenomenon (D'Costa et al, 2011). Another study discovered that bacteria isolated from a cave that had been isolated for 4 million years were highly resistant to antibiotics, with one strain showing resistance to 14 commercially available drugs (Bhullar et al, 2012). These isolates represent a reservoir of resistance genes with the potential to be mobilised and disseminated into the wider microbial community via plasmids or other MGE's. Indeed, Forsberg et al, 2012 demonstrated that a number of resistance genes in a previously sensitive pathogenic strain of *E. coli* were shared with soil bacteria.

1.5.2 Modified cell wall

Gram-negative bacteria are intrinsically less permeable than Gram-positive bacteria due to their double-membrane cell envelope and liposaccharide rich outer membrane. Lipopolysaccharides consist of an O antigen polysaccharide, core oligosaccharide and a hydrophobic component known as lipid A. Lipid A is buried in the outer membrane and elicits a strong inflammatory response which can lead to septic shock in the host upon bacterial cell lysis by immune cells (Maldonado et al, 2016). Immune cells typically rely upon detection of lipid A to target the bacteria, therefore modification of lipid A

presents an opportunity to evade the immune system and establish an infection. Modifications to the acylation and phosphorylation patterns of lipid A; as well as changes to the charge of the bacterial surface, are made during and after trafficking to the outer membrane and directly affect pathogenesis by diminishing the host inflammatory response, altering membrane permeability and promoting resistance to antibiotics (Needham et al, 2013).

1.5.3 Porins

Besides protecting bacteria from toxicity, the outer membrane contains channels known as porins; outer membrane proteins (OMPs) with a beta-barrel structure that permit the uptake of soluble molecules (Masi et al, 2013). In *E. coli*, hydrophilic antibiotics are able to cross the outer membrane by diffusion through OmpC and OmpF, the major porins. Down-regulation or replacement of porins with more selective channels therefore limits antibiotic entry by reducing the permeability of the cell. One study demonstrated that cells with porin alteration or loss have carbapenem resistance even when carbapenamases are not present, indicating that they could contribute significantly to resistance (Wozniak et al, 2012). A strain of *K. pneumoniae* carrying a mutated OmpK36 porin variant also caused an outbreak in a Greek hospital in 2012 (Poulou et al, 2013). Additionally, porin loss has been associated with a significant increase in resistance in clinical isolates of extended spectrum β-lactamase-producing *E. coli* and *K. pneumoniae* (Baroud et al., 2013). This study also demonstrated that efflux pump activity also plays a role in resistance to carbapenems.

1.5.4 Efflux pumps

Although bacterial membranes are generally impermeable, some toxic compounds are still able to penetrate the cell. These toxic compounds are expelled from the cell by transmembrane transporters known as efflux pumps. Efflux of antibiotics or toxins is often the fastest acting bacterial stress response and owing to broad specificity for multiple types of compounds, they contribute substantially to virulence and are often referred to as multi-drug resistance (MDR) efflux pumps (Sun et al., 2014).

The movement of drugs against a concentration gradient requires energy. To date, six groups of multi-drug transporters have been characterised in depth: one group which

utilises ATP to drive efflux (the ATP binding cassette (ABC) family), and five others which use electrochemical energy from ion gradients: the resistance-nodulation-cell division (RND) superfamily, major facilitator superfamily (MFS), small multi-drug resistance (SMR) family, proteobacterial antimicrobial compound efflux (PACE) family and the multi-drug and toxin extrusion (MATE) family (Du et al, 2018). RND and MF efflux pumps are the most common. The RND family of pumps are found extensively in Gram-negative bacteria and are the best characterised and most clinically relevant. They are tripartite assemblies which span both membranes and the periplasm and consist of a cytoplasmic membrane pump, a periplasmic protein and an outer membrane protein channel (Piddock, 2006). The AcrAB-TolC pump in *E. Coli* is a well-studied example and has two distinct binding pockets that accommodate substrates with a wide variety of sizes and properties, explaining how these pumps are able to export and provide resistance against such a wide range of antibiotics (Nakashima et al, 2011).

The overexpression of efflux pumps in bacteria has been detected in clinical samples since the 1900s. This is thought to occur in response to both environmental signals and as a result of mutations in repressors and transcription factors (Blair et al, 2015). All species of bacteria possess numerous genes that encode MDR efflux pumps, but most concerning is that some of these genes have been shown to be mobilised to plasmids that can be passed between bacteria by conjugative transfer. An IncHI1 plasmid isolated from a *Citrobacter freundii* strain was shown to contain resistance determinants that included genes encoding both an RND efflux pump and NDM-1 (Dolejska et al, 2013). The plasmid also contained proteins sharing 63 - 74 % homology with proteins from 3 other bacterial species. This is further evidence to support the hypothesis that resistance mechanisms are easily transmissible and rapidly disseminated between clinically relevant pathogens.

In addition to protecting bacteria against toxic compounds, some of the efflux pumps have been shown to export virulence and adhesion factors that facilitate bacterial aggregation into biofilm communities (Soto, 2013).

1.5.5 Biofilms

Most bacteria exist as one of two forms during growth and proliferation; either as single planktonic cells, or attached to surfaces in the form of multicellular aggregates known as biofilms. Acute infections normally involve planktonic bacteria and in general, are fairly susceptible to antibiotic treatment if diagnosed quickly. However, in untreated infections bacteria are capable of forming biofilms leading to chronic and often untreatable infections (Bjarnsholt, 2013). Biofilm infections such as pneumonia in cystic fibrosis patients, infections of the middle ear in patients with otitis media, chronic wounds and infections of implants and catheters, are relatively common and responsible for millions of deaths every year (Hall et al, 2017).

Biofilms consist of groups of cells enclosed in a self-produced extracellular matrix composed of proteins, polysaccharides, lipids and DNA which provides structural stability and protection to the biofilm. As biofilms, bacteria have been shown to be substantially less sensitive to antibiotics than non-adherent, planktonic cells of comparable density (Kirby et al, 2012). There are thought to be many reasons for this increased resistance (Figure 1.5).

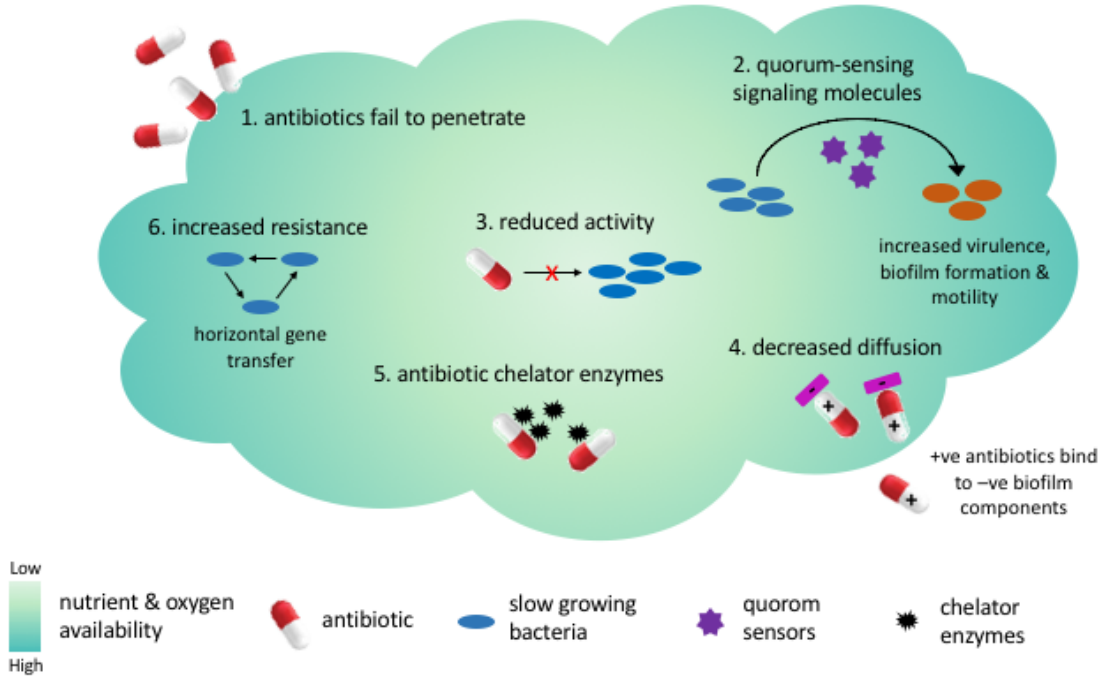

Figure 1.5: Challenges in treating biofilm associated bacterial infections: (1) Antibiotics may fail to penetrate beyond the surface layer of the biofilm. Outer layers of biofilm absorb damage. **(2)** Bacteria in biofilms interact through quorum-sensing signals; a signalling system that allows bacteria to communicate in polymicrobial infections. Quorom-sensing has been linked with the regulation of biofilm growth, virulence, and motility of bacteria. **(3)** Antibiotic action may be impaired in areas of waste accumulation or altered environment. Additionally, antibiotics such as β-lactams target rapidly dividing bacterial cells but bacteria in biofilms have a reduced growth rate. **(4)** Negatively charged components in the biofilm could bind to positively charged antibiotics (such as the aminoglycosides) and prevent their diffusion. **(5)** Antimicrobial agents may be altered or destroyed by enzymes in the biofilm matrix. **(6)** Mutation frequency and horizontal gene transfer are much higher in biofilms and results in development of resistance mechanisms such as over expression of efflux pumps or up-regulation of porin proteins. Adapted from Sherrard et al, 2014.

The efficacy of the antibiotic used is characterised by the amount that is able to reach and act upon the desired target. The observation that sub-optimal doses of antibiotics can act as agonists of biofilm formation was first demonstrated by Gordon Christensen in 1988 when he found that a strain of *Staphylococcus epidermidis* exhibited a 65 % increase in biofilm formation in the presence of 0.25 MIC of the antibiotic rifampin (Schadow et al, 1988). Numerous studies have since confirmed this observation for a wide variety of antibiotic classes and bacterial species, including the β-lactams (Kaplan, 2011). One study identified a novel regulatory mechanism in *E. coli* that induces biofilm

formation via ppGpp signalling. This report also confirmed that sub-MIC doses of various ribosome targeting antibiotics all resulted in a strong biofilm-formation response (Boehm et al, 2009). Additionally, sub-inhibitory doses of the β-lactam antibiotics vancomycin and oxacillin were shown to induce biofilm formation in a clinical strain of MRSA (Mirani et al, 2011).

As mentioned previously, the horizontal transfer of genes between bacterial species plays a crucial role in the rapid spread of resistance elements and it has previously been observed that *bla*$_{\text{NDM-1}}$ can be passed between *Enterobacteriaceae* species by conjugative transfer. Recent research has also established that *bla*$_{\text{NDM-1}}$ can be passed between species of biofilm; from *Enterobacteriaceae* to *Pseudomonas aeruginosa* and *Acinetobacter baumannii*, suggesting that biofilms might play a crucial role in the interspecies spread of plasmids carrying the NDM-1 gene in natural and clinical settings (Tanner et al, 2017).

1.5.6 Outer membrane vesicles

Outer membrane vesicles (OMVs) are spherical membrane-enclosed structures that originate from the outer membrane of Gram-negative bacteria. They contain cytoplasmic and periplasmic proteins, DNA, RNA, phospholipids, lipopolysaccharides and OMPs, and play a critical role in interactions between bacteria (Jan, 2017). They have a diverse range of functions and are involved in biofilm formation, transmission of virulence and signalling factors, cellular communication, bacterial pathogenicity and host infection. It has also been shown that OMVs are involved in bacterial defence against both physical and chemical stress and can protect bacteria against several classes of antibiotics (Kim et al, 2018).

OMVs act as a first line of defence and are able to protect bacteria in the early stages of antibiotic attack. Circulating β-lactam antibiotics are able to penetrate the outer membrane of OMVs where they are inactivated by transported β-lactamases (Schwechheimer et al, 2015). This was first confirmed 2 decades ago, when enzymatic and microscopy analysis showed that membrane vesicles isolated from 3 resistant clinical samples contained β-lactamase (Ciofu et al, 2000). Both OXA-24 and NDM-1 have since been isolated from OMVs and shown to protect nearby populations of

bacteria (Rumbo et al, 2011 and Gonzalez et al, 2016). Additionally, a more recent study by Kim et al, 2018 demonstrated that OMVs taken from β-lactam resistant strains of *E. coli* could confer antibiotic resistance in non-susceptible strains.

1.5.7 Modification of target

A common mechanism of bacterial resistance is to prevent antibiotics binding by modifying the target. These changes are either point mutations in genes encoding the target site, enzymatic alterations of the binding site (by addition of methyl groups), or replacement or bypass of the original target (Munita et al, 2016).

Rifampicin is a semi-synthetic rifamycin, a broad-spectrum antibiotic commonly used to treat tuberculosis, leprosy, AIDS-associated infections and MRSA. It inhibits DNA-dependent RNA polymerase by binding to the β subunit of the RNA polymerase (encoded by *rpoB*), and blocking transcription. Studies in *E. coli* revealed that high level rifampicin resistance is due to single point mutations in the *rpoB* gene that are expected to alter the confirmation of the binding pocket. Substitutions at three sites in particular confer high level resistance and accordingly were frequently associated with resistant clinical isolates (Alifano et al, 2015).

A classic example of resistance by enzymatic modification of the target site is the methylation of ribosomes catalysed by methyltransferases which results in resistance to the aminoglycosides. The aminoglycoside antibiotics function by binding to the ribosome and inhibiting protein synthesis. Eight plasmid-mediated 16S rRNA methyltransferase genes have been identified in pathogenic bacteria worldwide and confer high-level resistance to almost all clinically available aminoglycosides (Fritsche et al, 2008). Additionally, these methyltransferase genes have been found in association with NDM-1 in species of *Enterobacteriaceae* isolated in India and the UK and were also found in three different plasmid backbones suggesting that they are easily transmissible (Hidalgo et al, 2013).

Bacteria are capable of evolving new targets that have a similar function to the original target but are not susceptible to the antibiotic molecule. Resistance to β-lactam antibiotics in MRSA is due to expression of an extra exogenous penicillin-binding protein

2a (PBP2a) encoded by the gene *mecA*, which isn't present in other *S. aureus* species. PBP2a is only mildly inhibited by β-lactam antibiotics and can therefore continue peptidoglycan crosslinking under treatment with these drugs, when other PBPs are inhibited (Fishovitz et al, 2014).

1.5.8 Inactivating enzymes

Antibiotics can be inactivated through the addition of chemical groups via bacterial enzymes. These enzymes can cause antibiotic resistance by preventing the drug molecule from binding to its intended target as a result of steric hindrance. These enzymes form a diverse family of inactivating enzymes which can transfer various chemical groups including phosphates, acyls, ribitoyls and nucloetidyls (Blair et al, 2014).

Aminoglycoside antibiotics such as kanamycin and streptomycin are susceptible to modification by phosphorylating, acetylating, and nucleotidylating enzymes. These modifications prevent the antibiotic from binding to ribosomes and interfering with translation, a mode of action that is normally bactericidal. Many aminoglycoside-modifying enzymes (AMEs) have broad ligand specificity and some are able to modify more than 15 diverse aminoglycoside antibiotics (Norris et al, 2013). Worryingly, AME encoding genes were detected in 93.1 % of clinical isolates of *Enterobacteriaceae* collected from European and adjacent countries between 2014–15 (Castanheira et al, 2018).

Rifampin is a rifamycin antibiotic commonly used to treat tuberculosis and has increasingly become a reserve antibiotic for the treatment of resistant staphylococcal infections. Rifampin can be inactivated by glycosylation, ADP ribosylation, and phosphorylation. These inactivating enzymes chemically modify rifampin, reducing its affinity for the β-subunit of RNA polymerase and effectively blocking its mode of action (Spanogiannopoulos et al, 2014).

1.5.9 Penicillin binding protein mutations

Peptidoglycan is a three-dimensional net-like mesh that forms a key component of the bacterial cell wall. Penicillin binding proteins (PBPs) are membrane-bound enzymes involved in polymerisation of glycan strands and cross-linking between glycan chains in the final stages of peptidoglycan synthesis (Figure 1.6). They are named after their ability to bind to penicillin and are the targets of β-lactam antibiotics (Sun et al, 2014). PBPs vary between bacterial species in terms of their number, size, amount and affinity for β-lactam antibiotics. They can be classified into two major groups of high molecular weight (HMW) (>60 kDa) or low molecular weight (LMW) (<49 kDa), with LMW-PBPs serving mainly as monofunctional DD-carboxypeptidases. HMW-PBPs are divided into subclasses; A and B, both of which have transpeptidase function and are considered to be the main targets of β-lactam antibiotics (Bush et al, 2016).

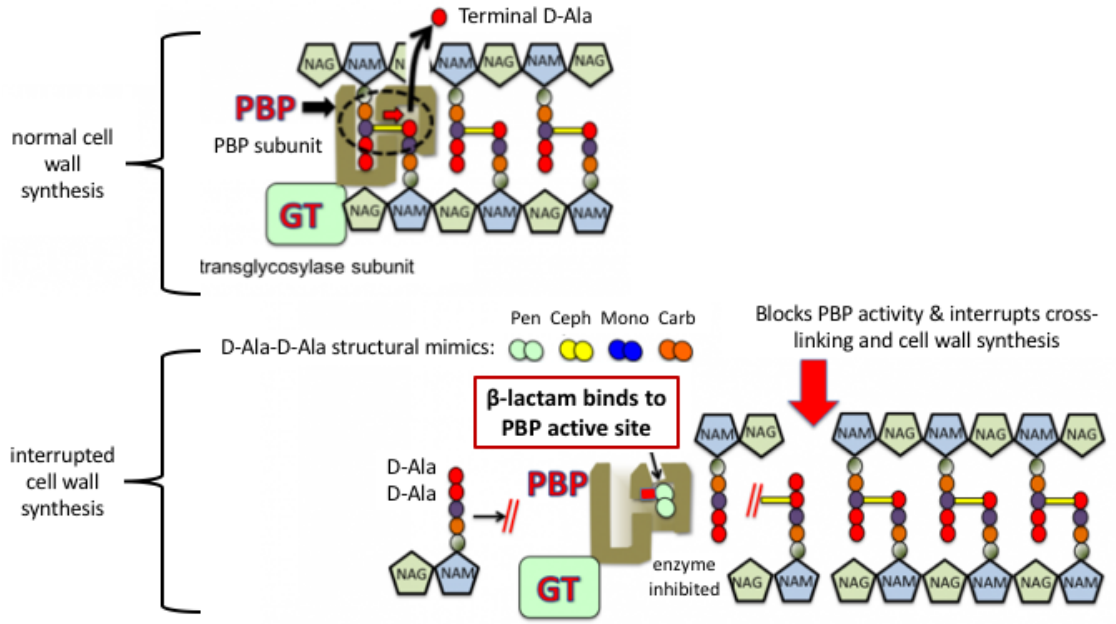

Figure 1.6: Mechanism of action of β-lactam antibiotics. (Top) During normal cell wall synthesis PBPs in the cell wall catalyse cross linking between glycan strands, which involves the removal of a terminal D-alanine residue from one of the peptidoglycan precursors (circled). Glycosyltransferases (GT) create covalent bonds between adjacent NAM/NAG peptide subunits creating a rigid cell wall that protects the cell from osmotic forces that would otherwise result in cell rupture. **(Bottom)** The β-lactam antibiotics, which include penicillins (Pen), cephalosporins (Ceph), monobactams (Mono) and carbapenems (Carb), are analogues of the D-Ala-D-Ala precursor for PBP, and are able to tightly bind to the active site and inhibit cell wall synthesis. NAG: N-acetylglucosamine; NAM: N-acetylmuramic acid (Clarks, 2015).

The superfamily of antibiotics known as the β-lactams are currently the most prescribed class of antibacterial agents. In the US they account for 65 % of all prescriptions for antibiotics and cephalosporins comprise nearly half of these prescriptions (Bush et al, 2016). β-lactams are broad-spectrum and have a core structure consisting of a 4-member β-lactam ring. The β-lactam ring is structurally similar to the D-Ala-D-Ala peptide sequence that is the substrate for PBPs and is able to mimic the substrate and bind to their active site with high affinity. This inhibits PBP activity and prevents cell wall formation leading to osmotic instability or autolysis (Figure 1.6). There are four major β-lactam subgroups; penicillins, cephalosporins, monobactams and carbapenems (Figure 1.7).

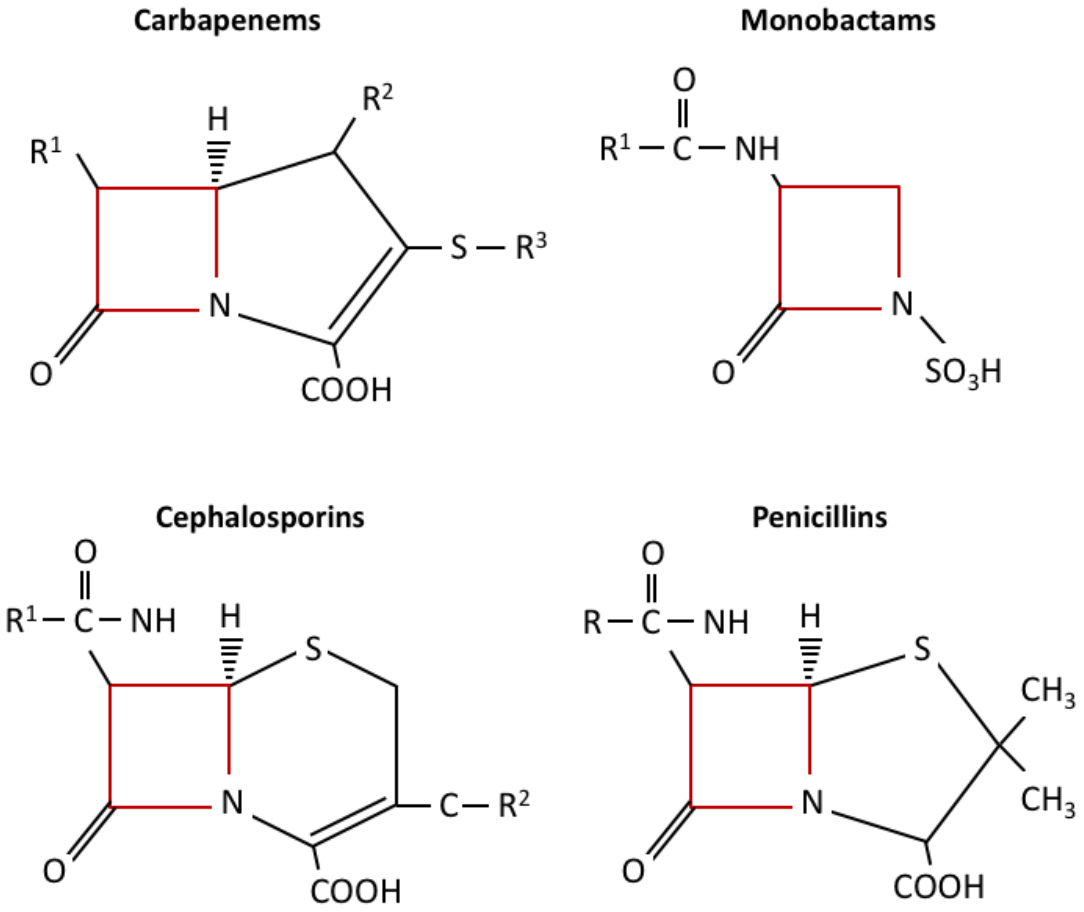

Figure 1.7: Chemical structures of the β-lactam antibiotics. Carbapenems, monobactams, cephalosporins and penicillins all contain a β-lactam ring which is structurally similar to the D-Ala-D-Ala peptide sequence that is the substrate for PBPs. R represents side chains that differ among members of the same class of beta-lactam antibiotics, the β-lactam ring is highlighted in red.

Resistance to β-lactam antibiotics occurs through mutational alterations in PBPs which reduces binding of the antibiotic to the active site; or by evolving a β-lactamase activity that degrades the antibiotic. Bacteria are capable of expressing mutated PBPs which still have enzymatic activity for cell wall synthesis, but have reduced affinity for β-lactam antibiotics (Kong et al, 2010). This has been shown for many PBPs and in a variety of bacterial species. Examples of PBPs with low affinity for β-lactams have been described for *Acinetobacter baumannii* (Gehrlein et al, 1991), *Staphylococcus aureus* (Hamilton et al, 2017), *Salmonella enterica* (Sun et al, 2014) and *E. coli* (Hedge et al, 1985).

1.5.10 β lactamases

The inactivation of antibiotics by enzymes has been a major mechanism of resistance since the first use of antibiotics, when penicillinase (a β-lactamase) was discovered in 1940 (Abraham et al, 1940). Many enzymes that target antibiotics have since been discovered, some of which are able to degrade several different antibiotics within the same class; for example, β-lactamases, which are effective against penicillins, cephalosporins, clavams, carbapenems and monobactams. The emergence of diverse β-lactamases, including IMP (imipenemase), VIM (Verona integron encoded metallo β-lactamase), KPC (*K. pneumoniae* carbapenemases), OXA (oxacillinase) and NDM enzymes in Gram-negative bacteria such as *K. pneumoniae, E. coli, P. aeruginosa* and *A. baumannii,* has led to the materialisation of multi-drug resistant isolates with serious clinical implications (Blair et al, 2015).

Beta lactamases protect bacteria by hydrolysing the four-membered β-lactam ring in β-lactam antibiotics. They thereby destroy the antimicrobial activity by deactivating the chemically reactive acylating group that modifies the active site serine side chains in PBPs, preventing the inhibition of cell wall synthesis. There are two general chemical mechanisms by which β-lactamases operate. Class A, C and D are serine β-lactamases (SBLs) and hydrolyse their substrates by forming an acyl-enzyme through an active site serine (Rotondo et al, 2017). Class B metallo β-lactamases (MBLs) require the participation of one or two active site Zn^{2+} ions to activate a nucleophilic water molecule for hydrolysis of the β-lactam ring (Figure 1.8).

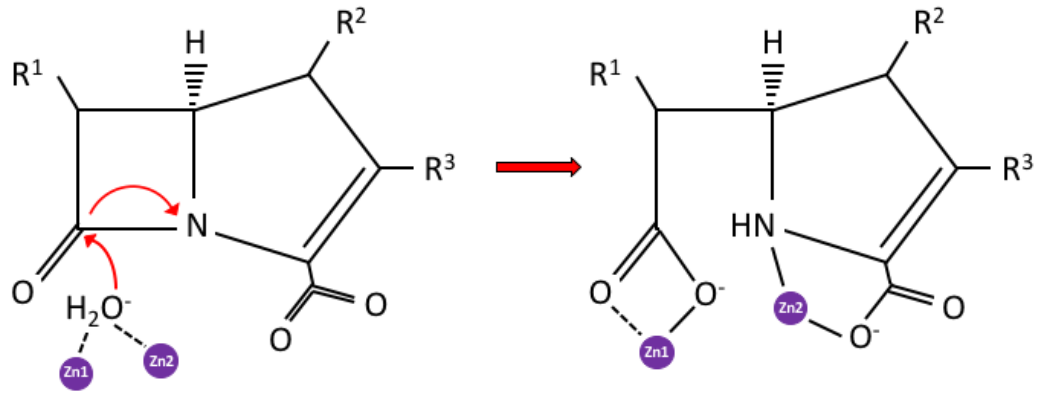

Figure 1.8: Hypothesised mechanism of carbapenem hydrolysis by metallo β-lactamases. Hydrolysis involves a nucleophilic attack to the carbonyl group, amide bond cleavage and the protonation of the nitrogen.

Until relatively recently, the SBLs were dominant in the clinic as the principle mechanism for β-lactam antibiotic resistance and as a result, research had focussed predominantly on developing inhibitors against this class of enzyme. There are currently four SBL inhibitors commercially available; avibactam, clavulanate, tazobactam and sulbactam, and a further eight in various stages of clinical development (Docquier et al, 2018). In comparison, the MBLs have only become clinically prominent relatively recently and there are currently no commercially available MBL inhibitors (McGeary et al., 2017).

1.6 Metallo β-lactamases

Metallo β-lactamases (MBLs) were discovered in the mid-1960s and were initially only detected in species with low pathogenic potential. However, since 1990 numerous MBLs have been discovered and isolated from a wide variety of major Gram-negative pathogens and they are now considered a major threat to global healthcare (Somboro et al, 2018). The MBLs are characterised by their broad-spectrum substrate specificity and are able to hydrolyse all β-lactam antibiotics, including the carbapenems; one of the last drugs still effective against multidrug-resistant infections. These carbapenem-resistant *Enterobacteriaceae* (CRE) are associated with mortality rates of up to 50 % and have recently been identified as “critical priority pathogens” by WHO (WHO, 2017).

MBLs are divided into 3 structural subclasses; B1, B2 and B3, defined primarily by differences in the primary zinc coordination shell and sequence similarities, although sequence homology is not large and ranges from 2 to 24 % (Palzkill, 2013). All MBLs possess a distinctive αβ/βα sandwich fold and possess a shallow active-site groove bordered by flexible loops. However, there has been some controversy regarding the number of zinc ions required for catalysis between the subclasses. Recent evidence suggests that for B1 and B3 subclasses, the presence of 2 zinc ions in the active site shows positive cooperativity and that the di-zinc enzyme is the most catalytically relevant. Paradoxically, subclass B2 enzymes are active in the mono-zinc form, but inhibited in the presence of a second zinc ion (Karsisiotis et al, 2014). The B1 subclass has the broadest substrate specificity and contains the largest number of clinically significant MBLs, including the transferable IMP, VIM and NDM-type enzymes.

1.7 New Delhi Metallo β-lactamase 1 (NDM-1)

New Delhi metallo-β-lactamase 1 (NDM-1) is a class B MBL that was first discovered in 2008 from a *Klebsiella pneumoniae* strain isolated from a Swedish patient who had undergone elective surgery in India (Yong et al, 2009). Molecular examination revealed that *bla*NDM-1 was found on a 180 kb plasmid alongside genes encoding CMY-4 (another β-lactamase), and genes that inactivated the antibiotics erythromycin, ciprofloxacin, rifampicin, and chloramphenicol. Additionally, genes encoding growth promoters and an efflux pump were observed. This isolate was resistant to all antibiotics tested apart from fluoroquinolones and colistin.

By 2009, isolates carrying NDM-1 were the predominant carbapenem-resistant Enterobacteriaceae in the UK and had been identified in *Klebsiella*, *E coli*, *Enterobacter* and *Morganella morganii* species - demonstrating the capability of the NDM-1 carrying plasmid to disseminate among strains of Enterobacteriaceae (Yong et al, 2009). Since then, NDM-1 has become one of the most prevalent carbapenemases worldwide. NDM-1 positive isolates have recently been reported in more than 40 countries covering all continents except South America and at least 17 variants differing by just 1 or 2 residues are now known (Khan, 2017). There are several proposed reasons for its rapid dissemination:

i) The plasmids detected in Gram-negative bacteria are easily transferrable by horizontal transmission and are capable of rearrangement, indicating genetic flexibility amongst bacterial populations
ii) A likely prevalence of undiagnosed asymptomatic carriers
iii) Shortage of effective antibiotics for the treatment of multi-drug resistant NDM-1 expressing bacteria

Sequence alignments of *bla*NDM-1 suggest that it may have originated as a chimera from *A. baumannii.* Sequences corresponding to the first six amino acids of the aminoglycoside phosphotransferase AphA6 and the insertion sequence IS*Aba125,* are strongly associated with *A. baumannii* and are often observed upstream of the *bla*NDM-1 (Toleman et al, 2012). The NDM-1 gene is rarely chromosomally integrated and is primarily found on various plasmids of different sizes including IncF, IncA/C, IncL/M, IncH, IncN and IncX3 (Poirel et al, 2011). Sequence analysis of some of these plasmids indicate that *bla*NDM-1 is often associated with insertion sequences and transposons, facilitating its dissemination by horizontal transfer. The transposon Tn3000 is reported as being primarily responsible for the spread of NDM-1 amongst Enterobacteriaceae (Campos et al, 2015).

There are numerous studies reporting the coexistence of NDM-1 alongside other β-lactamases including IMP-1 in Acinetobacter species (Tran et al, 2017), OXA-232 in *E. coli* (Both et al, 2016), OXA-48 in *K. pneumoniae* (Xie et al, 2017), OXA-23 in *A. baumannii* (Joshi et al, 2017) and VIM-1 in *K. pneumoniae* (Papagiannitsis et al, 2016). Additionally, the co-expression of NDM-1 alongside genes for methyltransferases conferring resistance against aminoglycosides has been observed (Rahman et al, 2015). In the E. coli strain ST471, NDM-1 was detected alongside CTX-M-9, TEM, SHV and RmtC (Kapmaz et al, 2016). The co-existence of NDM-1 with these other resistance elements drastically reduces treatment options. Concerningly, emergence of strains containing both MCR-1 and NDM-1 has resulted in isolates that are also resistant to colistin, a last resort drug that was previously effective against strains expressing NDM-1 (Zheng et al, 2016).

NDM-1 contains the αβ/βα protein fold that is characteristic of all MBLs, in which a central β sheet sandwich is flanked by solvent-exposed α helices (Figure 1.9). A number of X-ray crystal structures of apo NDM-1 and NDM-1 in complex with a variety of substrates or inhibitors and with varying occupation of the zinc binding sites have been reported and are listed in Section 4.3, Figure 4.18. These structures combined with molecular modelling reveal that NDM-1 has a wider and shallower binding groove than other MBLs and is therefore able to bind a wider variety of β-lactam antibiotics (Feng et al, 2014). Additionally, superposition of structures demonstrates a range of conformations for the flexible loop 3 which is adjacent to the active site (Green et al, 2011). This loop is involved in substrate binding and its increased flexibility and hydrophobicity compared to other MBLs is the proposed rationale for its broad substrate specificity.

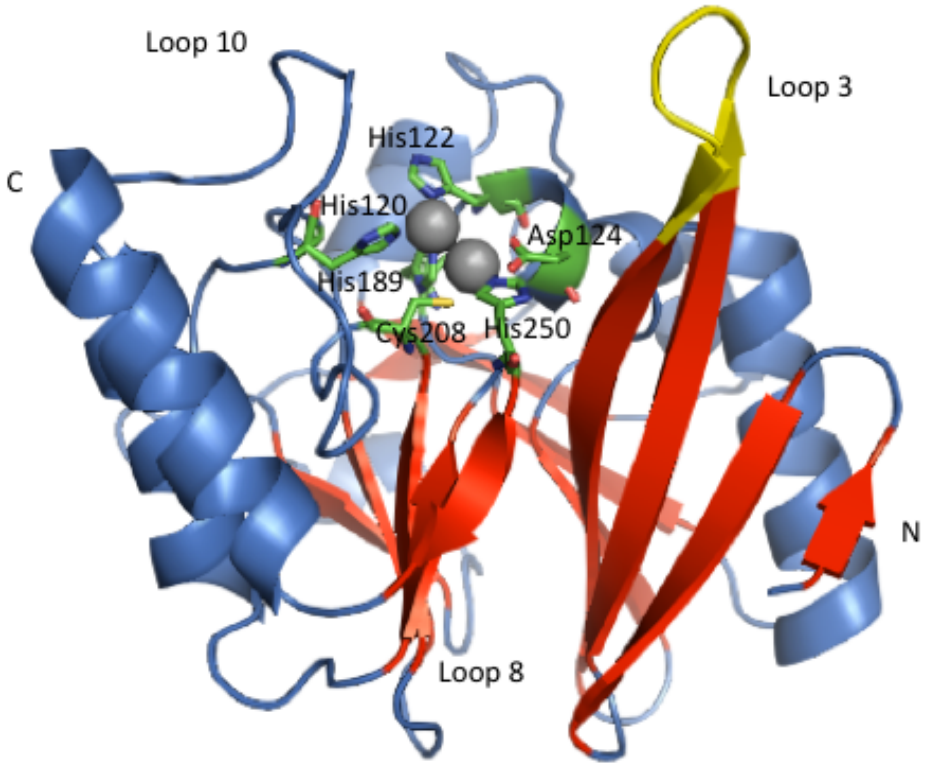

Figure 1.9: Structure of apo-NDM-1 (PDB: 3SPU) Cartoon of apo NDM-1 structure showing the αβ/βα sandwich common to all MBLs (α helix blue, β sheets red). Highlighted are the active site zinc ions (grey spheres), zinc ligands (sticks, green), and the flexible active site loop 3 (yellow). Zinc binding site 1 is coordinated by His120, His122 and His189. Zinc binding site 2 is coordinated by Asp124, Cys208 and His250 (adapted from King et al, 2011).

The active site typically contains either one or two zinc ions, with zinc binding site 1 tetrahedrally coordinated by His120, His122 and His189 and zinc binding site 2 octahedrally coordinated by Asp124, Cys208 and His250. Both zinc binding sites are coordinated by a catalytic water/hydroxide molecule with a further two water molecules coordinating zinc binding site 2 (Kim et al, 2013). The hydrolytic mechanism is subtle and some details are yet to be fully elucidated. What is currently understood is that the catalytic water/hydroxide molecule acts as a nucleophile and attacks the carbonyl carbon (C7) which hydrolyses the amide bond. However, details regarding substrate coordination, the identity and source of the catalytic water/hydroxide molecule, the individual roles of the zinc ions and the protonation of nitrogen after amide bond cleavage, are still to be explained (Zhang et al, 2018).

NDM-1 has a deeper and more open active site cavity than other B1 MBLs and structural comparison with VIM-2 reveals that NDM-1 has more positive residues in proximity to zinc ion 1 which are proposed to aid substrate positioning for more efficient catalysis (Mojica et al, 2017). Other unique features that differ from other MBLs include an unusual sequence insertion (FAAN) between residues 162 and 166, an alanine insertion between the two His residues in the HXHXD motif common to all MBLs, and a Tyrosine at position 242 rather than the universally conserved Tryptophan (Yong et al, 2009). The FAAN insertion forms part of loop 8 and forms key contacts with residues in the α3 helix that suggest a role in dimerization but are distant to the active site and unlikely to affect enzymatic activity (King et al, 2011). This study also observed the presence of a lipidation signal peptide and reported NDM-1 protein in high percentage sucrose fractions, suggesting its localisation to the bacterial outer membrane.

Most MBLs are soluble proteins that fold and bind zinc ions in the periplasm (Crowder et al, 2006). In Gram-negative bacteria periplasmic zinc levels are not regulated and zinc availability rapidly depletes during infection when the innate immune response triggers the release of the metal chelator calprotectin from neutrophils. This metal deprivation inhibits MBL activity and stability and research indicates that MBLs formed under these conditions are rapidly degraded in the periplasm (Gonzalez et al, 2016). In contrast, NDM-1 remains relatively stable under zinc deprivation when compared to levels of VIM-2 and it has been suggested that it is protected from degradation by membrane

anchoring. Gonzalez et al also reported the selective secretion of NDM-1 into OMVs, further protecting NDM-1 from zinc deprivation and proteases in the extracellular environment. As previously mentioned, NDM-1 containing OMVs are able to protect nearby colonies of susceptible bacteria and act as vehicles for DNA and protein delivery. The intra and inter-species horizontal transfer of plasmids carrying *bla*NDM-1 via OMVs has recently been confirmed in *A. baumannii* (Chatterjee et al, 2017).

1.8 Reversing resistance

1.8.1 β-lactamase inhibitors currently in clinical development

The production of β-lactamases is currently the most relevant mechanism of antibiotic resistance in Gram-negative bacteria. To try to combat these pathogens the pharmaceutical industry employed two strategies: a) optimising the remaining antibiotics that are effective against β-lactam resistant bacteria and b) developing inhibitors to be co-administered with antibiotics (Docquier et al, 2018). The discovery of the β-lactamase inhibitor clavulanic acid, isolated from *Streptomyces clavuligerus* was a significant breakthrough (Reading et al, 1977). Despite sharing the β-lactam ring common to β-lactam antibiotics, clavulanic acid has negligible antimicrobial activity but is a potent inhibitor of most of the β-lactamases that were circulating in the 80s. This led to the development of the first β-lactam-β-lactamase inhibitor combination: Augmentin or Co-Amoxiclav (amoxycillin and clavlulanic acid); effective against class A β-lactamase producing staphylococci, *E. coli*, *H. influenzae*, *M. catarrhalis* and *K. pneumoniae*, and is a combination that is still commonly prescribed today (NICE, 2018).

Combining β-lactam antibiotics with β-lactamase inhibitors is considered amongst the most reliable of strategies for tackling resistant pathogens and a number of new combinations have entered clinical development in the past decade (Table 1.2). The combinations which have been clinically approved all show a similar spectrum of activity in that they are all most effective against class A β-lactamases but do not inhibit class B MBLs due to the differences underlying their mechanisms of action. Following clinical approval, pathogens displaying resistance to these combinations began to appear. This was well documented for SHV and TEM enzymes where mutations in the β-lactamase genes yielded alterations in the properties of the enzymes (Mendonca et al, 2007 and Chaibi et al, 1999).

Table 1.2: β-lactam-β-lactamase inhibitor combinations that have reached the stage of clinical development

Antibiotic	Inhibitor	Inhibitor type	Status	Effective against	Reference
Amoxicillin	Clavulanic acid	Clavulanate	Approved	A β-lactamases	Reading et al, 1977
Ceftolozane	Tazobactam	Penicillanic acid sulfone derivative	Approved	A, C and D β-lactamases	Sorbera et al, 2014
Ceftazidine	Avibactam	Diazabicyclooctane	Approved	A, C and D β-lactamases	Levasseur et al, 2015
Ceftaroline	Avibactam	Diazabicyclooctane	Phase 2 initiated 2017	A, C and D β-lactamases	Sader et al, 2013
Aztreonam	Avibactam	Diazabicyclooctane	Phase 3 initiated 2018	A, C and D β-lactamases	Sader et al, 2018
Meropenem	Vaborbactam	Cyclic boronic acid	Approved USA	A and C β-lactamases	Lomovskaya et al, 2017
Imipenem-Cilistatin	Relebactam	Diazabicyclooctane	Phase 3 completed 2018	A and C β-lactamases	Rhee et al, 2018
Meropenem	Nacubactam	Diazabicyclooctane	Phase 1 trials completed in 2014 and 2017	A, B, C and D β-lactamases	Monogue et al, 2018
Cefepime	Zidebactam	Diazabicyclooctane	Phase 2 completed 2016	A, B, C and D β-lactamases	Livermore et al, 2017
Cefepime	AAI101	Penicillanic acid sulfone derivative	Phase 3 initiated 2018	A, C and D β-lactamases	Crandon et al, 2015
Sulbactam	ETX2514	Diazabicyclooctane	Phase 2 initiated 2018	A, C and D β-lactamases	Durand-Reville et al, 2017
Cefepime	VNRX-5133	Cyclic boronic acid	Phase 1 completed 2018	A, B, C and D β-lactamases	VenatoRx Pharmaceuticals, 2018

* **Combinations highlighted in green are effective against class B MBLs**

1.8.2 Metallo-β-lactamase inhibitors in clinical development

Of those listed in Table 1.2, only three combinations show any activity against the Class B MBLs. Two of these; nacubactam and zidebactam, are diazabicyclooctanes; small molecular scaffolds that mimic the β-lactam structure (Coleman, 2011). Nacubactam is predominantly effective against class A and C β-lactamases with some minor activity against class D enzymes. However, a reduction in MIC was also observed for 4 *Enterobacteriaceae* isolates co-expressing class B NDM-1 when treated with meropenem-nacubactam compared to meropenem only (Monogue et al, 2018). It remains unclear whether this reduction is due to effectivity against other co-expressed lactamases or whether nacubactam is able to inhibit NDM-1 specifically. Another trial investigating the effects of the inhibitor zidebactam in combination with cefepime also reported some effectiveness against strains containing MBLs, although isolates containing NDM were small in number and required further evaluation (Sader et al, 2017). The most promising β-lactam-β-lactamase inhibitor combination seems to be cefepime-VNRX-5133, which has shown effectiveness against both SBL and MBL containing pathogens. Cefepime MIC reductions from 8 to ≥ 2048-fold in NDM-1 expressing *Enterobacteriaceae* were observed (Hamrick et al, 2018); and ED_{50} reductions of 5-fold in murine models infected with NDM-1 producing *E. coli* strains (Weiss et al, 2018). A phase 1 clinical trial was completed earlier this year.

1.8.3 Zinc binding and zinc chelating metallo-β-lactamase inhibitors

Inhibitors that act by zinc binding or chelation are an obvious way of inhibiting metallo-β-lactamases. Although effective, such compounds act by binding or sequestering zinc ions in the active site, and in a human environment where approximately 10 % of enzymes interact with zinc, are likely to be associated with cytotoxicity issues (McCall et al., 2000). Known zinc chelators are restricted in clinical use because of these side effects. As an example, the median lethal dose of EDTA was calculated to be 28.5 mg/kg when administered intravenously in mice (Matsuura et al, 1993). In contrast, the natural fungal product Aspergillomarasmine A (AMA) was better tolerated with a median lethal dose of 159.8 mg/kg. AMA is also one of the few compounds reported to inactivate NDM-1. AMA inhibits VIM-2 and NDM-1 (IC_{50} in the low μM range) by chelating both of the active site zinc ions and was able to potentiate carbapenem activity in a murine model (King et al., 2014). Other reported zinc chelating inhibitors

include a spiro-indoline-thiadiazole compound (Falconer et al, 2015) and the PET imaging agents 1,4,7-triazacyclononane-1,4,7-triacetic acid (NOTA) and 1,4,7,10-tetraazacyclododecane-1,4,7,10-tetraacetic acid (DOTA) (Somboro et al, 2015); all have been shown to restore antibiotic activity in MBL expressing bacterial strains, and with MICs lower than that reported for AMA.

Following a previous line of research which demonstrated that azolythioacetamide scaffolds show inhibitory activity against MBLs (Yang et al, 2015), triazolylthioacetamide scaffolds have also been explored and show potent inhibition of NDM-1 with IC_{50} values below 1 μM. Docking studies suggest that the triazole ring replaces the bridging water/hydroxide molecule between the two active site zinc ions (Zhai et al, 2016). L and D captopril isomers have a similar mechanism of inhibition. Captopril is a drug already widely used for the treatment of hypertension. High resolution crystal structures of L and D captopril isomers in complex with MBLs reveal that the sulphur atom of the captopril isomers replaces the bridging water/hydroxide molecule of the dizinc cluster (Brem et al., 2016). D-captopril was found to be the most potent inhibitor and was able to potentiate the effects of meropenem against pathogens containing a variety of MBLs.

Mercaptoacetic acid thioester derivatives towards NDM-1, ImiS-1 and L1 have also been reported but despite showing strong inhibition of L1, only weak inhibition was observed for Imis-1 and NDM-1 (Liu et al., 2015). A range of bizthiazolidine inhibitors are described (Hinchcliffe et al, 2016). Crystal structures of these isomers in complex with MBLs of all subclasses demonstrates their versatility and indicates a wide range of binding modes. Despite this, cross-class inhibition is mostly due to zinc binding and it is therefore likely that affinity can be increased by introducing groups that are able to establish H-bonds or hydrophobic interactions with the surrounding residues (Docquier et al, 2018).

More recently, 1,2,4-triazole-3-thione compounds were identified as inhibitors of MBLs, with five analogues showing inhibition of at least four of the clinically important enzymes, including IMP-1, VIM-2 and NDM-1 (Sevaille et al, 2017). A derivative of dipicolinic acid (DPA) was also recently identified by a fragment based approach and showed inhibitory activity against these same three enzymes. Whilst DPA is a zinc

chelator, the modified derivative acts as a metal-binding competitive inhibitor with a 10-20 fold potentiation of imipenem in *Enterobacteriaceae* (Chen et al, 2017).

1.8.4 Covalent metallo-β-lactamase inhibitors

There are few reported covalent inhibitors of MBLs. Covalent inhibitors are generally disfavoured by pharmaceutical companies due to concerns over toxicity and side effects. However, roughly 30 % of commercially available drugs are actually covalent inhibitors and often have increased ligand efficiency and better resistance to mutations (Singh et al, 2011). Ebselen is a selenium-containing compound that is already safely used in human studies. Ebselen inactivates NDM-1 by forming a S-Se bond with the zinc binding Cys^{221} residue in the active site of the enzyme. However, its anti-oxidant activity and toxicity has raised concern over its potential (Chiou et al, 2015).

The reversible covalent inhibitor 3-formylchromone inhibits NDM-1 by binding to Lys^{224} in the active site (Christopeit et al., 2016). However, this inhibitor contains an aldehyde group which are generally avoided in drug discovery due to their increased reactivity and susceptibility to metabolic oxidation. The already approved early β-lactam drug Cefaclor has also been shown to irreversibly inactivate NDM-1 by binding to a different active site Lysine (Lys^{211}) (Thomas et al., 2014). Unfortunately, supratherapeutic doses were needed to inactivate NDM-1, precluding the clinical use of this drug for NDM-1 bearing pathogens.

1.8.5 Other metallo-β-lactamase inhibitors

It remains notoriously difficult to identify potent inhibitors of the MBLs. The selection of broad spectrum inhibitors is hampered by their diversity and the fact that the selected inhibitor must remain inactive towards similar human proteins (Bebrone et al., 2010). For this reason, several new strategies have recently started to be explored. These include screening of already approved compounds for possible repositioning in antibacterial therapy which has yielded, besides captopril, three molecules that show inhibition of NDM-1, VIM-1 and IMP-7 with IC_{50}s in the low µM range (Klingler et al., 2015). However, the concentrations required to restore antibacterial activity could not be reached in pathogenic strains. Similarly there has been much investigation into a variety of boronic acids, some of which were already known SBL or penicillin-binding-

protein (PBP) inhibitors. Boron compounds behave as Lewis acids, reacting with nucleophiles to form tetrahedral covalent products that resist hydrolysis by enzymes. Recent studies have identified cyclic boronates that show promise against SBL, MBL and PBP enzymes. (Brem et al., 2016b). One of these compounds has already been patented and was able to restore meropenem activity in Gram-negative strains carrying both serine and metallo-β-lactamases. Additionally, as previously mentioned, the cyclic boronic acid compound VNRX-5133 also shows promise against both SBL and MBL containing strains and is currently in clinical development (Table 1.2).

Natural compounds have played an important role in the discovery of antibiotics. Virtual molecular docking of 35 natural compounds into the active site of NDM-1 identified 2 compounds; Isomargololone and Nimbolide, with IC_{50} values of 1.25 and 1.34 µM respectively (Thakur et al, 2013). Extracts from the fungus *Chaetomium funicola* were found to inhibit IMP-1 and CfiA MBLs, and bind with the conserved Lys residue (Lys^{184}) (Payne et al, 2002). Additionally, a recent report found that Magnolol, a natural compound widely used in traditional Chinese medicine, inhibited NDM-1 carrying strains when combined with meropenem with an IC_{50} of 6.47 µg/mL and had little toxicity in mice, rats or dogs (Liu et al, 2018).

1.8.6 Novel biologics as metallo-β-lactamase inhibitors

Novel biologics that are able to inhibit MBLs have started to be explored and have already had some success. Many of these biologics display affinities for their targets which are comparable to those observed for monoclonal antibodies. However, unlike antibodies, simple modification of the selected reagents can improve their binding to target molecules and enhance their stability. A 10 residue DNA aptamer was developed as an isoform-specific non-competitive inhibitor for the *Bacillus cereus* 5/B/6 MBL that interferes with metal ion coordination at one of the zinc sites (Kim S K et al., 2009). The aptamer was isolated by SELEX where target molecules are incubated with a library of ssDNA aptamers; and the isolated aptamer showed strong affinity to its target with an IC_{50} of just 1.2 nM. Similarly, a camelid nanobody with a reported IC_{50} of 10 µM was selected by phage display as an inhibitor of VIM-4 and hypothesised to work by interfering with the dynamic of the metal-coordinating L7 loop (Sohier et al., 2013).

These studies demonstrate the potential of investigating novel biologics for the isolation and selection of highly specific inhibitors.

1.9 Affimer reagents

Affinity reagents that can be generated rapidly and cost effectively represent a major advance in the development of tools for improving understanding of biological processes and studying protein-protein interactions, expression and localisation (Škrlec et al, 2015). Attractive properties that differentiate most engineered scaffolds from antibodies include a small size, high thermal stability, high solubility, a lack of cysteines and low production costs in bacteria. Their applications range from therapy and diagnostics to research. A large number of new scaffolds have been reported in the past 2 decades, with some already gaining clinical approval. These include Adnectins (Lipovsek, 2011), Anticalins (Gebauer et al, 2012), Avimers (Jeong et al, 2005), Kunitz domains (Hosse et al., 2006), Knottins (Ackerman et al, 2014), Affibodies (Nord et al., 1997) and DARPins (Binz et al., 2003). They have been used in diverse applications including the treatment and diagnosis of cancer and inflammatory disorders (Mross et al, 2013 and Jonsson et al, 2010), structural studies (Batyuk et al, 2016), imaging applications (Terwisscha van Scheltinga et al, 2014 and Yang et al, 2014) and intracellular targeting of protein function (Kummer et al, 2012).

Affimers are a class of small protein scaffolds that have been developed for molecular recognition applications (Tiede et al, 2014). The scaffolds were originally termed ‘Adhirons’ but are now licensed as ‘Affimers’ by Avacta Life Sciences Ltd. There are two Affimer scaffolds based on similar protein conformations, Type I one based on the naturally occurring human protease inhibitor Stefin A (Woodman et al, 2005), and Type II based on a phytocystatin consensus sequence (Tiede et al, 2014). The Affimer scaffold used in this study was Type II. The consensus design strategy is centred around the assumption that at a given position, a consensus residue contributes more to the stability of the protein than non-conserved residues. Proteins generated through consensus design have demonstrated increased stability in a number of studies; including antibody CH3 domains (Demarest et al, 2004), phytase enzymes (Lehmann et al, 2002), ankyrin repeat proteins (Binz et al, 2003) and FN3 domains (Porebski et al, 2015). The phytocystatin Affimer scaffold is based on a consensus alignment of 57

phytocystatin sequences to create a highly stable synthetic structure with a Tm of 101 °C. The Affimer has range of attributes that make it ideal as an engineered scaffold protein; it is small in size (~12 kDa), monomeric, lacks disulphide bonds and is easily produced in E coli (up to 100 mg/L). Diverse libraries of up to 1.3 x 10^{10} have been constructed in the scaffold by incorporating two randomised nine amino acid variable regions (VR). The crystal structure of the Affimer has been solved (Figure 1.10) (Tiede et al, 2014), and there are now 10 published structures of Affimer reagents in the PDB database, both apo and in complex with its targets.

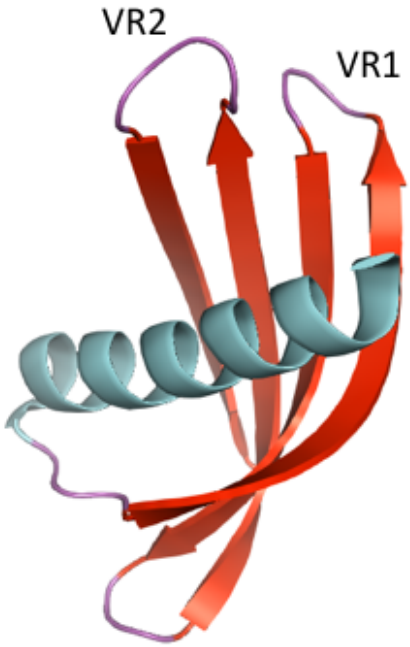

Figure 1.10: Crystal structure of the Affimer scaffold. (PDB 4N6T), 1.75 Å resolution. The Affimer consists of a single alpha helix and a four-strand anti-parallel β sheet core, a structure which is characteristic of proteins belonging the cystatin family. The insertion sites for library production are labelled VR1 and VR2. Residues 1–10 and 90–92 were not visible in the structure and presumed to be disordered. VR1 is positioned between the first and second β strands and VR2 between the third and fourth β strands.

Affimer reagents have been successfully utilised in a wide range of applications, illustrating their potential for isolating novel binding molecules against a wide range of targets. They have been shown to be useful tools in imaging (Bedford et al, 2017, Schlichthaerle et al, 2018 and Lopata et al, 2018), biosensors (Zhurauski et al, 2018 and Sharma et al, 2016) and immunoassays (Xie et al, 2017 and Koutsoumpeli et al, 2017).

In addition, they have demonstrated applicability for the study of protein-protein interactions. The HIF-1α/p300 protein–protein interaction leads to expression of multiple genes involved in angiogenesis and proliferation in cancer. Affimers were used to probe the interaction and identified novel binding motifs of p300 which could be used for future inhibitor design (Kyle et al, 2015). Affimers have also been isolated against Fc gamma receptors involved in the inflammatory response in autoimmune diseases and were shown to selectively block IgG binding (Robinson et al, 2017). Additionally, Affimers that bind to a range of Src-Homology 2 (SH2) domains were identified and shown to bind specifically with minimal cross-reactivity against other Grb family members (Tiede et al, 2017). Taken together, these studies provide evidence to suggest that Affimer reagents may represent a novel discovery platform for the isolation of highly selective inhibitors against MBLs.

1.10 Phage display and library generation

Over recent decades phage display as a selection-based system has become an important source for discovering new biological drug candidates (Rahbarnia et al, 2017). Methods have been adapted for presenting large libraries of antibody fragments, peptides and artificial binding proteins. A phage display strategy for the isolation of highly selective Affimer reagents has been described (Tang et al, 2017).

1.10.1 Library generation

Screening to obtain binding reagents for a desired target requires large and diverse libraries to ensure the selection of binders that have optimal binding specificity and affinity. Oligonucleotide-directed mutagenesis is a well-established method for completely randomising a residue at a defined location. Degenerate oligonucleotides that incorporate mixtures of the four natural bases to randomly code for amino acids are commercially available for the generation of diverse libraries. However, for randomisation introduced in this manner it is almost impossible to control diversity and this inevitably leads to bias where one combination is often more or less represented than another (Neylon, 2004). Additionally, the incorporation of undesired amino acids or stop codons cannot be controlled for. Bias is also introduced due to the mismatch between the number of coding sequences per amino acid - for example, arginine is represented by six codons, whereas histidine is only represented by two. To overcome

this bias, trinucleotide phosphoramidites were developed which utilise codon mixtures rather than nucleotide mixtures (Virnekas et al, 1994). This method can be used to remove codon bias and allows for randomisation with all twenty amino acids, or a desired subset.

All of the primers used to generate libraries in this work were produced by Ella Biotech GmbH. Ella Biotech use the scheme developed by Kayushin et al., 1996 to generate 20 trinucleotide phosphoramidites that each correspond to one of the 20 amino acids (excluding stop codons). These 20 trimers are chosen from a possible 64 combinations in the randomisation scheme NNN and are selected as they are major codons in *E. coli* and will not cause low transcription. Additionally, codon synthesis is relatively challenging and these 20 selected trimers are the best in terms of quality. Quality in terms of rate of dimer/tetramer directly influences the frameshift rate and is therefore extremely important to create high diversity. Reaction factors for all of the trimers are calculated and used to calculate the ratio needed to ensure equal incorporation into the primers. It is also possible to request specific subsets of trimers and we therefore requested the exclusion of cysteines to reduce the possibility of non-specific cross-linking via disulphide bonds and to allow for the addition of a cysteine at a later date for site specific labelling, if required. A lack of disulphide bonds also makes Affimers better tolerated for use in cellular reducing environments.

1.10.2 M13 bacteriophage

The filamentous bacteriophages are viruses containing a circular single-stranded DNA genome inside a long, thin protein capsid cylinder. Among the phage which specifically infect *E. coli*, the F pilus-specific phage (M13, fd and f1) have been the most studied. As their name suggests, they use the tip of the F conjugative pilus as a receptor and are specific for *E. coli* cells containing the F episome. In this work we have used the filamentous bacteriophage M13 (Figure 1.11).

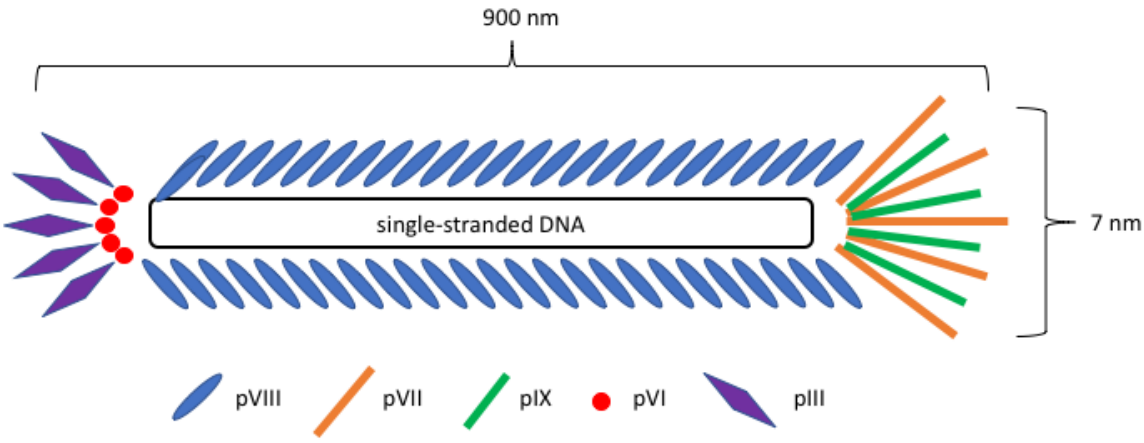

Figure 1.11: The M13 bacteriophage particle. M13 bacteriophage has a cylindrical shape with an approximate length of 900 nm and a diameter of 7 nm. It encapsulates a single-strand genome that encodes five different capsid proteins which comprise two groups, major coat proteins (pVIII) and minor coat proteins (pVII, pIX, pVI and pIII).

The phage genome is encapsulated in a flexible protein cylinder that is composed of approximately 2700 molecules of the major coat proteins pVIII. Each end of the phage is constructed of two different pairs of proteins: approximately five molecules each of pIII and pVI proteins, and on the other end five molecules each of pVII and pIX proteins. This end contains the packaging signal and is the first part of the particle to be assembled (Rakonjac et al, 2011).

1.10.3 M13 phage infection and life cycle

Unlike many phage, M13 phage particles do not kill the host cell during active infection. Phage particles are continually produced and extruded through the cell membrane as the host cell continues to grow and divide (Figure 1.12).

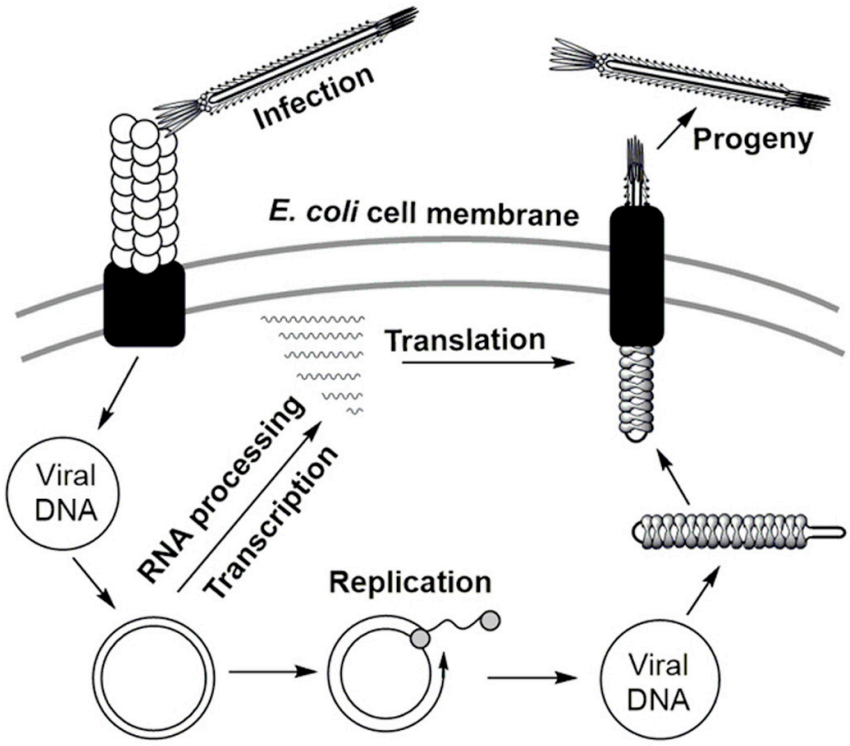

Figure 1.12: Schematic of the M13 bacteriophage life cycle from cell entry to release of progeny phage. The reproductive life cycle of M13 starts with the absorption of the phage to the tip of the F pilus of the host *E. coli*. The phage is then transported to the cell surface. The outer-membrane proteins TolQ, TolR and TolA are thought to mediate uncoating and DNA penetration. During this process, the phage genome is injected into the cell cytoplasm where it is replicated and repackaged as new phage particles at the cell membrane (Smeal et al, 2017).

The M13 infection cycle begins with the interaction of the phage particle with the F pilus of the bacterial cell, specifically mediated by pIII, the viral absorption coat protein. The phage and bacterial cell are drawn together by retraction of the pilus, to allow for conjugation to take place. The outer membrane proteins Tol Q, R and A are thought to mediate uncoating and DNA translocation (Click et al, 1998). Once inside the bacterial cytoplasm, the single-stranded phage genome is converted into a double-stranded replicative form (RF), which is further duplicated and used as the template for the production of the 11 phage proteins. Eventually, the parental RF is also used as the template for generating new single-stranded viral DNA via a rolling-circle mechanism (Sidhu, 2001). Proteins pII, pIV, and pX regulate the amount of RF DNA and single-stranded DNA, which determines the rate of phage protein biosynthesis and the rate of

phage assembly and extrusion, respectively. Dimers of protein pV bind to the newly synthesized viral strands and prevent RF formation. This results in single-stranded viral genome which is assembled into progeny phage particles at the membrane-bound assembly site (Barbas et al, 2001).

1.10.4 Phage display

The virions of F1 filamentous phage are relatively easy to manipulate and have exceptional stability compared to tailed phage such as T7 and lambda, making them ideal for applications such as phage display. Polypeptides fused to M13 coat proteins are displayed on the surface of phage particles. All of the phage coat proteins have been used successfully as display platforms but pIII is the most commonly used. It has the disadvantage of having only 5 copies displayed per phage particle, but an advantage in that chimeric pIII proteins containing large inserts are well tolerated.

For phage display of Affimer scaffolds, the scaffold coding region is cloned into the phagemid vector pBSTG1 (GenBank KJ474865), between the *Nhe*I and *Not*I restriction sites. The genome encodes a DsbA secretion signal peptide, Affimer, TAG codon, C-terminal half of gene III of bacteriophage M13 and a gene encoding ampicillin resistance. The DsbA signal sequence is fused to the protein coding sequence to allow efficient translocation to the periplasm and a C-terminal His tag has been introduced to allow for purification by metal ion affinity columns. The resulting phagemid is termed pBSTG-Aff (Figure 1.13).

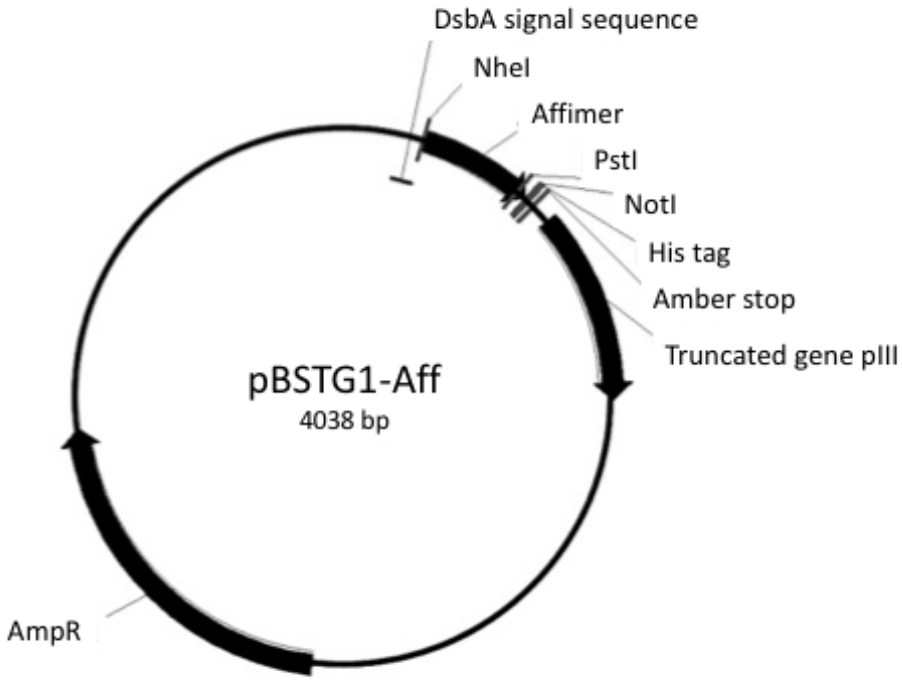

Figure 1.13: Schematic representation of the pBSTG1-Aff phagemid vector. Relevant features of the construct and the coding region for the Affimer are highlighted. The Affimer sequence is flanked by *Nhe*I and *Not*I restriction sites followed by a 6 histidine tag. The truncated pIII gene helps in incorporating the fusion proteins into pIII phage coat proteins. DsbA signal sequence targets translocation of the fusion protein to the periplasm (Tiede et al, 2014).

The suppressible amber (TAG) stop codon is included between the Affimer and pIII coding sequences. Suppressor strains of E. coli such as ER2738 have a mutation in the tRNA anti-codon loop which reads the amber stop codon as a glutamine and allows for translational read-through (Weigert et al, 1965). In non-suppressor strains such as JM83, the stop codon is translated as normal and generates soluble protein fragments which are not linked to the pIII coat proteins.

The Affimer-truncated-pIII fusion contains the C-terminal of pIII (required for insertion into the phage coat), but is missing the N-terminal which prevents superinfection of a phage particle already infected with phage. This allows infection with helper phage containing the wild-type pIII. Infection of the bacteria with M13K helper phage provides structural proteins required for replication of the genome and packaging into phage particles (Barbas et al, 2001). Additionally, the helper phage bears a defective origin of

replication so that packaging of the phagemid genome is favoured over the helper phage genome. Bacteria can be infected with the phagemid-phage mixtures and cells selected by addition of antibiotic are those which contain the phagemid DNA.

1.10.5 Phage display screening

Binding peptides are normally isolated from recombinant-display libraries by affinity selection experiments in which a phage is captured, by its displayed peptide, to a target protein. This process is called screening or panning (Figure 1.14). The target protein-phage complex is immobilised in wells or to beads to allow for removal of non-binding phage by washing. The target-bound phage can then be eluted and amplified by infection and growth in *E coli*. The resulting phage pool is enriched for phage that bind to the desired target, this is reflected in the increased phage yield in subsequent panning rounds. Clones can be chosen from affinity-enriched pools which have a high yield compared to a negative control and can then be tested in an ELISA to confirm binding to the target. DNA sequencing reveals the amino acid sequence and identifies any consensus sequences between clones (Barbas et al, 2001).

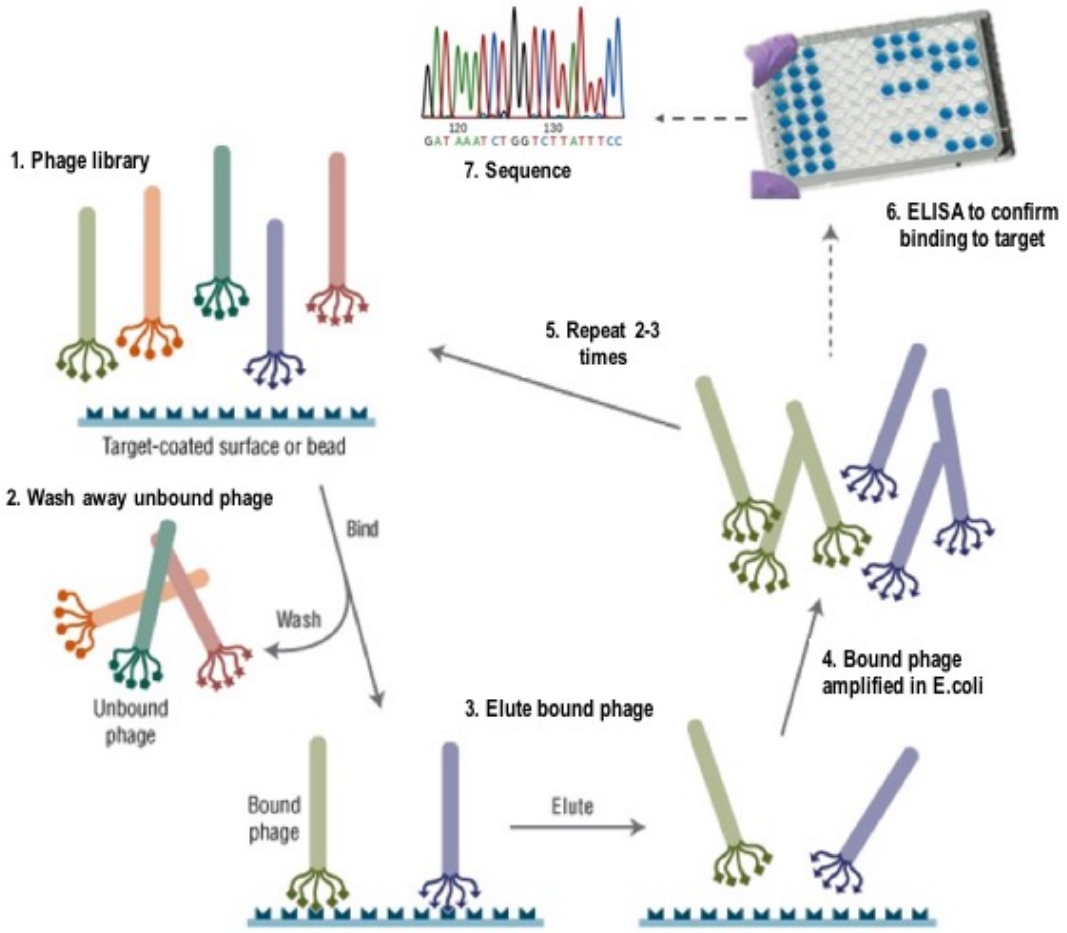

Figure 1.14: Phage display protocol. Immobilised target proteins are screened with the phage library in 2-3 panning rounds. In each panning round, the phage are introduced to the immobilised target so that binding can occur. Weak binders are removed in a series of washes. The strongest binding phage are eluted and amplified in *E coli*. This phage sample is then used in the next panning round. After several rounds of phage display isolated phage binders from the final panning round are taken forward for sequencing to determine variable region sequences.

Approximately thirty years after its discovery, phage display remains one of the most widely used *in vitro* selection methods. Initially developed to revolutionise the generation of therapeutic antibodies, phage display is now the first choice for screening artificial binding proteins. Using phage display, Affimer reagents isolated against a range of diverse molecular targets have been described (Tiede et al, 2017). However, the ability to inhibit proteins involved in antibacterial resistance is yet to be explored.

1.11 Objectives

Reagents that are able to detect and modulate metallo-β-lactamases are highly sought. The aim of this project was to identify and characterise Affimer reagents capable of inhibiting the metallo-β-lactamase NDM-1 using a range of molecular, structural, biochemical and cellular assays.

Chapter 2

Materials and Methods

2.1 Materials

2.1.1 Bacterial strains and cloning vectors

Escherichia coli XL1-Blue cells (Supercompetent, Agilent) (genotype: *recA1 endA1 gyrA96 thi-1 hdR17 supE44 relA1 lac [F´ proAB lacIq ZΔM15 Tn10 (Tetr)*]) were used for propagation of plasmid constructs.

BL21 Star™ (DE3) *E. coli* expression strain (Chemically competent; Invitrogen) (genotype: *F⁻ompT hdS$_B$ (r_B^-, m_B^-) galdcmrne131* (DE3)) encoding T7 RNA polymerase and ampicillin resistance were used for over-expression of protein from plasmid DNA.

E. coli B expression strain AVB101 (Avidity) (genotype: (*hdR, lon11, sulA1*) containing the IPTG inducible *birA* gene to over-express biotin ligase was used to produce biotinylated protein from biotin acceptor peptide (BAP) tagged pD861-pelB-NDM-1 plasmid DNA.

E. coli ER2738 cells (Lucigen) (genotype: [*F'proA+B+ lacIq Δ(lacZ)M15 zzf::Tn10 (tetr)] fhuA2 glnVΔ(lac-proAB) thi-1Δ(hdS-mcrB)5)* were used for the production of phage.

A clinical strain of *Klebsiella pneumoniae* provided by Dr A. O'Neill (School of Molecular and Cellular Biology, University of Leeds) was used for growth inhibition studies.

Three *Staphylococcus aureus* strains were provided by Dr Kenneth McDowall (School of Molecular and Cellular Biology, University of Leeds): SH1000, USA300 and UAMS-1

Cloning vectors used in this study were:

pET11a (Novagen) containing a T7 promoter, *lac* repressor gene and ampicillin resistance gene.

pBSTG-Aff phagemid vector (Tiede et al., 2014; originally pDHisII)) encoding a *dsbA* secretion signal, Affimer coding sequence, C-terminal coding region for domains 2 and 3 from gene III of bacteriophage M13 and ampicillin resistance.

pD861-pelB (Atum), containing a *rhaBAD* promoter, *pelB* signal sequence and kanamycin resistance gene.

2.1.2 Growth media and buffer recipes

2.1.2.1 Growth media

2TY broth

Tryptone (Oxoid) (16 g/L), yeast extract (Oxoid) (10 g/L) and NaCl (Fisher Scientific) (5 g/L) were dissolved in deionized water and the solution was autoclaved at 121 °C, 15 psi for 20 min.

LB broth

LB broth powder (Invitrogen) (20 g/L) was dissolved in deionized water and the solution was autoclaved at 121 °C, 15 psi for 20 min.

LB agar plates

LB agar powder (Invitrogen) (32 g/L) was added to deionized water and the solution was autoclaved at 121 °C, 15 psi for 20 min. After autoclaving, the solution was cooled to ca. 50 °C before addition of antibiotic to the appropriate concentration followed by dispensing of approximately 25 ml per petri dish under aseptic conditions.

TYH media

Tryptone (Oxoid) (20 g/L), yeast extract (Oxoid) (10 g/L), HEPES (Sigma) (11 g/L), NaCl (Fisher Scientific) (5 g/L) and $MgSO_4$ (Fisher Scientific) (1 g/L) were dissolved in 1 L deionized water. The pH was adjusted to 7.3 with KOH (Fisher Scientific) and autoclaved at 121 °C, 15 psi for 20 min.

2.1.2.2 Buffer recipes

2x blocking buffer 10 x blocking buffer diluted 1:5 in PBS-T

4x loading buffer 200 mM Tris-HCl, pH 6.8, 20 % (v/ v) glycerol, 8 % (w/ v) SDS, 0.4 % (w/ v) bromophenol blue, 20 % (v/ v) β-mercaptoethanol

10x Orange G loading dye 30 % glycerol, 0.2 % Orange G

Assay buffer 50 mM HEPES pH7, 20 µM $ZnSO_4$, 10 µg/ml BSA

Destain H_2O, methanol, and acetic acid in a ratio of 50/40/10 (v/v/v)

Elution buffer 50 mM NaH_2PO_4, 500 mM NaCl, 300 mM imidazole, 10 % glycerol, pH 7.4

Lysis buffer 50 mM NaH_2PO_4, 300 mM NaCl, 30 mM Imidazole, 10 % glycerol, pH 7.4

PBS 137 mM NaCl, 4.3 mM Na_2HPO_4, 1.47 mM KH_2PO_4, 2.7 mM KCl, pH 7.4

PBS-T 1% (v/v) solution of Tween-20 in PBS

PEG-NaCl 20% (w/v) PEG 8000, 2.5 M NaCl

Periplasmic lysis buffer 100 mM Tris, 20 % sucrose, 1 mM EDTA, pH 8

SDS PAGE running buffer 25 mM Tris, 200 mM glycine, 0.1 % (w/v) SDS, pH 8.3

TE buffer 10 mM Tris, 1 mM EDTA, pH 8

Wash buffer 50 mM NaH_2PO_4, 500 mM NaCl, 20 mM imidazole, pH 7.4

2.1.3 Antibiotics

Stock solutions of antibiotics were made up in deionised water, filter sterilised through a 0.2 µm syringe-end filter and stored in 1 ml aliquots at -20 °C. The final concentrations used in cultures and agar plates are shown in Table 2.1. Carbenicillin was used in place of ampicillin as it acts on the β-lactamase protein but is more stable, resulting in the formation of fewer satellite colonies.

Table 2.1: Stock and working concentrations of antibiotics

Antibiotic	Stock concentration	Working concentration
Chloramphenicol	34 mg/ml	10 µg/ml
Carbenicillin	50 mg/ml	100 µg/ml
Tetracycline	12 mg/ml	12 µg/ml
Kanamycin	25 mg/ml	50 µg/ml

2.2 Methods

2.2.1 DNA manipulation

2.2.1.1 Polymerase chain reaction (PCR)

All PCR reactions were set up in 0.2 ml tubes (Sarstedt) and thermal cycling carried out using a G-Storm GS2 thermal cycler.

Table 2.2: Reaction components for PCRs using Phusion High-Fidelity (HF) DNA polymerase (ThermoFisher):

Component	Volume (50 μl reaction)	Final concentration
5 x HF buffer	10 μl	1x
dNTP mix, 25mM	0.4 μl	200 μM of each
Forward primer 10 μM	4 μl	0.8 μM
Reverse primer 10 μM	4 μl	0.8 μM
Template DNA	X μl	1 ng/μl
DMSO	1.5 μl	3%
Deionised water	Y μl	to a final volume of 25 μl
Phusion HF DNA polymerase	0.5 μl	0.02 U/μl

Table 2.3: Reaction conditions for PCRs carried out using Phusion HF DNA polymerase:

Cycle step	Temperature (°C)	Time (s)	Cycles
Initial denaturation	98	30	1
Denaturation Annealing Extension	98 54 72	20 20 15 per kb	30
Final extension Hold	72	600	1

Table 2.4: Reaction components for PCRs using KOD Hot Start DNA polymerase:

Component	Volume (50 μl reaction)	Final concentration
10 x KOD buffer	5 μl	1x
dNTPs	5 μl	200 μM of each
Forward primer 10 μM	4 μl	0.8 μM
Reverse primer 10 μM	4 μl	0.8 μM
Template DNA	X μl	10 ng
25mM $MgSO_4$	3 μl	1.5 mM
Deionised water	Y μl	to a final volume of 25 μl
KOD DNA polymerase	1 μl	0.02 U/μl

Table 2.5: Reaction conditions for PCRs carried out using KOD Hot Start DNA polymerase:

Cycle step	Temperature (°C)	Time (s)	Cycles
Polymerase activation	95	120	1
Denaturation Annealing Extension	95 60 70	20 20 20	20
Final extension Hold	70 4	300 ∝	1

2.2.1.2 Splice overlap extension (SOE)

All SOE reactions were set up in 0.2 ml tubes (Sarstedt) and thermal cycling carried out using a G-Storm GS2 thermal cycler. Equimolar quantities of the two DNA fragments to be spliced were added to a total DNA concentration of 40 ng/ µl.

Table 2.6: Reaction components for SOE using Phusion HF DNA polymerase:

Component	Volume (25 µl reaction)	Final concentration
5 x HF buffer	5 µl	1x
dNTP mix, 25 mM	0.2 µl	200 µM of each
Fragment 1 DNA	X µl*	500 ng
Fragment 2 DNA	Y µl*	500 ng
DMSO	0.75 µl	3%
Deionised water	Z µl	to final volume of 25 µl
Phusion HF DNA polymerase	0.25 µl	0.02 U/µl

***To give a 1:1 molar ratio of fragment 1 : fragment 2 DNA**

Table 2.7: Reaction conditions for SOE carried out using Phusion HF DNA polymerase:

Cycle step	Temperature (°C)	Time (s)	Cycles
Initial denaturation	98	30	1
Denaturation Annealing Extension	98 54 72	20 20 120	10
Final extension Hold	72 4	600 ∝	1
Addition of 0.02 U/ul Phusion DNA polymerase			
Initial denaturation	98	30	1
Denaturation Annealing Extension	98 54 72	20 20 120	10
Final extension Hold	72 4	600 ∝	1

2.2.1.3 Final amplification of the SOE product

All final amplification reactions were set up in 0.2 ml tubes (Sarstedt) and thermal cycling carried out using a G-Storm GS2 thermal cycler.

Table 2.8: Reaction components for final amplification reaction carried out using KOD Hot Start DNA polymerase (Millipore):

Component	Volume (25 μl reaction)	Final concentration
10 x KOD buffer	2.5 μl	1x
dNTP mix	2.5 μl	200 μM of each
Forward primer 10 μM	2 μl	0.8 μM
Reverse primer 10 μM	2 μl	0.8 μM
SOE product	5 μl	X ng
25mM $MgSO_4$	1.5 μl	1.5 mM
Deionised water	9 μl	to a final volume of 25 μl
KOD DNA polymerase	0.5 μl	0.02 U/μl

Table 2.9: Reaction conditions for final amplification reactions carried out using KOD Hot Start DNA polymerase:

Cycle step	Temperature (°C)	Time (s)	Cycles
Initial denaturation	95	120	1
Denaturation Annealing Extension	95 54 72	20 20 20	5
Final extension Hold	72 4	600 ∝	1

2.2.1.4 BAP tag cloning

A Biotin Acceptor Peptide (BAP) sequence of G-L-N-D-I-F-E-A-Q-K-I-E-W-H-E was added after the *pelB* signal sequence at the N-terminus of pD861-pelB-NDM-1 to allow for biotinylation. An inverse PCR mutagenesis method was used as shown in Figure 2.1.

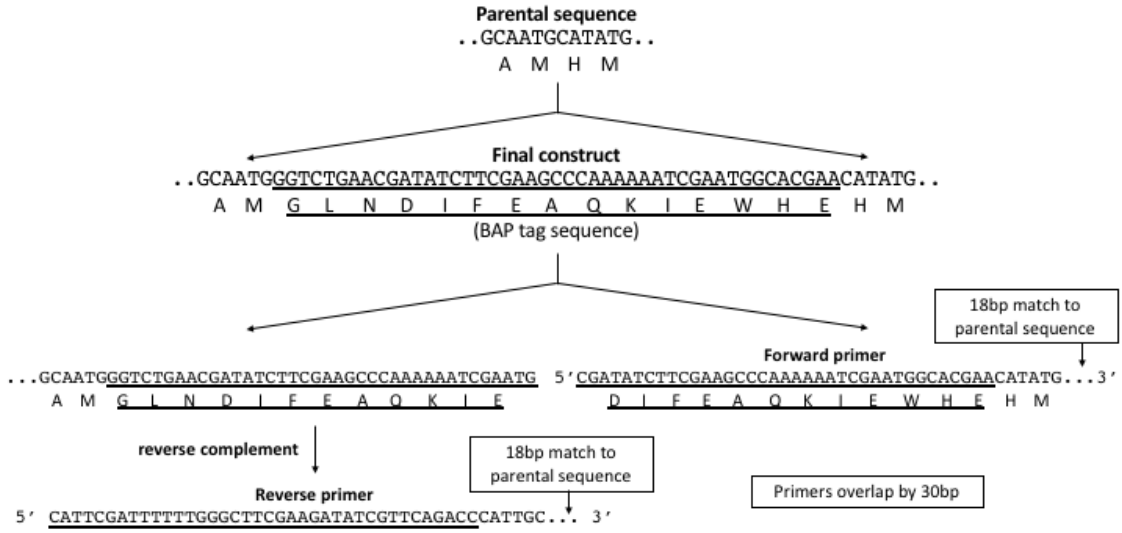

Figure 2.1: Design of primers for BAP tag insertion using the inverse PCR mutagenesis method. Full primer sequences listed below.

The following primers were designed and synthesised (Sigma):

5' CGATATCTTCGAAGCCCAAAAAATCGAATGGCACGAACATATGGAAATCCGTCCG 3' and 5' CATTCGATTTTTTGGGCTTCGAAGATATCGTTCAGACCCATTGCCATGGCTGGTTG 3' (BAP tag coding sequence is underlined). PCR reactions were set up using KOD Hot Start DNA polymerase (Millipore) as described in Section 2.1.1.1, but with 50 μl reaction volumes and longer annealing and extension times of 60 seconds and 4 min per cycle, respectively (Table 2.4 and 2.5). The DNA product was *DpnI* (NEB) digested to ensure the original template DNA was destroyed and cleaned up using a NucleoSpin® Gel and PCR clean-up kit (Machery Nagel) (Section 2.2.1.15). Supercompetent XL1-Blue cells were transformed with the DNA (Section 2.2.1.11) and a single colony picked and used to inoculate 5 ml of 2TY broth containing 50 μg/ml kanamycin and grown overnight at 37 °C, 230 rpm. Plasmid purification was carried out using QIAprep Spin Miniprep (Qiagen) according to the manufacturer's instructions (Section 2.2.1.13). DNA was eluted in 50 μl of nuclease free H_2O and sent for sequencing to confirm BAP tag inclusion (Section 2.2.1.17). BL21 Star™ (DE3) or AVB101 cells were then transformed with the DNA for protein production (Section 2.2.3.2)

2.2.1.5 Construction of Aff21ΔVR1 and Aff21ΔVR2 mutants

Affimer 21 constructs consisting of either variable region 1 (Aff21ΔVR2) or variable region 2 (Aff21ΔVR1) were created to determine whether one or both of the VRs were responsible for activity of the Affimer. Aff21ΔVR2 and Aff21ΔVR1 were created by amplifying DNA for each respective variable region from the pBSTG-Aff phagemid vector and SOEing with amplified DNA from a wild type (WT) Affimer scaffold with variable regions containing 2 or 3 Alanine residues (Figure 2.2).

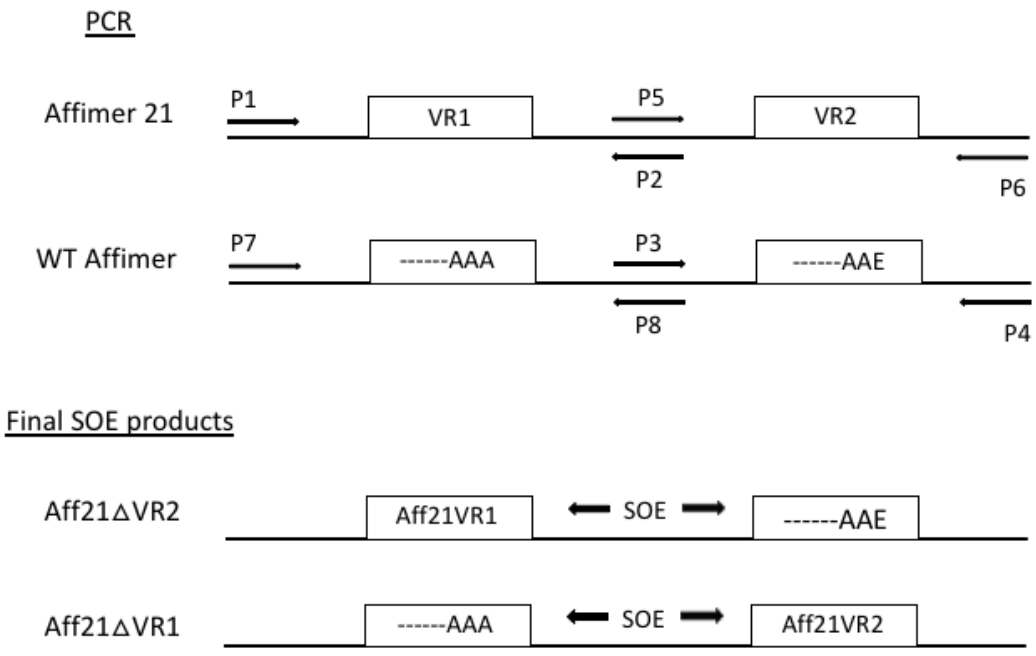

Figure 2.2: Generation of Aff21ΔVR1 and Aff21ΔVR2 DNA: Schematic showing the strategy for creating Aff21ΔVR1 and Aff21ΔVR2 DNA. Template DNA was pBSTG-Aff phagemid vector containing the Affimer 21 sequence and wild-type (WT) Affimer. Primers are listed in Table 2.10. VR1: variable region 1 and VR2: variable region 2.

Affimer 21 variable region DNA was amplified by PCR from the pBSTG-Aff phagemid vector using primers P1 and P2 (for VR1), and P5 and P6 (for VR2) (primer sequences listed in Table 2.10). Variable region DNA from the WT Affimer scaffold was amplified using primers P3 and P4 (empty VR1), and P7 and P8 (empty VR2).

Table 2.10: Primers for construction of Aff21ΔVR1 and Aff21ΔVR2 mutants

Construct	Vector	Primer	Sequence
Aff21ΔVR2	pBSTG-Aff	P1	Forward 5' TTCTGGCGTTTTCTGCGTCTGC 3'
		P2	Reverse 5' CACCGTCTTTAGCTTCCAGG 3'
Aff21ΔVR2	WT-Aff	P3	Forward 5' CCTGGAAGCTAAAGACGGTG 3'
		P4	Reverse 5' GTCAGGAAACAGCTATGACC 3'
Aff21ΔVR1	pBSTG-Aff	P5	Forward 5' CCTGGAAGCTAAAGACGGTG 3'
		P6	Reverse 5' TACCCTAGTGGTGATGATGGTGATGC 3'
Aff21ΔVR1	WT-Aff	P7	5' AGTAAAACGACGGCCAGTG 3'
		P8	5' CACCGTCTTTAGCTTCCAGG 3'

The respective DNA segments were then separated on agarose gels (Section 2.2.1.7), gel purified (Section 2.2.1.14), recombined in an SOE reaction (Section 2.2.1.2) and the final products amplified using primers P1 and P4 for Aff21ΔVR2, and primers P7 and P6 for Aff21ΔVR1 (Section 2.2.1.3). DNA was then digested with *NheI*-HF™ and *NotI*-HF™ (NEB) (Section 2.2.1.8) and ligated into similarly digested pET11a vector. XL1-Blue cells were then transformed with the DNA (Section 2.2.1.11), grown up and miniprepped (Section 2.2.1.13) before being sequenced (2.2.1.17) to confirm the correct insert. BL21 star™ (DE3) cells were then transformed with the DNA (Section 2.2.1.11) and protein produced as described in Section 2.2.3.2 .

2.2.1.6 Alanine scanning mutagenesis

Systematic alanine-scanning by Quikchange-based mutagenesis was performed on the two variable regions of Affimer 21. Mutations were introduced using the mutant primers listed in Table 2.11 and pET11a vector containing Affimer 21 sequence as template. PCR reactions were established using KOD Hot Start DNA Polymerase Kit (Millipore) as described in Section 2.2.1.1. The mutated products were digested for 1 h at 37°C with the restriction enzyme *DpnI* (New England Biolabs) to eliminate the original methylated template and to increase mutation efficiency. Supercompetent XL1-Blue cells were transformed with the digested products, plasmid DNA was purified from transformant colonies, and the presence of the mutation was confirmed by DNA sequence analysis (Section 2.2.1.17). For protein production, BL21 star™ (DE3) cells

were transformed with plasmid DNA and protein produced as described in Section 2.2.3.2.

Table 2.11: Complementary primer pairs (F and R) for generation of site-directed mutants (codon altered is highlighted in red)

Primer	Sequence 5' to 3'	Generated mutation
Affimer 21 1.1F	GTTAAAGCGAAAGAACAGGCTTACAAAGTTTGGACTCCG	G1.1A
Affimer 21 1.1R	CGGAGTCCAAACTTTGTAAGCCTGTTCTTTCGCTTTAAC	G1.1A
Affimer 21 1.2F	GTTAAAGCGAAAGAACAGGGTGCTAAAGTTTGGACTCCGTACGG	Y1.2A
Affimer 21 1.2R	CCGTACGGAGTCCAAACTTTAGCACCCTGTTCTTTCGCTTTAAC	Y1.2A
Affimer 21 1.3F	GCGAAAGAACAGGGTTACGCTGTTTGGACTCCGTACGG	K1.3A
Affimer 21 1.3R	CCGTACGGAGTCCAAACAGCGTAACCCTGTTCTTTCGC	K1.3A
Affimer 21 1.4F	GCGAAAGAACAGGGTTACAAAGCTTGGACTCCGTAC	V1.4A
Affimer 21 1.4R	GTACGGAGTCCAAGCTTTGTAACCCTGTTCTTTCGC	V1.4A
Affimer 21 1.5F	GAAAGAACAGGGTTACAAAGTTGCTACTCCGTACGGTACCATGTAC	W1.5A
Affimer 21 1.5R	GTACATGGTACCGTACGGAGTAGCAACTTTGTAACCCTGTTCTTTC	W1.5A
Affimer 21 1.6F	CAGGGTTACAAAGTTTGGGCTCCGTACGGTACCATGTAC	T1.6A
Affimer 21 1.6R	GTACATGGTACCGTACGGAGCCCAAACTTTGTAACCCTG	T1.6A
Affimer 21 1.7F	GTTACAAAGTTTGGACTGCTTACGGTACCATGTACTACC	P1.7A
Affimer 21 1.7R	GGTAGTACATGGTACCGTAAGCAGTCCAAACTTTGTAAC	P1.7A
Affimer 21 1.8F	GGTTACAAAGTTTGGACTCCGGCTGGTACCATGTACTACCTG	Y1.8A
Affimer 21 1.8R	CAGGTAGTACATGGTACCAGCCGGAGTCCAAACTTTGTAACC	Y1.8A
Affimer 21 1.9F	CAAAGTTTGGACTCCGTACGCTACCATGTACTACCTGAC	G1.9A
Affimer 21 1.9R	GTCAGGTAGTACATGGTAGCGTACGGAGTCCAAACTTTG	G1.9A
Affimer 21 2.1F	GCGAAAGTTTGGGTTAAGGCTCATTGGGATAACGGCGGC	T2.1A
Affimer 21 2.1R	GCCGCCGTTATCCCAATGAGCCTTAACCCAAACTTTCGC	T2.1A
Affimer 21 2.2F	GAAAGTTTGGGTTAAGACCGCTTGGGATAACGGCGGCCTG	H2.2A
Affimer 21 2.2R	CAGGCCGCCGTTATCCCAAGCGGTCTTAACCCAAACTTTC	H2.2A
Affimer 21 2.3F	GTTTGGGTTAAGACCCATGCTGATAACGGCGGCCTGAGAAAC	W2.3A
Affimer 21 2.3R	GTTTCTCAGGCCGCCGTTATCAGCATGGGTCTTAACCCAAAC	W2.3A
Affimer 21 2.4F	GGGTTAAGACCCATTGGGCTAACGGCGGCCTGAGAAAC	D2.4A
Affimer 21 2.4R	GTTTCTCAGGCCGCCGTTAGCCCAATGGGTCTTAACCC	D2.4A
Affimer 21 2.5F	GTTAAGACCCATTGGGATGCTGGCGGCCTGAGAAACTTC	N2.5A
Affimer 21 2.5R	GAAGTTTCTCAGGCCGCCAGCATCCCAATGGGTCTTAAC	N2.5A
Affimer 21 2.6F	GTTAAGACCCATTGGGATAACGCTGGCCTGAGAAACTTCAAA	G2.6A
Affimer 21 2.6R	TTTGAAGTTTCTCAGGCCAGCGTTATCCCAATGGGTCTTAAC	G2.6A
Affimer 21 2.7F	CATTGGGATAACGGCGCTCTGAGAAACTTCAAAG	G2.7A
Affimer 21 2.7R	CTTTGAAGTTTCTCAGAGCGCCGTTATCCCAATG	G2.7A
Affimer 21 2.8F	CCCATTGGGATAACGGCGGCGCTAGAAACTTCAAAGAACTG	L2.8A
Affimer 21 2.8R	CAGTTCTTTGAAGTTTCTAGCGCCGCCGTTATCCCAATGGG	L2.8A
Affimer 21 2.9F	GGGATAACGGCGGCCTGGCTAACTTCAAAGAACTGCAGGAG	R2.9A
Affimer 21 2.9R	CTCCTGCAGTTCTTTGAAGTTAGCCAGGCCGCCGTTATCCC	R2.9A

2.2.1.7 Agarose gel electrophoresis

DNA samples were mixed with 1x DNA loading buffer [30 % (v/v) glycerol, 0.25 % (w/v) Orange G] and 3 µl of each sample was loaded onto a 0.8 or 2 % (w/v) agarose gel made up in 1x TAE buffer (1 mM EDTA, 20 mM glacial acetic acid, 40 mM Tris base) and containing 1x SYBRsafe DNA gel stain (Invitrogen). A 3 µl aliquot of MassRuler DNA Ladder Mix (ThermoFisher) was also loaded. Gels were run in a RunOne Electrophoresis

Cell (EmbiTec) at 50 V for 40 min and bands were visualised under UV using a Amersham Imager 600 (GE Healthcare).

2.2.1.8 Restriction digests

Restriction digests were carried out according to the manufacturer's instructions (New England Biolabs) in a total volume of 50 µl. Each digestion reaction contained 20 U of each restriction enzyme, 1 µg DNA, 1x CutSmart Buffer and nuclease free dH_2O added to 50 µl. Reactions were incubated for >4 h at 37 °C. DNA fragments were analysed on either 0.8 % (plasmid) or 2% w/v (insert) agarose gels and then excised and purified from the gel where required (Section 2.2.1.14).

2.2.1.9 Dephosphorylation

Dephosphorylation of digested plasmid removes the 5' phosphate and prevents self-ligation. (Sambrook et al., 1989). Dephosphorylation was carried out by adding 0.1 U/ µl Antarctic Phosphatase and 1x Antarctic Phosphatase Reaction Buffer (New England Biolabs) to the completed restriction digestion reaction (Section 2.2.1.8) and incubating at 37 °C for 15 min.

2.2.1.10 Ligations

Ligation of plasmid and insert was carried out using T4 DNA ligase from either NEB or Roche. Digested insert DNA was combined with similarly digested and dephosphorylated plasmid in either 10 µl or 100 µl reaction volumes containing 1x T4 DNA ligase buffer, 1x T4 DNA ligase (400 units per 10 µl reaction volume), 10 ng/µl plasmid DNA, deionized water and varying amounts of insert DNA to give a range of molar ratios (a 4:1 molar ratio of insert to plasmid was found to be the most effective and was generally used). Reactions were incubated overnight at either room temperature (NEB ligase) or 4 °C (Roche ligase).

2.2.1.11 Transformation of *E. coli* by heat shock

A 10 µl (Supercompetent XL1-Blue) or 50 µl (BL21 Star™ DE3) aliquot of competent cells (Section 2.1.1) was thawed on ice for 10 min before addition of 10-50 ng plasmid DNA in a 1-5 µl volume. The mixture was gently mixed and incubated on ice for 30 min before being transferred to a 42 °C water bath for 45 seconds. The tube was then transferred

immediately to ice for a minimum of 2 min before addition of 190 µl (for Supercompetent XL1-Blue cells) or 450 µl (for BL21 Star™ DE3 cells) of SOC media. The culture was then incubated in a shaking incubator at 37 °C with shaking at 230 rpm to permit recovery. After 1 h, a 100 µl aliquot was plated onto an agar plate containing the appropriate antibiotic, inverted and incubated at 37 °C overnight.

2.2.1.12 Transformation of *E. coli* by electroporation

A 250 µl aliquot of electrocompetent ER2738 cells (Section 2.1.1) was defrosted on ice for 10 min and then added to 400 ng DNA in a chilled microcentrifuge tube and gently mixed by tapping the tube. The mixture was then transferred to a chilled, sterile electroporation cuvette with a 0.2 cm gap (BioRad), being careful not introduce air bubbles. The samples were electroporated in a MicroPulser Electroporator (BioRad) at 2.5 V. the cuvette was washed with 3x 1 ml SOC media (Invitrogen) and the cells transferred to a 50 ml Falcon tube containing a further 12 ml SOC media (Sigma). The 15 ml culture was split into 2 x 7.5 ml in 50 ml Falcon tubes and incubated at 37 °C, 230 rpm for 45 min to permit recovery and production of the antibiotic resistance protein. Cell samples (10 µl) were plated out at a range of dilutions (1:10 - 1:100,000) onto 245 x 245 mm bio-assay agar plates containing the appropriate antibiotic to allow for estimation of the library size. The plates were inverted and incubated at 37 °C overnight. The remaining cells were added to 250 ml of pre-warmed LB-carb media in a 2 L flask and incubated at 37 °C, 230 rpm until an OD_{600} of 0.6 measured on a spectrophotometer (Jenway). The culture was then inoculated with 10 µl M13K07 helper phage (titre ca. 10^{11}/ml) at 25 °C, 90 rpm for 1 h. Kanamycin (60 µg/ml) was added to select for cells that had successfully been infected by the M13K07 helper phage and the culture was incubated at 25 °C, 170 rpm overnight. Phage were precipitated with 6% polyethylene glycol 8000 and 0.5 M NaCl and incubated overnight at 4 °C. The following day the mixture was centrifuged at 4816 xg for 30 minutes to pellet the phage and the pellet resuspended in 320 µl TE buffer. The phage were then centrifuged again at 16,000 xg for 10 min and the supernatant mixed with 40% glycerol for storage.

2.2.1.13 Purification of DNA from *E. coli* by mini or maxiprep

Single colonies containing the plasmid of interest were used to inoculate an appropriate volume of 2TY broth containing selective antibiotic and grown overnight at 37 °C, 230 rpm. Plasmid purification was carried out using QIAprep Spin Miniprep or HiSpeed Plasmid Maxiprep kit (Qiagen) according to the manufacturer's instructions. DNA was eluted in an appropriate volume of nuclease free H_2O and stored at -20 °C.

2.2.1.14 Purification of DNA from an agarose gel

The DNA sample was first separated by agarose gel electrophoresis and visualised using a Amersham Imager 600 (GE Healthcare) (Section 2.2.1.7). Bands of interest were excised using a sterile scalpel and placed in a 1.5 ml microcentrifuge tube. Extraction of the DNA was performed using a NucleoSpin® Gel and PCR clean-up kit (Machery Nagel) according to the manufacturer's instructions. DNA was eluted in an appropriate volume (normally 50 µl) of nuclease free H_2O and stored at -20 °C.

2.2.1.15 Purification of PCR products

A NucleoSpin® Gel and PCR clean-up kit (Machery Nagel) was used to purify DNA products following PCR, SOEing or ligation in which the removal of reaction components was required for the highest efficiency of downstream processes, such as digestion or transformation. DNA was purified according to the manufacturer's instructions but eluted in nuclease free H_2O and stored at -20 °C.

2.2.1.16 Measuring DNA concentration

DNA concentration was determined using a Nanodrop-lite spectrophotometer (ThermoScientific). The spectrophotometer was blanked using the same buffer as that of the DNA sample. A 2 µl aliquot of the DNA solution was then applied to the sample pedestal and the concentration determined from the A_{260} reading according to the rearranged Beer-Lambert equation: $C = A.\varepsilon/l$ where C is the nucleic acid concentration in ng/µl, A is the absorbance in AU, ε is the wavelength dependent extinction coefficient (50 (ng-cm/µl) and l is the path length in cm.

2.2.1.17 DNA sequencing

Purified DNA was diluted to 100 ng/µl and DNA sequencing carried out by GeneWiz using the primers listed in Table 2.12. Results were analysed using MacVector version 13.5.2.

Table 2.12: Sequencing primers

Plasmid	Name	Primer position	Sequence
pET11a	T7F	Forward	5'TAATACGACTCACTATAGGG 3'
pBSTG-Aff	M13R	Reverse	5' CAGGAAACAGCTATGAC 3'
pD861-pelB	pD861-NDM-1	Forward	5' GACTGGTCGTAGAGACCATG 3'

2.2.2 Phage display techniques

2.2.2.1 Biotinylation of target proteins with EZ-Link® NHS-SS-Biotin

To biotinylate target protein, EZ-Link® NHS-SS-Biotin (ThermoScientific) was equilibrated to room temperature and diluted to 5 mg/ml in DMSO immediately before use. NH-SS-biotin was added at a 20-fold molar excess to 1 mg/ml protein in a total volume of 100 µl PBS and incubated at room temperature for 1 h. Excess biotin was removed using Zeba™ Spin Desalting Columns, 7K MWCO (ThermoScientific) according to the manufacturer's instructions. Samples were mixed with an equal volume of 80 % (v/v) glycerol and stored at -20 °C.

2.2.2.2 ELISA to confirm biotinylation

Biotinylated target were added as a range of dilutions (1, 0.1, 0.01 µl) to Nunc-Immuno™ MaxiSorp™ Strips (ThermoScientific) containing 50 µl PBS and incubated overnight at 4 °C. Wells were washed 3 times with 300 µl PBST on a HydroFlex plate washer (TECAN) and blocked with 250 µl 10x blocking buffer (Sigma) and incubated for 3 h at 37 °C. The wells were washed 3 times with PBST on a plate washer and incubated with High Sensitivity Streptavidin-HRP (ThermoScientific) diluted 1:1000 in 2x blocking buffer (10x blocking buffer diluted in PBST) for 1 h at room temperature on a VIBRAMAX 100 shaking platform (Heidolph). Wells were washed 6 times with 300 µl PBST on a

plate washer and incubated with SeramunBlau® fast TMB/substrate solution (Seramun) and allowed to develop for 3 min at room temperature. Absorbance was recorded at 620 nm using a Multiskan Ascent 96/384 Plate Reader (MTX Lab Systems Inc). Absorbance was read again at 6 min developing time.

2.2.2.3 Phage display for biotinylated targets

Phage display screening was carried out using Protein LoBind Tubes (Eppendorf) unless otherwise stated. Targets were biotinylated using EZ-Link NH-SS-Biotin (ThermoScientific), as described in Section 2.2.2.1. Biotinylation was confirmed using High Sensitivity Streptavidin-HRP (ThermoScientific) (Section 2.2.2.2).

2.2.2.3.1 First panning round

ER2738 *E coli* cells were grown overnight on LB agar with 12 µg/ml tetracycline at 37 °C. A single colony was used to inoculate 5 ml of 2TY media with 12 µg/ml tetracycline and the culture grown overnight at 37 °C, 230 rpm. Streptavidin coated (HBC) 8-well strips (ThermoScientific) were blocked using 2x blocking buffer at 37 °C overnight, with four wells per target. Wells were washed once with 300 µl PBST on a TECAN HydroFlex plate washer and 100 µl 2x blocking buffer added to the wells. The phage library was pre-panned three times against the streptavidin coated plates: 5 µl of the phage library was added to the first pre-pan well and incubated for 1 h at room temperature on a Heidolph VIBRAMAX 100 shaker. Blocking buffer was removed from the second pre-pan well and the phage-containing supernatant from the first pre-pan well transferred to the second and incubated for 1 h at room temperature with shaking. This was repeated for the third pre-pan well. During the pre-panning steps, biotinylated target (diluted 1:6 in 2x blocking buffer) was added to the panning well for 2 h at room temperature on a vibrating platform shaker and then washed 6 times with 300 µl PBST. Pre-panned phage was transferred into the well containing immobilised target and incubated at room temperature for 2 h with shaking at 400 rpm.

Meanwhile, fresh cultures of ER2738 cells were set up (8 ml per target) by diluting the overnight culture 1:15 and incubating for 1 h at 37 °C , 230 rpm to give an A_{600} of 0.6 at the time of phage infection. The panning well was washed 27 times with PBST on a plate washer and the phage eluted and used to infect ER2738 cells. Phage were eluted in 100

µl 0.2 M glycine, pH 2.2 for 10 min at room temperature followed by neutralisation with 15 µl 1 M Tris-HCl, pH 9.1 before addition to the prepared 8 ml of ER2738 cells. Remaining phage were eluted in 100 µl 100 mM triethylamine (Sigma) for 6 min at room temperature and neutralised with 50 µl 1 M Tris-HCl, pH 7 before addition to the same aliquot of ER2738 cells. The cells were incubated at 37 °C for 1 h and were mixed gently at least once during the incubation.

Phage infected ER2738 cells (1 µl) were plated onto LB agar carbenicillin plates. The remaining cells were centrifuged for 5 min at 3,000 xg, resuspended in a smaller volume and plated onto LB agar carbenicillin plates. Plates were inverted and incubated at 37 °C overnight. The following day, the number of colonies on the plate with the 1 µl inoculation were counted and this number multiplied by 8000 to determine the number of cells per 8ml. The cells were then scraped from both plates using 2TY media with carbenicillin (100 µg/ml) and transferred to a 50 ml Falcon tube. The A_{600} of a 1:10 dilution was measured and used to calculate the dilution factor for a fresh 8 ml culture with an A_{600} of 0.2 (log phase). The cells were then diluted as calculated into 2TY with carbenicillin (100 µg/ml) and grown for 1 h at 37 °C, 230 rpm. A 0.32 µl aliquot of M13K07 helper phage (titre ca. 10^{14}/ml) was added and the cells incubated for 30 min at 37 °C, 90 rpm before the addition of 400 µg kanamycin and incubation overnight at 25 °C, 170 rpm.

Cells were harvested by centrifugation at 3,500 xg for 10 min and the phage-containing supernatant transferred to fresh Falcon tubes. The required volume (125 µl per target) of phage-containing supernatant was removed for use in the second panning round. A 2 ml aliquot of PEG-NaCl was added to the remaining supernatant to precipitate the phage and incubated overnight at 4 °C. Phage were pelleted by centrifugation at 4,816 xg for 30 min and the supernatant discarded. The pellet was resuspended in 320 µl TE buffer transferred to microcentrifuge tubes and centrifuged at 16,000 xg for ten min. The supernatant was removed and diluted at 1:1 ratio with 40 % glycerol (made up in water) and stored at -80 °C.

2.2.2.3.2 Second panning round

ER2738 cells were grown overnight in 5 ml 2TY media with 12 µg/ml tetracycline at 37 °C, 230 rpm. Streptavidin beads (20 µl per target) (Dynabeads® MyOne™ Streptavidin T1, 10 mg/ml), were blocked with 100 µl 2x blocking buffer and incubated overnight at room temperature on a Stuart SB2 fixed speed rotator at 20 rpm. Plates for the KingFisher Flex robotic platform (ThermoScientific) were blocked at 37 °C for 2 h; panning wells were blocked with 1 ml 2x blocking buffer in a deep 96 well plate (ThermoScientific) and elution wells were blocked with 300 µl 2x blocking buffer in two KingFisher (200 µl) 96 well plates (ThermoScientific). Sufficient wells in 4x deep 96 well plates were prepared with 950 µl 2x blocking buffer directly before use.

Pre-panning of phage was carried out using pre-blocked streptavidin coated beads. The pre-blocked streptavidin beads were centrifuged at 800 xg for 1 minute and immobilised on a magnet before removing the 2x blocking buffer. The beads were resuspended in 2x blocking buffer, 100 µl per 20 µl beads. A 125 µl aliquot of phage-containing supernatant from the first panning round was mixed with 125 µl 2x blocking buffer (or 5 µl purified phage with 245 µl 2x blocking buffer) and added to 25 µl pre-blocked streptavidin beads and incubated for 1 h at RT on the rotator. The beads were centrifuged at 800 xg for 1 minute and placed on a magnet. The supernatant containing the phage was transferred to a fresh tube and another 25 µl pre-blocked streptavidin beads were added and incubated for 1 h at room temperature on the rotator. During the pre-pans, the biotinylated target protein was incubated with 50 µl pre-blocked streptavidin beads and mixed for 2 h at room temperature on the rotator. Immediately before use, the 2x blocking buffer was removed from the deep 96-well plate used for panning and the two (200 µl) 96-well plates used for elution. Glycine, 100 µl of 0.2 M, pH 2.2, was aliquoted per target into the pre-blocked wells of one elution plate and 100 µl 1.4 % triethylamine aliquoted per target into the pre-blocked wells of the second elution plate. The tubes containing the streptavidin beads and biotinylated target were centrifuged at 800 xg for 1 min, immobilised on a magnet and washed with 2x blocking buffer; repeating three times. The tubes containing the pre-panned phage were centrifuged at 800 xg for 1 min, immobilised on a magnet and the supernatant removed and mixed with the target protein bound to streptavidin beads. The beads were resuspended and transferred to the pre-blocked wells of the deep 96-well plate.

The KingFisher Flex protocol 'Phage_display_pH_elution' was selected (Table 2.13) and the plates placed into the machine in the appropriate order. 1 h before elution of phage, a fresh 8 ml culture of ER2738 cells was setup from the overnight culture as previously described (Section 2.2.2.3.1) and grown at 37 °C, 230 rpm. Phage were eluted, added to the culture of ER2738 cells and plated out as described for the first panning round.

Table 2.13: KingFisher Flex 'Phage_display_pH_elution' protocol

Protocol Step	Plate	Volume (µl)	Settings
Tipcomb	96 DW tip comb		
Pick-Up: Tipcomb	KingFisher 96 KF plate		
Collect Beads	Plate: Binding Microtiter DW 96 plate		Collect count 1 Collect time (s) 1
Binding	Plate: Binding Microtiter DW 96 plate	300	**Beginning of Step** Release beads [hh:mm:ss]: 00:00:00 **Mixing/Heating Parameters** Mix time [hh:mm:ss]: 00:00:10 Speed: fast **End of step** Collect beads, count: 5 Collect time (s): 30
Wash 1	Plate: Wash 1 Microtiter DW 96 plate	950	**Beginning of Step** Release beads [hh:mm:ss]: 00:00:00 **Mixing/Heating Parameters** Mix time [hh:mm:ss]: 00:01:00 Speed: slow **End of step** Collect beads, count: 5 Collect time (s): 30
Wash 2	Plate: Wash 2 Microtiter DW 96 plate	950	**Beginning of Step** Release beads [hh:mm:ss]: 00:00:00 **Mixing/Heating Parameters** Mix time [hh:mm:ss]: 00:01:00 Speed: slow **End of step** Collect beads, count: 5 Collect time (s): 30
Wash 3	Plate: Wash 3 Microtiter DW 96 plate	950	**Beginning of Step** Release beads [hh:mm:ss]: 00:00:00

			Mixing/Heating Parameters Mix time [hh:mm:ss]: 00:01:00 Speed: slow **End of step** Collect beads, count: 5 Collect time (s): 30
Wash 4	Plate: Wash 4 Microtiter DW 96 plate	950	**Beginning of Step** Release beads [hh:mm:ss]: 00:00:00 **Mixing/Heating Parameters** Mix time [hh:mm:ss]: 00:01:00 Speed: slow **End of step** Collect beads, count: 5 Collect time (s): 30
pH Elution	Plate: pH elution KingFisher 96 KF plate	100	**Beginning of Step** Release beads [hh:mm:ss]: 00:00:00 **Mixing/Heating Parameters** Mix time [hh:mm:ss]: 00:07:30 Speed: slow Postmix[hh:mm:ss]: 00:00:05 Speed: Bottom mix **End of step** Collect beads, count: 5 Collect time (s): 30
Triethylamine Elution	Plate: Triethylamine KingFisher 96 KF plate	100	**Beginning of Step** Release beads [hh:mm:ss]: 00:00:00 **Mixing/Heating Parameters** Mix time [hh:mm:ss]: 00:03:30 Speed: slow Postmix[hh:mm:ss]: 00:00:05 Speed: Bottom mix **End of step** Collect beads, count: 5 Collect time (s): 30
Leave: Tipcomb	96 DW tip comb		

2.2.2.3.3 Third panning round

The third panning round used NeutrAvidin coated high binding capacity strips (ThermoScientific) in place of the Streptavidin coated high binding capacity strips, as previously described for the first panning round. A 200 µl aliquot of phage containing supernatant or 8 µl of purified phage from the second pan was used. Phage were eluted

from wells containing target protein and empty control wells and plated at a range of dilutions to compare the level of amplification in the target wells.

2.2.2.4 Phage display for non-biotinylated targets

Phage display screening against large, unbiotinylated targets such as bacterial cells and spores was carried out in Protein LoBind Eppendorf tubes (Eppendorf), using centrifugation steps (2 min at 12,000 xg) to separate target from unbound phage.

2.2.2.4.1 Isolation of Affimer proteins against individual strains of *S. aureus* biofilm

Three strains of *Staphylococcus aureus* were used: SH1000, USA300 and UAMS-1.

ER2738 *E. coli* cells were grown overnight on LB agar with 12 µg/ml tetracycline at 37 °C. A single colony was used to inoculate 5 ml of 2TY media with 12 µg/ml tetracycline and the culture grown overnight at 37 °C, 230 rpm.

To isolate Affimer proteins specific to each individual *S. aureus* biofilm strain, an aliquot of naïve phage library was pre-panned 4 times against a combination of cells grown as biofilms from the other two strains: 20 µl of the phage library was added to a tube containing 1200 µl PBS and a 1:1 mixture of the 2 non-target strains and incubated for 1 h at room temperature on a Stuart SB2 fixed speed rotator. The mixture was centrifuged for 2 min at 12,000 xg in a Genfuge 24D centrifuge (Progen) and the supernatant containing the unbound phage was transferred to a second tube containing a 1:1 mix of the 2 non-target strains and incubated for 1 h at room temperature on a Stuart SB2 fixed speed rotator. This was repeated for a third and fourth pre-pan. During the pre-panning steps, fresh cultures of ER2738 cells were set up (8 ml per target) by diluting the overnight culture 1:15 and incubating for 1 h at 37 °C , 230 rpm to give an A_{600} of 0.6 at time of infection.

The pre-panned phage were incubated with the target strain for 2 h at room temperature on a rotator. The cells were pelleted at 12000 xg for 2 min, washed with 300 µl PBS to remove unbound phage and transferred to a fresh tube. This was repeated for 5 washes. Bound phage were eluted with 200 µl 0.2 M Glycine (pH 2.2) for 10 min, neutralised with 30 µl 1 M Tris-HCl (pH 9.1), further eluted with 200 µl of 100 mM

triethylamine (Sigma-Aldrich, St Louis, USA) for 6 min, and neutralised with 100 µl 1 M Tris–HCl (pH 7). Eluted phage were used to infect the pre-prepared ER2738 cells for 1 h at 37 °C and plated onto LB agar plates containing 100 µg/ml carbenicillin and grown overnight at 37 °C. Colonies were scraped into 7 ml of 2TY medium with 100 µg/ml carbenicillin. Absorbance was measured at 600 nm and the cells diluted to A_{600} 0.2 in an 8 ml culture. Cells were plated and phage were generated and precipitated as described in Section 2.2.2.3.1. This was repeated for two further panning rounds. During the final pan, the pre-panned phage were split into 4x 300 µl and incubated with either target strain, a negative control (magnetic beads) or controls (biofilm cells from the other two non-target strains) for 2 h at room temperature on a rotator. The bound phage were eluted and plated as before and the number of phage-infected colonies on each plate was recorded.

2.2.2.4.2 Isolation of Affimer proteins that bind *S. aureus* biofilm but not planktonic cells of the same strain

ER2738 *E. coli* cells were grown overnight on LB agar with 12 µg/ml tetracycline at 37 °C. A single colony was used to inoculate 5 ml of 2TY media with 12 µg/ml tetracycline and the culture grown overnight at 37 °C, 230 rpm.

To isolate Affimer proteins specific to biofilm-grown cells of each individual *S. aureus* strain, an aliquot of naïve phage library was pre-panned 4 times against planktonically grown cells of the target strain: 20 µl of the phage library was added to a tube containing 1200 µl PBS and planktonically grown cells of the target strain and incubated for 1 h at room temperature on a Stuart SB2 fixed speed rotator. The mixture was centrifuged for 2 min at 12,000 xg in a Genfuge 24D centrifuge (Progen) and the supernatant containing the unbound phage was transferred to a second tube containing planktonically grown cells of the target strain and incubated for 1 h at room temperature on a Stuart SB2 fixed speed rotator. This was repeated for a third and fourth pre-pan. During the pre-panning steps, fresh cultures of ER2738 cells were set up (8 ml per target) by diluting the overnight culture 1:15 and incubating for 1 h at 37 °C , 230 rpm to give an A_{600} of 0.6 at time of infection.

The pre-panned phage was then incubated with biofilm-grown cells of the target strain for 2 h at room temperature on a rotator. The cells were pelleted at 12000 xg for 2 min, washed with 300 µl PBS to remove unbound phage and transferred to a fresh tube. This was repeated for 5 washes. Bound phage were eluted with 200 µl 0.2 M glycine (pH 2.2) for 10 min, neutralised with 30 µl 1 M Tris-HCl (pH 9.1), further eluted with 200 µl of 100 mM triethylamine (Sigma-Aldrich, St Louis, USA) for 6 min, and neutralised with 100 µl 1 M Tris–HCl (pH 7). Eluted phage were used to infect the pre-prepared ER2738 cells for 1 h at 37 °C and plated onto LB agar plates containing 100 µg/ml carbenicillin and grown overnight at 37 °C. Colonies were scraped into 7 ml of 2TY medium with 100 µg/ml carbenicillin. Absorbance was measured at 600 nm and the cells diluted to A_{600} 0.2 in an 8 ml culture. Cells were plated and phage was generated and precipitated as described in Section 2.2.2.3.1. This was repeated for 2 further panning rounds. During the final pan, the pre-panned phage were split into 3x 400 µl and incubated with either biofilm-grown cells of the target strain, a negative control (magnetic beads) or controls (planktonically-grown cells from the target strain) for 2 h at room temperature on a rotator. The bound phage were eluted and plated as before and the number of phage-infected colonies on each plate was recorded. This protocol was used for each of the three strains of *S. aureus*: SH1000, USA300 and UAMS-1.

2.2.2.5 Phage display with competition

For a more stringent screening using the affinity-matured focused phage library, the screens were carried out as described in Section 2.2.2.3.1 but with the following adjustments:

The focused phage library (5 µl) was pre-panned 3 times as before but in a volume of 200 µl 2x blocking buffer. BAP-tagged and biotinylated NDM-1 was bound to 9 x Streptavidin-Coated (HBC) strips (ThermoScientific) for 2 h, then pre-panned phage was split and 100 µl added to the well containing the immobilised target and 100 µl added to an empty control well for 10 min with shaking. Any unbound phage were then removed by washing 27x in PBST and 1 well was eluted (Day 1). 100 µl of 2x blocking buffer and 50 µg un-biotinylated NDM-1 added to all remaining wells to act as competition. On each consecutive day, all panning wells were washed 27 times with 300 µl PBST on a plate washer and fresh un-biotinylated NDM-1 was added to all except one well. This well was eluted and used to re-infect ER2738 cells as described

previously. An extra elution step was then performed using 200 µl of 0.1 mg/mL bovine trypsin in 1x TBS elution buffer (1x TBS and 20 mM $CaCl_2$) for 5 minutes and used to infect a separate aliquot of ER2738 cells.

2.2.2.6 Phage ELISA

Phage ELISA was performed on randomly selected clones to confirm binding to the target. Streptavidin (Molecular Probes) was diluted to 5 µg/ml in PBS and 50 µl added to each well of a F96 Maxisorp Nunc-Immuno plate (ThermoScientific) and incubated for at least 4 h at room temperature or 4 °C overnight. Strep-coated ELISA plates were stored at 4 °C for up to a week.

200 µl 2TY media containing 100 µg/ml carbenicillin was aliquoted into the appropriate number of wells in a 96-well V-bottom deep-well plate (Greiner). Individual colonies from the panning round were used to inoculate wells and incubated overnight at 37 °C, 1050 rpm in an incubating microplate shaker (Heidolf Incubator 1000 and Titramax 1000). The next day, 200 µl 2TY media with 100 µg/ml carbenicillin was aliquoted into a new 96-well V-bottom deep-well plate and 25 µl of the overnight culture transferred into the corresponding well and incubated for 1 h at 37 °C, 1050 rpm. M13K07 helper phage (titre ca.10^{14}/ml) was diluted 1/1000 in 2TY with 100 µg/ml carbenicillin and 10 µl added per well and incubated for 30 min at room temperature, 450 rpm. Kanamycin (25 mg/ml) was diluted 1/20 in 2TY media with 100 µg/ml carbenicillin and 10 µl added per well and incubated overnight at room temperature, 750 rpm. Phage was harvested by centrifugation at 3500 xg for 10 min and phage containing supernatant transferred directly to a prepared ELISA plate for binding to immobilised target protein.

The pre-prepared streptavidin plates were blocked with 200 µl 2x blocking buffer and the plates incubated overnight at 37 °C. The following day the wells were washed once with 300 µl PBST on a TECAN HydroFlex plate washer. Biotinylated target protein was diluted 1/100-1000 in 2x blocking buffer and 50 µl added per well and control wells treated with 50 µl 2 x blocking buffer. The plates were incubated for 1 h at room temperature on a vibrating platform shaker (Heidolph VIBRAMAX 100). Wells were washed once with 300 µl PBST on a plate washer and 10µl 10x blocking buffer aliquoted per well. A 40 µl aliquot of the prepared phage-containing supernatant was added to

the target-containing well and a corresponding control well and incubated at room temperature for 1 h on a vibrating platform shaker. Each well was washed once with PBST on a plate washer and 50 µl of a 1/1000 dilution of anti-Fd-Bacteriophage-HRP antibody (Seramun Diagnostica) was added before incubation for 1 h at room temperature with shaking. Wells were washed 10 times with PBST on a plate washer and 50 µl of SeramunBlau® fast TMB/substrate solution (Seramun) added and allowed to develop for 3 min. Tetramethylbenzidine (TMB) is a substrate for HRP and develops a water-soluble blue reaction product that can be read spectrophotometrically at 620 nm. Absorbance per well was measured at 620 nm using a Multiskan Ascent 96/384 Plate Reader (MTX Lab Systems Inc). An additional reading was taken after 6 min.

2.2.3 Protein production and purification

2.2.3.1 Subcloning into pET11a plasmid

Affimer coding sequences were sub-cloned from the pBSTG-Affimer phagemid vector into a pET11a-derived vector for production of Affimer proteins.

Supercompetent XL1-Blue cells were transformed with pET11a plasmid DNA by heat shock (Section 2.2.1.11) and single colonies were picked into media, grown overnight and maxiprepped as described in Section 2.2.1.13. The high fidelity restriction enzymes *NheI*-HF and *NotI*-HF (NEB) were used to digest pET11a plasmid as per Section 2.2.1.8. Dephosphorylation (2.2.1.9), gel separation (2.2.1.7) and purification (2.2.1.14) were carried out as described previously. The digested vector was stored at -20°C.

The Affimer DNA sequence was amplified from the pBSTG phagemid vector by PCR using Phusion polymerase (Section 2.2.1.1) and the primers listed in Table 2.14. The primer pBSTG-Aff reverse (+ cysteine) was used to add a cysteine to an Affimer that might require downstream labelling by biotinylation with EZ-Link® NH-SS-Biotin (Section 2.2.2.1).

Table 2.14: PCR primer sequences

Primer	Sequence
pBSTG-Aff forward	5' - ATGGCTAGCAACTCCCTGGAAATCGAAG
pBSTG-Aff reverse	5' - TACCCTAGTGGTGATGATGGTGATGC
pBSTG-Aff reverse (+ cysteine)	5' - TTACTAATGCGGCC**GCA**CAAGCGTCACCAACCGGTTTG

*His-tag is underlined, cysteine is in bold

After amplification, the reaction mixture was incubated with *DpnI* enzyme (NEB) at 37 °C for 1 h and purified using a NucleoSpin Gel and PCR Clean-up kit (Machery-Nagel) (Section 2.2.1.15). The PCR-amplified Affimer sequence was digested with *NheI* and *NotI* restriction enzymes (2.2.1.8), purified again (2.2.1.15) and stored at -20 °C. The *NheI-NotI* digested inserts were ligated into the similarly digested pET11a vector using T4 DNA ligase (NEB) (Section 2.2.1.10). A negative control without insert DNA was also set up. Supercompetent XL1-Blue *E. coli* cells were transformed with the pET11a vectors containing ligated inserts (2.2.1.11) and plated onto LB plates containing 100 µg/ml carbenicillin. Plates were incubated at 37 °C overnight. Plasmid DNA was extracted from single colonies (Section 2.2.1.13) and DNA sequenced to confirm the correct insert (2.2.1.17).

2.2.3.2 Protein production

2.2.3.2.1 Production in BL21 Star (DE3) cells

BL21 Star (DE3) cells were transformed with pET11a-Affimer or pD861-NDM-1 plasmid DNA (Section 2.2.1.11) for production of protein. Single colonies were picked and used to inoculate 5 ml selective LB medium (Invitrogen) and grown overnight at 37 °C, 230 rpm. The following day, overnight cultures were inoculated into a larger culture volume of selective LB medium at a 1:100 dilution. Cultures were grown to an OD_{600} of 0.8 at 37 ^{o}C, 230 rpm and induced with a final concentration of either 0.5 mM IPTG (for pET11a-Affimer) or 0.2 % w/v L-rhamnose (pD861-NDM-1) and cultured overnight at 25 °C, 150 rpm. Cells were harvested by centrifugation at 4000 xg for 20 min in a Heraeus Multifuge X3R centrifuge (ThermoScientific).

2.2.3.2.2 Production of biotinylated NDM-1 in AVB101 cells

AVB101 cells were transformed with pD861 plasmid DNA encoding BAP-tagged NDM-1 (Section 2.2.1.11) for production of biotinylated protein. Single colonies were picked and used to inoculate 10 ml TYH media (Section 2.1.2) supplemented with 10 µg/ml chloramphenicol and 50 µg/ml of kanamycin. Cultures were grown overnight at 37 °C, 230 rpm. The following day, overnight cultures were inoculated into a larger culture volume of TYH media containing 50 µg/ml kanamycin and 0.5 % sterile glucose, at a 1:200 dilution. Cultures were incubated at 37 ^{o}C, 230 rpm until they reached an OD_{600} of 0.7. A 5 mM d-biotin (Invitrogen) solution was prepared in 10 mM pre-warmed bicine buffer (pH 8.3) (Sigma) and filter sterilised. The biotin solution was added to the culture at a final concentration of 50 µM and the culture induced with 1.5 mM IPTG and 0.2 % w/v L-rhamnose and incubated overnight at 25 °C, 150 rpm. Cells were harvested by centrifugation at 4000 xg for 20 min in a Heraeus Multifuge X3R centrifuge (ThermoScientific).

2.2.3.3 Protein purification

2.2.3.3.1 Purification of Affimer proteins

Following protein production and cell harvesting (Section 2.2.3.2.1), cell pellets were resuspended at 1:50 of the original culture volume in lysis buffer supplemented with 1% v/v Triton X-100 (Sigma), 100 µg/ml Lysozyme, 10 U/ml Benzonase Nuclease (Novagen) and 1x Halt Protease Inhibitor Cocktail EDTA-free (ThermoScientific), and incubated for 20 min on a SB2 rotator (Stuart) at room temperature. A 20 minute incubation at 50 °C denatured non-specific proteins and lysates were centrifuged at either 16,000 xg for 20 min in a Genfuge 24D centrifuge (Progen) (for small culture volumes); or (for larger volumes), centrifuged at 4816 xg for 20 min followed by isolation of the supernatant and a further centrifugation step at 12,000 xg for 20 min in a Heraeus Multifuge X3R centrifuge (ThermoScientific). A sample of the supernatant was kept for SDS-PAGE analysis and the remainder was added to an appropriate volume of washed Amintra Ni^{2+}NTA resin (Expedeon) and incubated for 1-2 h on a SB2 rotator (Stuart) at room temperature. The mixture was then added to a disposable polypropylene column containing a porous polyethylene disc (ThermoScientific) and the flow through (containing unbound protein) kept for SDS PAGE analysis. The Ni^{2+}NTA

resin was then washed with wash buffer (50 mM NaH_2PO_4, 500 mM NaCl, 30 mM Imidazole, pH 7.4) until the flow through measured less than 0.09 mg/ml of protein as measured on a Nanodrop Lite Spectrophotometer (Section 2.2.3.5.1). A sample of the final wash flow through was kept for SDS PAGE analysis. The His-tagged Affimer was eluted from the resin by incubation with 100-500 µl elution buffer (50 mM NaH_2PO_4, 500 mM NaCl, 300 mM Imidazole, 10% glycerol, pH 7.4), for 5 min. Elution steps were repeated until no more protein was eluted (as measured on a Nanodrop Lite Spectrophotometer), and analysed by SDS-PAGE with Coomassie staining to assess purity as described in Section 2.2.3.5.2.

2.2.3.3.2 Purification of NDM-1

Following protein production and cell harvesting (Section 2.2.3.2.2), cell pellets were very gently resuspended at 1:10 volume of the original culture volume in chilled periplasmic lysis buffer (100 mM Tris, 20% sucrose, 1 mM EDTA, pH 8) and incubated on a tube roller (StarLabs) for 10 min at 4 °C. Lysates were centrifuged at 4000 xg for 20 min in a Heraeus Multifuge X3R centrifuge (ThermoScientific) and the supernatant removed and kept for SDS-PAGE analysis. Pellets were gently resuspended in 20 ml of chilled 5 mM $MgSO_4$ and incubated on a tube roller (StarLabs) at 4 °C for 30 min before being centrifuged again at 10,000 xg for 20 min in a Heraeus Multifuge X3R centrifuge. The supernatant (periplasmic fraction) was added to an appropriate volume of washed Amintra Ni^{2+}NTA resin (Expedeon) (typically 1 ml slurry per 400 ml culture) and incubated for 1-2 h on a tube roller at 4 °C. The mixture was then added to a disposable polypropylene column containing a porous polyethylene disc (ThermoScientific) and the flow through (containing unbound protein) kept for SDS-PAGE analysis. The Ni^{2+}NTA resin was then washed with wash buffer (50 mM NaH_2PO_4, 500 mM NaCl, 30 mM Imidazole, pH 7.4) until the flow through measured less than 0.09 mg/ml of protein as measured on a Nanodrop Lite Spectrophotometer (Section 2.2.3.5.1). A sample of the final wash flow through was kept for SDS PAGE analysis. The His-tagged NDM-1 was eluted from the resin by incubation with 100-500 µl elution buffer (50 mM NaH_2PO_4, 500 mM NaCl, 300 mM Imidazole, 10% glycerol, pH 7.4), for 5 min. Elution steps were repeated until no more protein was eluted (as measured on a Nanodrop Lite Spectrophotometer), and analysed on a SDS PAGE gel with Coomassie staining to assess purity as described in Section 2.2.3.5.2.

2.2.3.3.3 Dialysis of purified protein

Proteins were buffer exchanged into 1x PBS (137 mM NaCl, 10 mM Phosphate, 2.7 mM KCl, pH 7.4) + 10% (Affimer proteins) or 40% (NDM-1) of glycerol, by dialysis. Slide-A-Lyzer dialysis cassettes (ThermoScientific) with a MWCO of 7000 K and a volume capacity of either 0.5 or 3 ml were hydrated in the dialysis buffer by immersion for 5 min. Protein was loaded into a syringe with mixing needle (Terumo) attached and injected into the cassette via one of the syringe ports. Air was removed from the cassette and the cassette attached to a buoy before being floated in 5 L of dialysis buffer for 2 h at room temperature with stirring. The buffer was replaced with fresh buffer and the protein dialysed for a further 2 h before the buffer being replaced again and dialysed overnight at 4 °C. To remove the dialysed protein, a small amount of air was injected into the cassette followed by withdrawal of the sample into a fresh syringe.

2.2.3.4 Protein analysis

2.2.3.4.1 Protein concentration

Protein concentration was determined using a Nanodrop-lite spectrophotometer (ThermoScientific). The spectrophotometer was blanked using the same buffer as that of the protein sample. A 2 µl aliquot of the protein solution was then applied to the Nanodrop sample pedestal and the A_{280} was recorded. The extinction coefficient and absorbance 0.1 % for each protein was determined from the amino acid sequence using ExPASy ProtParam. The extinction coefficient indicates how much light a protein absorbs at a given wavelength. From the molar extinction coefficient of tyrosine, tryptophan and cysteine at a given wavelength, the extinction coefficient of the native protein in water can be computed using the equation:

ε(Prot) = (No.Tyrosine * εTyrosine) + (No.Tryptophan * εTryptophan) + (No.Cysteine * εCysteine)

The absorbance (optical density) can be then be calculated using the formula: Absorb(Prot) = ε(Prot) / Molecular weight.

The concentration of the sample was then determined according to the Beer-Lambert equation when solved for concentration: $C = A / \varepsilon.l$ where C is the concentration, A is the absorbance in AU, ε is the extinction coefficient and l is the path length in cm. Calculations using the extinction coefficient ($M^{-1}cm^{-1}$) yielded the molar concentration

of the protein solution. Replacing ε with the absorbance 0.1 % (= 1 mg/ml) yielded the concentration of protein in mg/ml.

2.2.3.4.2 SDS PAGE gel electrophoresis

Protein samples were separated according to their mobility through a SDS-polyacrylamide gel by electrophoresis. Samples were mixed with 4 x loading buffer and heated at 95 °C for 5 min. Using a Bio-Rad mini-PROTEAN casting system a 15 % resolving gel (15 % (v/v) acrylamide (Severn Biotech Ltd), 375 mM Tris, pH 8.8, 0.1 % (w/v) SDS, 0.15 % (w/v) ammonium persulfate (APS), 0.04 % (v/v) N N N' N' tetramethyl-ethylenediamine (TEMED)) was poured between casting plates and allowed to polymerise for 1 h overlaid with isopropanol to ensure a flat interface. Isopropanol was removed and a stacking gel (5 % (v/v) acrylamide, 125 mM Tris pH 6.8, 0.1 % (w/v) SDS, 0.1 % (w/v) APS, 0.1 % (v/v) TEMED) poured before addition of a 10 or 15 well comb to create sample wells. Protein samples and PageRuler™ Prestained Protein Ladder (ThermoScientific) were loaded and gels electrophoresed at 170 V in SDS PAGE running buffer for 1 h.

2.2.3.4.3 Coomassie Blue staining of SDS PAGE gels

To visualise total protein, SDS PAGE gels were stained with Coomassie Blue stain (45 % (v/v) methanol, 7 % (v/v) acetic acid, 0.25 % (w/v) Coomassie Brilliant Blue R-250 (Fluka)) for 1 h before applying destain (25 % (v/v) methanol, 7.5 % (v/v) acetic acid) overnight. Gels were imaged using an Amersham Imager 600 (GE Healthcare).

2.2.3.4.4 Western blot analysis of SDS PAGE gels

Proteins were transferred from SDS-PAGE gels onto a mini format PVDF membrane with 0.2 µm pore size (Bio-Rad) using a Trans-Blot Turbo transfer system (Bio-Rad) according to the manufacturer's instructions. Transferred membranes were incubated in 3 % (w/v) BSA in TBS-T (500 mM NaCl, 20 mM Tris-base, 0.1 % (v/v) Tween-20) for 1 h at room temperature or 4 ˚C overnight. Membranes were then washed in TBS-T at room temperature for 5 min, three times, followed by incubation with primary antibody diluted in TBS-T + 3 % BSA for a minimum of 1 h and washed again for three five minute intervals. The membrane was then incubated in secondary antibody diluted in TBS-T for a minimum of 1 h before being washed for three five minute intervals. Membranes

were incubated for 5 min with 3 ml Luminata Forte Western HRP Substrate (Millipore) and visualised using chemiluminescence on an Amersham Imager 600 (GE Healthcare).

2.2.3.4.5 Competition ELISA

Streptavidin (Molecular Probes) was diluted to 5 µg/ml in PBS and 50 µl added to each well of a F96 Maxisorp Nunc-Immuno plate (ThermoScientific) and incubated for at least 4 h at room temperature or 4 °C overnight. Streptavidin-coated ELISA plates were stored at 4 °C for up to a week.

The pre-prepared streptavidin plates were blocked with 200 µl 2x blocking buffer and the plates incubated overnight at 37 °C. The following day the wells were washed once with 300 µl PBST on a TECAN HydroFlex plate washer. Biotinylated target protein was diluted 1/100 in 2x blocking buffer and 50 µl added per well and the 'no target' control well treated with 50 µl 2 x blocking buffer. The plates were incubated for 1 h at room temperature on a vibrating platform shaker (Heidolph VIBRAMAX 100). Wells were washed three times with 300 µl PBST on a plate washer. Solutions of different concentrations of Diclofenac (DCF) (not biotinylated) in PBST were prepared from a 10 mM stock solution of diclofenac sodium (Sigma) to give final concentrations ranging from 16 nM to 16 µM. The DCF solutions were mixed with DCF-Affimer (final concentration of 0.2 µg/ml) and incubated for 30 minutes. Then, 50 µl per well of each Affimer:DCF mixture were added into the plate wells and 50 µl of 2 x blocking buffer was added to the 'no Affimer' control well and all wells were incubated at room temperature for 1 h on a vibrating platform shaker. Each well was washed three times with PBST on a plate washer. Subsequently, HRP conjugated anti-6x His tag antibody (1 µg/mL in 2x blocking buffer) was added (50 µL/well) and incubated for 1 hour at room temperature with shaking. Wells were washed 10 times with PBST on a plate washer and 50 µl of SeramunBlau® fast TMB/substrate solution (Seramun) added and allowed to develop for 3 min. Absorbance per well was measured at 620 nm using a Multiskan Ascent 96/384 Plate Reader (MTX Lab Systems Inc).

2.2.4 Library generation

2.2.4.1 Generation of focused phage libraries

Two phage libraries were generated. Library 1 involved the randomisation of residues in VR1 of Affimer 21 that were shown to be essential for inhibition of NDM-1 activity. Library 2 involved the randomisation of residues in VR1 that had been shown not to be essential for inhibition of NDM-1 activity. Supercompetent XL1-Blue cells were transformed with pBSTG-Aff phagemid vector DNA by heat shock (Section 2.2.1.11) and single colonies were picked into media, grown overnight and DNA maxiprep prepared as described in Section 2.2.1.13. The high fidelity restriction enzymes *NheI*-HF and *PstI*-HF (NEB) were used to digest 20 µg pBSTG-Aff phagemid vector as per Section 2.2.1.8. Dephosphorylation (2.2.1.9), agarose gel separation (2.2.1.7) and purification (2.2.1.14) were carried out as described previously. The digested vector was stored at -20 °C.

Library insert DNA was constructed by SOE of two PCR products (fragments) that were amplified from the pBSTG-Aff phagemid vector containing the Affimer 21 sequence (Figure 2.3).

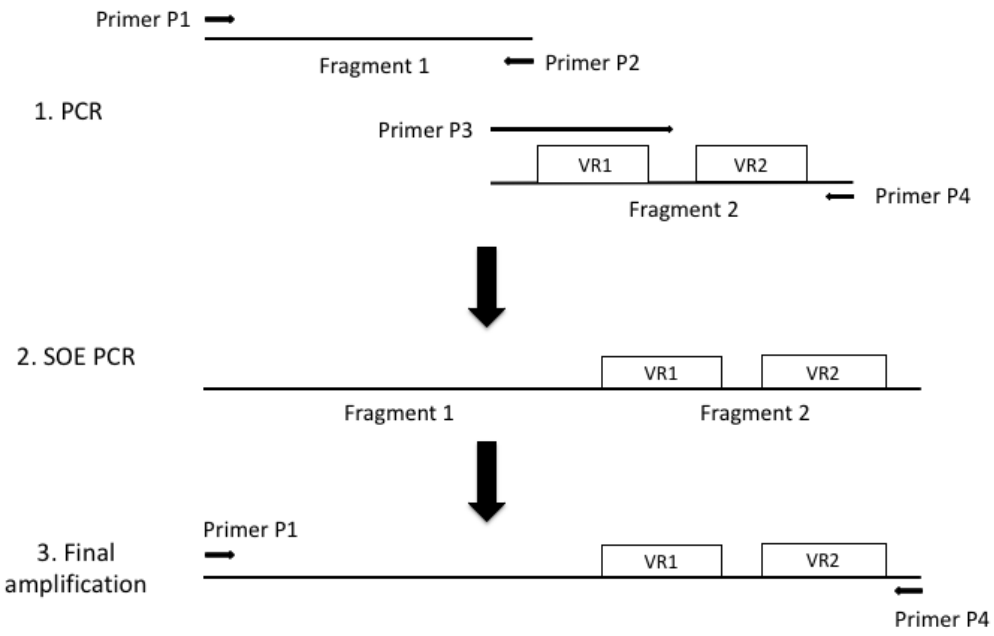

Figure 2.3: Generation of library insert DNA: Schematic showing the strategy for creating library insert DNA. Template DNA was pBSTG-Aff phagemid vector containing the Affimer 21 sequence. Primers are listed in Table 2.15. VR1: variable region 1 and VR2: variable region 2.

The first PCR product extended from the *dsbA* signal coding sequence up to the first variable loop and the second PCR product introduced the two nine amino acid variable regions of the Affimer 21 sequence, whilst randomizing the residues in variable region 1 (VR1). Primers were designed as shown in Table 2.15 and sent to Ella Biotech for synthesis.

Table 2.15: Library generation primers

Library 1	**Name**	**Sequence**
Fragment 1 For	P1	5' TTCTGGCGTTTTCTGCGTC 3'
Fragment 1 Rev	P2	5' **TGTTCTTTCGCTTTAACAAC** 3'
Fragment 2 For	P3	5'**GTTGTTAAAGCGAAAGAACA**GGGTNNNNNNGTTNNNNNNNNNTACGGTACCATGTACTACCTG 3' *
Fragment 2 Rev	P4	5' GTCACCAACCGGTTTGAACTC 3'
Library 2	**Name**	**Sequence**
Fragment 2 For	P3	5'**GTTGTTAAAGCGAAAGAACA**GNNNTACAAANNNTGGACTCCGNNNNNNACCATGTACTACCTGACC-3' *

* The coding sequence for variable region 1 is underscored, overlapping primer sequence regions are in bold.

Primers P1, P2 and P4 were the same for generation of both libraries. Primer P3 introduced the degenerate positions (NNN) as trimers representing a single codon for each of the 19 amino acids excluding cysteines and stop codons (Kayushin et al., 1996). Eight PCR reactions for each fragment were carried out using Phusion HF polymerase as described in Section 2.2.1.1. PCR products for each fragment were pooled, separated on an agarose gel (2.2.1.7), purified by gel extraction (2.2.1.14) and combined in 10 cycles of SOE PCR (2.2.1.2) followed by a final amplification using primers P1 and P4 and KOD Hot Start DNA Polymerase Kit (2.2.1.3). SOE efficiency was confirmed by analysis on an agarose gel. DNA product was digested with *Nhe*I and *Pst*I (2.2.1.8) gel extracted and cloned into the similarly digested pBSTG-Aff phagemid (2.2.1.10). The pBSTG-library DNA was then purified (2.2.1.15), electroporated into ER2738 cells and phage were generated (2.2.1.12). The phage library was snap frozen in liquid nitrogen and stored at -80 °C.

2.2.4.2 Estimation of phage library titre by spectrophotometer

The phage library was diluted 1:20 and 1:50 in TE buffer and loaded into High Precision Cell quartz cuvettes (Hellma Analytics), alongside a blank consisting of TE buffer only. A Genova spectrophotometer (Jenway) was blanked against the TE buffer and measurements of the 1:20 and 1:50 phage dilutions made at A_{269} (the wavelength at which absorbance for filamentous phage is at a maximum). This was repeated to obtain a baseline measurement at A_{320}. At the wavelength A_{320} there is little light absorption from phage chromophores, so deducting this crudely corrects for light scattering from phage particles and non-phage particulate contaminants. The A_{269} measurements were corrected for the baseline (A_{320}) measurements ($A_{269} - A_{320}$) and the virion concentration (in phage particles/ml) was calculated for the 1:20 and 1:50 phage library dilutions: phage particles/ml = (corrected A_{269} x 6 x 10^{16}) / number of nucleotides in the phage genome (Barbas et al., 2001).

2.2.4.3 Estimation of phage library titre by plating out

ER2738 cells were grown overnight on an LB agar plate containing 12 µg/ml tetracycline and used to inoculate 5–10 ml of LB/tet media (Invitrogen). The culture was incubated with shaking for 4–8 h to mid-log phase (OD_{600} ~ 0.5).

Serial dilutions of the phage library were prepared at 10^3, 10^4, 10^5, 10^6 and 10^7 in 1 ml of LB media, a fresh pipette tip was used for each dilution. When the ER2738 culture reached mid-log phase, 200 µl was dispensed into microcentrifuge tubes, one for each phage dilution. To carry out infection, 10 µl of each phage dilution was added to each tube, mixed briefly, and incubated at room temperature for 5 min. The phage-infected cells were then plated onto LB agar plates containing 100 µg/ml carbenicillin, inverted and incubated at 37 °C overnight. The LB agar plates were pre-warmed for at least 1 h at 37°C before use. The following day, colonies on each plate were counted and multiplied by the dilution factor for that plate to get the phage titre in colony forming units (cfu) per volume.

2.2.5 Enzyme assays

2.2.5.1 β-Lactamase activity assays

NDM-1 activity was quantified by spectrophotometric measurement of nitrocefin hydrolysis at 482 nm and at 25 °C on a Tecan Spark® microplate reader (Tecan Trading AG) and readings for each well were taken every 12 secs for 15 min. All dilutions were made up in assay buffer containing 50 mM HEPES buffer pH 7, 20 μM $ZnSO_4$ and 10 μg/ml bovine serum albumin (Sigma) in a final volume of 150 μl in a 96 well Nunc® Microwell plate (ThermoScientific). Reactions included 100 nM NDM-1, 10 μM clavulanic acid, either 200 or 500 nM of Affimer and 65 μM nitrocefin (Millipore); which was added immediately prior to spectrophotometric measurement. Controls included an EDTA control (5 mM EDTA, 100 nM NDM-1, 65 μM nitrocefin), a no Affimer control (100 nM NDM-1, 65 μM nitrocefin, 50 μl assay buffer) and a no NDM-1 control (200 or 500 nM Affimer, 65 μM nitrocefin, 50 μl assay buffer). All reactions and controls were set up in triplicate on each plate. Initial rates were calculated from the first 250 seconds during which the rates were constant.

IC_{50} values were determined after a 5 minute pre-incubation of NDM-1 enzyme with Affimer. Final concentrations of NDM-1 in the assays was 100 nM. Affimer was tested at a range of concentrations between 10 nM to 3 μM made up in assay buffer. Reactions also included 65 μM nitrocefin and 10 μM clavulanic acid with controls as described previously. Initial rates of nitrocefin hydrolysis were determined during the first 250 seconds of the reaction during which the rates were constant.

All data were processed using GraphPad Prism 7 (GraphPad Software Inc.). Measurements were normalised to the mean of the EDTA control wells and converted to concentration in μM using Beer-Lambert's Law: $C = A / \varepsilon.l$ where C is the concentration, A is the absorbance value, ε is the extinction coefficient and l is the path length in cm (0.473764). Linear regression analysis was performed ($y = mx + c$ where y is concentration, x is time, m is the slope of the fitted line and c is the intercept) and the mean and standard error values were calculated from the slopes of the graph. The rates in μM/s were then plotted and IC_{50} values determined.

2.2.5.2 Kinetic analysis

The hydrolysis of a range of concentrations of nitrocefin, from 0.4 to 4 µM, by 30 nM NDM1 was followed by measuring the formation of product at 486 nm in a UV-2401PC UV-Vis spectrophotometer (Shimadzu) at 25 °C for two min. This was performed both in the presence and absence of 10 nM Affimer 21. The initial rate of the reaction was recorded and absorbance units were converted to concentration units using the extinction coefficient of Nitrocefin (20500 $M^{-1}cm^{-1}$) and Beer Lambert's Law (described above), and then multiplied by 10^6 to convert the units to µM per second.

Kinetic parameters were determined by fitting the plot of rate against substrate concentration to the Michaelis-Menten equation using non-linear regression: Rate = $(V_{max}[S]) / (K_M + [S])$ where V_{max} (µM/s) is the maximum rate of the enzyme, [S] (mM) is the substrate concentration and K_M (mM) is the Michaelis constant (the [S] at half V_{max}) and gives an indication of the affinity of the enzyme for the substrate. The turnover number, k_{cat} (s^{-1}) was determined by dividing V_{max} by the enzyme concentration (µM).

Mechanism of inhibition was visualised using a Lineweaver-Burk (double reciprocal) plot, which plots the reciprocal of substrate concentration vs. the reciprocal of enzyme velocity: $1/rate = (1 / V_{max}) + (K_M / V_{max} [S])$.
All assays were performed in assay buffer. Data was processed using OriginPro 8.6 software.

2.2.6 Cell assays

2.2.6.1 Minimum inhibitory concentration (MIC)

A clinical strain of *Klebsiella pneumoniae* constitutively expressing NDM-1 was used. Measurement of MIC was performed in 96-well microtitre plates in a volume of 200 µl per well. Serial dilutions of meropenem (Sigma) were made in Mueller Hinton broth (MHB) (Sigma) at 10x final concentration. Bacteria were prepared from an overnight culture and diluted in MHB to an OD_{600} of 0.001, equivalent to a CFU of 2×10^5 (Lorian, 2005). Diluted culture (180 µl) was placed in each well and supplemented with 20 µl of meropenem to give final concentrations ranging from 1 µg/ml to 128 µg/ml. Three technical repeats of each condition were performed. The microtitre plate was sealed

with a plate sealer and lid, followed by sealing with parafilm to ensure no evaporation. The plate was then incubated on an orbital rotator at 300 rpm, 37 °C for 18 h. The MIC of the antibiotic was determined as the lowest concentration that did not show growth.

2.2.6.2 Cell growth assay

A clinical strain of *Klebsiella pneumoniae* constitutively expressing NDM-1 was used. Assays were performed aerobically at 37 °C in a 96-well microtitre plate in a FLUOstar Omega dual orbital shaker. Cell density was quantitatively assessed by means of measuring absorbance at OD_{600} every 5 min for 20 h. LB media (2 ml) was inoculated with either *K. pneumoniae* or *E. coli* BL21 (DE3) star cells and grown overnight at 37 °C, 230 rpm. Overnight cultures were then diluted 50-fold in LB media and density adjusted to fall between OD_{600} 0.08 and 0.1. Diluted cultures were diluted again 1:50 in LB and then 180 µl was added to 9 ml for a final dilution of 2500-fold. Diluted cells (33 µl) were added to each well. Meropenem was added to give a final concentration of 6 µg/ml and Affimer 21 was dosed at final concentrations ranging from 1 µg/ml to 10 µg/ml. The final reaction volume of each well was 100 µl. Multiple controls were used; no antibiotics to assess cell viabilities; and LB only to confirm aseptic technique. Both cell lines with meropenem and without Affimer 21 were used to give a survival reference point and to test the potency of meropenem.

2.2.6.3 U-2 OS cell toxicity assay

Human osteosarcoma (U-2 OS) cells (ATCC) were cultured in DMEM media (Sigma) supplemented with 10 % FBS (Gibco) and 1 % pen-strep for 72 h in Costar® TC-treated 24-well plates (Corning). DMEM was replaced with Affimer 21 at final concentrations of 0.1, 1, 10 and 100 µg/ml or yeast-sumo Affimer at 100 µg/ml. Cells were incubated at 37 °C for 24 h and then washed in 500 µl PBS. Trypsin (200 µl) was added and incubated for 5 min at 37 °C. Cells were then diluted to a final volume of 1 ml with 800 µl DMEM + 10 % FBS broth. A Muse® cell counter was used to determine total cell count and % viability.

2.2.7 Complex formation and crystallization trials

2.2.7.1 Complex formation

Affimer 21 production (Section 2.2.3.2.1) was scaled up to 3 L of culture volume and NDM-1 production (Section 2.2.3.2.2) was scaled up to 8 L of culture volume. Affimer 21 protein was added in excess to Amintra Ni^{2+}NTA resin (Expedeon) and purified as described in Section 2.2.3.4.1 but not eluted from the resin. NDM-1 protein was purified as per Section 2.2.3.4.2 and the periplasmic fraction was mixed with the Affimer-bound resin and incubated at 4 ˚C overnight on a Tube Roller (StarLabs). The resin was then added to a fresh polypropylene column (ThermoScientific) and washed and eluted as described previously. The protein sample was then immediately applied to a HiPrep™ 16/60 Sephacryl S-100 HR column and purified by size exclusion chromatography.

2.2.7.2 Size exclusion chromatography

Size exclusion chromatography (SEC) was performed on a HiPrep™ 16/60 Sephacryl S-100 HR column attached to an Akta Explorer system. The column was flushed with de-gassed pure water to remove the storage ethanol (20 %) and equilibrated with de-gassed buffer (20 mM HEPEs, 150 mM NaCl, pH7). A 2 ml aliquot of protein sample was loaded onto the column using a 2 ml injection loop. Absorbance of the protein sample was measured at 280 nM at a flow rate of 0.5 ml/min and 2 ml fractions were collected. Upon completion, the column was washed with de-gassed pure water and stored in 20 % ethanol. The collected protein fractions were separated and analysed by SDS-PAGE (Section 2.2.3.5.2).

2.2.7.3 Concentration of protein

Protein was concentrated using Vivaspin® 5000 MWCO centrifugal concentrators (Sartorius) by centrifugation at 4000 xg in a Heraeus Multifuge X3R centrifuge (ThermoScientific) until the desired concentration was reached. Concentration of protein was monitored and measured using a Nanodrop lite spectrophotometer.

2.2.7.4 Crystallization trials

Crystallization trials were set up with the NDM-1 : Affimer 21 protein complex purified by Ni^{2+}NTA and SEC as described in Section 2.2.7.1. Protein was concentrated in

Vivaspin® 5000 MWCO centrifugal concentrators (Sartorius) up to concentrations varying between 3 and 40 mg/ml. Initial screens were set up using the commercially available screens JCSG Core Suites I, II, III, and IV (Qiagen). Trials were set up on 96 well 3-drop plates (Molecular Dimensions) using a NT8® Drop Setter robotics system (Formulatrix). Protein was mixed at 1:1, 2:1 and 1:2 ratios with mother solution in each of the three drops to a total volume of 0.2 µl. Plates were sealed with VIEWseal pressure adhesive seals stored at 20 °C on a Sonicc RI 1000 Crystal Detector (Formulatrix) for imaging over a 34-day period.

2.2.7.5 Crystallisation optimisation

Conditions that looked promising from the initial commercial screens were optimised and a 96-well deep well plate (Greiner) of buffer conditions that centred on the variation of precipitant and pH was created using a Formulator® Screen Builder (Formulatrix). A 96 well 3-drop plate of crystallisation trials was then set up using these optimised conditions with Affimer 21 : NDM-1 complex protein, as before.

Chapter 3

Hitting difficult targets: proof of concept

Note

My initial PhD project was titled ‘synthetic approaches to developing novel biosensors for rapid, in-field detection of yellow wheat rust, *Puccinia striiformis*’. However, due to an unforeseen shortage in the availability of yellow rust fungal spores, I was not able to attempt an Affimer screen to isolate binders to these targets. Therefore the work carried out during the first year of my PhD and the subsequent results described in this section focussed upon exploring the capability of isolating Affimers that bind to a range of unusual or difficult to target molecules. After this year it was decided that I should focus on a new PhD project in order to obtain enough results to complete my PhD and I therefore started working on a project entitled ‘modulation of metallo-β-lactamase activity using Affimers’, for which the main part of this thesis is focussed upon.

Affimers have been successfully selected against more than 300 protein targets but the potential for identifying binding reagents against more 'difficult' targets has not yet been fully explored. To examine the potential and flexibility of Affimer technology, the libraries were screened against a) individual fluorescent proteins, b) a small molecule and c) prokaryotic biofilms. Here we present results demonstrating the ability to generate and exploit binding reagents against such targets. The potential to isolate binding reagents that recognise difficult targets offers new scope for the development of tools to understand biological function and for detection and diagnostic applications.

3.1 Isolation of Affimer reagents against individual fluorescent proteins for imaging applications

Imaging techniques are rapidly evolving and researchers are continuously searching for more accurate methods of labelling cellular components to achieve maximum resolution. Traditional immunostaining techniques often rely upon antibodies which can be larger than the protein of interest, limiting localisation accuracy by placing the dye or fluorophore further away from the intended target. This distance is known as the linkage-error and can be as much as 25 nm for primary-secondary antibody complexes, a distance which is not only often outside of the resolution limit of the instrument, but which causes low labelling density by steric hindrance (Fornasiero et al, 2015).

Single molecule localisation microscopy (SMLM) techniques such as photoactivation localization microscopy (PALM) and stochastic optical reconstruction microscopy (STORM) rely upon the presentation of bright fluorophores close to the target without adding substantial background. While PALM relies on genetically encoded fluorescent proteins, STORM uses organic dyes to give better localisation precision as they emit greater numbers of photons and are therefore brighter (Moerner, 2012). However, delivery to the target still requires conjugation to antibodies, displacing the dye with linkage errors of approximately 10 nm (Ries et al, 2012). Such limitations have resulted in the development of smaller probes that can be utilised to improve the staining precision of biological samples.

The small size of novel affinity reagents makes them an attractive alternative to antibodies for use in imaging technologies. They are able to penetrate tissues and access tightly packed subcellular spaces more readily than antibodies and are often better tolerated in the cytosol, enabling live cell imaging. SMLM techniques have begun to explore the use of nanobodies as one such alternative. The nanobody is derived from a single antigen binding variable domain (VHH region) found in cameloids and can be cloned in phage display vectors for the selection of binders (Hamers-Casterman et al, 1993). In 2012 it was demonstrated that nanobodies targeting GFP can be used to deliver bright organic flurophores to GFP-tagged proteins, providing a significant improvement in the localisation precision of super-resolution microscopy when compared to traditional staining techniques (Ries et al, 2012). Nanobodies have also been fused to fluorescent proteins and endogenously expressed for visualising antigens in live cells (Rothbauer et al, 2006); and used in DNA-PAINT (DNA-points accumulation in nanoscale topography) (Agasti et al, 2017). In parallel, nanobodies that bind to GFP were explored as possible tools for the purification and cellular engineering of fluorescent protein fusions (Kubala et al, 2010). Additionally, these GFP-nanobodies have been shown to be capable of isolating GFP-tagged proteins from cell extracts and redirecting them to alternative cellular locations (Rothbauer et al, 2008).

DNA and RNA aptamers are single-stranded lengths of oligonucleotides ranging from 15 to 100 nucleotides (Ellington et al, 1990). The nucleotide sequence of the aptamer is responsible for the 3D structure that establishes specific binding to a target molecule. Similarly to nanobodies, aptamers have also demonstrated improved precision obtained in super-resolution microscopy and single molecular localisation microscopy when compared to antibodies (Opazo et al, 2012 and Gomes de Castro, 2017). RNA aptamers that bind GFP, YFP and CFP (Fluorescent Protein-Binding Aptamers; FPBA) with low nanomolar affinity for the detection and localization of RNA and other biological molecules in living cells have also previously been described (Shui et al, 2012). It is expected that these FPBAs could also be used for tracking cellular molecules by tethering them to FPs through heterovalent aptamers, where one arm binds the FP and the others the target. Additionally, the ability of FPBAs to alter the fluorescence of target FPs could be utilized in quantitative detectors for target molecules.

Succeeding the work carried out in this project, Affimer reagents have been successfully exploited for use in a number of imaging applications including in vivo imaging of tumours, affinity fluorescence in fixed cells and as probes for imaging tubulin and a receptor tyrosine kinase in super resolution microscopy (Tiede et al, 2017). Interestingly, the Affimers against tubulin were shown to target interphase microtubules in a similar way to antibodies, but they also labelled the cytokinetic furrow, which is inaccessible to antibodies. Even more recently, Affimer reagents that target F-actin for imaging applications have been described (Lopata et al. 2018). The isolated Affimer reagents were able to image F-actin in both fixed and live cells. These results suggest that Affimer reagents are able to selectively bind structures of F-actin with only small differences, a property that makes them ideal for imaging proteins with high homology. Furthermore, actin-specific Affimers were also used in DNA-PAINT imaging (Schlichthaerle et al, 2018). The Affimers were labelled with single DNA strands at a C-terminal cysteine to achieve quantitative, site specific labelling and were shown to give comparable results to the commonly used labelling molecule phalloidin.

Additionally, highly specific Affimer reagents that are able to distinguish between proteins of high homology have previously been reported. Using negative selection techniques, Affimer reagents that are able to differentiate between different isoforms of SUMO were isolated (Tang et al, 2017), and another study identified Affimer reagents that bind specifically to Fc gamma receptors (FcγRs) that share 98 % homology (Robinson et al, 2018). One Affimer demonstrated direct competition for the Fc binding site whilst another was shown to act through allosteric modulation. The Affimer that acted via direct competition was able to discriminate between FcγRIIIa and FcγRIIIb due to subtle differences in amino acid composition at just two positions.

Accurate staining procedures and the size of affinity tools used are highly important in super-resolution microscopy. The small size of Affimer proteins (12 kDa, ~2 nm), similar to that of nanobodies (13 kDa, ~3 nm) and aptamers (15 kDa, ~4 nm), and the ability to specifically introduce a cysteine for addition of biotin or a fluorophore, makes them good alternatives as reagents for use in imaging applications. Affimer reagents that selectively bind individual fluorescent markers could represent alternatives for use in detection, imaging and purification of fluorescent protein fusions.

3.1.1 Results

Fluorescent proteins (FPs) have revolutionized cell biology and biochemistry by providing easy to use genetically encodable FP tags. Much research has been focussed on identifying and developing FPs with novel characteristics and enhanced properties for visualising the structure and dynamic processes of living cells and organisms (Rodriguez et al, 2017). The green fluorescent protein (GFP) from the jellyfish *Aequorea victoria* and its homologs are extensively used as genetically encodable fluorescent protein tags and enhanced GFP (eGFP) is now one of the most widely used commercial probes. GFP has been engineered to produce a vast number of other variants including the widely used cyan fluorescent protein (CFP) and yellow fluorescent protein (YFP). As a result, eGFP, CFP and YFP sequences share some homology (Figure 3.1).

```
CLUSTAL O(1.2.4) multiple sequence alignment

eGFP ---MVSKGEELFTGVVPILVELDGDVNGHKFSVSGEGEGDATYGKLTLKFICTTGKLPVP 57
YFP  MRGSGSSGALLFHGKIPYVVEMEGNVDGHTFSIRGKGYGDASVGKVDAQFICTTGDVPVP 60
CFP  ----MSGGEELFAGIVPVLIELDGDVHGHKFSVRGEGEGDADYGKLEIKFICTTGKLPVP 56
          * *  ** * :* ::*::*:*.**.**: *:* ***  **:  :******.:***

eGFP WPTLVTTFSYGVQCFSRYPDHMKQHDFFKSAMPEGYVQERTIFFKDDGNYKTRAEVKFEG 117
YFP  WSTLVTTLTYGAQCFAKYGPEL--KDFYKSCMPDGYVQERTITFEGDGNFKTRAEVTFEN 118
CFP  WPTLVTTLAWGIQCFARYPEHMKMNDFFKSAMPEGYIQERTIHFQDDGKYKTRGEVKFEG 116
     * *****:::* ***::*  .:  :**:**.**:**:***** *:.**::***.**.**.

eGFP DTLVNRIELKGIDFKEDGNILGHKLEYNYNSHNVYIMADKQKNGIKVNFKIRHNIED--G 175
YFP  GSVYNRVKLNGQGFKKDGHVLGKNLEFNFTPHCLYIWGDQANHGLKSAFKICHEITGSKG 178
CFP  DTLVNRVELKGEGFKEDGNILGHKLEYSAISDNVYIMPDKANNGLEANFKIRHNIEG--G 174
     .:: **::*:* .**:**::**::**:.   . :**  *: ::*::  *** *:* .  *

eGFP SVQLADHYQQNTPIGDGPVLLPDNHYLSTQSALSKDPNEKRDHMVLLEFVTAAGITHGMD 235
YFP  DFIVADHTQMNTPIGGGPVHVPEYHHMSYHVKLSKDVTDHRDNMSLKETVRAVDCRKTYL 238
CFP  GVQLADHYQTNVPLGDGPVLIPINHYLSCQSAISKDRNEARDHMVLLESFSAYCHTHGMD 234
     .. :*** * *.*:*.*** :*  *::* :  :*** .: **:* * * . *    :

eGFP ELYK-------------------------- 239
YFP  ----------------------------
CFP  ELYRSGLRSRAQASNSAVDGTAGPGSTGSR 264
```

Figure 3.1: Alignment of protein sequences for eGFP, CFP and YFP. The protein sequences for eGFP (RayBioTech), CFP (BioVision) and YFP (BioVision) were aligned using the UniProt alignment tool (The UniProt Consortium, 2017). Percentage homology between each pair of fluorescent proteins was calculated: eGFP and CFP = 70 %, YFP and CFP = 48 % and eGFP and YFP = 51 %.

To determine whether Affimer reagents could be isolated that are capable of binding specifically to individual FPs, a phage display screen was carried out using biotinylated eGFP, CFP and YFP proteins (Section 2.2.2.3). To isolate Affimers that bind specifically to each FP, the naïve phage library was pre-panned against a combination of the other two FPs. After three rounds of panning, ninety-six colonies were picked from each plate and a phage ELISA was carried out to check binding to the biotinylated targets (Section 2.2.2.6). From these, sixteen clones were chosen as showing potential binding. The binding of the sixteen pre-selected clones was confirmed in a second phage ELISA against each of the biotinylated fluorescent proteins. Each clone was also checked for non-specific binding against a negative control (wells with no target present). Absorbance readings were recorded at 620 nm on a MultiSkan Ascent plate reader (Figure 3.2).

a.

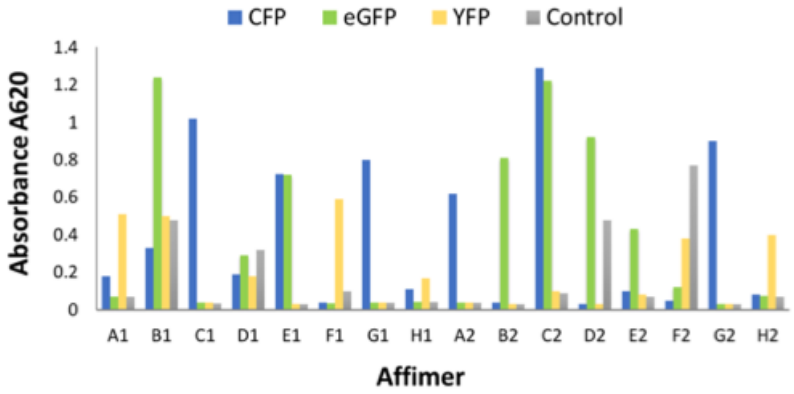

b.

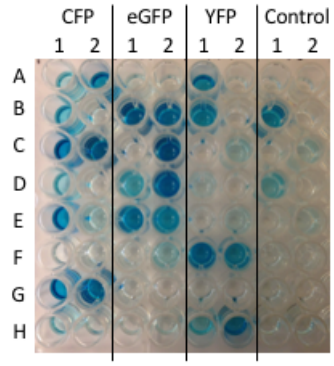

c.

Affimer	CFP	eGFP	YFP	-ve
A1	+	-	+	-
B1	+	+	+	+
C1	+	-	-	-
D1	+	+	+	+
E1	+	+	-	-
F1	-	-	+	-
G1	+	-	-	-
H1	-	-	-	-

Affimer	CFP	eGFP	YFP	-ve
A2	+	-	-	-
B2	-	+	-	-
C2	+	+	-	-
D2	-	+	-	+
E2	-	+	-	-
F2	-	-	+	+
G2	+	-	-	-
H2	-	-	+	-

Figure 3.2: Phage ELISA results for Affimer reagents selected against individual fluorescent proteins (FPs). (a) 16 pre-selected colonies (A1 to H2) were tested in a phage ELISA. Each colony represented one Affimer and was tested for binding against each FP or an empty control well. Phage binding was detected with anti-Fd bacteriophage-HRP antibody and visualised on addition of TMB. Absorbance at 620nm was measured for each well. **(b)** Photograph of the phage ELISA plate. Binders A1 to H2 were tested against each FP and an empty control well. **(c)** Summary table of isolated Affimer binding to FP targets: + indicates binding, - indicates binding of less than 0.1 as measured by absorbance at 620 nm. Green shading indicates the Affimer binders which had the highest absorbance values for each of the three FPs and were therefore taken forward for sequencing analysis

Out of the sixteen clones, eight displayed binding to one specific fluorescent protein, two showed binding to both eGFP and CFP and six showed either low level binding to all targets or displayed non-specific binding to the negative control. Affimer binders which had the highest absorbance for each FP were sequenced (Section 2.2.1.17) (Table 3.1).

Table 3.1: Variable region sequences for Affimer reagents selected against FPs

Affimer	Specific for	Variable region 1	Variable region 2
C1	CFP	QYIYKWQQS	KGTSFRVLD
F1	YFP	FWEPNYYNT	NDFMTQPYY
B2	eGFP	WQQRMFSDE	IDYFMKKRK

The three selected Affimers were then sub-cloned from the phagemid vector into a pET11a plasmid for production and purification to allow for future characterisation (Section 2.2.3). The Affimers were subcloned with and without cysteine for possible future downstream labelling. An SDS PAGE gel confirmed the presence of the purified Affimers at ~12 kDa (Figure 3.3).

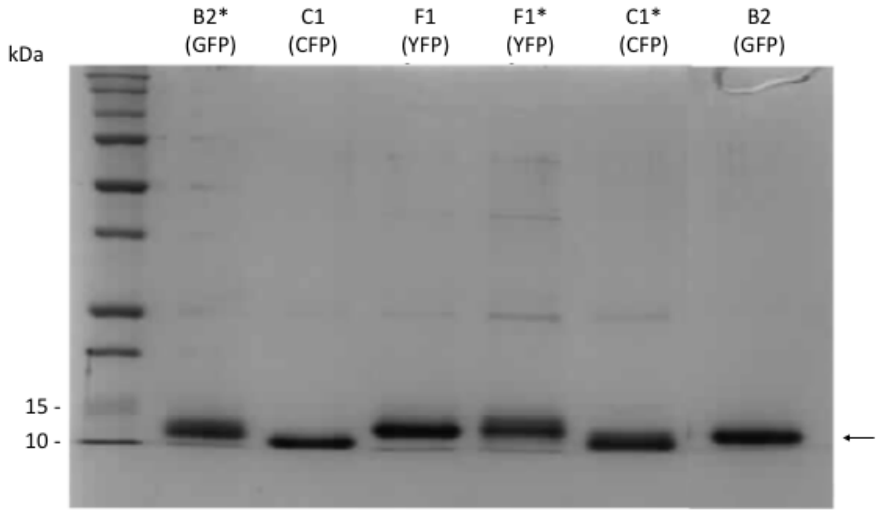

Figure 3.3: Purification of isolated Affimers that bind to FPs. Purified and dialysed Affimer proteins produced from pET11a vector. * indicates the addition of a cysteine. The proteins were purified from bacterial cell lysate using nickel ion affinity chromatography. Proteins were analysed by SDS-PAGE and Coomassie blue staining to confirm purity. The Affimers visualised at 12 kDa as indicated by the arrow.

The purified FP Affimer binders were dialysed into 1x PBS + 10 % v/v glycerol and stored at -80 °C (Section 2.2.3.4.3).

3.2 Identifying Affimer reagents that bind small molecules

The isolation of reagents that bind to small organic compounds is technically challenging. Small molecules do not display innate immunogenicity and suitable binding sites are often limited. Phage display has proven to be a useful tool in both drug discovery and environmental sciences for the selection of reagents that bind to small molecules (Takakusagi et al, 2010). Phage display is able to detect proteins expressed at low levels and allows identification of the binding site on target proteins; limitations that are difficult to overcome using transcriptomic and proteomic investigation. Large numbers of potential binders can also be screened simultaneously. These advantages make phage display particularly useful for applications such as ecotoxicology, where identification of novel binders against small molecules can be used to detect low levels of toxicological targets, both in humans, and the environment (Van Dorst et al, 2012).

Anticalins are a class of novel biologics derived from human lipocalins; low molecular weight proteins found in blood plasma (Pieris Pharmaceuticals Inc.). They have a simple, compact fold dominated by a central β-barrel, supporting four structurally variable loops that form a binding pocket of variable size and shape. Natural lipocalins play a role in the complexation of small molecules for various physiological roles and Anticalins maintain a similar predominant specificity for small molecules (Schiefner et al, 2015). Indeed, Anticalin proteins have been used for targeting a number of high-profile targets in human diseases (e.g. HER2, VEGF, Interleukins, Hepcidin), several of which are now in clinical development (Rothe et al, 2018). Affimers have also recently been reported that bind to the small molecule, 2,4,6-trinitrotoluene (TNT) (Tiede et al, 2017). These studies demonstrate the potential for using novel non-antibody scaffolds for the detection of small molecules.

Recent increases in the world's population and subsequent urbanisation has magnified the effects of agricultural and economic activities on the ecosystem (United Nations, 2018). The impact of population increase on the environment takes two major forms: a) an increase in consumption of resources such as land, food, water, air, fossil fuels and minerals and b) an increase in waste products such as air and water pollutants, toxic materials and greenhouse gases (Dovers et al, 2015). Pharmaceuticals and personal care products (PCPs) are commonly used in many fields including medicine,

industry, livestock farming, aquaculture and daily life. In addition, a rise in the incidence of diseases associated with urbanisation such as diabetes, obesity and mental illnesses along with an increasingly aging population have led to a huge proliferation in the use of pharmaceuticals (Redshaw et al, 2013). These increases in consumption coupled with inadequate waste removal systems have meant that PCPs and pharmaceuticals are now ubiquitous in the environment (Wang et al, 2016).

The non-steroidal anti-inflammatory drug Diclofenac (2-[(2,6-dichlorophenyl) amino]benzeneacetic acid) (DCF) is widely used in both human and animal health care (Figure 3.4).

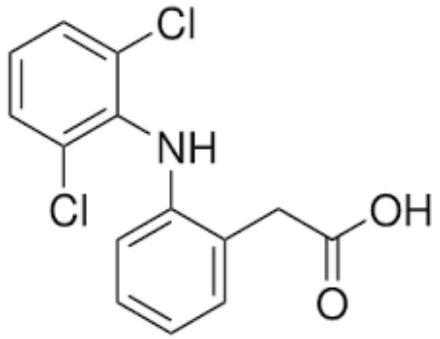

Figure 3.4: Chemical structure of Diclofenac. Molecular Weight: 296.14864 g/mol, Chemical classification: Non-steroidal anti-inflammatory compound.

Diclofenac contamination is frequently detected in sewage treatment plants, rivers, lakes and marine waters and research has shown that DCF and its metabolites are difficult to remove during biological wastewater treatment (Vieno et al, 2014). Removal efficiency of DCF varies greatly between laboratory, pilot and full-scale plants with efficiency values of < 5-40 % (Rigobello et al, 2013). Increased efficiency would invariably include the addition of an additional purification stage to the treatment process; especially designed to remove micro-pollutants. Ozonation (as used in the treatment of drinking water) and the use of activated carbon are technologies that have been developed as advanced water treatment options but often result in by-products of DCF which have not yet been studied for toxicity (Oulton et al, 2010). The use of micro-organisms such as bacteria and algae has also been explored. These have several advantages in that they are capable of removing nitrates and phosphates to meet safety requirements, and that wastewater naturally provides a stable nutrient source for these organisms (Escapa et al, 2016). However, further research is still required to fully

understand the effects of several biotransformation products and abiotic nitro-products on the environment (Vieno et al, 2014). The use of a bacterial consortium was able to remove 56 % of DCF and were resistant to most antibiotics and heavy metals commonly found in wastewater (Aissaoui et al, 2017).

There are growing concerns in regard to the persistence of DCF; the drug has been shown to have acute toxic effects in bacteria, algae and invertebrates (Ferrari et al, 2003 and Bonnefille et al, 2018) and was responsible for the near extinction of three species of vulture in India (Oaks et al, 2004). Diclofenac was extensively used in this area as a veterinary drug to treat inflammation or other symptoms of disease in cattle. Due to the social and legal need for environmental assessment and monitoring, ecotoxicology faces pressure to produce cost effective, sensitive and reliable tools to detect early impacts before the ecosystem is irreversibly damaged (Feito et al, 2012). To date, several methods for detecting DCF have been reported. These include potentiometry, capillary electrophoresis, HPLC, HPLC–MS, spectrophotometry, spectrofluorometry and gas chromatography (Yilmaz et al, 2015). However, these methods are time-consuming and require sophisticated and expensive instrumentation. Several methods for the rapid determination of DCF in biological samples have been reported, but little other research reported for the quantitative determination of DCF in water supplies. An aptamer-based electrochemical biosensor has recently been developed for the detection and quantification of DCF (Azadbakht et al, 2018). However, the sensitivity of this method is still to be tested for the detection of DCF in the aquatic environment.

Currently there is a shortage of rapid and cost-effective methods for the monitoring of DCF contamination. Electrochemical methods such as biosensors have fast responses, excellent sensitivity and simple operation and could help address some of these challenges. Knowledge relating to the factors involved in urban pollution is essential to support well-informed decision making for developing effective approaches to combat environmental contamination. An Affimer-based biosensor that could detect DCF in the aquatic environment could provide a useful tool in monitoring and quantifying the active compound in water supplies. Furthermore, an Affimer that selectively binds DCF could represent a novel extraction method for improving the capture and removal efficiency of DCF molecules at treatment plants.

3.2.1 Results

A phage display screen was carried out using biotinylated DCF (provided by Dr Robin Bon, University of Leeds). Following three rounds of panning, forty-eight colonies were randomly selected from the test plate and a phage ELISA was carried out to check binding to the biotinylated target (Figure 3.5). Figure 3.5a shows the 96 well ELISA plate, wherein the binding of the forty-eight selected clones was checked against biotinylated DCF (well A1 to H6) and against a negative control (wells with no target present) from well A7 to H12. The absorbance readings were read at 620 nm on a MultiSkan Ascent plate reader (Figure 3.5b).

a.

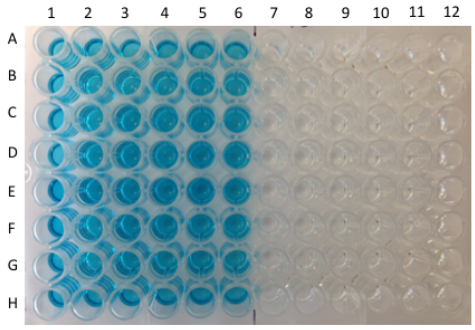

b.

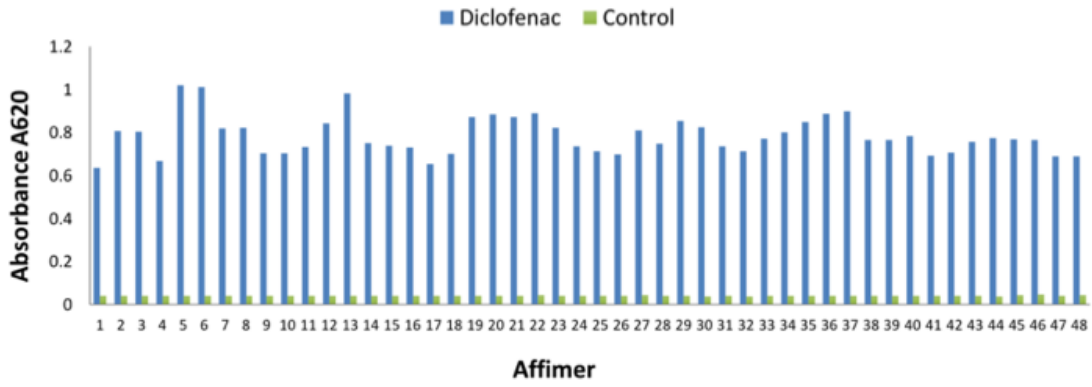

Figure 3.5: Phage ELISA results for Affimer reagents selected against Diclofenac (DCF). **(a)** Following three rounds of phage display against DCF, 48 colonies were tested in a phage ELISA. Each colony represented one Affimer and was tested for binding against Diclofenac or an empty control well. Phage binding was detected with anti-Fd bacteriophage-HRP antibody and visualised on addition of TMB. **(b)** Absorbance at 620 nm was measured for each well.

All of the forty-eight clones displayed a high level of Affimer-target binding with very low levels of binding in the negative control wells. Sequencing and protein alignment in MacVector revealed that all forty-eight clones had identical sequences in both loops of the Affimer scaffold (Section 2.2.1.17) (Table 3.2).

Table 3.2: Variable region sequences for Affimer reagents selected against FPs

Variable region 1	Variable region 2	No. of sequencing appearances
TSMAYMQWG	EEAVYMGWL	48

The selected Affimer was then subcloned from the phagemid vector into a pET11a plasmid for production and purification to allow for future characterisation (Section 2.2.3). The Affimer was subcloned with and without cysteine for possible future downstream labelling. An SDS PAGE gel confirmed the presence of the purified Affimer at ~12 kDa (Figure 3.6).

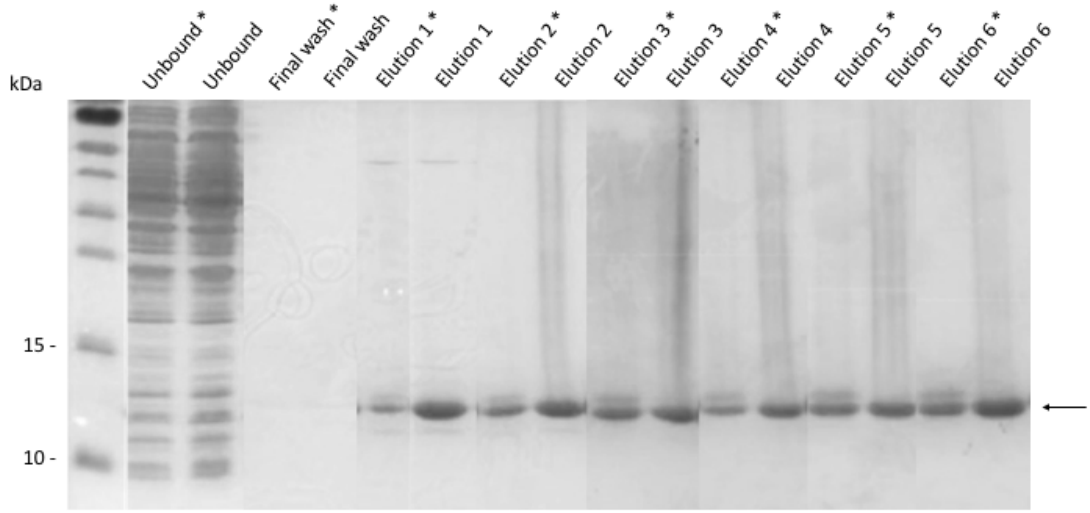

Figure 3.6: Purification of isolated Affimer that binds to Diclofenac. Purified and dialysed Affimer proteins produced from pET11a vector. * indicates the addition of a cysteine. The proteins were purified from bacterial cell lysate using nickel ion affinity chromatography. Proteins were analysed by SDS-PAGE and Coomassie blue staining to confirm purity. The Affimers visualised at 12 kDa as indicated by the arrow.

The purified FP Affimer binders were dialysed into 1x PBS + 10 % v/v glycerol (Section 2.2.3.4.3).

The potential of the DCF-Affimer to be used in a competition ELISA was evaluated. Competition ELISAs are able to quantify the concentration of an antigen in a sample by essentially measuring the interference. Free-DCF competes with the immobilised DCF for Affimer binding. Consequently, the number of Affimers bound to the immobilised DCF decreases with increasing concentration of free-DCF. The higher the free Diclofenac concentration, the weaker the output signal, indicating that the signal output inversely correlates with the amount of Diclofenac in the sample. Following washing, only those Affimers bound to surface-DCF remain in the plate wells to be detected by the HRP-conjugated antibody. This format is commonly used for small sized antigens that usually have limited epitopes (Lisitsyn et al, 2014).

Prior to testing the DCF-Affimer in a competition ELISA, the concentration of Affimer required for these assays was determined. A gradient of concentrations of DCF-Affimer were tested against immobilised DCF in an ELISA in order to determine a concentration of Affimer that gives a strong absorbance measurement but which does not fully saturate the target. Any excess Affimer in the assay could bind to the free-DCF and prevent it from competing with immobilised DCF. Initially concentrations of DCF-Affimer ranging from 0.1 to 10 µg/mL were tested (Figure 3.7).

a.

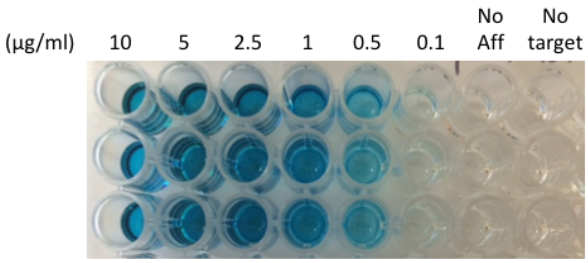

b.

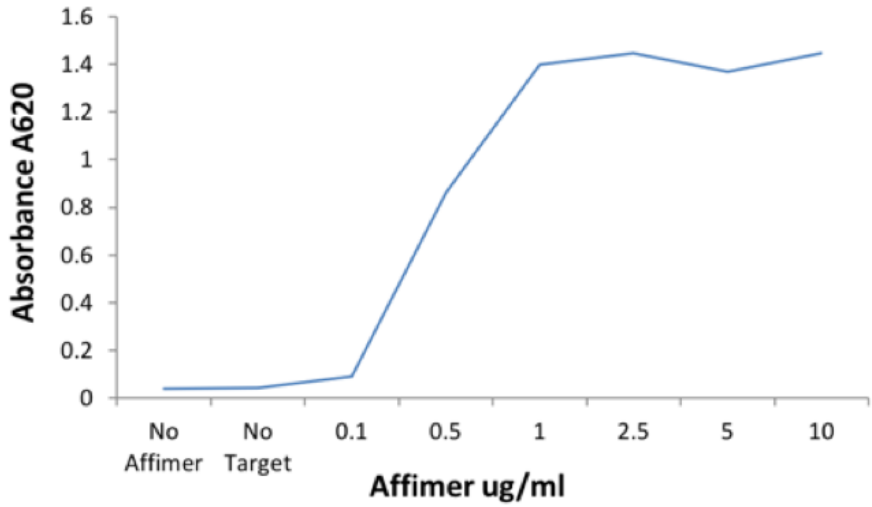

Figure 3.7: Direct ELISA using a gradient of concentrations of DCF Affimer. Concentrations of DCF-Affimer ranging from 0.1 to 10 µg/ml were introduced to immobilised DCF. Bound Affimer was detected using Anti-6x His Tag antibody conjugated with HRP and visualised upon addition of TMB **(a)** ELISA plate wells showing the TMB colour product (each triplicate of wells corresponds to different concentration of Affimer, including negative controls) **(b)** Average absorbance measured at 620 nm plotted against Affimer concentration in µg/ml.

From this initial ELISA it was evident that a concentration of 1 µg/ml DCF-Affimer or greater was fully saturating the immobilised DCF. To obtain a more accurate estimate the ELISA was repeated using concentrations of Affimer between 0.1 and 0.5 µg/ml (Figure 3.8).

a.

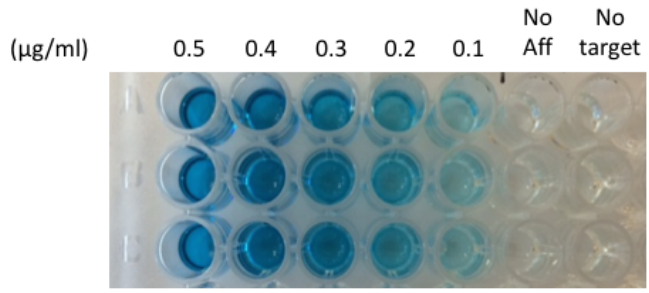

b.

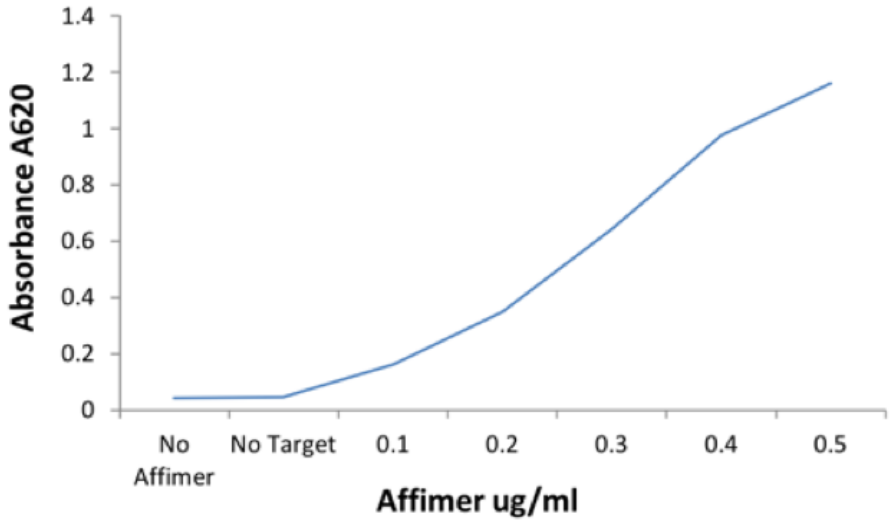

Figure 3.8: Direct ELISA using a gradient of concentrations of DCF Affimer. Concentrations of DCF-Affimer ranging from 0.1 to 0.5 µg/ml were introduced to immobilised DCF. Bound Affimer was detected using Anti-6x His Tag antibody conjugated with HRP and visualised upon addition of TMB **(a)** ELISA plate wells showing the TMB colour product (each triplicate of wells corresponds to a different concentration of Affimer, including negative controls) **(b)** Average absorbance measured at 620 nm was plotted against Affimer concentration in µg/ml.

A concentration of 0.2 µg/ml DCF-Affimer was selected as the concentration that gives a good visible signal without fully saturating the target and was used for all subsequent ELISA experiments.

Once the concentration of Affimer to be used had been determined, a DCF-Affimer competition ELISA was performed in collaboration with a visiting PhD student, Eleni Koutsoumpeli, from the University of York (Figure 3.9) (Section 2.2.3.5.5). DCF-Affimer was used at the pre-determined concentration of 0.2 µg/mL (equivalent to 15.8 nM), while the free-DCF solution concentrations ranged from 16 nM (1:1 molar ratio of Affimer to DCF) to 16 µM (1:1000 ratio). The absorbance readings were read at 620 nm on a MultiSkan Ascent plate reader.

a.

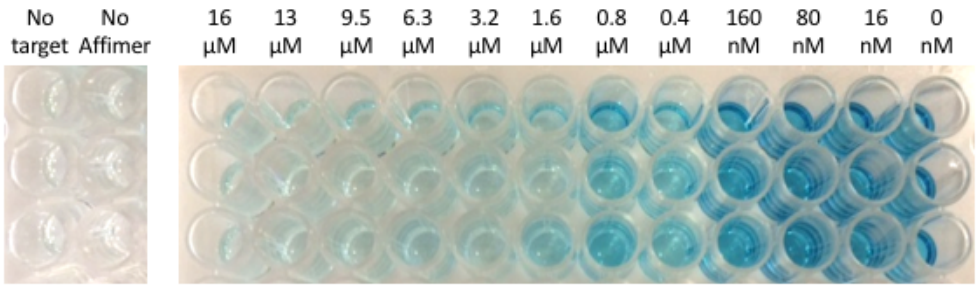

b.

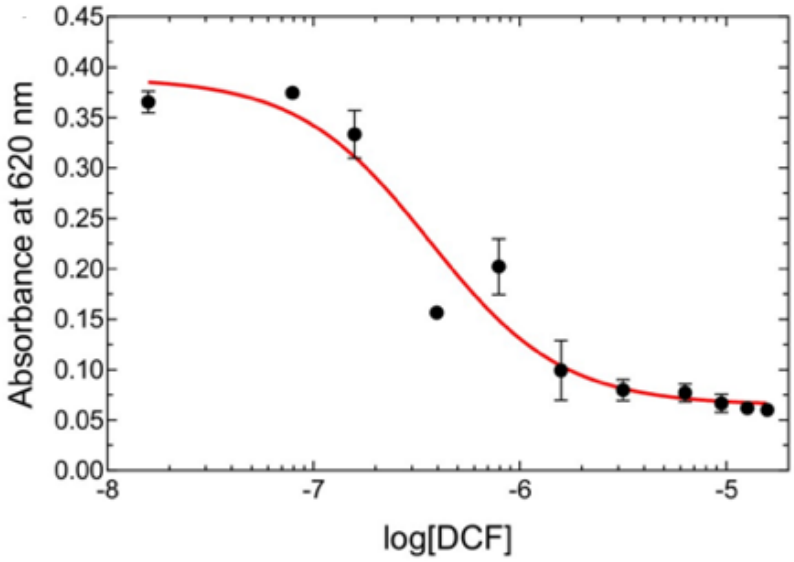

Figure 3.9: Competition Diclofenac (DCF)-Affimer ELISA: DCF-Affimer concentration was 0.2 µg/mL (equivalent to 15.8 nM) whilst free DCF solution concentrations ranged from 16 nM to 16 µM. Affimer bound to immobilised DCF was detected using Anti-6x His Tag antibody conjugated with HRP and visualised upon addition of TMB **(a)** ELISA plate wells showing the TMB colour product (each triplicate of wells corresponds to different concentration of free-DCF, including negative controls) **(b)** Absorbance measured at 620 nm plotted as a function of the logarithm of DCF concentration (red line shows 4PL curve fitting).

At higher free-DCF concentrations the measured absorbance signal was decreased, showing that the free-DCF exhibited considerable competition with the immobilised DCF for binding with the Affimer. The response was plotted against the logarithm of DCF concentration and the data were fitted using a four parameter logistic (4PL) curve, which is the curve typically used for concentration-response data in competition assays:

$$Y = \text{bottom} + (\text{top} - \text{bottom}) / (1 + 10^{((\text{LogIC50} - X) * \text{Slope})})$$

where Y is response, X is the free-DCF concentration, *bottom* is response at infinite free DCF concentration, *top* is response when the free DCF is absent and *slope* refers to the steepness of the curve. The IC_{50} (inhibitory concentration) is the concentration of competitor causing 50 % inhibition of binding (50 % inhibition of DCF-Affimer binding to immobilised DCF due to free-DCF). The curve was shown to be a good model of the experimental data ($R^2 = 0.941$) and yielded an IC_{50} of 0.36 µM.

3.3 Affimers against prokaryotic biofilms as potential diagnostic tools for infective endocarditis

Infective endocarditis (IE) is an infection of the inner lining of the heart and heart valves, most commonly caused by *Staphylococcus aureus*. Although incidence is rare, it is associated with high morbidity and mortality (Hoerr et al, 2018). With an increasingly aging population there has been an increase in cardiac associated conditions such as symptomatic bradycardia and degenerative heart valve disease including aortic stenosis and mitral regurgitation. Subsequently the number of invasive procedures such as pacemaker implantation and valve replacement have also increased (Thuny et al, 2012). *Staphylococcus aureus* are capable of forming biofilms on these cardiovascular prostheses, complicating the diagnosis and treatment of infective endocarditis. Bacteria that grow as biofilms are far more resistant (100 to 1000 times) to antimicrobial agents than their planktonic counterparts, often necessitating surgical intervention; this prolongs hospitalisation and increases the risk of recurrent infections (Ceri et al, 2009).

The poor outcome of patients acquiring IE is partly due to the non-specific clinical presentation and a lack of biomarkers resulting in a shortage of diagnostic methods for detecting the disease (Habib et al, 2015). The Duke criteria are the current standard for diagnosis of IE and are based on clinical presentation/symptoms, laboratory

parameters, imaging, and microbiology (Li et al, 2000). Microbiological culture is considered the most sensitive and reliable for diagnosis, but these tests are time consuming, require trained technicians and are not suitable for bedside use. Additionally, possible infections are often pre-treated with antibiotics before confirmation of a diagnosis which hampers results (Hoerr et al, 2018). Rapid detection and identification of the causative pathogen is required for timely and targeted therapy. There is a subsequent need for culture-free diagnostic assays that can be carried out rapidly, and maintain a high degree of sensitivity and specificity.

A number of biosensors have been developed to try and fulfil this requirement. Examples include those that utilise MEMS (Micro Electro Mechanical Systems) (Ceylan Koydemir et al, 2011) and SPR (surface plasmon resonance) (Tawil et al, 2013). One study reported the development of a biosensor called LPG-ISAM (long period grating – ionic self-assembled multilayer) (Bandara et al, 2015). The LPG-ISAM consists of an ISAM deposited on the surface of an optical fibre which can be conjugated to monoclonal antibodies that bind to methicillin-resistant *S. aureus* strains (MRSA). When binding occurs there is a change in the emitted light. The LPG-ISAM biosensor can provide results in 1 hour. However, this device relies upon the production of expensive monoclonal antibodies and the optical fibre and functional coating need replacing after each use; adding to the production costs and making it unsuitable for high-throughput testing.

Biosensors that incorporate engineered biorecognition elements are able to recognise bacteria but have higher stability than enzymes or antibodies (Hoyos-Nogues et al, 2018). A DNA aptamer-based detection system that recognises live MRSA cells has been developed (Turek et al, 2013). Aptamers that bind to MRSA cells are selected by SELEX and then conjugated to gold nanoparticles. MRSA cells are added and unbound nanoparticles removed. MRSA cells that are bound to the aptamers are then visualised using transmission electron microscopy. Although two of the selected aptamers bound selectively to strains of MRSA and did not bind to *E. faecalis*, they were not able to differentiate between strains of MRSA. In addition, the use of transmission electron microscopes makes this a costly method of analysis.

Hospital-acquired and community-acquired *Staphylococcus aureus* infections have different spectrums of antimicrobial susceptibility and therefore early detection of the specific strain could provide healthcare professionals with vital information as to the most efficient antimicrobial treatments for effective eradication and to the known risk factors associated with the infecting strain. Additionally, rapid results could lead to earlier isolation of infected patients and therefore lower rates of transmission. In this regard, biosensors are now being investigated as attractive alternatives to traditional methods for detecting pathogens. An Affimer-based biosensor that could detect *Staphylococcus aureus* infections and differentiate between strains could allow for the early detection and treatment of infective endocarditis, reducing morbidity and mortality rates and allowing faster control actions in healthcare units.

3.3.1 Results

A modified phage display screen was carried out using the phage display method for non-biotinylated targets as described previously (Section 2.2.2.4.1.1). Three strains of *Staphylococcus aureus* were used (provided by Dr Kenneth McDowall, University of Leeds): SH1000, USA300 and UAMS-1 (Table 3.3). The three strains were grown as biofilms by PhD student Fayez Alsulaimani, University of Leeds.

Table 3.3: *Staphylococcus aureus* strains used in this study

Strain	Description
S. aureus SH1000	*S. aureus* 8325-4 lineage with functional rsbU
S. aureus UAMS-1	oxacillin-susceptible clinical isolate
S. aureus USA300	methicillin-resistant *S. aureus*

To isolate Affimers that bind specifically to biofilms of each individual strain, naïve phage library was pre-panned against a mixed combination of biofilm from the other two strains. Three rounds of panning were carried out. On the final pan, the pre-panned phage was split and panned against biofilm from the target strain, a negative control (magnetic beads) and controls (biofilm from the other two strains). The number of phage-infected colonies on each plate was recorded (Figure 3.10).

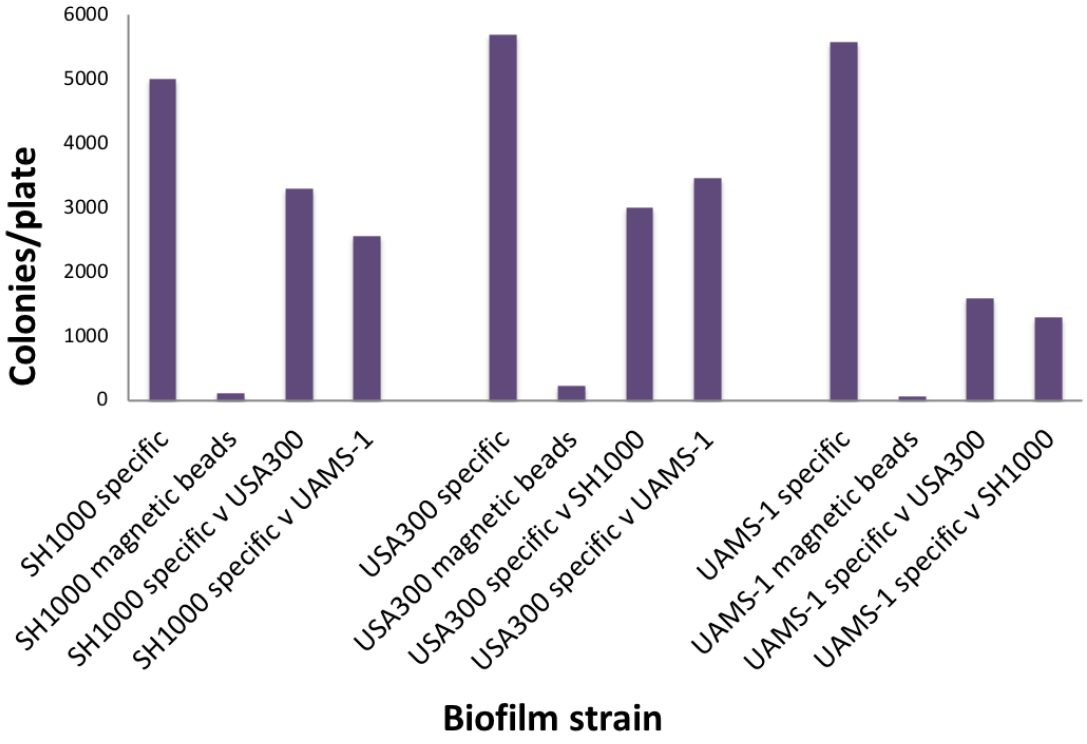

Figure 3.10: Numbers of phage infected colonies after panning to isolate Affimers that bind specifically to individual strains of *S. aureus*. Following three panning rounds, eluted phage were incubated with ER2738 cells and plated onto LB carb agar plates. The following day, the number of colonies on each agar plate were counted and recorded for each strain of biofilm. Isolated phage were also split and panned against magnetic beads (negative) and the other two strains (controls).

A ~1.5 to 3-fold increase in the number of colonies on the strain specific plates compared to the control plates was observed and suggested that some of the selected Affimers might be strain specific. Additionally, low levels of non-specific binding to magnetic beads was observed. Further study of these isolated Affimers was carried out by PhD student Fayez Alsulaimani, University of Leeds. Binding of the isolated Affimer proteins to the three strains of *Staphylococcus aureus* was confirmed by ELISA and the results are summarised in Figure 3.11.

Affimer	SH1000	UAMS-1	USA300
UAMS-1_1	NS	++	+++
SH1000_2	NS	+	+
SH1000_10	+	+++	+
UAMS-1_11	NS	+++	+
SH1000_27	NS	NS	NS
SH1000_30	+++	NS	NS
SH1000_31	+++	+++	+++
USA300_49	+++	+++	+++
USA300_50	NS	+++	++++
USA300_51	NS	NS	++++
USA300_65	+	+++	+++
Anti-Actin	NS	NS	NS

Figure 3.11: ELISA screen to confirm Affimer binding to *S. aureus* strains.
+ = P< 0.01, ++ = P<0.001, +++ = P<0.0001, ++++ = P<0.00001, NS = non-significant.
P value for screening ELISA results was calculated based on *S. aureus* biofilm specific Affimers compared to non-biofilm specific anti-Actin Affimer. This was done in triplicates and also done blind. (carried out by PhD student Fayez Alsulaimani, University of Leeds)

Affimer reagents that bound specifically to SH1000 and USA300 were identified (SH1000_30 and USA300_51). However, Affimers raised against UAMS-1 also displayed binding to USA300 (UAMS-1_1 and UAMS-1_11). Several Affimers bound to all three *S. aureus* strains.

To isolate Affimers that bind specifically to cells grown as biofilms of each individual strain, but not to planktonic cells of that strain, a phage display screen was performed (Section 2.2.2.4.1.2). Negative selection was performed by pre-panning the naïve phage library against planktonic cells. Following the final pan, the pre-panned phage was split and panned against biofilm cells from the target strain, a negative control (magnetic beads) and controls (planktonic cells of the same strain as the target). Eluted phage were incubated with ER2738 cells and plated onto LB carb plates. The number of phage-infected colonies on each plate was recorded (Figure 3.12).

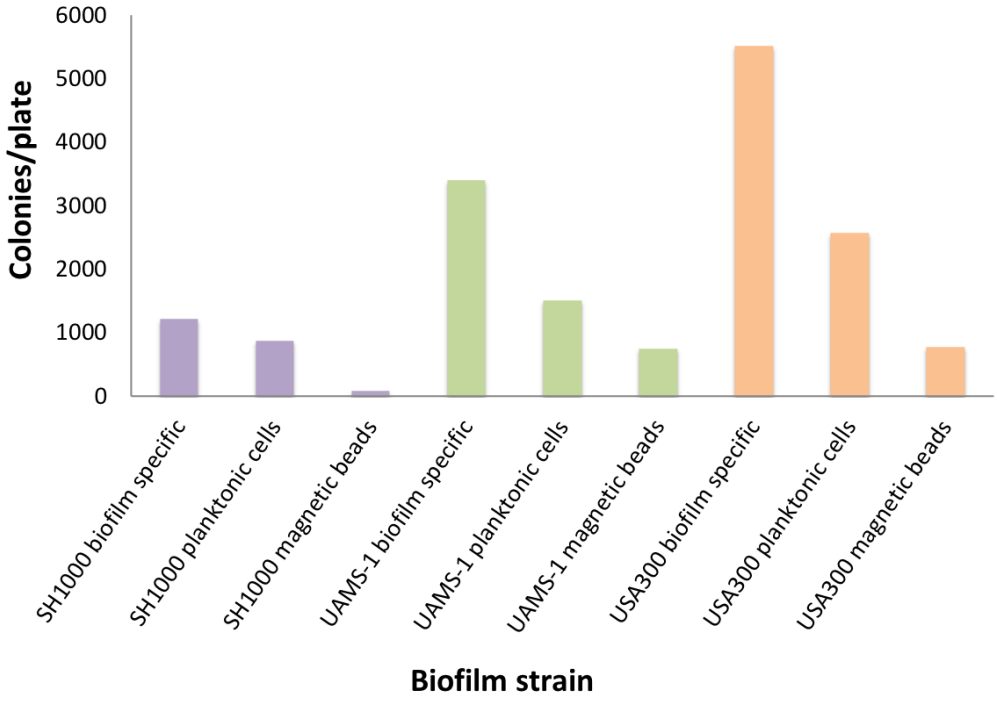

Figure 3.12: Numbers of phage infected colonies after panning to isolate Affimers that bind specifically to *S. aureus* cells grown as biofilms. Following three panning rounds, eluted phage were incubated with ER2738 cells and plated onto LB carb agar plates. The following day, the number of colonies on each agar plate were counted and recorded for each strain of biofilm. Isolated phage were also split and panned against magnetic beads (negative) and planktonic cells from the same strain (control).

A ~2-fold increase in the number of colonies on the UAMS-1 and USA300 biofilm specific plates compared to the corresponding planktonic control plates suggests that some of these Affimers may bind specifically to cells grown as biofilms. Fewer colonies were observed for the SH1000 strain but there was a small increase compared to the negative and control plate. Additionally, relatively low levels of non-specific binding to magnetic beads was observed.

3.4 Chapter summary and future work

Isolation of Affimer reagents against individual fluorescent proteins for imaging applications

One significant advantage of phage display screening is the ability to isolate highly specific binding reagents through counter-screening against homologous target molecules (Tang et al, 2017). Using this technique in combination with the Affimer library, we were able to isolate binders that bind specifically to eGFP, CFP or YFP. Two of the selected Affimers bound to both eGFP and CFP but did not bind to YFP. As eGFP and CFP were shown to be 70 % homologous this was not unsurprising and might suggest a common binding site. This ability to isolate Affimers that are able to differentiate between highly homologous targets was recently demonstrated in a study that identified Affimer reagents that bind specifically to Fc gamma receptors that share 98 % homology (FcγRs) (Robinson et al, 2018). Although YFP does share slightly less homology with CFP and eGFP, the sequences of all three are still markedly similar, suggesting that the Affimer we have isolated as a YFP-specific binder may bind at a divergent site to that of the other two proteins. Alternatively, YFP may have a different structural conformation wherein a possible common binding site of the other two proteins is not accessible to the Affimer. As has been demonstrated in other Affimer studies, X-ray crystallography could also be performed in order to determine the binding sites of the Affimers to all three fluorescent proteins to help elucidate the mechanisms of specificity (Hughes et al, 2017 and Robinson et al, 2018).

These results provide further evidence of the ability to isolate Affimer reagents capable of differentiating between protein targets sharing high homology. As has now been demonstrated, they offer similar benefits to nanobodies and aptamers when utilised for super resolution microscopy (Schlichthaerle et al, 2018), and have the additional advantage in that they negate the need to use animals for their generation. The preliminary results reported here suggest that these Affimers could offer similar advantages in imaging applications, and may offer a further alternative for targeting GFP-tagged proteins with organic fluorophores. It would also be interesting to determine whether the Affimer reagents isolated in this report could be utilised

similarly to the GFP-nanobodies for the purification of fluorescent protein fusions from cell extracts. A further useful property of non-antibody binding proteins is their ability to function in the cytosol, enabling live cell imaging. Nanobodies that target FPs have exploited this capability for targeting multiple endogenous proteins in live cells (Klein et al, 2018). Similarly, Affimer reagents have been shown to be well tolerated when imaging actin in live cells (Lopata et al, 2018), opening up avenues for the use of the FP Affimers described here in similar multiplexed imaging applications in the future.

Identifying Affimer reagents that bind small molecules

Using the Affimer scaffold, we have isolated a novel binding reagent to the small molecule drug, Diclofenac. Of the forty-eight individual colonies isolated by phage display, one unique sequence was identified. This is perhaps unsurprising given the small size of the target (~0.3 kDa) and suggests a limited number of binding sites.

Whilst direct ELISA assays are able to give an indication of molecular interactions, competition ELISAs are normally used for the detection of small molecules in the field. The potential of the isolated DCF-Affimer to be used in a competition assay format was therefore evaluated. Results showed strong competition between free-DCF and immobilised-DCF and a 4PL curve was plotted, showing a decreasing trend that corresponded to increasing free-DCF concentration. This also eradicates the possibility that an Affimer could have been isolated that binds partially to the biotin linker as such an Affimer would not be able to bind to free-DCF.

The IC_{50} is considered to be a good measure of the estimated binding inhibition potency of the free-DCF in the competition ELISA (Cox et al, 2012). The IC_{50} of 0.36 µM estimated here is higher than those reported for antibody-based competition ELISAs for Diclofenac detection in other studies (Huebner et al, 2015 and Rau et al, 2014). The detection limit of the assay can be estimated as the blank signal + three standard deviations and was calculated to be 75 nM (106 µg/L) (Shrivastava et al, 2011). Although this detection limit is not low enough to detect environmentally relevant concentrations of diclofenac (typically low picomolar), the results are promising and optimisation of the assay could bring the detection limit within the required range.

A recent study has demonstrated that Affimer reagents can be successfully selected against small organic compounds such as the 0.2 kDa chemical 2,4,6-trinitrotoluene (TNT) (Tiede et al, 2017). This ability to isolate Affimer binders that detect small molecules represents a useful tool for the generation of reagents that can be used for diagnostic and monitoring applications in health, security and environmental settings. The competition ELISA data presented here are preliminary results which further demonstrate the potential of Affimers as bioreceptors in immunoassays for the detection of small molecules. Affimers have already demonstrated potential for use as highly sensitive capture reagents in biosensor platforms (Sharma et al, 2016 and Zhurauski et al, 2018). While further work is needed to optimise the ELISA protocol, the results are very promising and suggest that Affimer-based assays could be incorporated into biosensors for rapid on-site monitoring of contaminants in the environment. There could also be potential in incorporating Affimers into an additional purification stage in water treatment processes for the capture and removal of micro-pollutants.

Affimers against prokaryotic biofilms as potential diagnostic tools for infective endocarditis

We have demonstrated the use of phage display for the selection of novel Affimer binding reagents capable of distinguishing between two strains of *Staphylococcus aureus* grown as biofilms. It was perhaps slightly surprising that no Affimer reagents were isolated that bind specifically to UAMS-1 as there were fewer colonies recorded for this strain when it was panned against the other two *S. aureus* strains. The ELISA demonstrated that isolated binders for UAMS-1 also bound to USA300. This suggests that the selected Affimers may bind to identical epitopes on these two strains. Future identification of the bound epitopes for all of the isolated Affimers is likely to be beneficial as it may allow rational modification of the Affimer sequence to tailor binding parameters. Additionally, optimisation of the phage display protocol to include more stringent negative selection steps might allow for the future identification of Affimers that specifically recognise UAMS-1. Characterisation of the Affimer reagents against other species of staphylococci to confirm specificity would also be valuable. It would also be interesting to test these isolated Affimer binders for bacteriostatic or bactericidal activity to determine possible additional therapeutic applications. Affimer

reagents that can differentiate between bacteria grown as biofilm and planktonic cells of the same strain may also have been identified, although further characterisation by ELISA is needed to confirm this.

Staphylococcus aureus is listed as number five on the antimicrobial resistant bacteria threat list published by the World Health Organisation (Willyard, 2017). Its ability to form biofilms on cardiac implants makes it a leading cause of infective endocarditis and better diagnostic methods are needed to identify the presence and species of a biofilm. The preliminary results reported here demonstrate the potential of Affimers for the detection of pathogenic bacteria. As previously mentioned, Affimers have already been demonstrated as highly sensitive capture reagents in biosensor platforms (Sharma et al, 2016 and Zhurauski et al, 2018). While further work is needed to characterise the selected binders, the results are promising and suggest that Affimer-based assays could be incorporated into biosensors for rapid detection and diagnosis of biofilms.

In summary, these results demonstrate the ability of the Affimer scaffold to offer a platform for the selection of novel binding reagents for a wide range of targets, including fluorescent proteins, small molecules and prokaryotic cells. The selected Affimers have the potential for incorporation into novel diagnostics, with huge potential as tools in environmental and health protection settings.

Chapter 4

Isolation & characterisation of NDM-1-specific Affimer reagents

4. Isolation & characterisation of NDM-1-specific Affimer reagents

4.1 Introduction

The β-lactams are the most successful and widely used class of antibiotic drugs but they are vulnerable to inactivation by β-lactamases. New Delhi metallo-β-lactamase 1 (NDM-1) is a class B β-lactam hydrolysing enzyme that confers bacteria with almost complete resistance to all β-lactam antibiotics, including carbapenems; one of the last drugs still effective against multidrug-resistant infections. With only a few new antibiotics discovered in the past 30 years, researchers are now looking for inhibitors to reinstate sensitivity to previously ineffective antibiotics. This strategy has represented a significant milestone in the field of antibacterial discovery, revitalising antibiotics such as amoxicillin, which may be potentiated by the β-lactamase inhibiting clavulanic acid (Ball et al., 1980). However, whilst there are currently four clinically approved serine β-lactamase inhibitors there are still no commercially available metallo-β-lactamase (MBL) inhibitors (McGeary et al., 2017). With few effective antibiotics against NDM-1 expressing bacteria, and resistance developing to those which remain, the search for new and potent MBL inhibitors has become of paramount importance.

The BioScreening technology group had previously isolated Affimer reagents that bind to NDM1 by phage display. NDM-1 protein was a kind gift from Oxford Protein Production Facility (OPPF). NDM-1 was biotinylated using EZ-Link® NH-SS-Biotin, immobilised for phage display and subjected to three rounds of panning using the naïve Affimer phage library. Ninety-six clones were selected at random from the final pan and checked for binding to NDM-1 by phage ELISA (Figure 4.1 a and b). Of the 96 clones tested, 10 were excluded as they did not display binding to the target and 4 were excluded for non-specific binding to the control wells.

a.

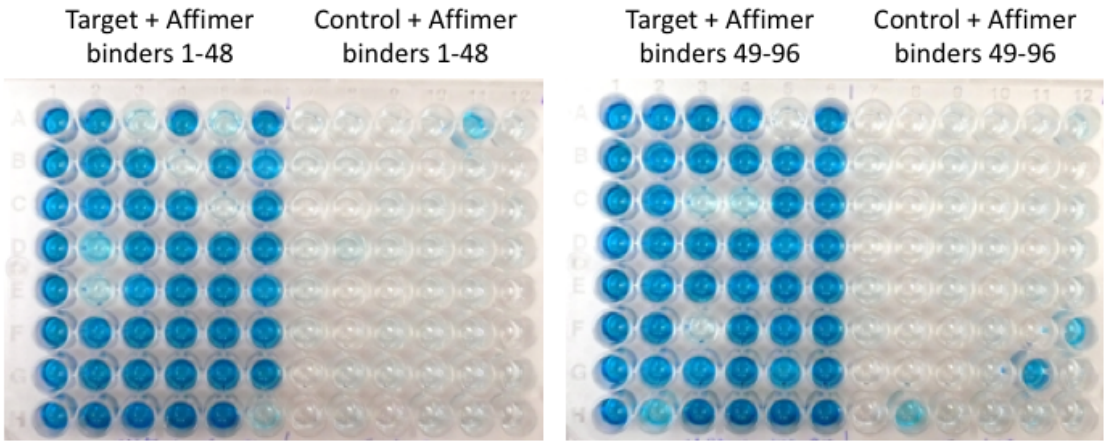

b.

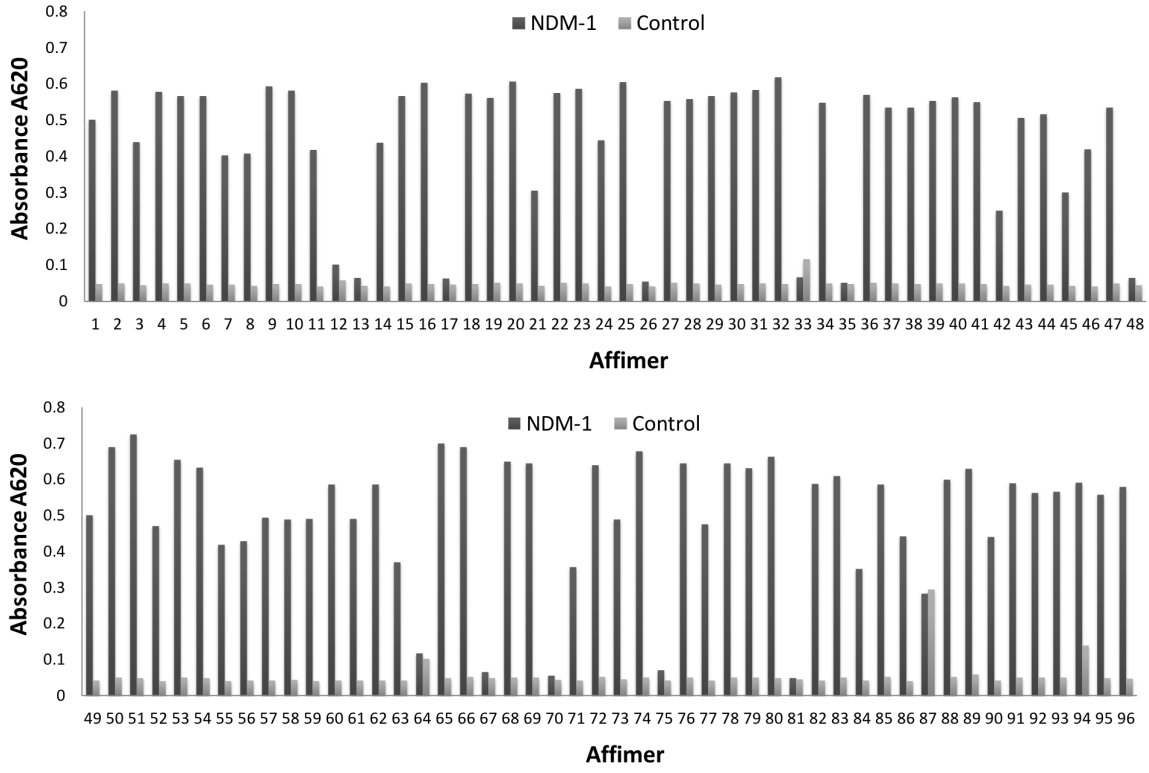

Figure 4.1: Phage ELISA results for Affimer reagents selected against NDM-1. (a) Following three rounds of phage display against NDM-1, 96 colonies were tested in a phage ELISA. Each colony represented one Affimer and was tested for binding against NDM-1 or an empty control well. Phage binding was detected with anti-Fd bacteriophage-HRP antibody and visualised on addition of TMB. **(b)** Absorbance at 620nm was measured for each well.

The 82 Affimer clones that exhibited specific binding to the target were sequenced (Section 2.2.1.17) and 10 Affimer reagents with unique variable regions were identified (Table 4.1).

Table 4.1: Variable region sequences for Affimer reagents selected against NDM-1

Affimer	Variable region 1	Variable region 2	No. of sequencing appearances
1	HSIWHHEIS	KWHGISYMP	1
2	QHVEGWSQV	AHVFKKSPK	54
3	AAVIEFLEV	TFHSGIKWR	17
21	GYKVWTPYG	THWDNGGLR	2
45	SQFNDMGEV	MIGSLVKWR	1
59	GRGPNHWRE	RYVKQDEWH	2
71	NAQIQYMHV	YFKGDVLWR	2
73	EYWVENMKV	RIGNMWFWR	1
75	VAKKMVQMY	FYKHQPIMF	1
95	QHSPPNWRE	GYYRNFHMR	1

Affimers 2 and 3 were identified 54 and 17 times respectively, which may suggest that these binders have either a higher affinity or are preferentially expressed on the pIII coat protein of the bacteriophage. A sequence logo indicates a prevalence of a valine residue at position 1.9 (variable region 1, position 9), a tryptophan at position 2.8 and either arginine, histidine or a lysine (positively charged side chains) at position 2.9 (Figure 4.2).

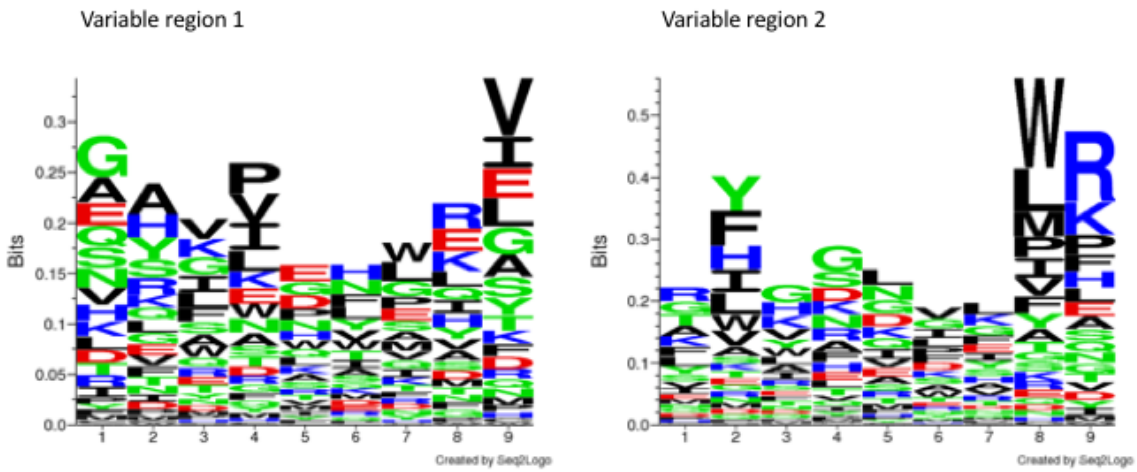

Figure 4.2: Sequence logo Sequence logo analysis of the two variable regions for the ten isolated Affimers gives a visual representation of amino acid consensus. Large symbols represent frequently observed amino acids, big stacks represent conserved positions and small stacks represent variable positions. Basic amino acids are coloured black, acidic amino acids are red and both polar and non-polar are green. Created using Seq2Logo (Frolund Thomsen et al, 2012)

Here we describe the characterisation of NDM-1 binding Affimer reagents. Validation by β-lactamase activity assays identified any Affimer reagents that have intrinsic effects on NDM-1 activity, with further characterisation conducted by kinetic analysis and bacterial and mammalian cell assays.

4.2 Results

4.2.1 Investigating the effects of isolated Affimer reagents on NDM-1 activity

Antibiotics containing β-lactam rings are highly susceptible to being hydrolysed by enzymatic activity, which deactivates their antibiotic potency. Nitrocefin is a chromogenic cephalosporin that lacks antibiotic potency but contains the characteristic β-lactam ring and is therefore susceptible to β-lactamase mediated hydrolysis. Upon hydrolysis, the absorption spectrum of nitrocefin shifts from intact (yellow) at 386 nm to hydrolysed (red) at 482 nm. This change in absorption can be measured over time and allows estimation of activity of a given β-lactamase enzyme based on the rate at which it hydrolyses nitrocefin (O'Callaghan et al., 1972, Meini et al., 2015). The 10 isolated Affimer binders that bind NDM-1 were sub-cloned into pET11a for production and purification (Section 2.2.3) then dialysed into 1x PBS + 10 % v/v glycerol (Figure

4.3a). Affimer 75 and 95 initially had very low production yields and were almost completely lost following dialysis. Production and purification of these two Affimers was therefore repeated and yields were improved (Figure 4.3b).

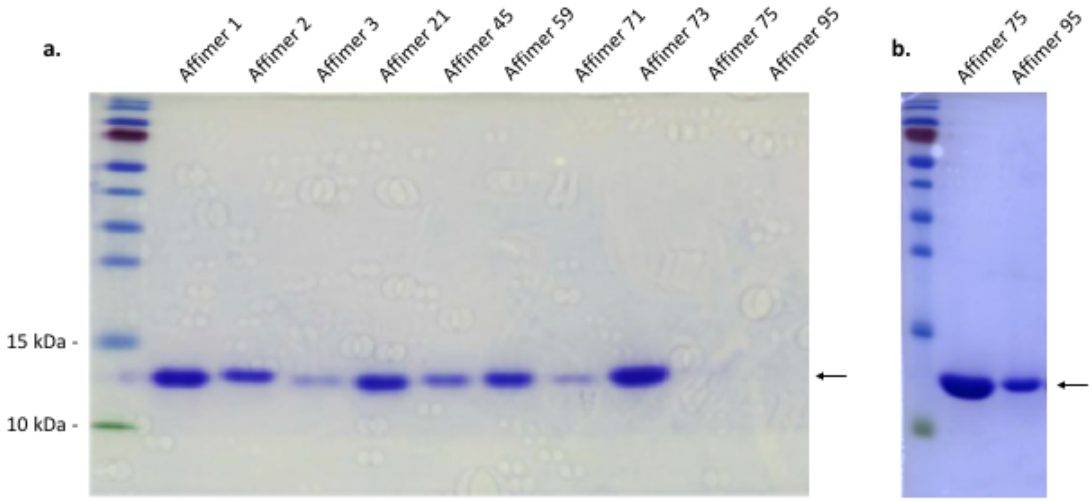

Figure 4.3: Purification of isolated Affimers that bind to NDM-1 (a) Purified and dialysed Affimer proteins produced from pET11a vector. The proteins were purified from bacterial cell lysate using nickel ion affinity chromatography. Proteins were analysed by SDS-PAGE and Coomassie blue staining to confirm purity. The Affimers visualised at 12 kDa as indicated by the arrow. Affimer 75 and 95 had very low yields **(b)** Production and purification of Affimer 75 and 95 was repeated as before. Proteins were analysed by SDS-PAGE and Coomassie blue staining to confirm purity. The Affimers visualised at 12 kDa as indicated by the arrow.

The 10 purified Affimer proteins were tested in β-lactamase activity assays with nitrocefin as the substrate (Section 2.2.5.1), to determine whether they had any effect on NDM-1 enzyme activity. Reactions included 100 nM NDM-1, 10 μM clavulanic acid, 200 nM of Affimer and 65 μM nitrocefin and all Affimer isolates were normalised to the EDTA control. As discussed previously, NDM-1 belongs to the metallo-β-lactamase (MBL; class B) family and relies upon Zn^{2+} in the active site to catalyse hydrolysis. EDTA is a potent zinc chelating agent (Auld D., 1988) and on addition of NDM-1, will sequester Zn^{2+} from the active site and render the enzyme inactive, serving as a positive control for enzyme inhibition. An Affimer that binds to yeast SUMO was used as a negative control to demonstrate that non-NDM-1 binding Affimer reagents have little effect on NDM-1 enzymatic activity. Additionally, a NDM-1 only control containing no Affimer

demonstrated the maximum rate of nitrocefin hydrolysis. Absorbance at 482 nm was plotted over time (s) to give an initial indication of trend (Figure 4.4a). After 3 replicate experiments, absorbance values measured during the first 250 seconds (during which the rates were constant) were converted to concentration in µM using Beer-Lambert's Law and then to rate in µM/s using linear regression analysis (Figure 4.4b). Of the 10 Affimer reagents tested, Affimer 21 showed a reduction in initial NDM-1 enzymatic activity of 69 % when compared to that of the NDM-1 only control ($p < 0.0001$, R^2 0.9998

a.

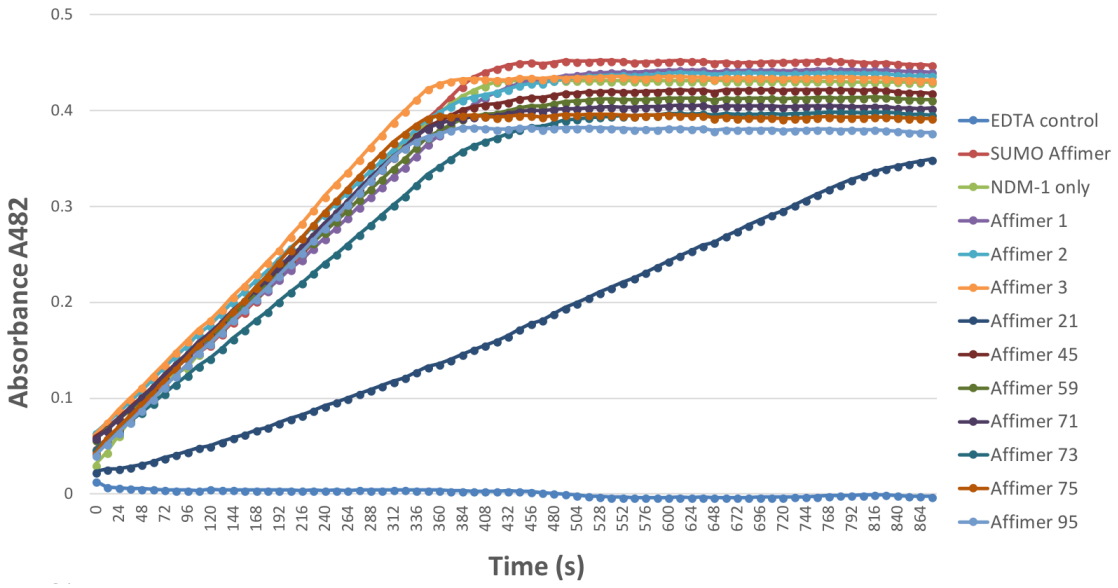

b.

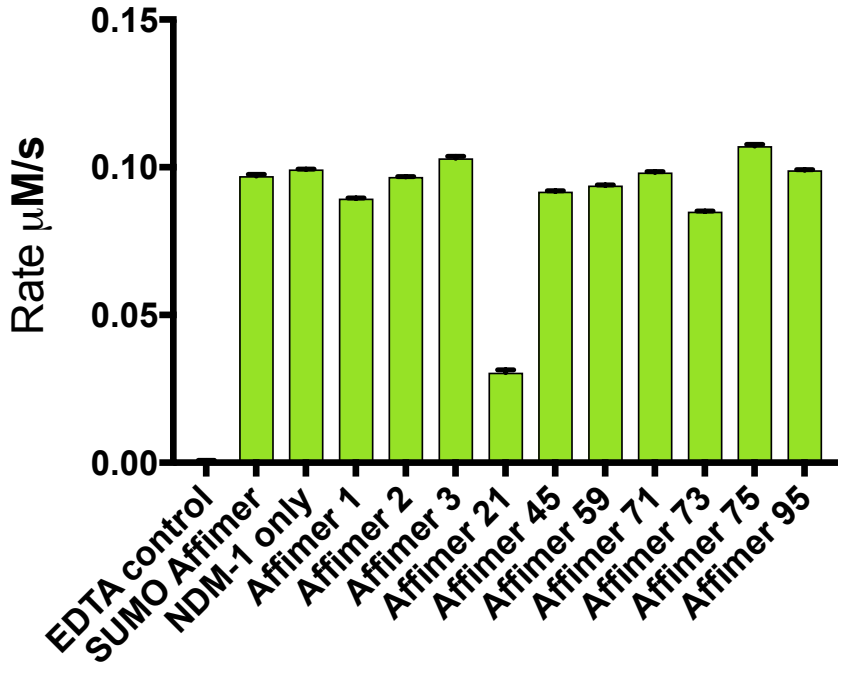

Figure 4.4: Effects of Affimer reagents on rate of nitrocefin hydrolysis by NDM-1. NDM-1 activity was quantified by spectrophotometric measurement of nitrocefin hydrolysis at 482 nm and at 25 °C on a Tecan Spark microplate reader and readings for each well were taken every 12 secs for 15 min. Data was normalised to the EDTA control. **(a)** The change in absorbance at 482 nm for NDM-1 only and upon addition of Affimer was recorded **(b)** Activity of NDM-1 only or with 200 nM Affimer recorded as rate of nitrocefin hydrolysis (μM/s). Error bars represent standard errors from 3 replicate experiments (n = 3).

4.2.2 Characterisation of Affimer 21

4.2.2.1 IC_{50} of Affimer 21

The IC_{50} (inhibitory concentration) is the concentration of inhibitor that causes a 50% decrease in activity of the enzyme and gives a measure of the potency of a substance. To determine the IC_{50} value, Affimer 21 was tested for inhibition of 100 nM NDM-1 in a β-Lactamase activity assay (Section 2.2.5.1) at a range of concentrations (10 nM to 3 μM). Plate wells were set up in triplicate and average absorbance readings calculated. Rate of nitrocefin hydrolysis (μM/s) was calculated over the initial 250 seconds as before, and the data were fitted using a four-parameter logistic curve (4PL), which is the curve typically used for dose response and/or receptor-ligand binding assays:

$$Y = \text{bottom} + (\text{top} - \text{bottom}) / (1 + 10^{((\text{LogIC50} - X) * \text{Slope})})$$

where Y is response, X is the Affimer concentration, *bottom* is response at infinite Affimer concentration, *top* is response when the Affimer is absent and *slope* refers to the steepness of the curve.

The response was plotted against the logarithm of Affimer concentration and the resulting 4PL curve (Figure 4.5) showed a decreasing trend with increasing concentration. The curve was shown to be a good model of the experimental data (R^2 = 0.9978) and yielded an IC_{50} of 0.37 μM.

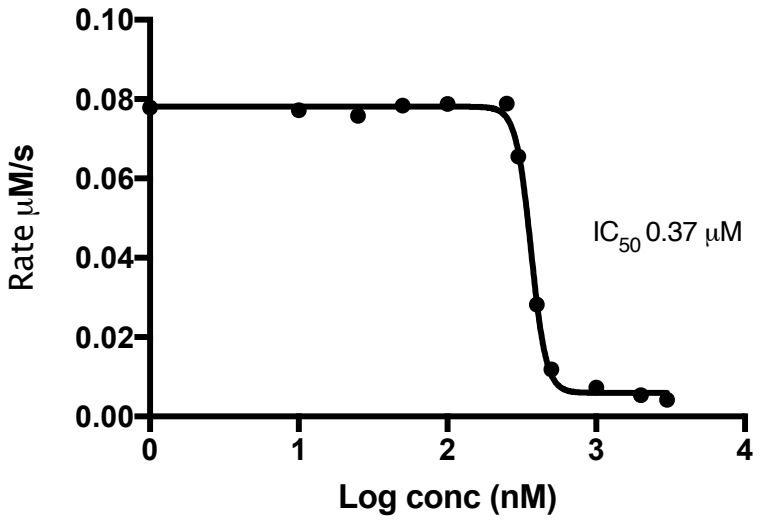

Figure 4.5: IC_{50} of Affimer 21. A four-parameter logistic curve was plotted to determine the IC_{50} value. Rate of nitrocefin hydrolysis (μM/s) by NDM-1 against logarithm of the concentration of Affimer 21 (10 nM to 3 μM) was calculated. IC_{50} was calculated as 0.37 μM, R^2 = 0.9978. n = 1

4.2.2.2 Kinetic analysis of Affimer 21

In order to further characterise the inhibition of NDM-1 by Affimer 21, activity was measured over a range of substrate concentrations with the aim of determining the kinetic parameters k_{cat} and K_M (Section 2.2.5.2). The initial rate of the reaction was recorded and absorbance units were converted to concentration using Beer Lambert's Law before fitting to a Michaelis-Menten curve (Figure 4.6). Kinetic analysis was carried out by undergraduate student, Sophie Saunders, supervised by myself at BSTG, University of Leeds.

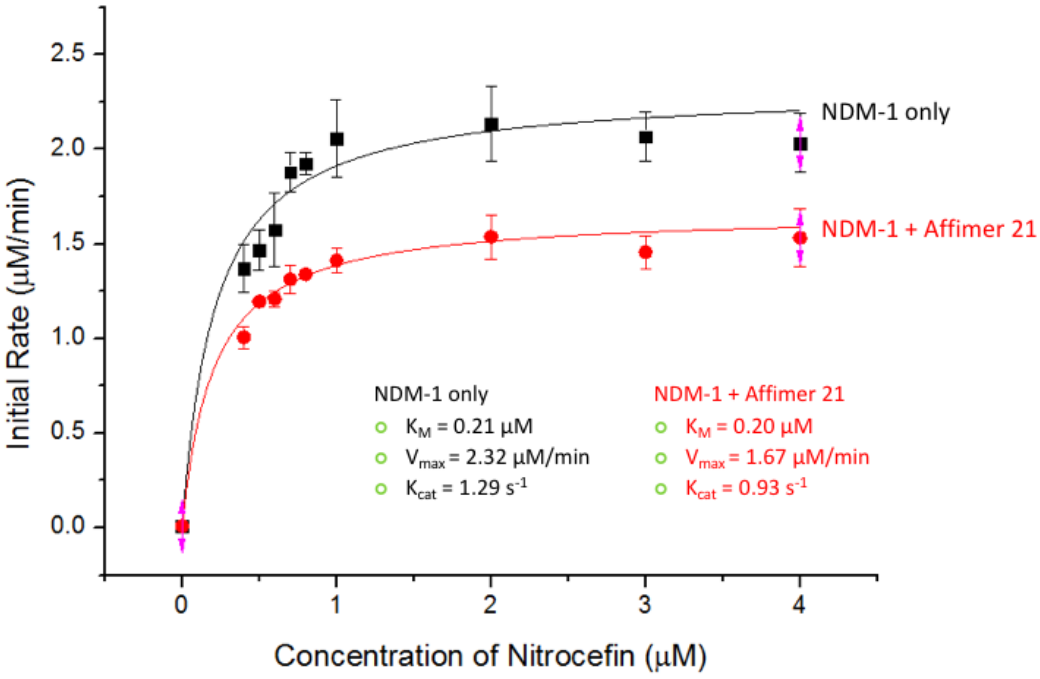

Figure 4.6: Kinetic analysis of inhibition of NDM-1 by Affimer 21. The hydrolysis of a range of concentrations of nitrocefin, 0.4 to 4 µM, by 30 nM NDM1 was measured at 486 nm, 25 °C for 2 min. This was performed with/without 10 nM Affimer 21. Initial rate of reaction was recorded and absorbance units converted to µM/s using Beer Lambert's Law. Kinetic parameters were determined by fitting the plot of rate against substrate concentration to the Michaelis-Menten equation using non-linear regression and reveals that the K_M remains constant and V_{max} and k_{cat} decrease upon addition of Affimer 21 when compared to the NDM-1 only control. All assays were performed in assay buffer. Data was processed using OriginPro 8.6 software. n = 3.

The kinetic efficiency of an enzyme is measured by k_{cat} / K_M and therefore higher values for k_{cat} and lower values for K_M indicate a more efficient enzyme for the reaction measured.

Table 4.2: Kinetic parameters for NDM-1 with and without Affimer 21

	k_{cat} (s^{-1})	K_M (µM)	k_{cat} / K_M (s^{-1} $µM^{-1}$)
NDM-1 only	**1.29**	**0.21**	**6.14**
NDM-1 + Affimer 21	**0.93**	**0.20**	**4.65**

Addition of Affimer 21 resulted in a 25 % decrease in the kinetic efficiency of NDM-1 when compared to the NDM-1 only control. A Lineweaver-Burk plot (Lineweaver et al., 1934) was used to give a visual indication of the mechanism of inhibition (Figure 4.7). Lineweaver-Burk plots were most commonly used prior to the development of non-linear regression software, when curved data had to be transformed in order to perform linear regression (Dowd et al., 1965). Although the V_{max} and K_M values from this kind of plot are unreliable due to distortion of the error by the transformations; it is still useful for giving a visual impression of the different forms of enzyme inhibition.

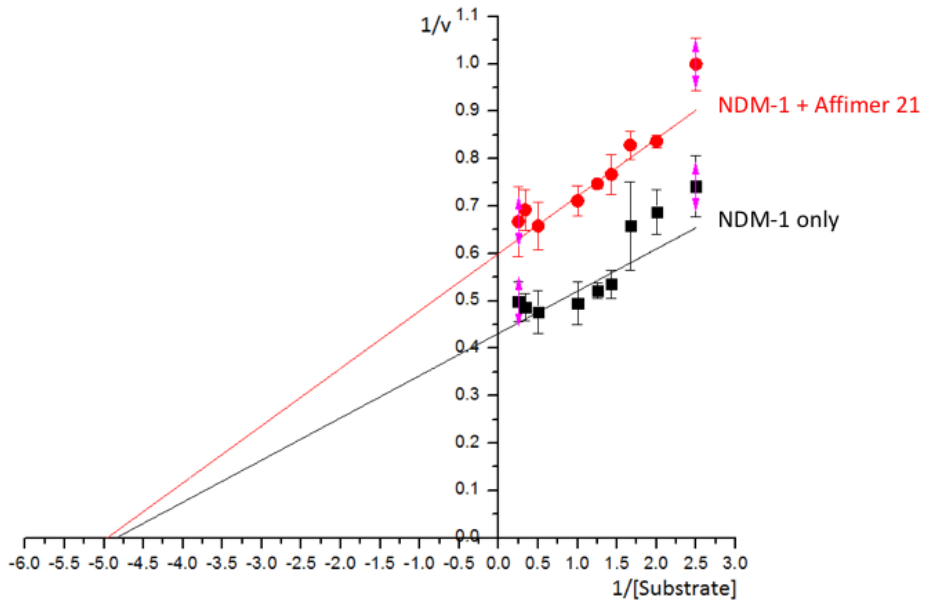

Figure 4.7: Mechanism of inhibition of NDM-1 by Affimer 21. Mechanism of inhibition was visualised using a Lineweaver-Burk (double reciprocal) plot, which plots the reciprocal of substrate concentration vs. the reciprocal of enzyme velocity: 1/rate = (1 / Vmax) + (KM / Vmax [S]). Lineweaver-Burk plot of NDM-1 only and NDM-1 on addition of Affimer 21 suggests non-competitive inhibition. All assays were performed in assay buffer. Data was processed using OriginPro 8.6 software. n = 3

The Lineweaver-Burk plot for NDM-1 with and without Affimer 21 is consistent with a plot that indicates non-competitive inhibition, where K_M is unaffected and therefore both sets of data have the same x intercept; but different slopes and y intercepts (V_{max} is reduced with addition of inhibitor).

4.2.2.3 Binding epitope

Determining the conformational epitope of binding proteins could provide valuable information regarding the binding interaction. Epitopes are generally divided into two classes, linear epitopes where a string of amino acids are sufficient for binding, or conformational epitopes where protein folding is necessary for binding. In western blot analysis, the protein is partially or wholly denatured and can therefore be used to investigate binding to a linearised target (Forsstrom et al., 2015). To determine the binding epitope of NDM-1 required for Affimer 21 binding, NDM-1 and Yeast SUMO proteins were probed with either Affimer 21 or Yeast SUMO 10 Affimer by western blot analysis (Section 2.2.3.5.4) (Figure 4.8).

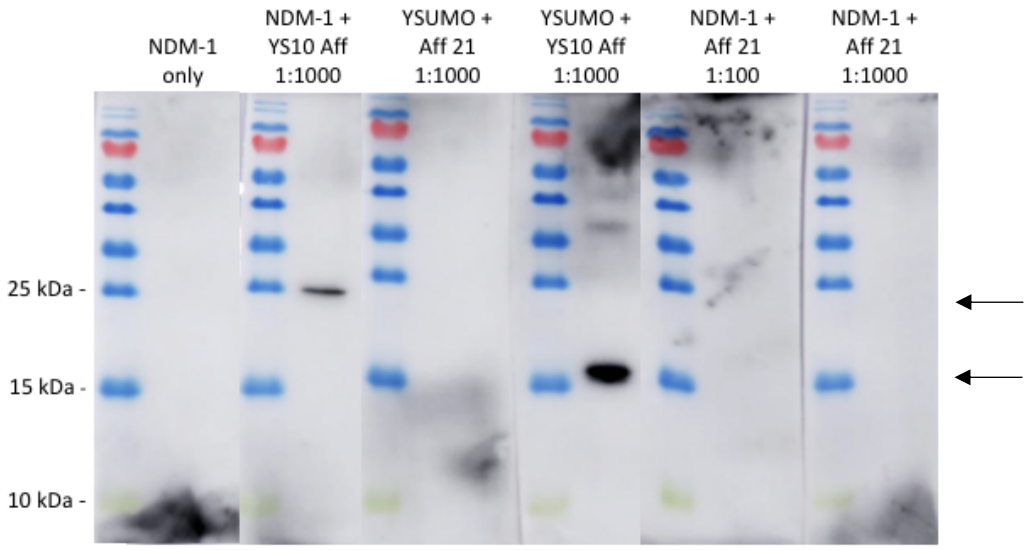

Figure 4.8: Assessment of the binding epitope of NDM-1 required for Affimer 21 binding. NDM-1 and yeast SUMO (YSUMO) proteins (100 ng) were separated according to their mobility by SDS-PAGE on a 15 % resolving gel. Proteins were transferred from SDS-PAGE gels onto a mini format PVDF membrane with 0.2 µm pore size using a Trans-Blot Turbo transfer system and probed with either 0.5 µg (1:1000) or 5 µg (1:100) of Affimer 21 (Aff 21) or Yeast SUMO 10 (YS10) Affimer by western blot analysis. Membranes were visualised using Luminata Forte Western HRP Substrate and chemiluminescence on an Amersham Imager 600). n = 1

Affimer 21 did not show binding to NDM-1 at either concentration, suggesting that a conformational epitope of NDM-1 is needed for Affimer 21 binding. The negative controls NDM-1 only and Yeast SUMO with Affimer 21 showed no binding and the positive control Yeast SUMO with Yeast SUMO 10 Affimer showed strong binding, as expected. Interestingly, the Yeast SUMO 10 Affimer also showed some binding to NDM-1 and had previously indicated a small increase in NDM-1 activity in a β-lactamase activity assay (Figure 4.4). This might suggest that the Yeast SUMO 10 Affimer has low specificity.

4.2.2.4 Effect of Affimer 21 on meropenem activity in *Klebsiella pneumoniae*

Klebsiella pneumoniae is one of the most commonly occurring carbapenem-resistant *Enterobacteriaceae* (CRE) species in the world (Munoz-Price et al, 2013). Infections are normally hospital-acquired and are associated with high mortality and morbidity rates. For the following assays, a clinical isolate of *Klebsiella pneumoniae* known to express the bla_{NDM1} gene was used. The minimum inhibitory concentration (MIC) of meropenem for this strain was determined as 32 µg/ml by MSc student, Ben Lawrence. Cell assays were carried out with an MSc student, Ben Lawrence, under my supervision.

The effect of Affimer 21 on meropenem potency in *Klebsiella pneumoniae* was tested (Section 2.2.6.1) (Figure 4.9). A final concentration of 6 µg/ml meropenem was used, to shorten the lag phase and make dose dependent inhibition visible over the assay period. Affimer 21 restored sensitivity to meropenem in a dose-dependent manner.

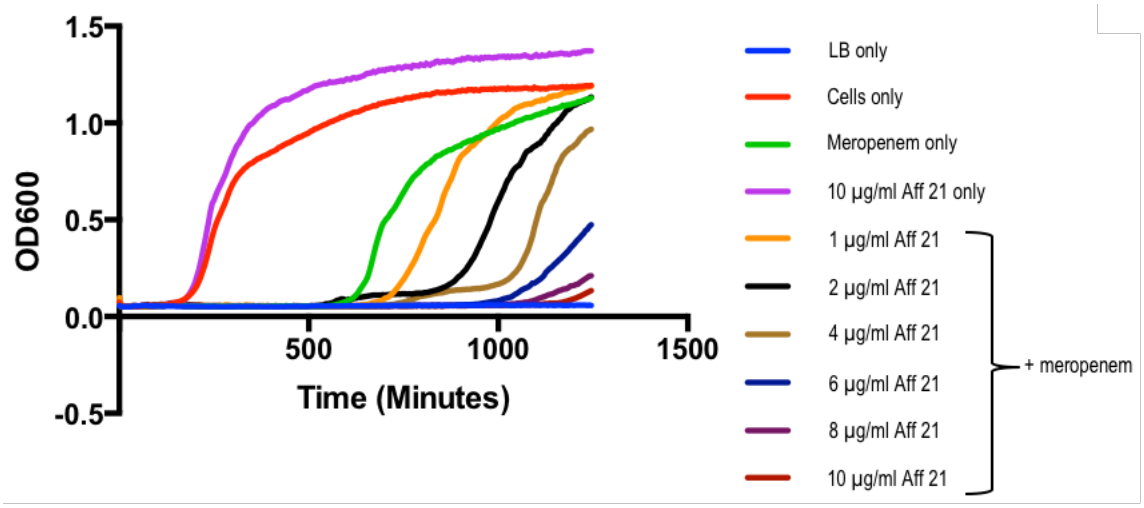

Figure 4.9: Restoration of meropenem potency by Affimer 21 in a clinical strain of *K. pneumoniae* expressing NDM-1. Assays were performed aerobically at 37 °C in a 96-well microtitre plate in a FLUOstar Omega dual orbital shaker. Cell density was assessed by measuring absorbance at OD_{600} every 5 min for 20 h. Meropenem was dosed at 6 µg/ml (0.2x MIC). Affimer 21 was dosed at concentrations between 1 - 10 µg/ml. n = 3

4.2.2.5 Tolerance of Affimer 21 in mammalian cells

An essential quality for any antimicrobial drug is selective toxicity, to selectively kill or inhibit the growth of microbial targets while causing minimal or no harm to the host. Nearly all of the previously reported MBL inhibitors act by zinc binding or chelation (McCall et al., 2000). An inhibitor that acts by sequestering zinc from the active site of NDM-1 might be expected to have off-target effects in mammalian cells due to the large number of human metalloproteins found in the cellular environment. It is therefore critical that any newly reported inhibitors are tested fairly early on in the discovery pipeline for possible cytotoxicity. An initial test for effect of Affimer 21 on survival of mammalian U-2 OS cells was carried out (Section 2.2.6.2) (Figure 4.10). Cell toxicity assays were carried out by an MSc student, Ben Lawrence, who was supervised by myself at BSTG, University of Leeds.

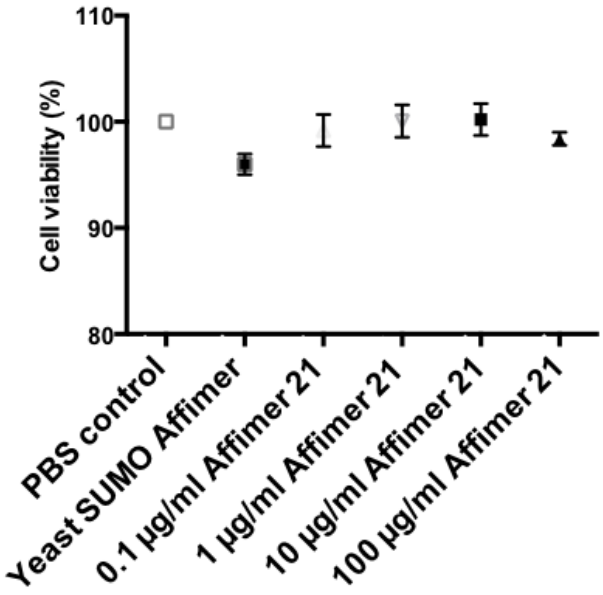

Figure 4.10: Affimer 21 is well tolerated in mammalian cells. U-2 OS cells were cultured in DMEM media supplemented with 10 % v/v FBS and 1 % w/v penicillin-streptomycin for 72 h in 24-well plates. DMEM was replaced with Affimer 21 at concentrations of 0.1 - 100 µg/ml or 100 µg/ml of yeast SUMO Affimer and incubated at 37 °C for 24 h. A Muse® cell counter was used to determine total cell count and % viability. n = 3

Results were subjected to a one-way ANOVA test and there was found to be no significant difference between the PBS control and any concentration of Affimer 21, suggesting that Affimer 21 is well tolerated in mammalian cells.

4.2.2.6 Structural characterisation by crystallography

The crystallisation of proteins depends upon the creation of a solution of protein and precipitant that is supersaturated (McPherson et al., 2014). Supersaturation is achieved beyond the concentration where the protein is soluble (the solubility curve), but before it reaches the point of precipitation (disordered aggregation). The concentration of precipitant changes the position of the solubility curve at a given protein concentration. Figure 4.11 represents a solubility phase diagram and illustrates the relationship between protein and precipitant concentrations. The region of supersaturation is divided into the metastable, labile and precipitation regions. Nucleation (ordered aggregation) of crystals occurs in the labile region, which reduces the protein concentration in the solution and drives the process back into the metastable region, where sustained crystal growth can occur (Krauss I et al., 2013). The final region, at very

high supersaturation, is where precipitation might be most probable. The method used in this study for crystal growth is vapour diffusion, where the evaporation of water from a protein/buffer drop concentrates the drop to the point where nucleation and crystal growth can occur.

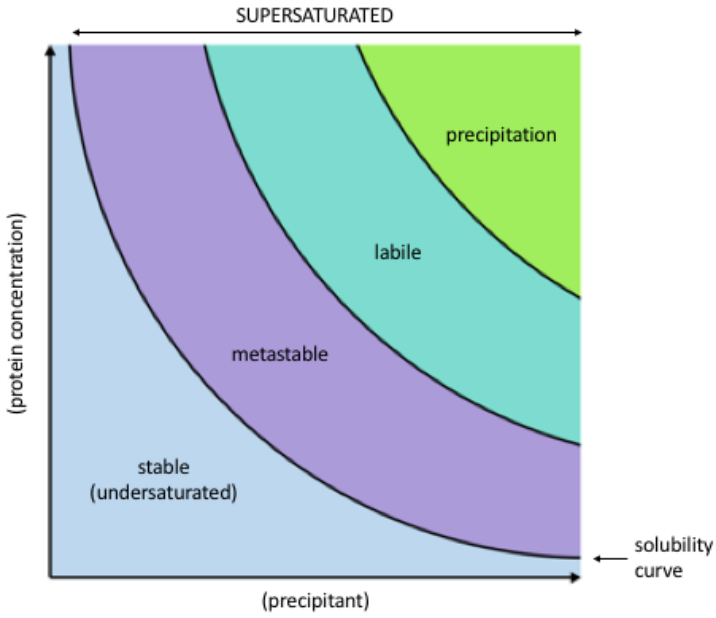

Figure 4.11: Phase diagram for crystallisation of macromolecules

There have been a number of crystal structures published of NDM-1, both apo and in various complexes with either antibiotics or inhibitors, as summarised in Table 4.3.

Table 4.3: Summary of apo and complex crystal structures of NDM-1

PDB	Substrate	Resolution Å	Protein conc. mg/ml	Conditions	Temp °C	Reference
3ZR9	apo	1.91	35	5 mM $CoCl_2$, 5 mM $NiCl_2$, 5 mM $MgCl_2$, 5 mM $CdCl_2$, 100 mM HEPES pH 7.5, 12 % (w/v) PEG 3350	20	Green et al, 2011
3SPU	apo	2.1	68	0.1 M Li_2SO_4, 0.63 M $(NH_4)_2SO_4$, 0.05 M Tris at pH 8.5	25	King et al, 2011
3RKJ	apo	2.0	40	0.17 M $(NH_4)_2SO_4$, 25.5 % (w/v) PEG 4000, 15 % glycerol	16	Kim et al., 2011
3S0Z	apo	2.5	5	20 mM/L $CdCl_2$, 20 mM/L $CaCl_2$, 20 mM/L $CoCl_2$ and 20 % (v/w) PEG 3350	18	Guo et al., 2011
5A5Z	apo	2.6	20	24 % PEG 1500, 0.05 M TBG pH 4	25	Klingler et al., 2015
4RL0	cefuroxime	1.3	36	30 % (w/v) PEG 3350, 0.1 M Bis-Tris pH 6.0, 0.2 M Li_2SO_4	-	Feng et al., 2014
4RL2	cephalexin	2.0	36	28 % (w/v) PEG 3350, 0.1 M Bis-Tris pH 5.8, 0.2 M $(NH_4)_2SO_4$	-	Feng et al., 2014
4EY2 4EYB 4EYF	methicillin oxacillin benzylpenicillin	1.17 1.16 1.8	60	0.2 M $MgCl_2$, 25 % PEG 3350, 0.1 M bis-tris pH 5.5	25	King et al., 2012
4EYL	meropenem	1.9	55	1M trisodium cacodylate, 0.1 M sodium cacodylate pH 6.5	25	King et al., 2012
5YPI 5YPL	meropenem imipenem	2.3 1.8	30	28 % (w/v) PEG 3350, 0.1 M Bis-Tris pH 5.8, 0.2 M $(NH_4)_2SO_4$ + crystal soaking with antibiotic	20	Feng et al., 2017
5XP6	bismuth Bi(III)	0.95	50-100	0.1 M Bis-Tris pH 5.5, 15 % PEG 3350 (w/v), 20 mM L-proline	20	Wang et al., 2018
4EXS	l-captopril	2.4	-	10% w/v PEG 8K, 8% v/v ethylene glycol, and 0.1 M HEPES pH 7.5	25	King et al., 2012

*Apo structures of NDM-1 highlighted in green, NDM-1 in complex with antibiotic highlighted in orange, NDM-1 in complex with inhibitor highlighted in blue

The reported crystal structures of inhibitors in complex with NDM-1 are shown to act by interaction with the Zn^{2+} ions in the active site. In order to gain further insight into the binding mechanism of Affimer 21 with NDM-1, as well as to confirm the mode of inhibition, structural studies are needed. Analysis of the Affimer binding site on NDM-1 might also reveal key features important for the informed design of novel inhibitors of NDM-1 and other metallo-β-lactamases in the future. Four attempts at obtaining a crystal structure of the Affimer 21 : NDM-1 complex were made during the course of this project.

4.2.2.6.1 Crystallisation screen 1

Initially, Affimer 21 and NDM-1 were produced and purified separately before being combined to allow the proteins to form a complex. A pure and homogenous sample of Affimer 21 was produced (Sections 2.2.3.2 and 2.2.3.4) and the size and purity confirmed by SDS-PAGE analysis (2.2.3.4.2) as shown in Figure 4.12. Samples from each stage of the purification process were also included.

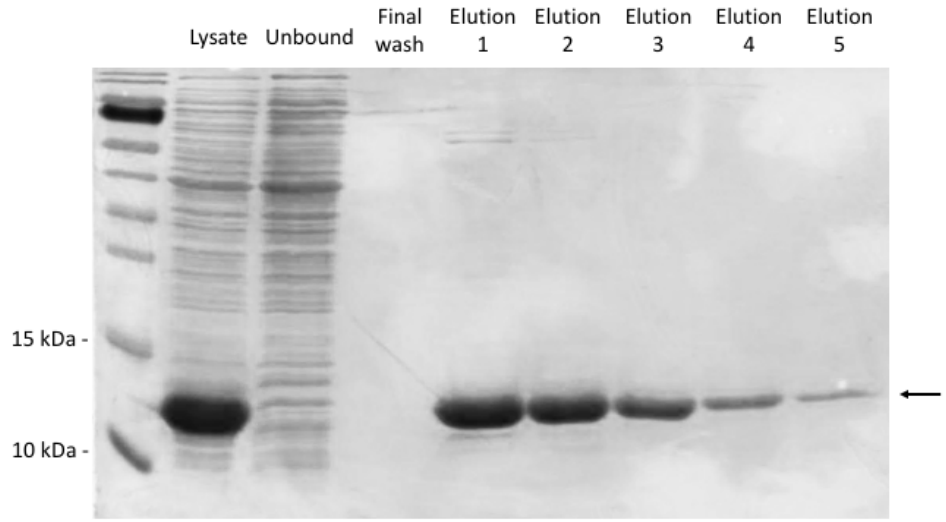

Figure 4.12: SDS-PAGE analysis of Affimer 21 production and purification. Affimer 21 protein was produced from pET11a vector in BL21 Star (DE3) cells. The protein was purified from bacterial cell lysate using nickel ion affinity chromatography and analysed by SDS-PAGE and Coomassie blue staining. The Affimer was eluted and visualised at 12 kDa as indicated by the arrow.

Affimer 21 was further purified by size exclusion chromatography. Salt is normally included in SEC buffers to reduce any protein-matrix interactions. However, the presence of high salt concentrations increases the potential of particulates in the mobile phase, thereby influencing the elution volume of proteins (Ahmed et al., 2010). Proteins were therefore dialysed into 25 mM HEPES, 100 mM NaCl pH 7.5 before being loaded on an 16/60 HiLoad Superdex 200 column (GE Healthcare) attached to an Äkta Xpress system (Section 2.2.7.2) (Figure 4.13a). This was carried out in collaboration with Dr Anil Verna at Oxford Protein Production Facility (OPPF), Research Complex at Harwell. The eluted fractions were analysed by SDS-PAGE (Section 2.2.3.4.2) to confirm the size of the expressed protein as Affimer 21 (Figure 4.13b). NDM-1 had been produced and purified to 35 mg/ml by Dr Anil Verna previously. Both proteins were eluted in 20 mM Tris, 200 mM NaCl, pH 7.5.

a.

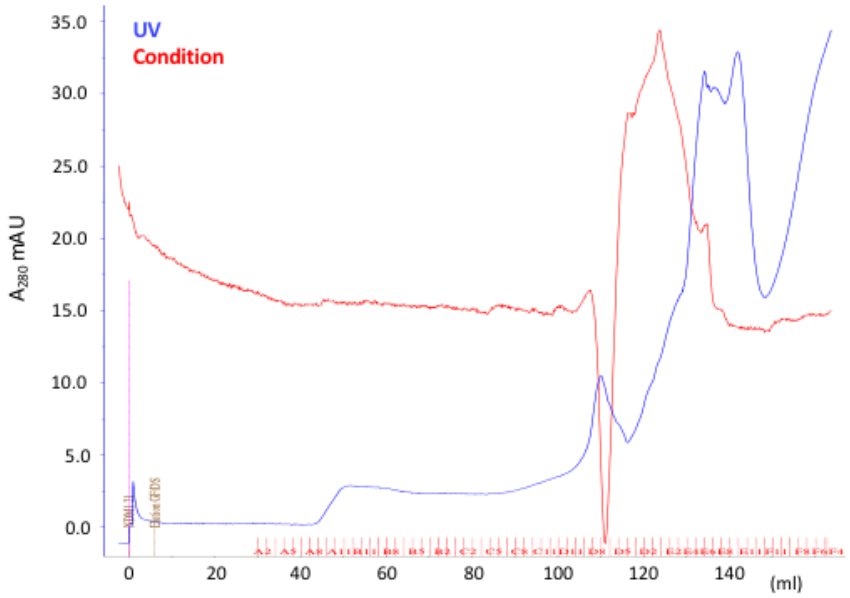

b.

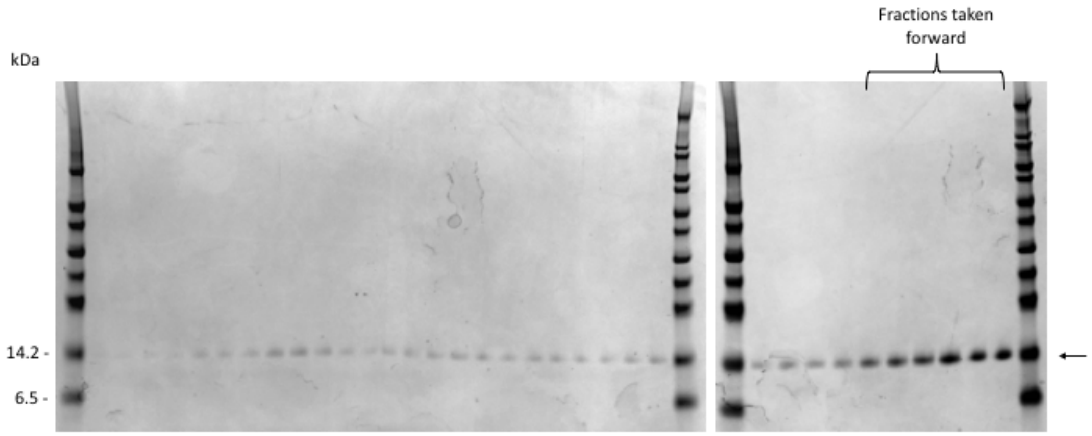

Figure 4.13: Purification of Affimer 21 by size exclusion chromatography (SEC). a) SEC trace showing the A_{280} (mAU) of the sample. **b)** SDS-PAGE analysis of the eluted protein fractions showing Affimer 21 at 14 kDa.

The Affimer eluted relatively late, suggesting that it might interact in some way with the column. It is likely that collection of much of the Affimer was missed. However, the six fractions that were of the highest concentration were pooled and concentrated to 8 mg/ml (Section 2.2.7.3). Ideally NDM-1 and Affimer 21 would be mixed at a 1:1 molar ratio to form the complex. However, due to low sample volume of the Affimer after concentrating, the proteins were mixed at approximately a 2:1 molar ratio of NDM-1 to Affimer 21. The protein mixture was then screened for initial crystallisation conditions across 2x 96 well plates of commercially available screening blocks from Hampton

Research. The screens were set up in sitting-drops with various protein : buffer ratios using a RoboGo robot (MWG) and stored on a Crystal Detector robot (Formulatrix) at 20 °C for imaging. No crystals grew and very little precipitation was seen, suggesting that a condition needed to be altered.

4.2.2.6.2 Crystallisation screen 2

In order to allow for visualisation of the Affimer : NDM-1 complex and to ensure that any unbound protein was removed prior to setting up crystallisation trials, a different method of purification was adopted. Affimer 21 and NDM-1 were produced and purified by Ni-NTA resin as described previously (Sections 2.2.3.2.1, 2.2.3.3.1 and 2.2.3.3.2) and dialysed (Section 2.2.3.3.3) before being combined at a 5:1 molar concentration of Affimer to NDM-1 to ensure that NDM-1 was fully saturated with Affimer and to produce as much complex as possible. The proteins were left to bind overnight at 4 °C on a rotator. Size exclusion chromatography of the complex was performed on a Superdex 75 (26/60) column (GE Healthcare) attached to an Äkta prime system at 4 °C (Section 2.2.7.2) (Figure 4.14a). The sample was eluted in 25 mM HEPES, 100 mM NaCl, pH 7.5, as HEPES buffer had been successful for NDM-1 crystallisation in other studies (Wang et al., 2018, King et al., 2012). SEC purification of the complex, rather than separate proteins, was hypothesised to reduce the time taken for Affimer to be eluted from the column by increasing the size of the target protein and reducing the amount of available unbound Affimer.

a.

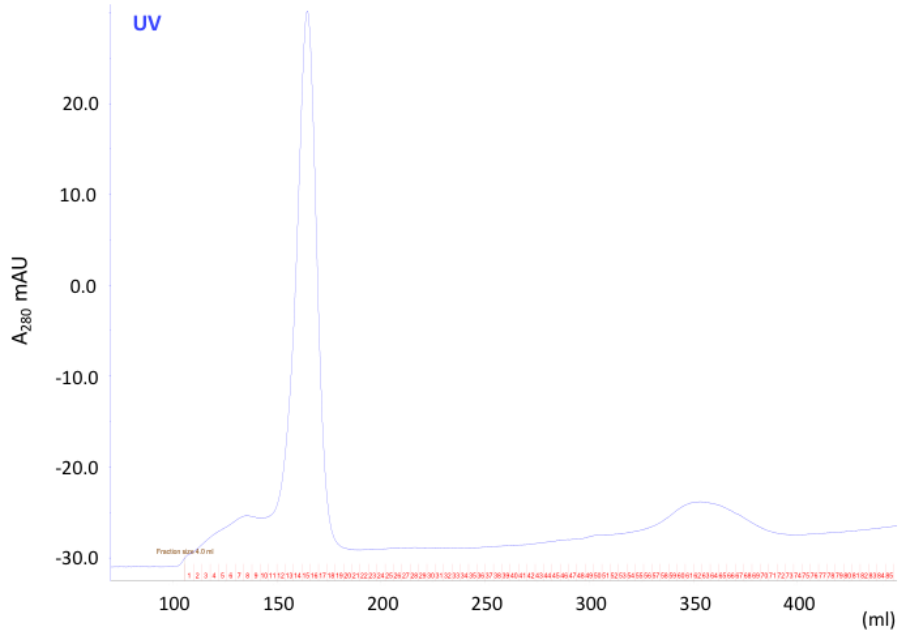

b.

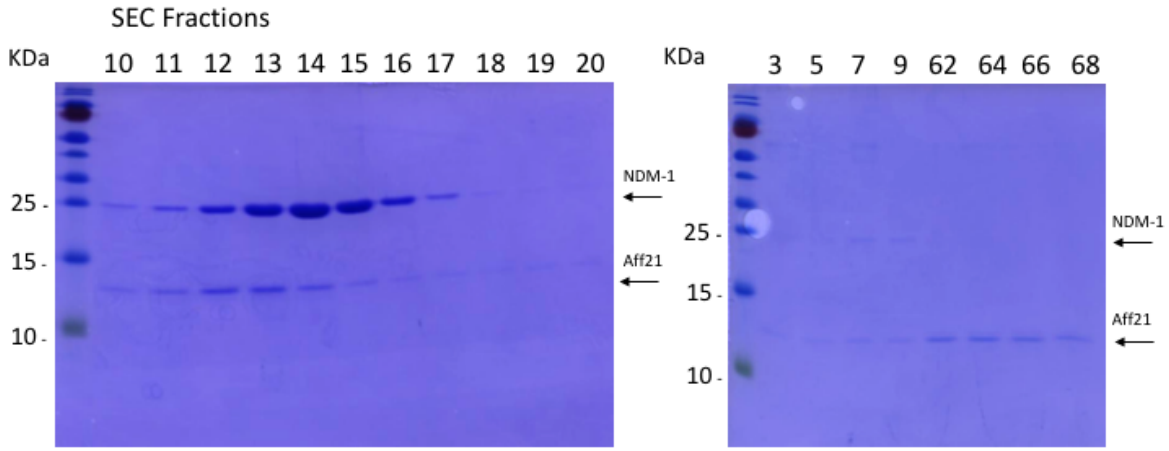

Figure 4.14: Purification of Affimer 21:NDM-1 complex by size exclusion chromatography. a) Size exclusion chromatography (SEC) was performed on a HiPrepTM 16/60 Sephacryl S-100 HR column attached to an Akta Explorer system. A 2 ml aliquot of protein sample was loaded onto the column using a 2 ml injection loop. Absorbance of the protein sample was measured at 280 nM at a flow rate of 0.5 ml/min and 2 ml fractions were collected. **b)** The collected protein fractions were separated by SDS-PAGE on a 15 % resolving gel and stained with Coomassie Blue to check purity. Arrows indicate bands showing Affimer 21 at 12 kDa and NDM-1 at 25 kDa.

The complex eluted in fractions 10-17 and unbound Affimer 21 eluted later at approximately fractions 62-68. SDS-PAGE analysis (Section 2.2.3.4.2) (Figure 4.14b) of the eluted fractions confirmed the presence of bands at 12 kDa (Affimer) and 25 kDa (NDM-1), which looked to both be present in fractions 10-20. However, in a 1:1 molar complex you would expect the protein bands to be of equal quantity on a gel. In fractions 11-17 there appears to be much more NDM-1 than Affimer, which might suggest either the presence of unbound NDM-1 mixed in with the complex or that more than 1 molecule of NDM-1 binds to each Affimer. Despite this, fractions 11-14 were pooled and concentrated to 6.25 mg/ml using VivaSpin columns (Section 2.2.7.3). The complex was then screened for initial crystallisation conditions across 4x 96 well plates of commercially available screening blocks from Qiagen (Section 2.2.7.4). The screens were set up in sitting-drops with various protein : buffer ratios using a NT8® Drop Setter robotics system (Formulatrix) and stored on a Sonicc RI 1000 Crystal Detector (Formulatrix) at 20 °C for imaging. Again, no crystals grew and very little precipitation was seen.

4.2.2.6.3 Crystallisation screen 3

Previously reported crystal structures of NDM-1 were obtained at concentrations ranging from 35 - 60 mg/ml (Green et al., 2011, Youngchang et al, 2011, King et al., 2012). As no crystals grew and very little precipitation was seen in the previous screens, the complex was deemed to be in an undersaturated state (Figure 4.11). To obtain higher concentrations of protein and push the protein towards the labile zone, production was scaled up to 8 L of culture volume for NDM-1 (expected yield of 135 mg) and 500 ml of Affimer 21 (expected yield of 70 mg). To obtain a more homogenous complex, purification was performed using a pull-down method in which Affimer 21 protein lysate was added in excess to 1 ml Ni^{2+}NTA resin (capacity 30 mg) to ensure full saturation, and washed. The periplasmic fraction of NDM-1 was then added to the Affimer-bound resin before being washed and eluted (Section 2.2.7.1). The elution buffer used contained a lower concentration of NaCl than usual (150 mM) to avoid having to dialyse the protein and possibly lose some of the sample. The production and purification process was analysed by SDS-PAGE (Section 2.2.3.4.2) (Figure 4.15).

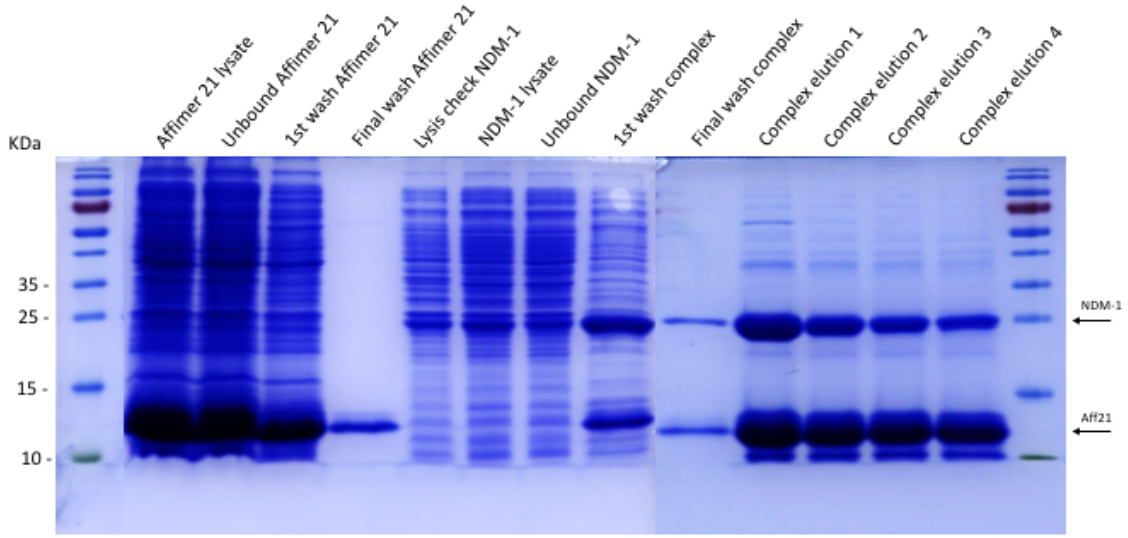

Figure 4.15: SDS-PAGE analysis of Affimer 21:NDM-1 complex production and purification. Affimer 21 production was scaled up to 500 mL of culture volume and NDM-1 production scaled up to 8 L of culture volume. Affimer 21 protein was added in excess to Amintra Ni^{2+}NTA resin and purified as described previously, but not eluted from the resin. Periplasmic fraction containing NDM-1 protein was mixed with the Affimer-bound resin, added to a polypropylene column and washed and eluted as described previously. Protein samples were separated by SDS-PAGE on a 15 % resolving gel and stained with Coomassie Blue to check purity. Affimer 21: NDM-1 complex was purified using 1 ml Ni^{2+}NTA resin. Affimer 21 is shown at 12 kDa and NDM-1 is shown at 25 kDa.

Both NDM-1 and Affimer 21 proteins contain a polyhistidine-tag and therefore it was necessary to ensure that the resin was fully saturated with Affimer 21 before addition of NDM-1 lysate to reduce the possibility of capturing NDM-1 protein that wasn't in complex. SDS-PAGE analysis showed a high level of Affimer 21 in the unbound sample suggesting the Ni-NTA resin was fully saturated with Affimer 21. The Affimer-bound resin was then saturated with NDM-1 as indicated by NDM-1 remaining in the unbound NDM-1 sample. Bands corresponding to Affimer and NDM-1 were visualised in the elutions of the complex. There appeared to be more Affimer 21 than NDM-1 but it was predicted that any excess unbound Affimer would be removed during size exclusion chromatography (SEC). Co-purification of the complex (25 mg) by SEC was performed on a HiPrep™ 16/60 Sephacryl S-100 HR column attached to an Äkta Explorer at 4 °C (Section 2.2.7.2) (Figure 4.16a). The sample was eluted in 25 mM HEPES, 100 mM NaCl, pH 7.5, as before.

a.

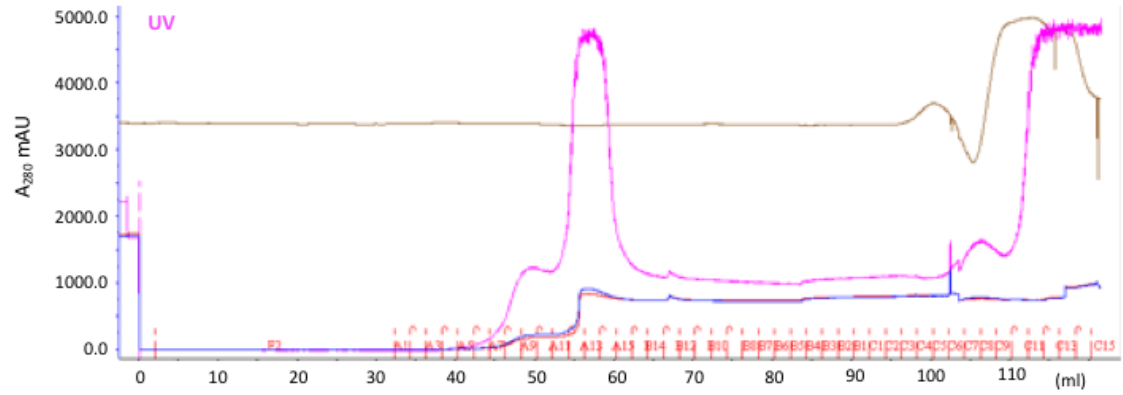

b.

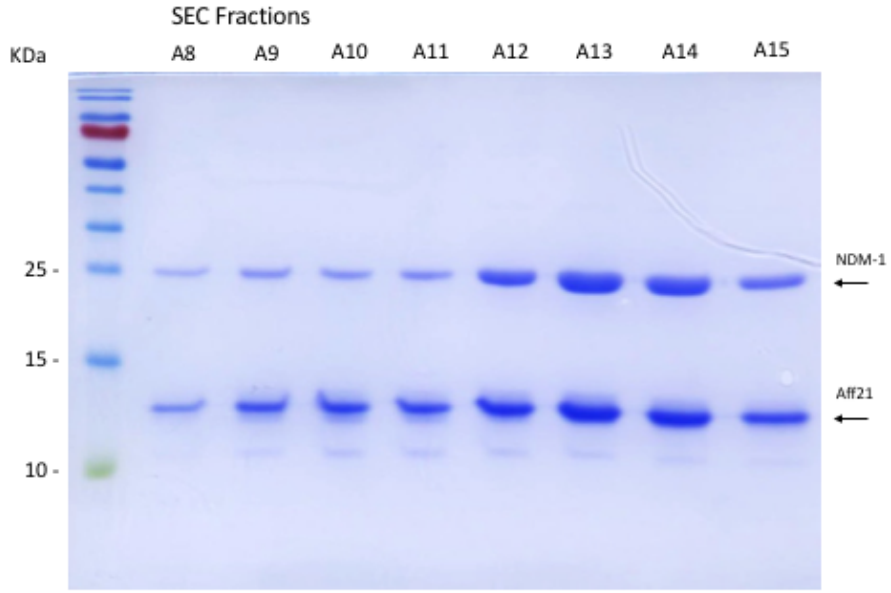

Figure 4:16. Purification of Affimer 21:NDM-1 complex by SEC. a) Size exclusion chromatography (SEC) of the complex was performed on a HiPrepTM 16/60 Sephacryl S-100 HR column attached to an Akta Explorer system. A 2 ml aliquot of protein sample was loaded onto the column using a 2 ml injection loop. Absorbance of the protein sample was measured at A_{280} (mAU) at a flow rate of 0.5 ml/min and 2 ml fractions were collected. **b)** The collected protein fractions were separated by SDS-PAGE on a 15 % resolving gel and stained with Coomassie Blue to check purity. Arrows indicate bands showing Affimer 21 at 12 kDa and NDM-1 at 25 kDa.

The complex eluted in fractions A8-A15. SDS-PAGE analysis (Section 2.2.3.4.2) (Figure 4.15b) of the eluted fractions confirmed the presence of bands at 12 kDa (Affimer) and 25 kDa (NDM-1). In fractions A8-A11 (the shoulder of the peak), there appeared to be slightly more Affimer than NDM-1. However, in fractions A12 to A15 the ratio of Affimer to NDM-1 appears to be more even, suggesting that the extra Affimer seen in the purification gel (Figure 4.15) was Affimer that has now been removed during SEC. Fractions A12-A15 were pooled and concentrated to 19 mg/ml using VivaSpin columns (Section 2.2.7.3). The complex was then screened for initial crystallisation conditions across 4x 96 well plates of commercially available screening blocks from Qiagen (Section 2.2.7.4). The screens were set up in sitting-drops with various protein : buffer ratios using a NT8® Drop Setter robotics system (Formulatrix) and stored on a Sonicc RI 1000 Crystal Detector (Formulatrix) at 20 °C for imaging. No crystals grew but around 30 % of conditions showed precipitation.

4.2.2.6.4 Crystallisation screen 4

To obtain higher concentrations of protein for crystallisation trials, protein was produced in 8 L of culture volume for NDM-1 (expected yield of 135 mg) and 1.5 L of Affimer 21 (expected yield of 210 mg). Purification of the complex was carried out by pull down as per screen 3, but with 2 x 2 ml Ni^{2+}NTA resin to capture a theoretical 120 mg of Affimer 21. The production and purification process was analysed by SDS-PAGE (Figure 4.17).

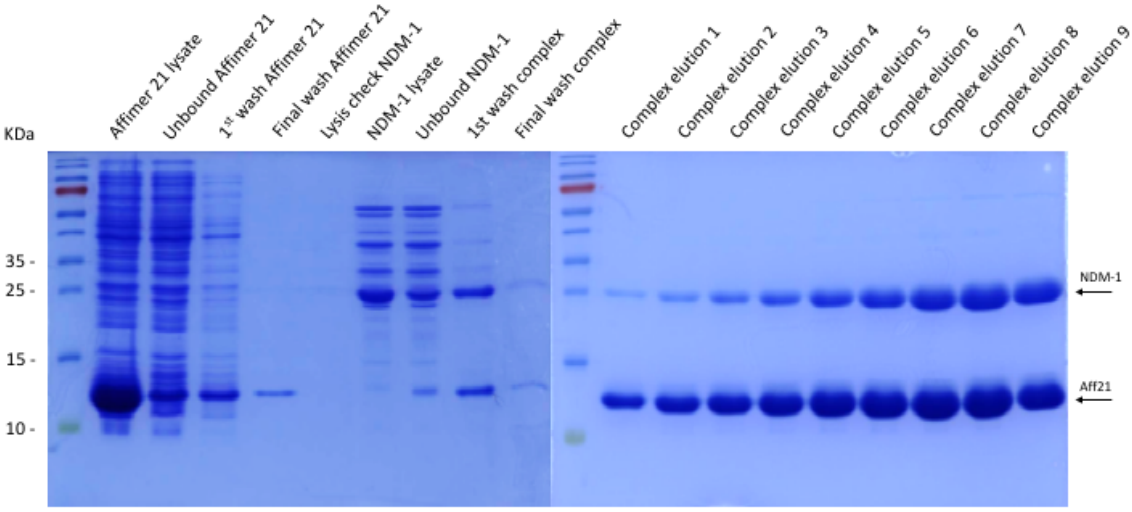

Figure 4.17: SDS-PAGE analysis of Affimer 21 : NDM-1 complex production and purification. Affimer 21 production was scaled up to 1.5 L of culture volume and NDM-1 production scaled up to 8 L of culture volume. Affimer 21 protein was added in excess to Amintra Ni^{2+}NTA resin and purified as described previously but not eluted from the resin. Periplasmic fraction containing NDM-1 protein was mixed with the Affimer-bound resin, added to a polypropylene column and washed and eluted as described previously. Protein samples were separated by SDS-PAGE on a 15 % resolving gel and stained with Coomassie Blue to check purity. Affimer 21 is shown at 12 kDa and NDM-1 is shown at 25 kDa**.** Affimer 21: NDM-1 complex was purified using 4 ml Ni^{2+}NTA resin. Affimer 21 is shown at 12 kDa and NDM-1 is shown at 25 kDa.

SDS-PAGE analysis confirmed that the Ni-NTA resin was fully saturated with Affimer 21, as indicated by the presence of Affimer 21 in the unbound sample. The Affimer-bound resin was then fully saturated with NDM-1 as shown by the NDM-1 remaining in the unbound NDM-1 sample. Two SEC runs were performed due to the larger volume of complex eluate. For the first run 2 ml at 13 mg/ml was loaded. For the second run, the complex was concentrated using VivaSpin columns and 2 ml at 30 mg/ml was loaded. Both runs were performed on a HiPrep™ 16/60 Sephacryl S-100 HR column attached to an Äkta Explorer at 4 °C (Section 2.2.7.2) (Figure 4.18a&b). The sample was eluted in 25 mM HEPES, 100 mM NaCl, pH 7.5, as before.

a.

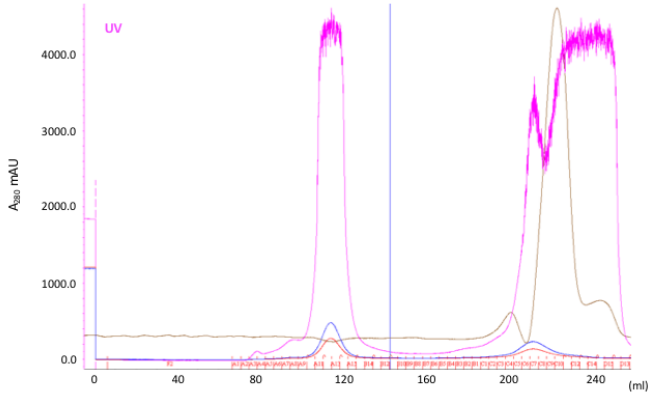

b.

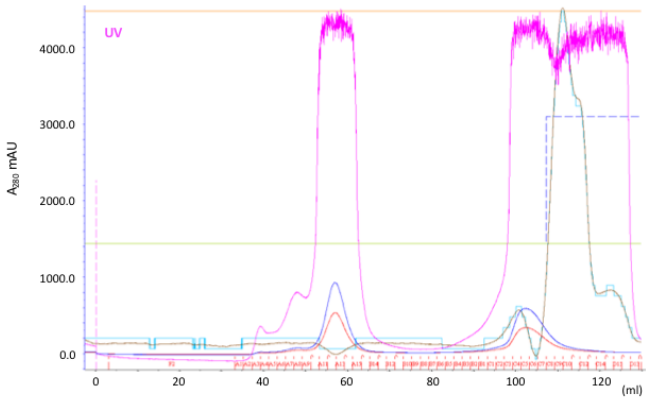

c.

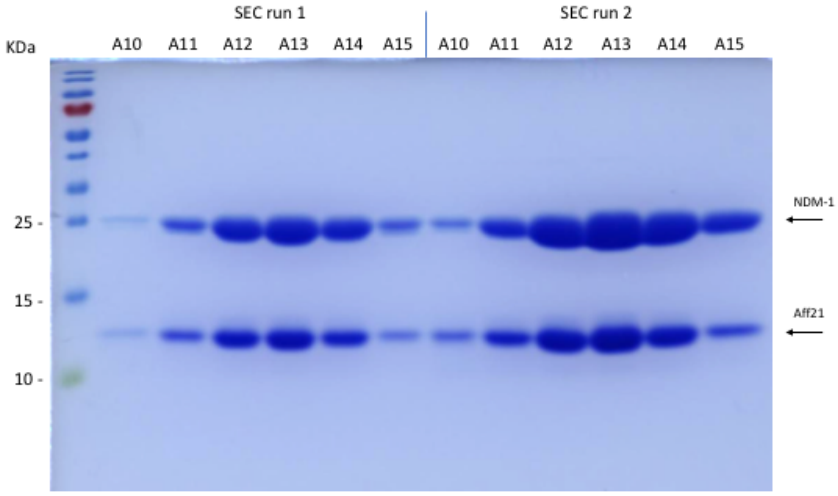

Figure 4.18: Purification of Affimer 21:NDM-1 complex by SEC. Size exclusion chromatography (SEC) of the complex was performed on a HiPrepTM 16/60 Sephacryl S-100 HR column attached to an Akta Explorer system. A 2 ml aliquot of protein sample was loaded onto the column for each run using a 2 ml injection loop. Absorbance of the protein sample was measured at A_{280} (mAU) at a flow rate of 0.5 ml/min and 2 ml fractions were collected. **a)** SEC trace of run 1 showing the A_{280} (mAU) of the sample. **b)** SEC trace of run 2 showing the A_{280} (mAU) of the sample. **c)** The collected protein fractions were separated by SDS-PAGE on a 15 % resolving gel and stained with Coomassie Blue to check purity. Arrows indicate bands showing Affimer 21 at 12 kDa and NDM-1 at 25 kDa.

The complex eluted in fractions A10-A15 in both runs. SDS-PAGE analysis (Section 2.2.3.4.2) (Figure 4.18c) of the eluted fractions confirmed the presence of bands at 12 kDa (Affimer) and 25 kDa (NDM-1). Fractions A11-A15 were pooled and concentrated to 40 mg/ml using VivaSpin columns (Section 2.2.7.3). The complex was then screened for initial crystallisation conditions across 4x 96 well plates of commercially available screening blocks from Qiagen (Section 2.2.7.4). The screens were set up in sitting-drops with various protein : buffer ratios using a NT8® Drop Setter robotics system (Formulatrix) and stored on a Sonicc RI 1000 Crystal Detector (Formulatrix) at 20 °C for imaging. Approximately 65 % of conditions showed precipitation and there were two conditions that showed possible crystal formation and were considered worth optimising (Figure 4.19).

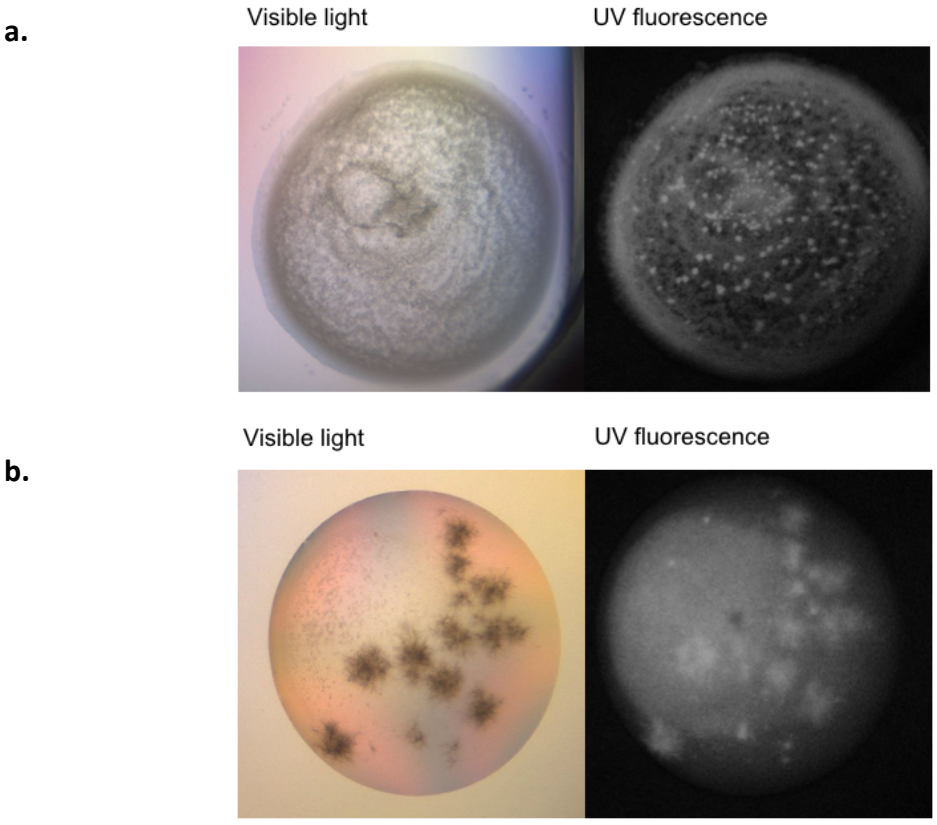

Figure 4.19: Crystallisation drop images for Affimer 21:NDM-1 protein complex. Conditions were set up using the commercially available screens JCSG Core Suites I, II, III, and IV from Qiagen. Trials were set up on 96 well 3-drop plates and imaged on a Sonicc RI 1000 Crystal Detector (Formulatrix). Total drop volume was 0.2 µl. Drops were imaged using both visible light and UV fluorescence. **a)** 1:1 ratio of protein to mother liquor. Mother liquor contained 0.2 M $NH_4H_2PO_4$, 0.1 M TRIS pH 8.5 and 50 % MPD (v/v). **b)** 1:1 ratio of protein to mother liquor. Mother liquor contained 0.16 M $(NH_4)_2SO_4$, 0.08 M Na Acet pH 4.6, 20 % PEG 4K (w/v) and 20 % glycerol (v/v)

4.2.2.6.5 Crystallisation optimisation

There were two conditions from the factorial screens in crystallisation screen 4 that showed possible crystal formation: 0.2 M $NH_4H_2PO_4$, 0.1 M TRIS pH 8.5 and 50 % MPD (v/v), and 0.16 M $(NH_4)_2SO_4$, 0.08 M Na Acet pH 4.6, 20 % PEG 4K (w/v) and 20 % Glycerol (v/v). A 96-well plate of new buffer conditions (48 conditions for each) that centred on the variation of precipitant and pH was created using a Formulator® Screen Builder (Formulatrix) (Section 2.2.7.5). A 96 well 3-drop plate of crystallisation trials containing various protein : buffer ratios was then set up using these optimised conditions with Affimer 21 : NDM-1 complex protein at 40 mg/ml, as before. At the time of writing, there were no visible crystals.

4.3 Chapter summary and future work

One advantage of phage display is that it allows for screening of diverse molecular targets to obtain high-potency binders suitable for development within a much faster timescale than that achievable for small molecules (Huang et al., 2012). For small molecules, hits from library screening are normally found with target affinities or IC_{50}s in the 1 to 5 µM range. In this study, an initial IC_{50} of Affimer 21 was estimated as 0.37 µM. Repeating the assay with Affimer concentrations ranging between 200-500 nM will allow for a more widely spread IC_{50} curve and a more accurate IC_{50} value. One advantage of using engineered protein scaffolds such as Affimers is that they can be easily manipulated through affinity maturation to allow for development of improved binding capabilities.

Kinetic analysis of the interaction between Affimer 21 and NDM-1 revealed that K_M remains constant and V_{max} and k_{cat} decrease upon addition of Affimer 21, as expected for an inhibitor. The kinetic efficiency of NDM-1 only was consistent with that previously reported for nitrocefin (Makena et al., 2015 and Kim et al., 2011), although there does seem to be much variation in the literature, depending on how the NDM-1 was produced. Addition of Affimer 21 resulted in a K_{cat}/K_M value of 4.65; which is a 25 % decrease in the kinetic efficiency of NDM-1 when compared to the NDM-1 only control. Additionally, a Lineweaver-Burk plot suggested that Affimer 21 is a non-competitive inhibitor of NDM-1. This was surprising as most reported MBL inhibitors act by zinc binding or chelation (Docquier et al., 2018).

Affimer 21 was shown to restore sensitivity to meropenem in a dose-dependent manner in a clinical strain of *Klebsiella pneumoniae* that carries the bla_{NDM-1} gene. Additionally, a control containing 10 µg/ml of Affimer and no meropenem showed no significant effect on cell growth, suggesting that the Affimer does not exhibit any off-target antimicrobial effects in this *Klebsiella* strain. Whilst these trends were replicated across experimental repeats, no statistical analyses were possible owing to the variable nature of cell culture in small volumes. These experiments require a substantial number of further repeats, in larger culture volumes and with a variety of antibiotics to confirm the results and allow for statistical analysis. Until relatively recently it was thought that all metallo-β-lactamases are localised to the periplasm. It was therefore surprising that Affimer 21 was able to inhibit NDM-1 in cell assays as the route of access to the periplasm was unclear. However, there has been recent evidence that indicates that NDM-1 may be anchored to the outer membrane of gram-negative bacteria (King et al., 2011). Additionally, a study by Gonzalez et al (2016) showed that NDM-1 was found in the outer membrane fraction in cellular fractionation experiments, and that membrane-anchoring contributes to the unusual stability of NDM-1 and favours its secretion in outer membrane vesicles (OMVs). Immunofluorescence microscopy of labelled Affimer 21 would further elucidate the cellular localisation of NDM-1 in gram-negative bacteria.

Initial results from cell culture experiments indicate that Affimer 21 is well tolerated in the mammalian cell line, U-2 OS. However, to fully validate the cytotoxicity of Affimer 21, testing in a variety of mammalian cell lines would need to be completed. As previously discussed, generalised zinc chelation is an undesirable characteristic for an effective antimicrobial. These early indications that Affimer 21 is well tolerated in mammalian cells may suggest that Affimer 21 does not work by zinc chelation which would support our kinetic data which indicates that Affimer 21 is an allosteric inhibitor. However, to fully confirm the binding interaction between NDM-1 and Affimer 21, structural data is needed. Four attempts at obtaining a crystal structure of the Affimer 21 : NDM-1 complex were made during the course of this project. However, at the time of writing no crystals had been obtained. It is well documented that crystallography of bio-macromolecules is a multi-parametric process and depends upon multiple factors (Table 4.4) (Krauss et al., 2013).

Table 4.4: Examples of some of the parameters affecting crystallisation

Physical factors	Chemical factors	Biochemical factors
Temperature	pH	Sample purity
Surface	Sample concentration	Sample homogeneity
Time	Precipitant type	Sequence modifications
Pressure	Precipitant concentration	Aggregation
Gravity	Buffer	Sample pI
Viscosity	Ionic strength	Proteolysis
Vibrations	Crosslinkers	

All of these thermodynamic and dynamic parameters can be used to influence supersaturation of the sample and therefore the rates of nucleation and crystal growth. Indeed, as previously indicated in Table 4.3, crystal structures of NDM-1 have been reported for a wide variety of buffer conditions, pH's, temperatures and protein concentrations. In this study, approximately 65 % precipitation was seen for concentrations of NDM-1 at 40 mg/ml. Therefore, increasing the sample concentration is unlikely to improve the possibility of obtaining crystals and could push the process too far past the metastable zone where most crystals are formed. One study used crystal soaking of the apo-structure of NDM-1 with various antibiotics to obtain a structure of the crystal complex (Feng et al., 2017). However, this method is unlikely to be effective in obtaining a co-crystal structure of NDM-1 in complex with Affimer as the Affimer is likely to be too large to fit through the solvent channels without disrupting the crystal lattice.

An alignment of the amino acid sequences of NDM-1 from the reported crystal structures reveals that the majority of the proteins were truncated at the N-terminus, with most having a truncation of 10-20 residues compared to the full-length protein used in this study (NDM-1 pD861) (Figure 4.18).

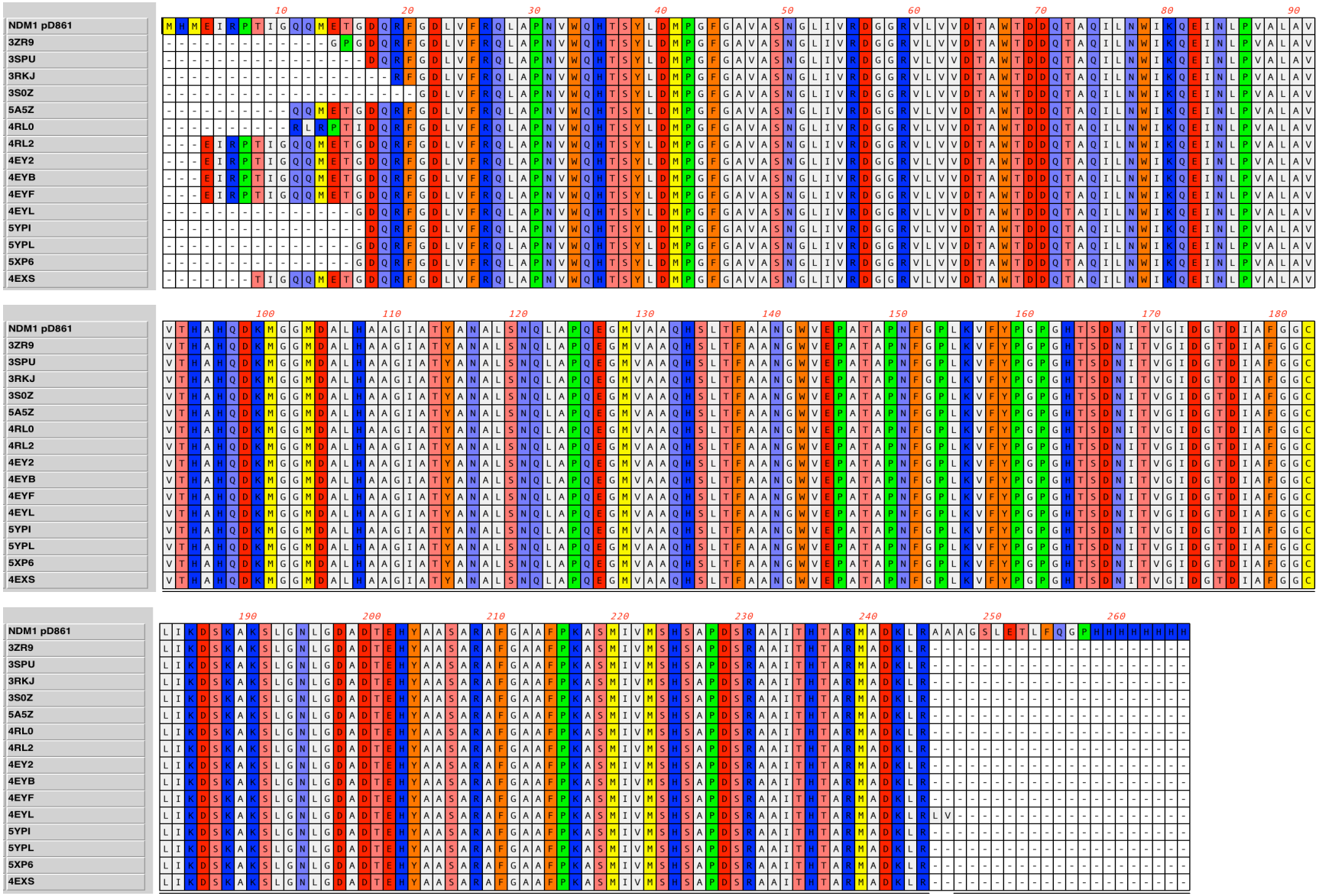

Figure 4.20: Alignment of protein sequences for reported crystal structures of NDM-1

Truncation of the N-terminal region has been reported to improve solubility and level of expression of NDM-1 (Kim., 2011). Additionally, all of the reported structures show cleavage of the C-terminal His-tag. For some of the studies, this is due to cleavage of the His-tag using HRV 3C protease following purification. However, as this is not reported for all of the structures, it might also be that this section of the protein is unresolved in some cases. Despite obtaining high levels of NDM-1 protein with the full-length protein, it seems likely that these modifications also render NDM-1 more amenable to crystallisation and this approach would therefore be worth exploring for future crystallisation trials.

As can be seen, there is much work that can be completed to further the project. However, characterisation thus far has revealed that Affimer 21 acts as a potent inhibitor of NDM1, in both β-lactamase activity assays and in cell-based assays with a clinically relevant bacterial strain. Affimer 21 was ascertained to have an IC_{50} of 0.37 μM and kinetic analysis suggested a non-competitive mechanism of inhibition, potentially excluding it as a zinc chelator. Additionally, Affimer 21 was shown to be non-toxic in the mammalian cell line U-2 OS. Although co-crystallisation has been so far unsuccessful, a protocol for the production of pure and homogenous protein complex has been optimised, and proposals for future trials suggested. These preliminary data are promising for the potential use of Affimer 21 in antibiotic combination therapy, however certain biochemical and mechanistic details are still to be elucidated.

Chapter 5

Identification of critical residues in the Affimer 21:NDM-1 interaction

5.1 Introduction

The mapping of protein-protein interactions is crucial for understanding the complex molecular relationships in biological processes. Many high-resolution structures have been solved to try to improve knowledge of the molecular details of protein interactomes. Obtaining a three-dimensional (3D) structure of a protein complex reveals useful information on the architecture and chemistry of a protein-protein interaction, including the residues involved, number of hydrogen bonds, the size and shape of the interface and the occurrence of bound water molecules (Lise et al., 2009). However, the co-crystallisation of protein-ligand complexes is not always possible, and although protein structures can provide information on the structural binding epitope (i.e. the residues involved in binding), they do not characterise the binding energetics or show how docking occurs. Therefore, in order to fully elucidate a molecular binding interaction, the residues within a protein structure that contribute to the binding interaction need to be resolved (Cunningham et al., 1993).

Site-directed mutagenesis is invaluable for investigating protein structure and function. Although there are many different mutagenesis strategies (Amin et al., 2004, Labrou., 2010, Knight et al., 2013), alanine scanning has been proven to be especially effective in mapping the residues involved in binding interactions for a number of proteins (Reimer et al., 2017, Kumarasinghe et al., 2018, Schomer et al., 2018). Alanine scanning is a widely used approach in which residues in the protein of interest are systematically substituted for an alanine at chosen positions by site-directed mutagenesis, and the altered protein assayed to determine any changes in function (Cunningham et al., 1989). Because substitution with an alanine removes all of the side chain atoms past the β-carbon, the effects of an individual alanine mutation can be used to interpret the role of the original residue side chain. Alanine lacks unusual backbone dihedral angle preferences; unlike glycine for example, which would also nullify the sidechain, but can introduce conformational flexibility into the backbone of the protein (Morrison et al, 2001). Alanine scanning mutagenesis can therefore provide a detailed map of a protein-ligand interaction, an important step for rational protein and drug design (Weiss et al, 2000).

Novel binding scaffolds can be easily modified and mutations are often well tolerated (Binz et al., 2005; Škrlec et al., 2015). Alanine scanning mutagenesis has therefore been successfully utilised to determine binding hot spots and to analyse the individual contributions of residues in the binding regions of various scaffolds, including Knottins, Kunitz domains and Monobodies (Glotzbach et al., 2013, Chen et al., 2012, Cheung et al., 2015). In a recent study, a RadA-based scaffold was probed by alanine scanning to identify two critical residues for TPX2/Aurora A kinase binding, an interaction involved in mitotic spindle assembly which is overactivated in tumour cells (Rossmann et al., 2017). As well as elucidating critical residues in a binding interaction, information obtained from alanine scanning has been shown to be a useful tool in guiding the design of affinity matured libraries that often leads to the selection of improved affinity binders. This technique was used to develop Affibodies that bind to VEGFR2 and block VEGF-A binding. The information obtained from an alanine scan was used to guide the design of an affinity matured library from which two improved affinity binders were obtained (Fleetwood et al., 2014).

As obtaining structural data of the NDM-1:Affimer 21 complex has so far been unsuccessful, the binding interaction at the protein interface is yet to be defined. As discussed above, information as to which residues are critical for binding, and those which impede the interaction, could be used to improve inhibitory efficacy and guide future rational design. Here we probe the interactions between enzyme and inhibitor by first investigating the contribution of each variable region to the interaction, and then by performing a complete alanine scan to determine the contribution of individual residues. Single alanine mutations (18 in total) were systematically introduced by site-directed mutagenesis and tested for potency of NDM-1 inhibition in β-lactamase activity assays.

5.2 Results

5.2.1 Construction and characterisation of Aff21ΔVR1 & Aff21ΔVR2 mutants

To determine whether one or both of the variable regions (VRs) of Affimer 21 are responsible for inhibitory activity of NDM-1 we created Affimer 21 constructs consisting of either variable region 1 (Aff21ΔVR2) or variable region 2 (Aff21ΔVR1). Aff21ΔVR2 and Aff21ΔVR1 were created by amplifying DNA for each respective variable region from the pBSTG-Aff phagemid vector and SOEing with amplified DNA from a wild type (WT) Affimer scaffold with variable regions containing either 2 alanine residues and a glutamic acid, or 3 alanine residues (Section 2.2.1.5, Figure 2.2). Final SOE products were amplified, DNA digested with *NheI*-HF™ and *NotI*-HF™ (NEB) (Section 2.2.1.8) and ligated into similarly digested pET11a vector. XL1-Blue cells were then transformed with the DNA (Section 2.2.1.11), grown up and miniprepped (Section 2.2.1.13) before being sequenced to confirm the correct insert (Table 5.1).

Table 5.1: Amino acid sequences of Aff21ΔVR1 and Aff21ΔVR2

	Variable Region 1									Variable Region 2									
Affimer 21	G	Y	K	V	W	T	P	Y	G	T	H	W	D	N	G	G	L	R
Aff21ΔVR1	-	-	-	-	-	-	A	A	A	T	H	W	D	N	G	G	L	R
Aff21ΔVR2	G	Y	K	V	W	T	P	Y	G	-	-	-	-	-	-	A	A	E

Following sequencing confirmation, BL21 star™ (DE3) cells were transformed with the DNA (Section 2.2.1.11) and protein produced and purified as described in Section 2.2.3.2. The size and purity of the proteins was confirmed by SDS-PAGE analysis (Section 2.2.3.4.2) as shown in Figure 5.1. Samples from each stage of the purification process were also included.

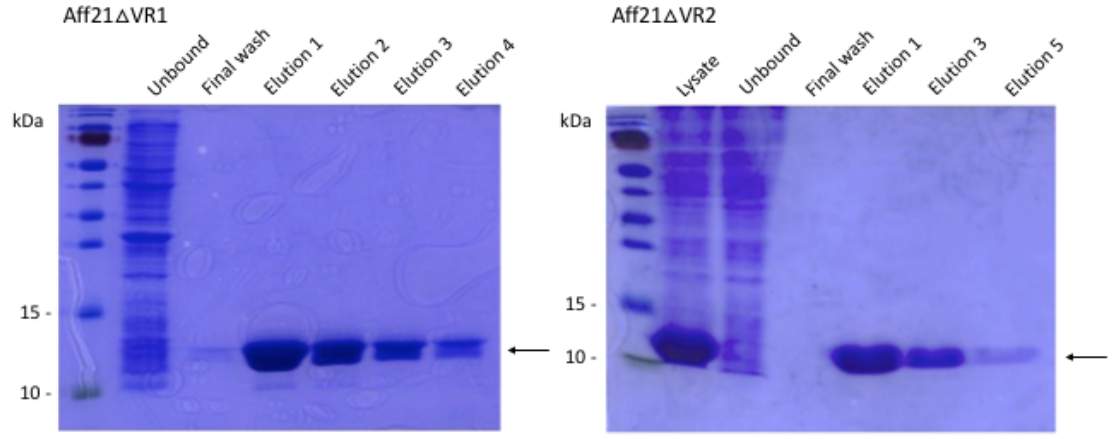

Figure 5.1: Production and purification of Aff21ΔVR1 and Aff21ΔVR2 mutants. Purification of proteins produced from pET11a vector. The proteins were purified from bacterial cell lysate using nickel ion affinity chromatography and separated by SDS-PAGE on a 15 % resolving gel and stained with Coomassie Blue to check purity. The Affimer was eluted and visualised at 12 kDa as indicated by the arrows.

The activity of each mutant was measured and compared to Affimer 21 in a β-lactamase activity assay with nitrocefin as the substrate (Section 2.2.5.1) to determine their effects on NDM-1 activity. Reactions included 100 nM NDM-1, 10 µM clavulanic acid and 65 µM nitrocefin and all results were normalised to the EDTA control. The concentration of Affimer used was increased to 500 nM (from 200 nM) to ensure that even small changes in activity caused by the variable region deletion were observed. The EDTA negative control sequesters Zn2+ from the active site and renders NDM-1 inactive. Additionally, a NDM-1 only positive control containing no Affimer demonstrated the maximum rate of nitrocefin hydrolysis. Absorbance at 482 nm was plotted over time (s) to give an initial indication of trend (Figure 5.2a). After 3 replicate experiments, absorbance values measured during the first 250 seconds (during which the rates were constant) were converted to concentration in µM using Beer-Lambert's Law and then to rate in µM/s using linear regression analysis (Figure 5.2b).

a.

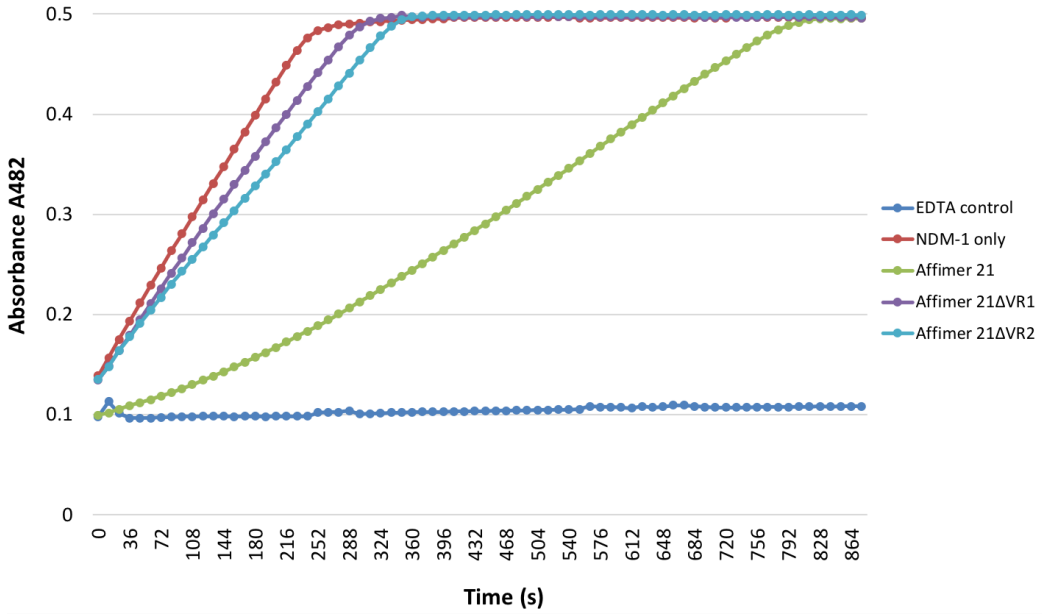

b.

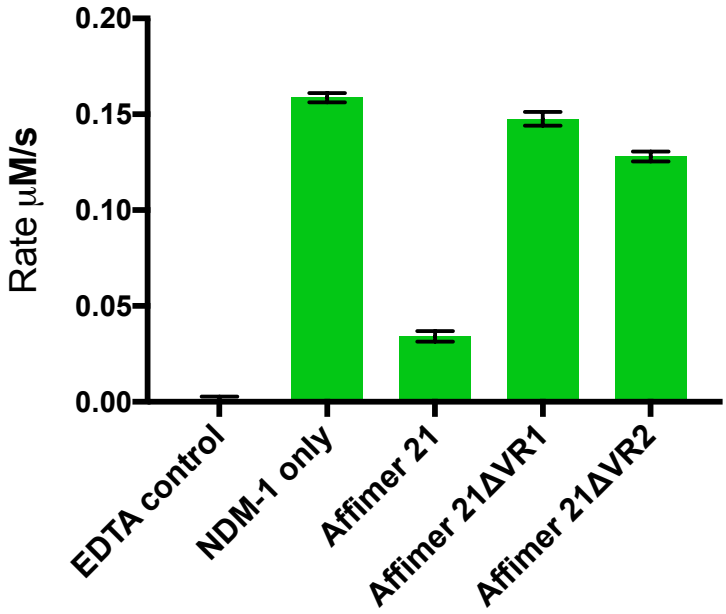

Figure 5.2: Effects of Aff21ΔVR1 and Aff21ΔVR2 on rate of nitrocefin hydrolysis by NDM-1. Reactions included 100 nM NDM-1, 10 µM clavulanic acid, 500 nM Affimer and 65 µM nitrocefin. Data was normalised to the EDTA control. **(a)** The change in absorbance at 482 nM for NDM-1 only and upon addition of Affimer was recorded. **(b)** Activity of NDM-1 only or with 500 nM Affimer recorded as rate of nitrocefin hydrolysis (µM/s). n = 3, error bars represent standard error from 3 replicate experiments.

The β-lactamase activity assay indicated that both variable regions of Affimer 21 are required for effective inhibition of NDM-1. Aff21ΔVR1 showed only a minimal reduction in initial NDM-1 enzymatic activity of 7 % ($p < 0.05$ R^2 0.8335), when compared to the NDM-1 only positive control. In comparison, Aff21ΔVR2 showed a 19 % reduction in NDM-1 activity compared to the NDM-1 only control ($p < 0.001$ R^2 0.9829) suggesting that variable region 1 may play a more fundamental role in the inhibition of NDM-1.

5.2.2 Site-directed mutagenesis of Affimer 21

To identify the functionally important residues in the 2 variable regions of Affimer 21, systematic alanine-scanning by site-directed mutagenesis was performed (Section 2.2.1.6). Primers were designed to enable the sequential substitution of each of the Affimer 21 variable region amino acids to an alanine (Table 2.11). Substitution with an alanine eliminates any side-chain interactions without altering the main-chain conformation or imposing electrostatic or steric effects, so it is often the preferred choice for testing the contribution of specific amino acids while preserving the native structure of the protein (Cunningham et al., 1989). The mutations were introduced using Quikchange-based mutagenesis and the linear amplification products for all 18 mutants were checked on agarose gels alongside a positive and negative control (Figure 5.3).

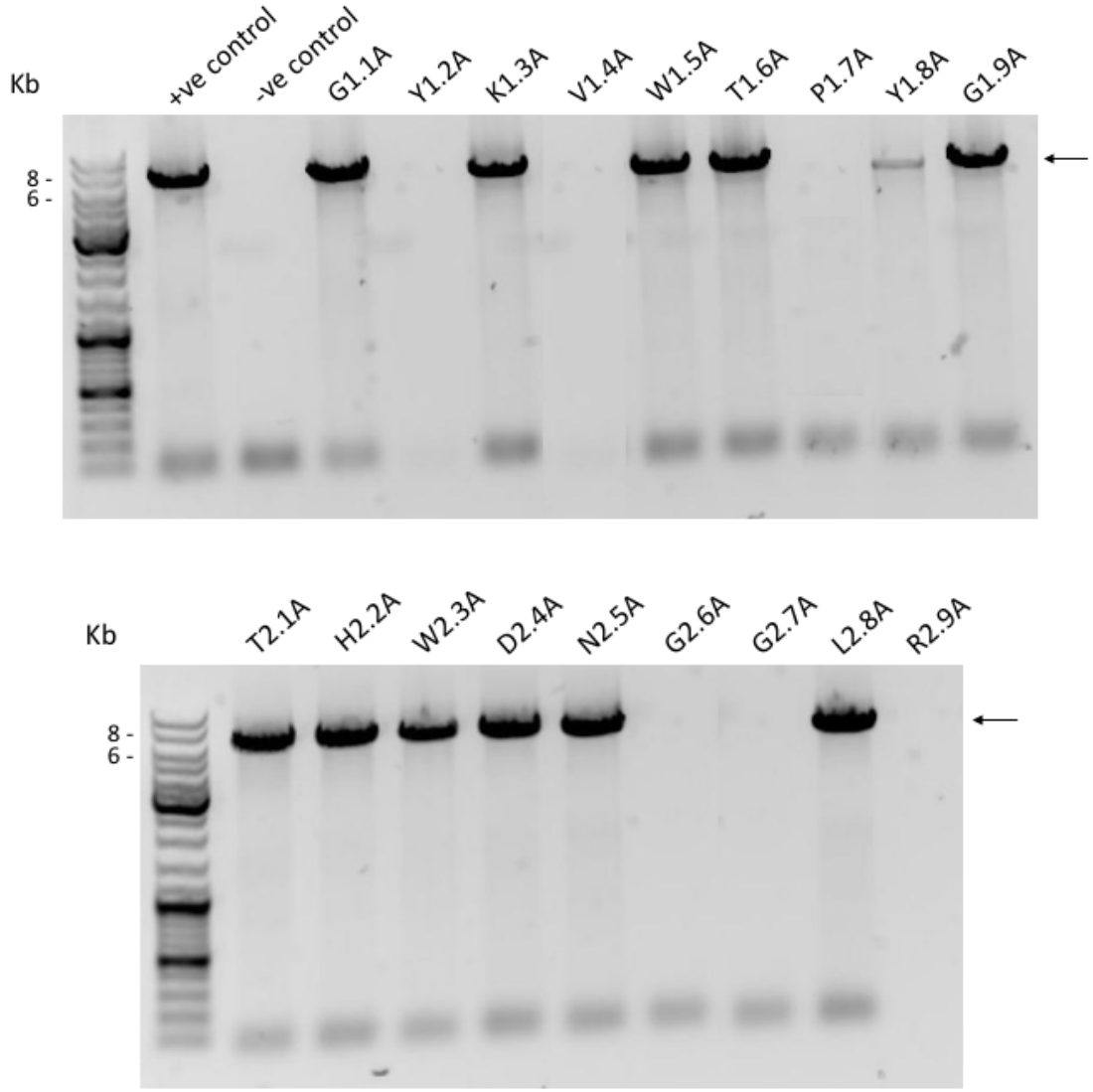

Figure 5.3: Production of Affimer 21 alanine scanning mutants. Quikchange-based mutagenesis of Affimer 21 from the pET11a vector to systematically introduce an alanine in all of the positions in the two variable regions. Positive and negative controls consisting of a DNA and primer set that had previously been shown to successfully amplify, and template DNA with no primers were also analysed. The DNA products were analysed by agarose gel electrophoresis resulting in an approximately 7000 bp product as indicated by the arrow.

The mutant constructs Y1.2A, V1.4A, P1.7A, G2.6A, G2.7A and R2.9A failed to amplify and therefore the linear amplifications were repeated, as before (Figure 5.4).

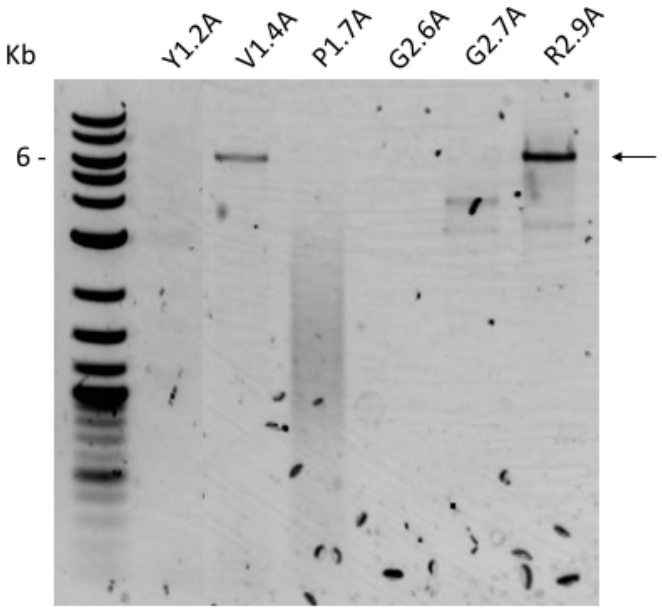

Figure 5.4: Repeat linear amplifications of Affimer 21 alanine scanning mutants. Quikchange-based mutagenesis of Affimer 21 from the pET11a vector to introduce an alanine in positions in the two variable regions that failed to amplify in the first batch. The linear amplification products were analysed by agarose gel electrophoresis resulting in an approximately 7000 bp product as indicated by the arrow.

DNA for the constructs that had successfully amplified up to this point were *DpnI* digested and supercompetent XL1-Blue cells were transformed with the DNA. Single colonies were picked and grown up, DNA extracted by miniprep and then checked by sequencing (Section 2.2.1.6). All sequences were correct and contained the expected alanine mutation, apart from G1.1A which was therefore repeated alongside the constructs Y1.2A, P1.7A, G2.6A and G2.7A which had failed to amplify after two attempts at the linear amplification. Gradient linear amplifications to try different annealing temperatures were therefore attempted. Additionally one of the samples, G2.7A, was trialled with Phusion HF DNA polymerase as well as the standard KOD Hot Start polymerase to see whether this improved amplification (Figure 5.5 and 5.6).

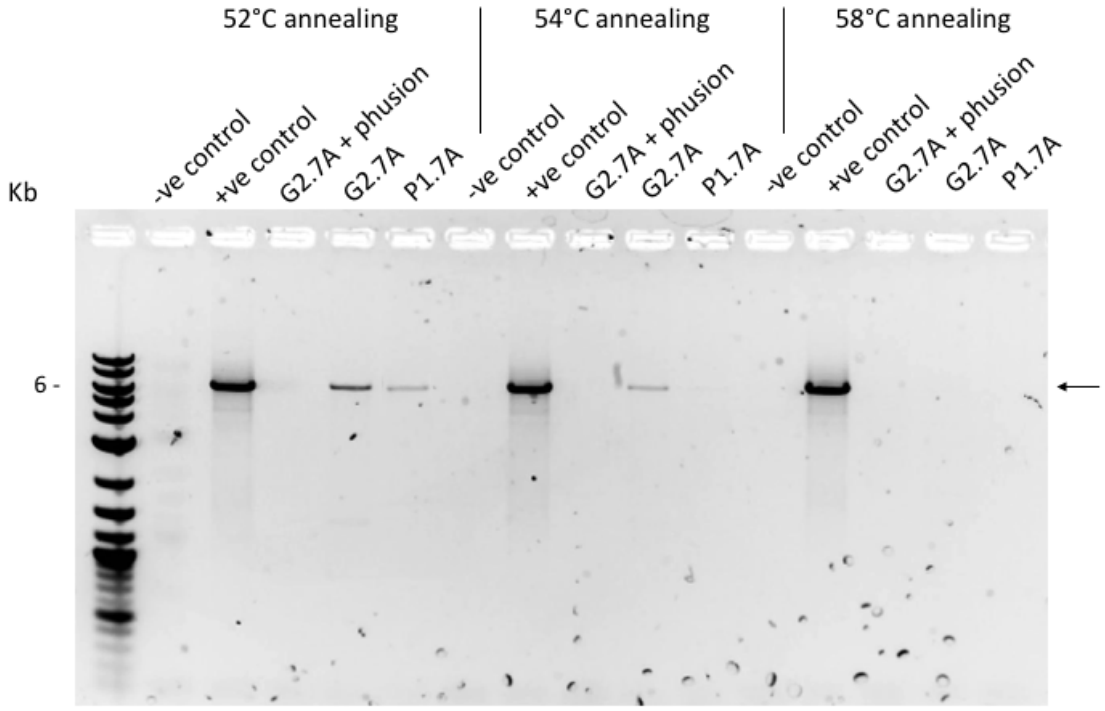

Figure 5.5: Gradient linear amplifications of Affimer 21 alanine scanning mutants G2.7A and P1.7A. Quikchange-based mutagenesis of Affimer 21 from the pET11a vector to introduce an alanine. Different annealing temperatures were trialled for each construct. Additionally, G2.7A was trialled with both Phusion HF polymerase and KOD Hot Start polymerase. An annealing temperature of 52 °C gave DNA product for both G2.7A and P1.7A. No product was seen at any temperature when KOD Hot Start polymerase was replaced with Phusion HF polymerase. Positive and negative controls consisting of a DNA and primer set for G1.9A that had previously been shown to successfully amplify, and template DNA with no primers were also analysed. The linear amplification products were analysed by agarose gel electrophoresis resulting in an approximately 7000 bp product as indicated by the arrow.

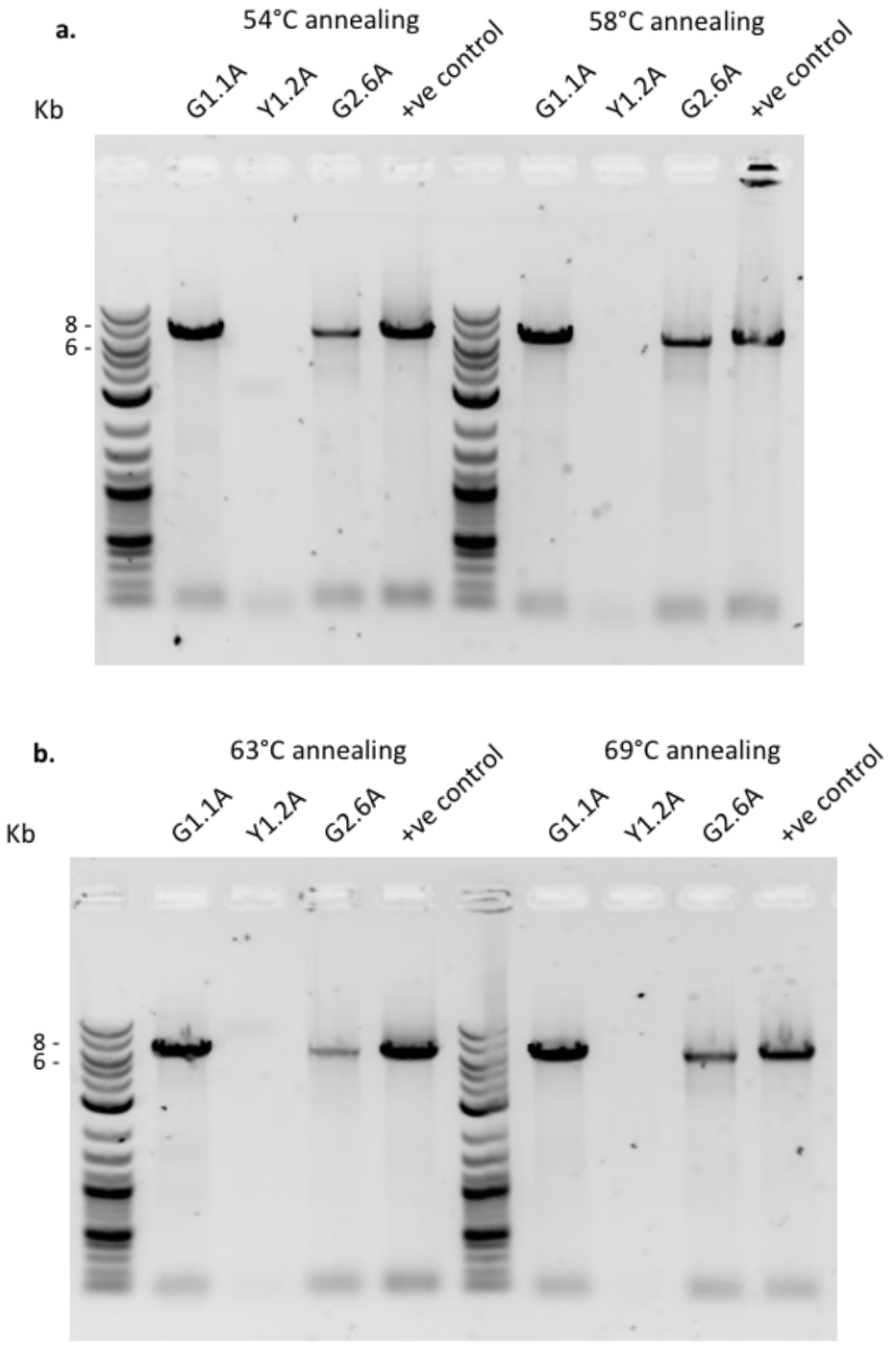

Figure 5.6: Gradient linear amplifications of Affimer 21 alanine scanning mutants G1.1A, Y1.2A and G2.6A. (a & b) Quikchange-based mutagenesis of Affimer 21 from the pET11a vector to introduce an alanine. Different annealing temperatures were trialled for each construct. DNA products were seen at all annealing temperatures for G1.1A and G2.6A but Y1.2A failed to amplify at any annealing temperature. A positive control consisting of a DNA and primer set for G1.9A that had previously been shown to successfully amplify, was also analysed. The linear amplification products were analysed by agarose gel electrophoresis resulting in an approximately 7000 bp product as indicated by the arrow.

The mutant constructs G2.7A and G1.7A amplified with an annealing temperature of 52 °C and there was also a faint band seen for G2.7A at 54 °C, substantially lower than the standard annealing temperature of 60 °C originally used.

Y1.2A had failed to amplify twice with standard amplification conditions and in linear amplifications with a range of annealing temperatures. The primers were redesigned with a slightly shorter length (reduced from 50 to 44 bases). These primers were trialled with the standard Quikchange-based mutagenesis method using KOD Hot Start Polymerase and gave a strong band on an agarose gel (Figure 5.7).

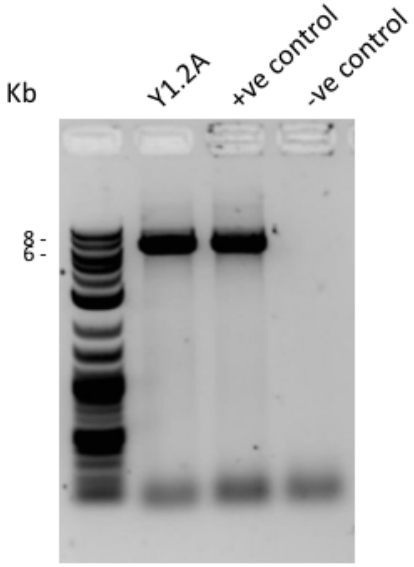

Figure 5.7: Repeat linear amplification of Affimer 21 alanine scanning mutant Y1.2A. Quikchange-based mutagenesis of Affimer 21 from the pET11a vector to introduce an alanine at position 1.2. Positive and negative controls consisting of a DNA and primer set for G1.9A that had previously been shown to successfully amplify, and template DNA with no primers were also analysed. The DNA products were analysed by agarose gel electrophoresis resulting in an approximately 7000 bp product as indicated by the arrow.

Supercompetent XL1-Blue cells were transformed with *DpnI* digested products, plasmid DNA was purified from transformant colonies, and the presence of the mutation was confirmed by DNA sequence analysis (Table 5.2) (Section 2.2.1.17).

Table 5.2: Amino acid sequences of the 18 alanine scanning mutants of Affimer 21

	Variable Region 1									Variable Region 2								
Affimer 21	G	Y	K	V	W	T	P	Y	G	T	H	W	D	N	G	G	L	R
G1.1A	A	Y	K	V	W	T	P	Y	G	T	H	W	D	N	G	G	L	R
Y1.2A	G	A	K	V	W	T	P	Y	G	T	H	W	D	N	G	G	L	R
K1.3A	G	Y	A	V	W	T	P	Y	G	T	H	W	D	N	G	G	L	R
V1.4A	G	Y	K	A	W	T	P	Y	G	T	H	W	D	N	G	G	L	R
W1.5A	G	Y	K	V	A	T	P	Y	G	T	H	W	D	N	G	G	L	R
T1.6A	G	Y	K	V	W	A	P	Y	G	T	H	W	D	N	G	G	L	R
P1.7A	G	Y	K	V	W	T	A	Y	G	T	H	W	D	N	G	G	L	R
Y1.8A	G	Y	K	V	W	T	P	A	G	T	H	W	D	N	G	G	L	R
G1.9A	G	Y	K	V	W	T	P	Y	A	T	H	W	D	N	G	G	L	R

	Variable Region 1									Variable Region 2								
Affimer 21	G	Y	K	V	W	T	P	Y	G	T	H	W	D	N	G	G	L	R
T2.1A	G	Y	K	V	W	T	P	Y	G	A	H	W	D	N	G	G	L	R
H2.2A	G	Y	K	V	W	T	P	Y	G	T	A	W	D	N	G	G	L	R
W2.3A	G	Y	K	V	W	T	P	Y	G	T	H	A	D	N	G	G	L	R
D2.4A	G	Y	K	V	W	T	P	Y	G	T	H	W	A	N	G	G	L	R
N2.5A	G	Y	K	V	W	T	P	Y	G	T	H	W	D	A	G	G	L	R
G2.6A	G	Y	K	V	W	T	P	Y	G	T	H	W	D	N	A	G	L	R
G2.7A	G	Y	K	V	W	T	P	Y	G	T	H	W	D	N	G	A	L	R
L2.8A	G	Y	K	V	W	T	P	Y	G	T	H	W	D	N	G	G	A	R
R2.9A	G	Y	K	V	W	T	P	Y	G	T	H	W	D	N	G	G	L	A

Once all the constructs had been successfully amplified and checked by sequencing, they were transformed into Supercompetent XL1-Blue cells for production and purification of protein (Section 2.2.3). The size and purity of the proteins was confirmed by SDS-PAGE analysis (Section 2.2.3.4.2) as shown in Figure 5.8. Samples from each stage of the purification process were also included.

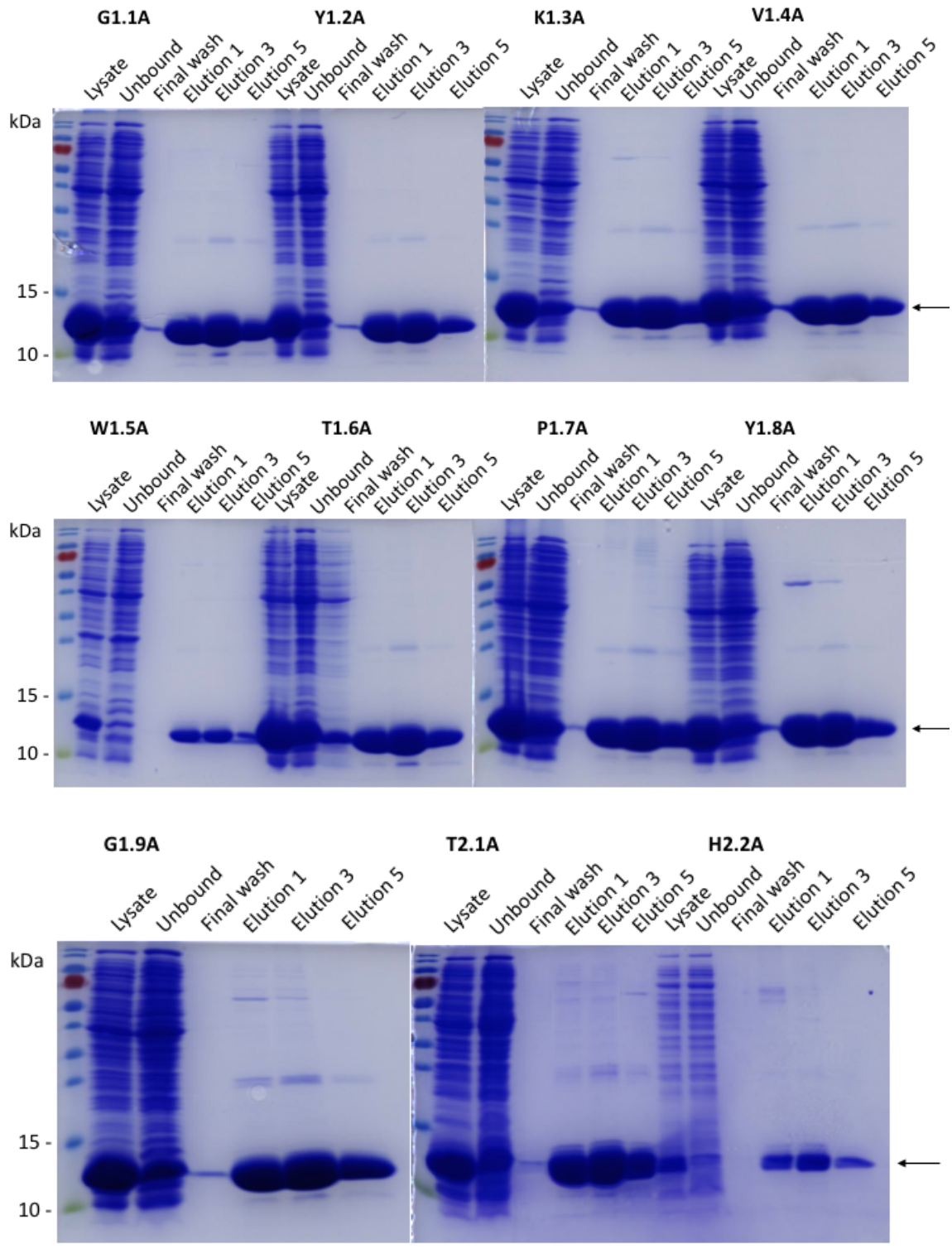
G1.1A
Y1.2A
K1.3A
V1.4A
W1.5A
T1.6A
P1.7A
Y1.8A
G1.9A
T2.1A
H2.2A
Lysate
Unbound
Final wash
Elution 1
Elution 3
Elution 5
kDa
15 -
10 -

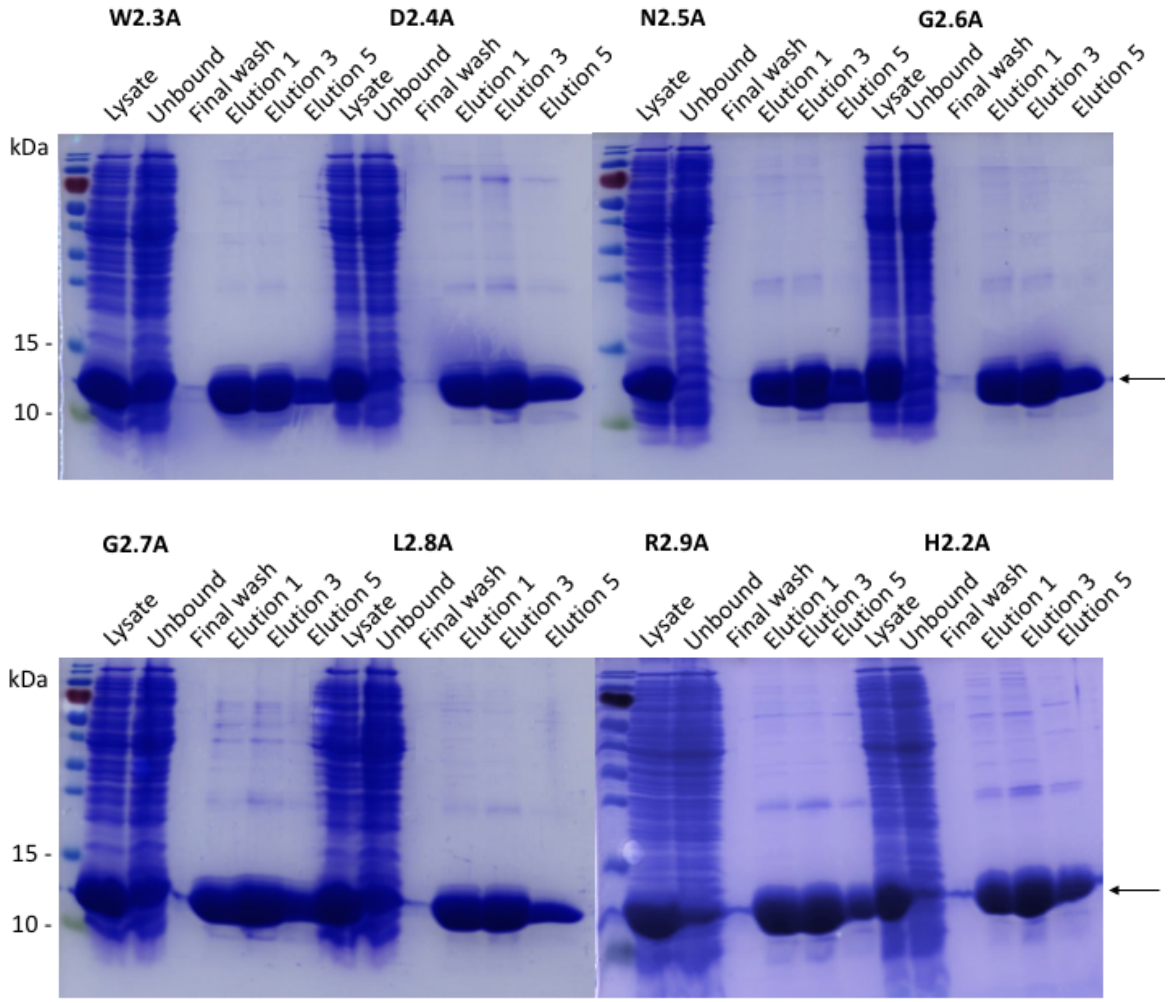

Figure 5.8: Production and purification of Affimer 21 mutants. Purification of proteins produced from pET11a vector. The proteins were purified from bacterial cell lysate using nickel ion affinity chromatography and analysed by SDS-PAGE and Coomassie blue staining. The Affimer was eluted and visualised at 12 kDa as indicated by the arrows. The construct H2.2A had a low yield and production was repeated (repeat shown in the final gel image). 10 µl of each sample was run on the gel.

Following production and purification, the mutant Affimer 21 constructs were dialysed into 1x PBS + 10 % v/v glycerol. The effects of the alanine substitutions on efficacy of NDM-1 inhibition were then measured in β-lactamase activity assays (Figure 5.9).

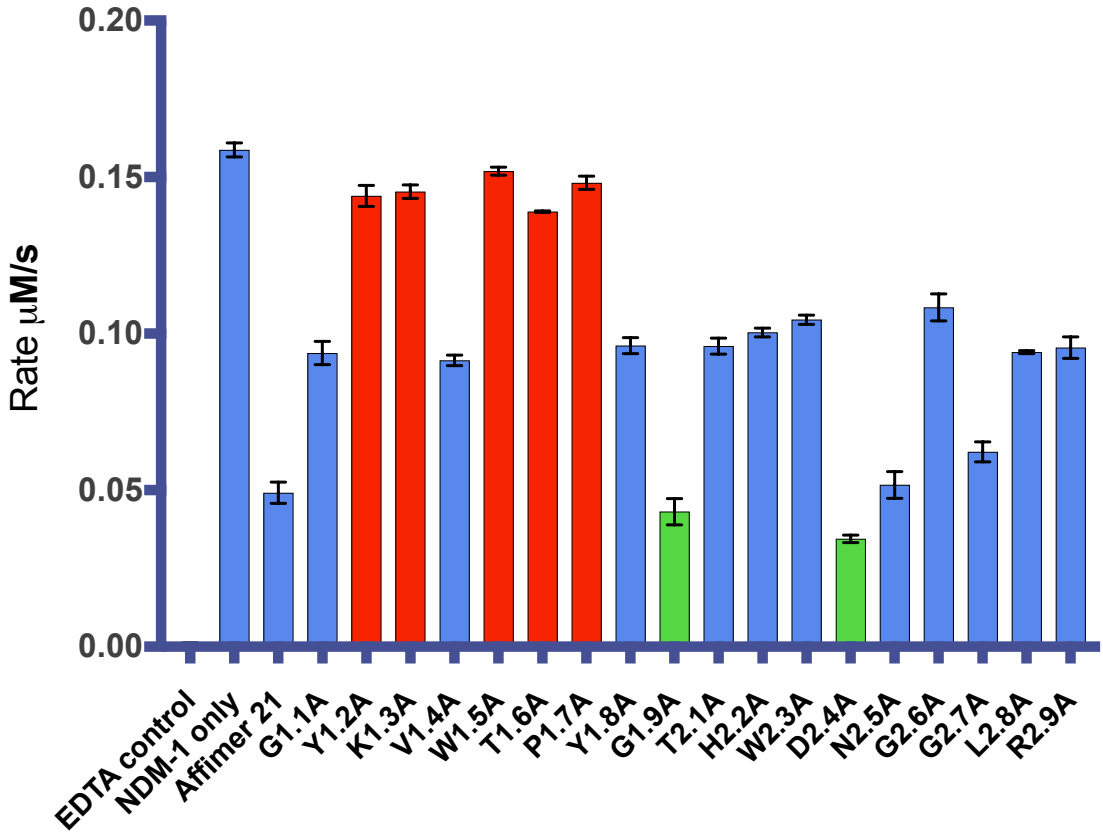

Figure 5.9: Effects of alanine substitutions in Affimer 21 on rate of nitrocefin hydrolysis by NDM-1. Reactions included 100 nM NDM-1, 10 µM clavulanic acid, 200 nM Affimer and 65 µM nitrocefin. Data was normalised to the EDTA control. Activity of NDM-1 only or with 200 nM Affimer recorded as rate of nitrocefin hydrolysis (µM/s). Y1.2A, K1.3A, W1.5A, T1.6A and P1.7A (highlighted in red) were shown to be the most critical residues for inhibition of NDM-1 activity. G1.9A and D2.4A (highlighted in green) were shown to slightly improve inhibition of NDM-1 when mutated to an alanine. n = 3, error bars represent standard error from 3 replicate experiments.

The Y1.2A, K1.3A, W1.5A, T1.6A and P1.7A mutants (red) demonstrated the lowest inhibitory activity, with inhibition between just 4 and 12 % compared to the NDM-1 only control (all significant different $p < 0.05$); suggesting that these residues are the most essential for the inhibitory activity of Affimer 21. These results are consistent with the earlier observation (Figure 5.2) that variable region 1 may encompass a more central role in the inhibition of NDM-1. Surprisingly, mutants G1.9A and D2.4A (green) demonstrated small increases in inhibitory efficacy. Mutant G1.9A increased inhibition by 12.3 % compared to Affimer 21 ($p = 0.1240$, $R^2 = 0.4854$) but was not significantly

improved, and D2.4A increased inhibition by 29.9 % ($p = 0.0021$ $R^2 = 0.9267$). This might suggest that the aspartate residue originally present at this position does not contribute to Affimer 21 binding, or might even negatively influence the Affimer-NDM-1 interaction.

5.2.2.1 IC_{50} of Affimer 21 D2.4A and G.19A

The G1.9A and D2.4A mutants were shown to slightly improve the inhibitory activity of Affimer 21. To confirm this result the IC_{50} values were estimated. D2.4A and G1.9A were tested for inhibition of 100 nM NDM-1 in β-Lactamase activity assays (Section 2.2.5.1) at a range of concentrations (10 nM to 3 μM). Rate of nitrocefin hydrolysis (μM/s) was calculated over the initial 250 seconds as before, and the data were fitted using a four parameter logistic curve (4PL). The curves were shown to be good models of the experimental data (D2.4A $R^2 = 0.9979$, G1.9A $R^2 = 0.9991$) and yielded IC_{50} values of 0.38 μM for both mutants (Figure 5.10). The IC_{50} for Affimer 21 had previously been calculated as 0.37 μM. It was therefore determined that there was unlikely to be any difference between the efficacy of Affimer 21 and the mutants G1.9A and D2.4A. However, to confirm this further repeats would be required. Repeating the assay with Affimer concentrations ranging between 200-500 nM will allow for a more widely spread IC_{50} curve and more accurate IC_{50} values.

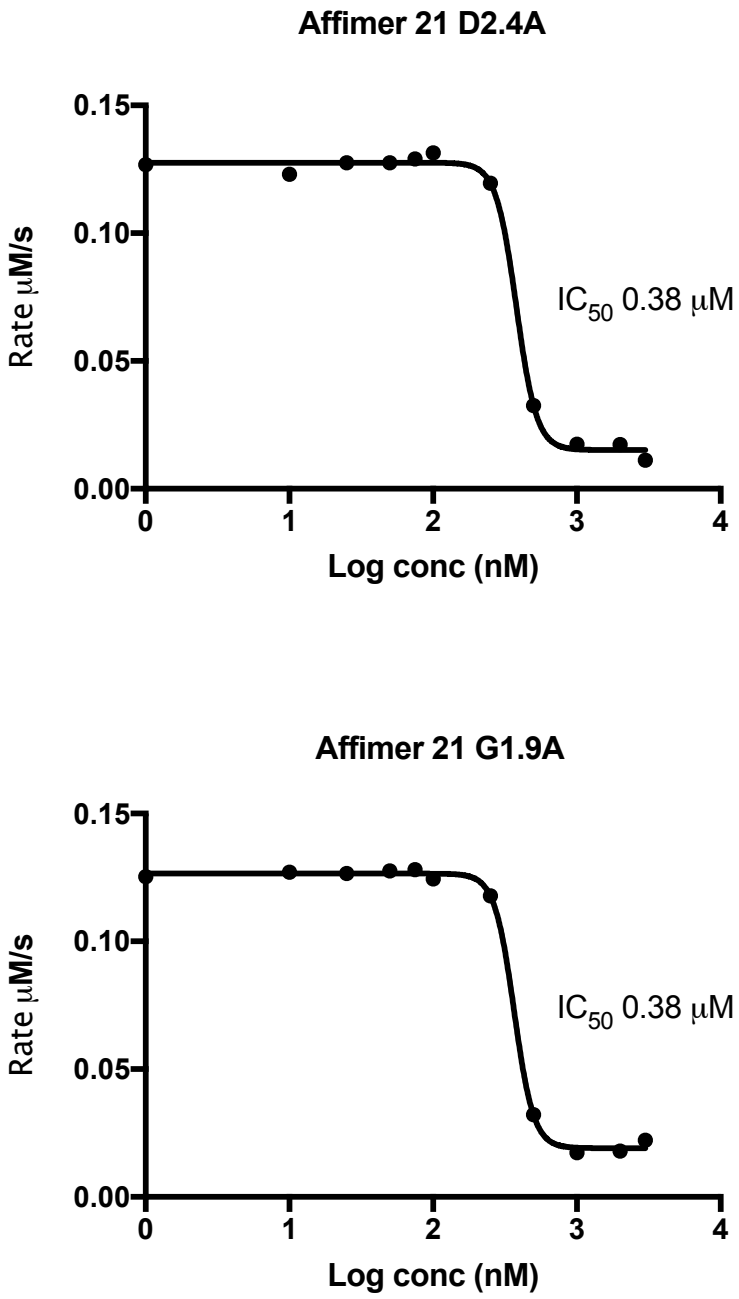

Figure 5.10: IC_{50} of Affimer 21 G1.9A and D2.4A. A four parameter logistic curve was plotted to determine the IC_{50} values of Affimer 21 G1.9A and D2.4A. Reactions included 100 nM NDM-1, 10 μM clavulanic acid and 65 μM nitrocefin. Rate of nitrocefin hydrolysis (μM/s) by NDM-1 against logarithm of the concentration of Affimer (10 nM to 3 μM) was calculated. n = 1. IC_{50} was calculated as 0.38 μM for both mutants, R^2 = 0.9979 and 0.9991

5.2.2.2 Combining alanine mutations

The Affimer 21 constructs G1.9A, D2.4A, N2.5A and G2.7A had been previously shown to increase or to almost match the inhibitory efficacy of the original Affimer 21. It was therefore hypothesised that combining these alanine mutations might increase inhibition by removing residues that appear to negatively influence the interaction between NDM-1 and Affimer 21. Constructs containing G1.9A + D2.4A, G1.9A + N2.5A and G1.9A + G2.7A were generated using Quikchange-based mutagenesis (Section 2.2.1.6) with G1.9A as the template DNA. The DNA products were checked on agarose gels (Figure 5.11a) and bands at approximately 7000 bp confirmed. The DNA was then checked by sequencing to confirm the alanine insertions. The construct G1.9A + G2.7A did not amplify well and contained an extra band on the agarose gel. It also failed to sequence and was therefore removed from this analysis. G1.9A + D2.4A and G1.9A + N2.5A were sub-cloned into pET11a for production and purification (Section 2.2.3) (Figure 5.11b) and checked by SDS-PAGE with Coomassie blue staining for protein bands of approximately 12 kDa.

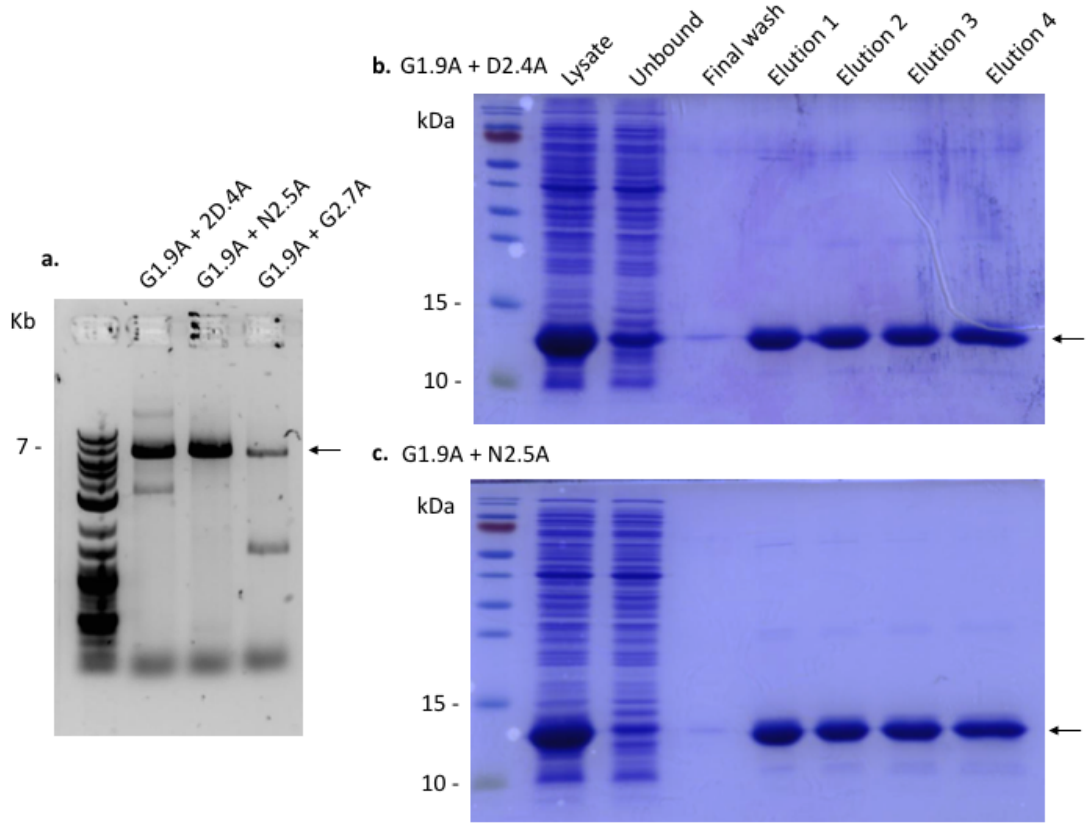

Figure 5.11: Production and purification of Affimer 21 mutants G1.9A + D2.4A and G1.9A + N2.5A. (a) Quikchange-based mutagenesis of Affimer 21 G1.9A from the pET11a vector to introduce extra alanine mutations. The linear amplification product was analysed by agarose gel electrophoresis resulting in an approximately 7000 bp products as indicated by the arrow. The construct G1.9A + G2.7A did not amplify as well and failed to sequence so was removed from the experiment. **(b)** Purification of G1.9A + D2.4A and G1.9A + N2.5A proteins produced from pET11a vector. The protein was purified from bacterial cell lysate using nickel ion affinity chromatography and analysed by SDS-PAGE and Coomassie blue staining. The Affimer was eluted and visualised at 12 kDa as indicated by the arrow.

Following purification, the effects of the double alanine substitutions on efficacy of NDM-1 inhibition were measured in β-lactamase activity assays with nitrocefin as the substrate (Figure 5.12).

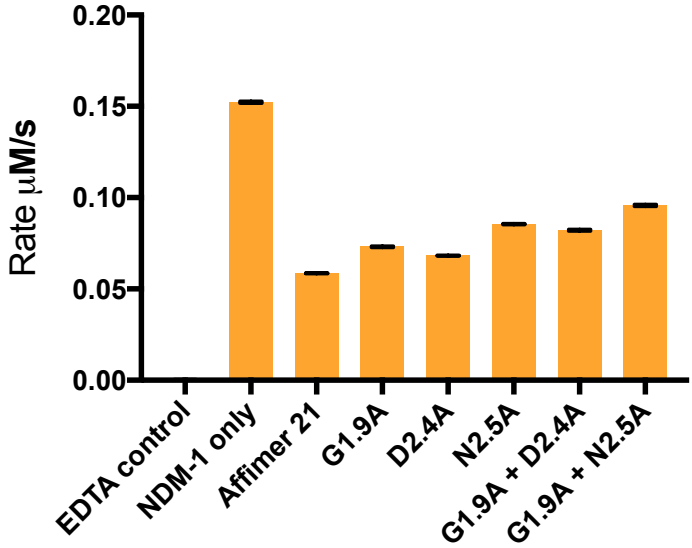

Figure 5.12: Effects of double alanine substitutions in Affimer 21 on rate of nitrocefin hydrolysis by NDM-1. Reactions included 100 nM NDM-1, 10 µM clavulanic acid, 200 nM Affimer and 65 µM nitrocefin. Data was normalised to the EDTA control. Activity of NDM-1 only or with 200 nM Affimer recorded as rate of nitrocefin hydrolysis (µM/s). The Affimer 21 constructs containing combined alanine mutations were shown not improve inhibition of NDM-1 when compared to their single mutation counterparts. n = 1, error bars represent standard error from 3 replicate wells.

The Affimers containing the double alanine mutations did not appear to improve the inhibitory activity of Affimer 21 and were slightly less effective at inhibiting NDM-1 compared to their single mutation counterparts.

5.3 Chapter summary and future work

As part of an affinity maturation strategy, the role of each variable region of Affimer 21 as well as the contribution of individual residues was investigated. The information obtained from these experiments was used to guide the generation of affinity matured libraries with the intention of selecting second generation Affimers with improved affinity and inhibitory efficacy for NDM-1 (Chapter 6). Initially the contribution of each variable region was explored to determine whether both were necessary for binding and/or inhibitory activity. Additionally, if only one variable region was required then the residues investigated by alanine scanning would be reduced by half. However, results indicated that both variable regions were required for inhibition of NDM-1, with variable region 1 possibly having a more fundamental role.

In an earlier study, the isolation and characterisation of highly specific Affimer reagents that inhibit SUMO-dependent protein-protein interactions was described (Hughes et al, 2017). In order to determine an explanation for the observed isoform specificity, SUMO-Affimers with deleted loops or chimeras in which a variable region was swapped between Affimer binders, were created. This revealed that for a SUMO Affimer that binds both SUMO-1 and SUMO-2, only variable region 1 was required. However, for another Affimer that bound only SUMO-2, both loops were required for binding. These results are similar to what was observed for Affimer 21, in that both loops were required for binding/inhibition of NDM-1, with the suggestion that variable region 1 may be slightly more involved in the interaction. It might be interesting to further investigate the role of variable region 2 by substituting it with a variable region 2 from an Affimer binder that bound NDM-1 but did not display inhibition, as described in chapter 4.

Affimer molecules can be easily modified by genetic or chemical means allowing easy investigation of the function of variable region residues. Alanine scanning mutagenesis of the two variable regions of Affimer 21 was performed. Initially, two residues in variable region 1 were shown to slightly improve inhibition when mutated to an alanine. However, further investigation showed that the IC_{50} values of these two mutants (G1.9A and D2.4A), were estimated to be 0.38 µM, 0.01 µM more than the IC_{50} for the original Affimer 21. Combining alanine mutations for the residues that had been shown to not contribute or negatively affect Affimer 21 binding, did not improve inhibition of NDM-1. This is similar to the observations made in the previously mentioned SUMO Affimer study, where double mutants were shown to be equally as effective as their single mutant counterparts in interacting with SUMO isoforms (Hughes et al, 2017).

Five mutated residues in variable region 1 demonstrated the lowest inhibitory activity, suggesting that these residues are the most essential for the inhibitory activity of Affimer 21. This was consistent with the earlier observation that variable region 1 may have a more significant role in inhibiting NDM-1 activity. The five critical residues were identified as Y1.2, K1.3, W1.5, T1.6 and P1.7. Tyrosine often plays a dominant role in antigen recognition by natural antibodies. Proline, threonine and lysine are frequently involved in maintaining protein structure, with proline in particular being often found in tight type II beta-turns in protein structures and playing a role in maintaining

conformational rigidity (Betts et al, 2003). Therefore, the substitution of these residues with an alanine may cause changes to the conformation of the binding region. Additionally, the ε-amino group of lysine often participates in hydrogen bonding, salt bridges and covalent interactions and the hydroxyl group of threonine is able to form hydrogen bonds with a variety of polar substrates. These amino acids may therefore play a critical role in the binding interaction with NDM-1. It is therefore perhaps unsurprising that a single mutation can almost completely remove the inhibitory action of Affimer 21. Indeed, there are many reports of single amino acid changes resulting in large alterations in protein function in the literature, with some reports of single mutations even converting inhibitory proteins into activators and vice versa (Brouwer et al, 2017 and Petti et al, 2013).

Variable region 2 also contains an HxD motif. The HxD motif is a highly conserved motif in the catalytic core of most protein kinases. It is hydrophobic, and it has been suggested that it may be a convergence point for catalytic, regulatory and substrate-binding elements because it forms several conserved hydrogen bonds with other residues (Kannan et al, 2005). Additionally, mutation of the HxD motif abolishes function in kinase enzymes (Zhang et al, 2015). It was therefore expected that mutation of these positions (H2.2 and D2.4) to an alanine might prevent inhibition of NDM-1 by the Affimer. However, whilst H2.2A was shown to reduce inhibitory potential, D2.4A had almost no effect on inhibition. This suggests that in this case, the HxD motif may not play such a crucial role in the binding interaction.

These studies demonstrate the ability to alter activity of protein modulators by small changes in their interactions. Here, the interaction between enzyme and inhibitor has been probed by alanine scanning and critical residues in the variable regions of Affimer 21 were identified. Further studies are required to fully elucidate the binding interaction between Affimer and NDM-1. However, the information gained regarding critical residues provides an important starting point for the creation of smaller, more focused sub-libraries varying the residues in these positions with the aim of improving the chance of isolating an Affimer with the best possible combination of residues for inhibition.

Chapter 6

Affinity maturation of Affimer 21

6. Affinity maturation of Affimer 21

6.1 Introduction

Saturation mutagenesis to evaluate the effects of every single possible combination of residues in a binding region is laborious and single mutations do not often result in large changes in the properties of a protein (Tiller et al, 2015). Additionally, to test all of the possible combinations of single and multiple mutations requires libraries with exceptionally high repertoires. For example, the maximum theoretical size of the Affimer library used in this project is approximately 1×10^{23} and the library produced by Tiede et al, 2014 was estimated to contain 1.3×10^{10} individual clones. Therefore, only a small subset of the possible variable region combinations can be probed using phage display; libraries for which are often dictated by the transformation efficiency of the host organism (approximately 10^{9}-10^{10} for *E. coli*) (Barbas et al, 2001). It is therefore expected that there may be Affimer proteins that were not represented in this library that may be better inhibitors than the isolated Affimer 21. As a result, it can be useful to generate sub-libraries that sample a relatively small number of residues at each of the variable region positions that are most likely to generate inhibitors with significant gains in activity (Shim, 2015).

The directed evolution of antibodies for affinity maturation is one of the most popular and effective protein engineering techniques (Wark et al, 2006). With an increase in the use of novel biologics as alternatives to antibodies, many of these techniques can be similarly applied for the isolation and improvement of non-antibody binding reagents with desirable properties. For example, directed evolution was used to develop Affibodies that bind to VEGFR2 and block VEGF-A binding. The information obtained from an alanine scan was used to guide the design of an affinity matured library from which two improved affinity binders were obtained (Fleetwood et al., 2014). Monobodies have been similarly developed. A Monobody targeting the Lyn SH3 domain has undergone directed evolution in which 130-fold increases in affinity were observed (Huang et al, 2016). The successful enhancement of desirable properties of binders in these studies suggests that similar techniques may be applied for affinity maturation of Affimer 21.

Chapter 4 described the isolation of Affimer 21, an inhibitor of NDM-1 with an IC_{50} of approximately 0.37 μM. Following alanine scanning and the identification of residues both critical and non-critical for the inhibition of NDM-1 (Chapter 5), two different approaches were trialled to generate two sub-libraries based around these residues, with the purpose of identifying an Affimer 21 variant with improved inhibitory properties.

6.2 Results

Residues which are critical for inhibition of NDM-1 were identified in variable region 1 of Affimer 21, however no critical residues were identified in variable region 2. Efforts at affinity maturation were therefore initially focused upon optimisation of variable region 1, with a view to then optimise variable region 2 through both randomisation and also modification of the size of the variable region.

6.2.1 Generation of Library 1

Alanine scanning by site-directed mutagenesis (Chapter 5) of Affimer 21 identified 5 residues (Y1.2, K1.3, W1.5, T1.6 and P1.7) in variable region 1 that when mutated to an alanine demonstrate almost complete loss of inhibitory activity of the Affimer, suggesting that these residues contribute to binding and inhibition of NDM-1. These 5 residues were therefore randomised using codon-selected semi-trinucleotide cassette synthesis (excluding cysteines); and a new library generated with the aim of finding the best possible combination of residues in these positions for improved inhibition of NDM-1.

The library was constructed by SOE of two PCR products that were amplified from the pBSTG-Aff phagemid vector containing the Affimer 21 sequence (Section 2.2.4). All primers were synthesized by Ella Biotech (Germany). The first PCR product extended from the *DsbA* coding sequence to the first variable loop (fragment 1) and the second PCR product (fragment 2) introduced the two nine amino acid variable regions of the Affimer 21 sequence (Figure 6.1), whilst randomizing the five residues in variable region 1 that had been shown to be essential for inhibition of NDM-1.

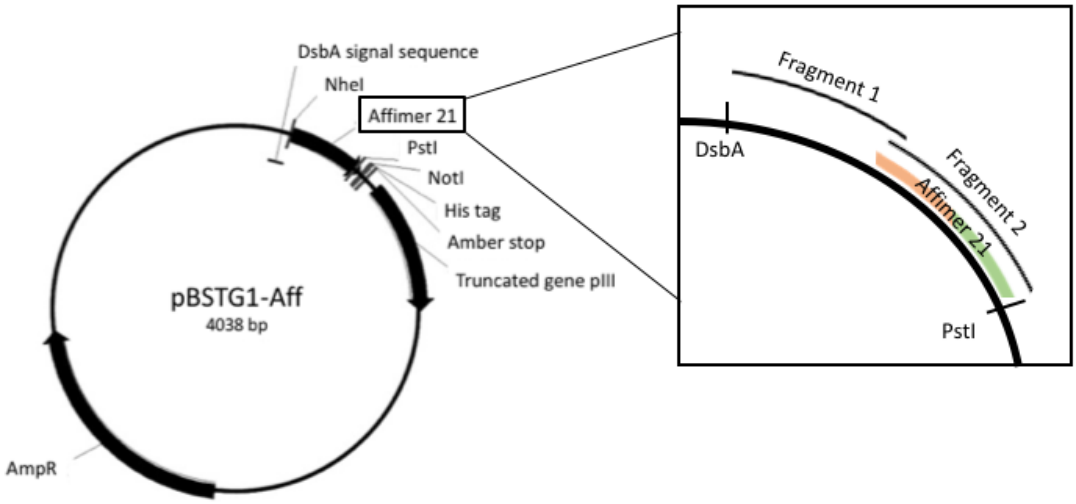

Figure 6.1: Fragment 1 and 2. The final PCR product was cloned into a pBSTG1-Aff plasmid to enable production of phage III coat proteins conjugated to the resulting library of Affimers. The first PCR product (fragment 1) extended from the DsbA coding sequence to the first variable loop, and the second PCR product introduced the two nine amino acid variable regions of the Affimer 21 sequence (fragment 2).

The degenerate positions (NNN) were introduced as trimers representing a single codon for each of the 19 amino acids excluding cysteines and stop codons. Following the SOE PCR to join the two fragments together, the fragment 1 forward primer (P1) and the fragment 2 reverse primer (P4) were used in a final reaction that incorporated five rounds of amplification to generate a final amplification product (Section 2.2.4.1, Figure 2.3). DNA products were analysed by agarose gel electrophoresis (Figure 6.2).

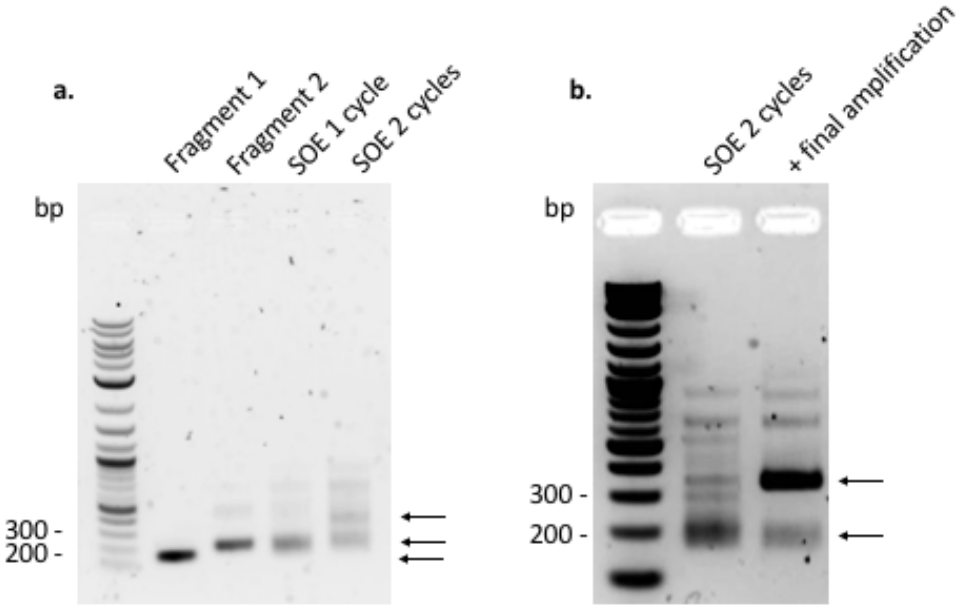

Figure 6.2: Construction of Library 1 insert DNA by splice overlap extension. Following initial PCRs to generate fragment 1 and 2, SOE reactions and final amplification, all products were analysed by agarose gel electrophoresis **(a)** Fragment 1 and fragment 2 amplified DNA were run on a 0.8 % agarose gel. Ten cycles of SOE PCR to join the two fragments was carried out (SOE 1 cycle), followed by addition of 0.02 U/ul extra Phusion DNA polymerase and a further ten cycles of SOE (SOE 2 cycles). 8 µl of DNA was loaded for each. **(b)** Five rounds of amplification to generate a final amplification product using primer P1 and P4 was carried out and run alongside the SOE 2 cycles product on a 2 % agarose gel. 4 µl of DNA was loaded.

After the final library insert PCR product had been generated, it was digested using *NheI*-HF and *PstI*-HF restriction enzymes and ligated into a pDHis vector digested with the same enzymes. The pDHis vector was dephosphorylated to prevent re-ligation. In order to determine the best ligation ratio of insert to vector DNA, a series of test ligations were performed. Additionally, two different ligases were compared (Figure 6.3). The resulting ligation products were transformed into *E. coli* XL1 Blue supercompetent cells and plated on LB agar plates supplemented with carbenicillin (Section 2.2.1.10). The following day, colonies were counted on each plate.

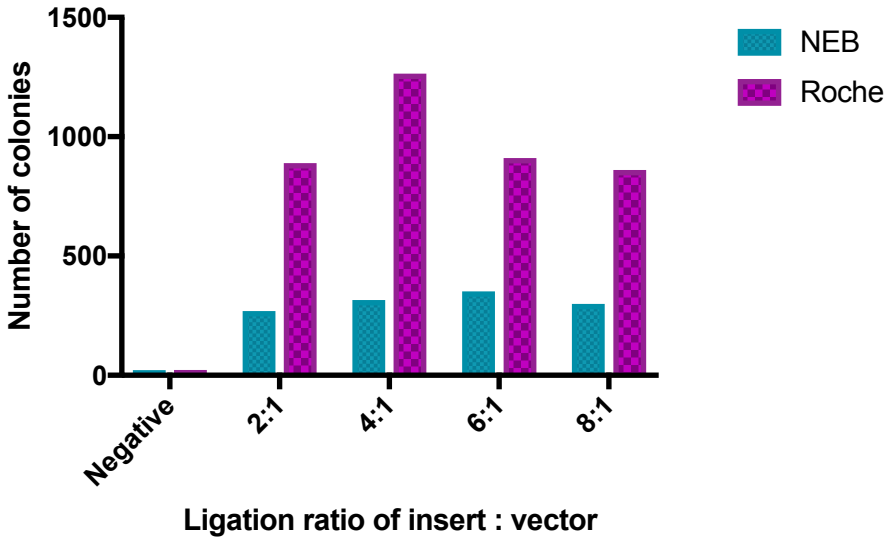

Figure 6.3: Number of colonies on ligation test plates. Ligation ratios of molar concentrations of insert to vector ranging from 2:1 to 8:1 were set up. Ligations were performed with both NEB and Roche T4 DNA ligase to compare efficiency. A negative control containing no insert DNA was also carried out.

A ligation ratio of 4:1 molar concentration of insert to vector using Roche T4 DNA ligase was found to give the most colonies and was used for all subsequent ligation reactions. There were very few colonies on the negative control plates which indicates that the vector was efficiently digested and dephosphorylated. Colonies selected at random were grown up and phagemid DNA extracted for DNA sequencing analysis using the pDHis-specific primer M13R (Table 6.1).

Table 6.1: Variable region amino acid sequences of 8 clones from Library 1

Affimer clone	Variable region 1	Variable region 2
1	**G**HA**V**TQG**YG**	**THWDNGGLR**
2	**G**NL**V**DET**YG**	**THWDNGGLR**
3	**G**EV**V**LVQ**YG**	**THWDNGGLR**
4	**G**QE**V**TQY**YG**	**THWDNGGLR**
5	**G**IQ**V**LAE**YG**	**THWDNGGLR**
6	**G**WW**V**WLW**YG**	**THWDNGGLR**
7	**G**KS**V**PSV**YG**	**THWDNGGLR**
8	**G**RH**V**ENK**YG**	**THWDNGGLR**

* residues in bold indicate those that were conserved from the original Affimer 21 sequence

The translated DNA sequencing results demonstrated a good level in the variety of residues incorporated in the randomised positions. Subsequently, the ligation was scaled up 10x and electroporated into electrocompetent *E. coli* ER2738 cells (Section 2.2.1.12). Cell samples were plated out at a range of dilutions (1:10 - 1:100,000) onto agar plates containing carbenicillin to allow for estimation of the library size (Table 6.2). The 1:10 dilution plate contained too many colonies to accurately count and was therefore excluded.

Table 6.2: Estimation of library size from total infected cells

Dilution factor	µl plated	Average no. of colonies	Cells per µl	Total cells in 15 ml
1:100	10	109.5	1095	1.64×10^7
1:1000	10	10.7	1070	1.6×10^7
1:10,000	10	1	1000	1.5×10^7
1:100,000	10	0	-	-

The mean library size was therefore estimated to be approximately 1.58×10^7. The maximum theoretical size of the library can be calculated as 19^5 (19 possible residues and 5 positions randomised), which is 2.48×10^6. The generated library was therefore estimated to give 6.37x coverage of the possible combinations in the theoretical library. A further 96 colonies were randomly selected from the ligation plates and sequenced to check the diversity of amino acid incorporation in the 5 randomised positions (Figure 6.4). The theoretical inclusion rate for each of the 19 amino acids at any given randomised position was calculated to be 5.26 % (100 ÷ 19).

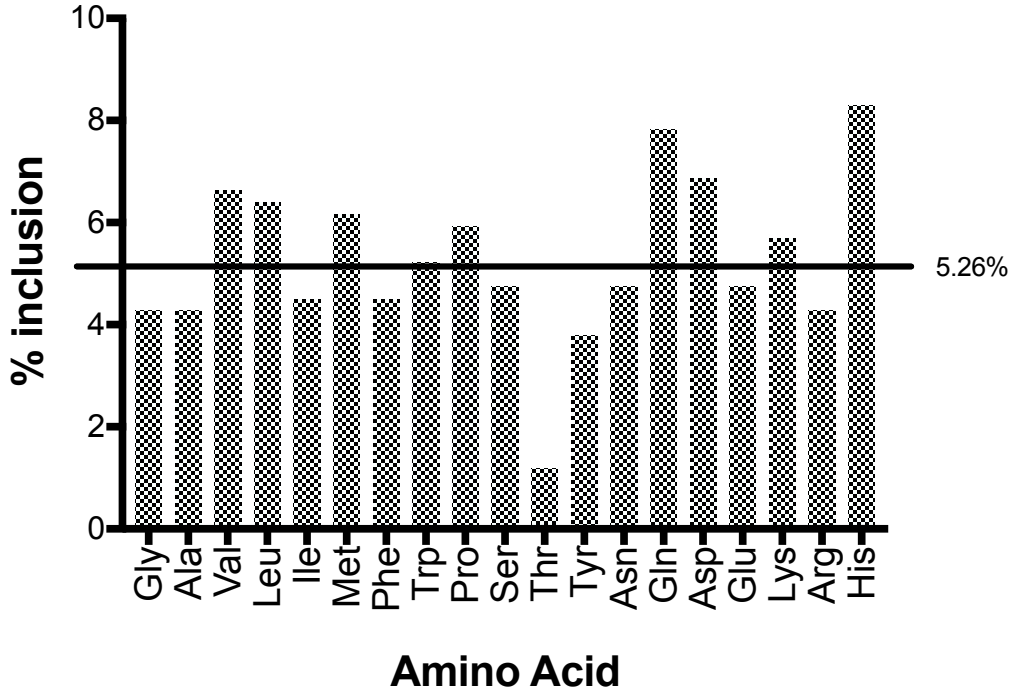

Figure 6.4: Inclusion rates (%) of amino acids in the 5 randomised positions of library 1. The theoretical inclusion rate for each of the 19 amino acids at any given randomised position was calculated to be 5.26 %.

The majority of amino acids are incorporated at close to the theoretical inclusion rate of 5.26 %. Histidines were the most frequently observed residue, with threonines being the least frequently observed. As Ella Biotech correct for the reaction factor of each trimer used in their primer synthesis process to ensure equal incorporation, this is most likely due to the relatively small number of clones sequenced and might be corrected for by increasing the observed population size.

To maintain the amount of input phage between phage display screens, it is necessary to first determine the phage titre of the library. The phage titre of library 1 was estimated via two methods and determined as 1.56×10^{14} and 9.3×10^{11} (per ml) by spectrophotometric quantification (Section 2.2.4.2) and plating out (Section 2.2.4.3), respectively. Spectrophotometric analysis is considered the most accurate method for measuring phage titre as there is less potential for introducing pipetting or counting errors (Barbas et al, 2001). It was also the method used for determining the phage titre

of the original Affimer library. Therefore, the titre determined by spectrophotometer was the measurement used to estimate the quantity of library needed for screening.

6.2.2 Isolation of Affimers against NDM-1 from Library 1

For phage display screening, the target protein is immobilised to allow for several cycles of phage introduction, washing and elution. The interaction between biotin and streptavidin is the strongest non-covalent binding known (K_D of 10^{-15} M), and is therefore commonly used for the immobilisation of target proteins in biotechnological applications (Green, 1990). Biotinylation is most commonly achieved via chemical reactions. However, a limitation of this is the uncontrollable binding of biotin to sites of the target protein that might be important for biological activity. To overcome this problem, techniques which mimic *in vivo* physiological biotinylation have been developed, using peptide 'tags' that are recognised as biotinylation sites as described below.

6.2.2.1 Insertion of an N-terminal biotin acceptor peptide to NDM-1 constructs

The chemical EZ-Link® NH-SS-Biotin enables biotinylation of target proteins via primary amines. NDM-1 contains several lysines that are in close proximity to the active site and it was hypothesised that biotinylation via NH-SS-Biotin at these sites might restrict both Affimer binding and substrate access (Figure 6.5). Therefore, primers to insert a unique 15 amino acid biotin acceptor peptide (BAP tag) for directed biotinylation of NDM-1 were designed to allow for enzymatic conjugation of a single biotin via biotin ligase (Section 2.2.1.4).

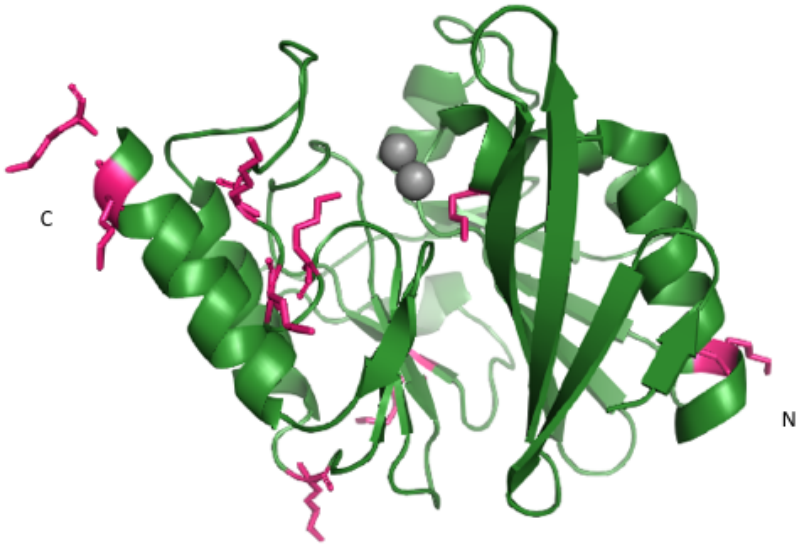

Figure 6.5: Structure of apo-NDM-1 (PDB: 3SPU) Cartoon of apo NDM-1 structure. Highlighted are the active site zinc ions (grey spheres) and lysine residues (pink), several of which are in close proximity to the active site (adapted from King et al, 2011).

The active site of NDM-1 is on the C-terminal side of the protein and therefore primers were designed to insert the BAP tag at the N-terminus after the *pelB* signal sequence of pD861-pelB-NDM-1. Immobilisation of biotinylated NDM-1 via streptavidin coated plates would then theoretically present the C-terminus and active site for Affimer binding during phage display screening (Section 2.2.2.3). The modified sequence of pD861-pelB-NDM-1 was checked using SignalP 4.0 (Petersen et al, 2011) to ensure that the BAP tag insertion was in frame and that the restriction sites would still cleave. An inverse PCR mutagenesis method was performed as described in Section 2.2.1.4 and digested with *DpnI* before being checked on an agarose gel (Figure 6.6a) (Section 2.2.1.7). Supercompetent XL1-Blue cells were transformed with the pD861-pelB-NDM-1 (+ BAP) DNA and 5 colonies picked at random from the agar plate. The cells were grown up and the plasmid purified and sent for sequencing to confirm BAP tag inclusion (Figure 6.6b). Sequencing results confirmed the insertion of a BAP after the *pelB* signal sequence of pD861-pelB-NDM-1. BL21 Star^{TM} (DE3) cells were then transformed with the DNA for protein production (Section 2.2.3.2). Purified protein was checked on a SDS-PAGE gel (Figure 6.6c) and dialysed into 1x PBS + 30% v/v glycerol for storage.

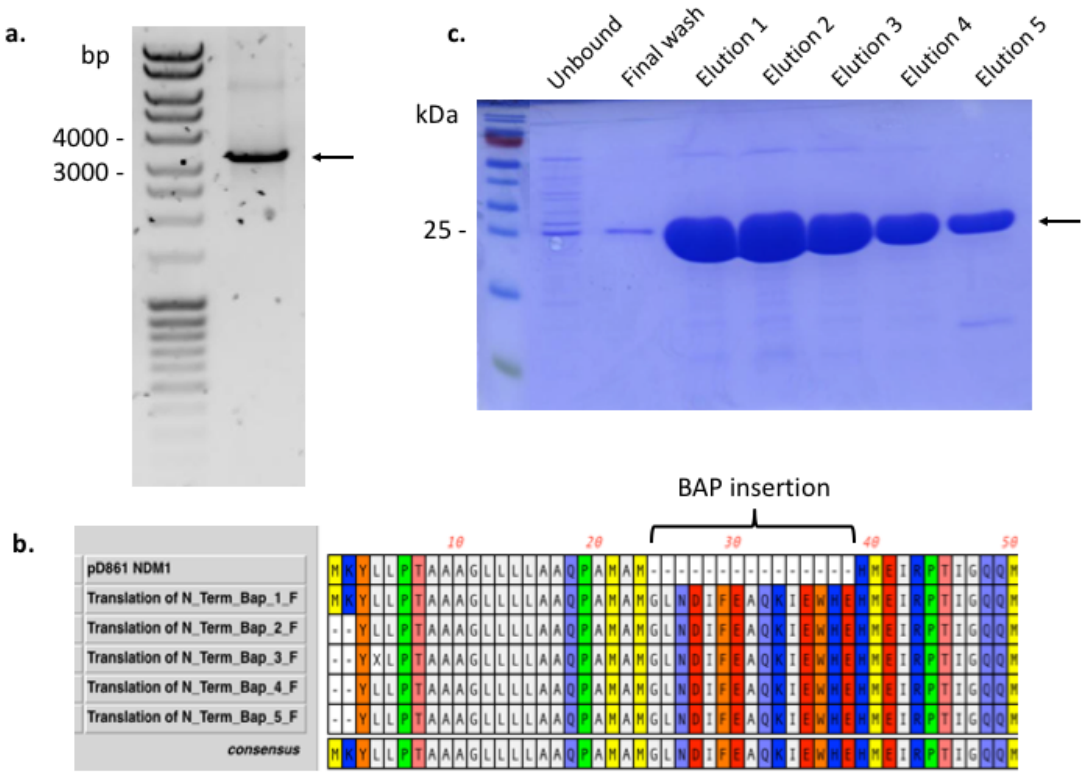

Figure 6.6: Insertion of an N-terminal biotin acceptor peptide to NDM-1 constructs. (a). Inverse PCR mutagenesis was used to introduce a biotin acceptor peptide (BAP tag) at the N-terminal of pD861-pelB-NDM-1 (Section 2.2.1.4., Figure 2.1). The DNA products were analysed on a 0.8 % agarose gel resulting in an approximately 3500 bp product as indicated by the arrow. 1 µl of DNA and 5 µl of MassRuler ladder were loaded. **(b)** Supercompetent XL1-Blue cells were transformed with the pD861-pelB-NDM-1 (+ BAP) DNA (Section 2.2.1.11) and 5 colonies picked at random. The cells were grown up and the plasmid purified (Section 2.2.1.13) and sent for sequencing to confirm BAP tag inclusion (Section 2.2.1.17). Sequencing results show the insertion of a biotin acceptor peptide (BAP insertion) after the *pelB* signal sequence of pD861-pelB-NDM-1. **(c)** Production and purification of pD861-pelB-NDM-1 from BL21 Star™ (DE3) cells. The protein was purified from bacterial cell lysate using nickel ion affinity chromatography and analysed by SDS-PAGE and Coomassie blue staining. NDM-1 was eluted and visualised at 25 kDa as indicated by the arrow.

Strains of *E. coli* contain a biotin ligase enzyme called *BirA* which biotinylates the BAP tag *in vivo* in the presence of ATP (Schatz, 1993). Strain AVB101 is an *E. coli* B strain that contains pBirAcm, an engineered pACYC184 plasmid with an IPTG inducible *birA* gene to overexpress biotin ligase. To optimise *in vivo* biotinylation, a trial to produce NDM-1 (+BAP) protein in AVB101 cells (Section 2.2.3.2.2) was conducted alongside production in BL21 Star™ (DE3) cells, with and without addition of d-biotin (Figure 6.7).

a.

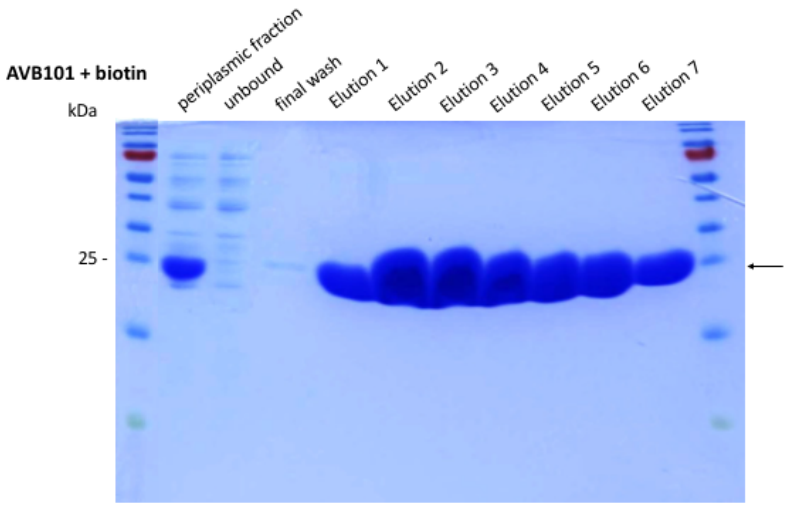

b.

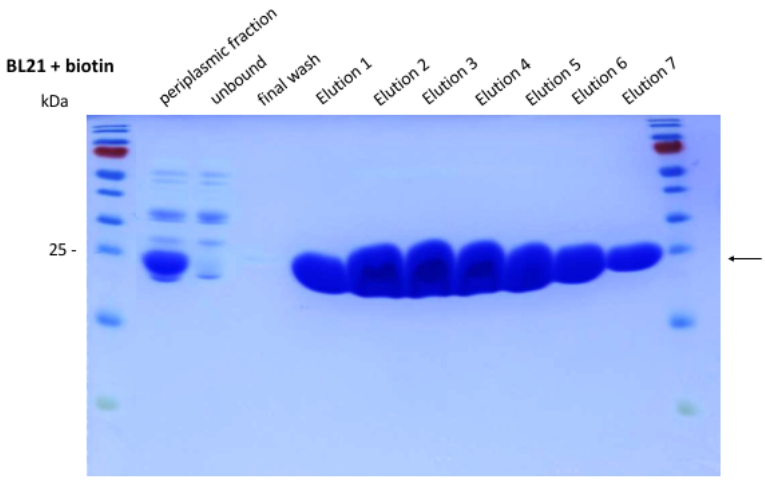

c.

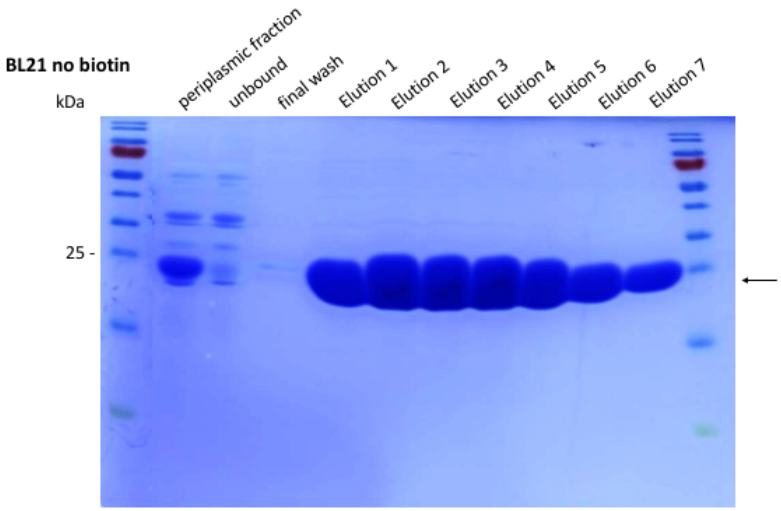

Figure 6.7: SDS-PAGE analysis of NDM-1 (+BAP) production and purification in AVB101 and BL21 Star™ (DE3) cells, with and without additional biotin. (a) NDM-1 (+BAP) produced in AVB101 cells with addition of 50 µM d-biotin. **(b)** NDM-1 (+BAP) produced in BL21 Star™ (DE3) cells with addition of 50 µM d-biotin. **(c)** NDM-1 (+BAP) produced in BL21 Star™ (DE3) cells with no additional biotin. The proteins were purified from bacterial cell lysate using nickel ion affinity chromatography and separated by SDS-PAGE on a 15 % resolving gel and stained with Coomassie Blue to check purity. NDM-1 was visualised at 25 kDa as indicated by the arrows.

The NDM-1 (+BAP) protein expressed well in both cell lines, with and without the additional D-biotin. To determine any differences in the level of biotinylation of the purified proteins, a biotin ELISA was performed (Section 2.2.2.2) (Figure 6.8a).

a.

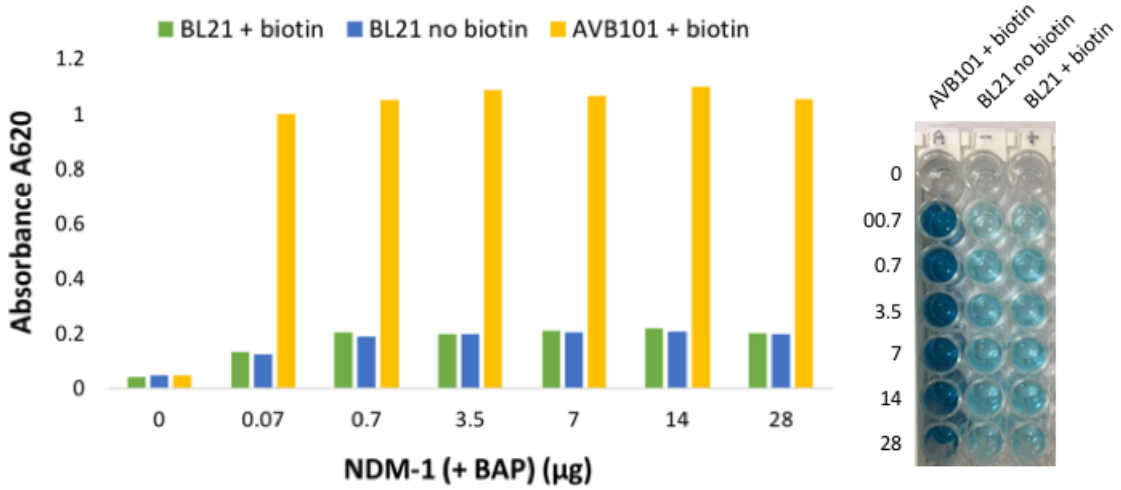

b.

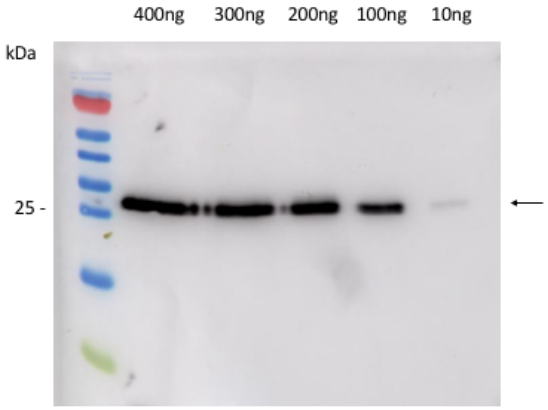

Figure 6.8: Biotinylation checks for NDM-1 (+ BAP) (a) Biotin ELISA using a gradient of concentrations of NDM-1 (+ BAP). A range of concentrations (0 to 28 µg) of NDM-1 (+ BAP) protein produced in either AVB101 or BL21 Star™ (DE3) cells, with or without additional biotin, were added to Nunc-Immuno MaxiSorp™ Strips. Biotinylated NDM-1 was detected using High Sensitivity Streptavidin-HRP and visualised upon addition of TMB. Absorbance was recorded at 620 nm using a Multiskan Ascent Plate Reader **(b)** A range of concentrations of NDM-1 (+ BAP) protein produced in AVB101 cells were separated according to mobility by SDS-PAGE on a 15 % resolving gel. Proteins were transferred onto a mini format PVDF membrane with 0.2 µm pore size using a Trans-Blot Turbo transfer system and probed with 1:10,000 Anti-Streptavidin-HRP antibody by western blot analysis. Membranes were visualised using Luminata Forte Western HRP Substrate and chemiluminescence on an Amersham Imager 600.

NDM-1 (+ BAP) produced in AVB101 cells with addition of d-biotin gave approximately 5x higher absorbance signal in a biotin ELISA than the NDM-1 produced in BL21 Star™ DE3 cells. Biotinylation of the NDM-1 (+BAP) produced in the AVB101 cells was also confirmed by western blotting analysis (Section 2.2.3.4.4) (Figure 6.8b). To determine whether Affimer- expressing phage are still able to bind to biotinylated and immobilised NDM-1 (+ BAP) in a phage display screen, a phage ELISA using Affimer 21 phage was also carried out (Figure 6.9).

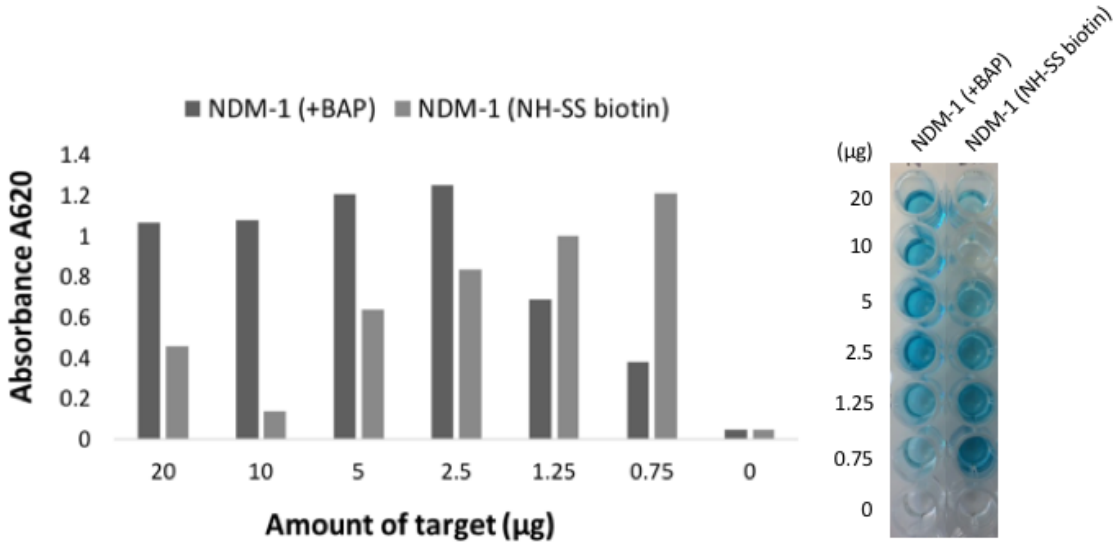

Figure 6.9: Phage ELISA results to confirm Affimer 21 phage binds to NDM-1 (+BAP). Affimer 21 phage was tested in a phage ELISA against NDM-1 (+BAP) and NDM-1 which had been chemically biotinylated using NH-SS biotin, at a range of target concentrations. Phage binding was detected with anti-Fd bacteriophage-HRP antibody and visualised on addition of TMB. Absorbance at 620nm was measured for each well.

The phage ELISA confirmed that Affimer 21 phage was able to bind to both in vivo biotinylated NDM-1 (+BAP) and chemically biotinylated NDM-1 (NH-SS biotin). Chemically biotinylated NDM-1 (NH-SS biotin) seemed to give a stronger absorbance signal at lower concentrations, which might suggest that the phage has difficulty accessing the binding site when more target molecules are presented and there is greater steric hindrance. As these target molecules are randomly biotinylated, it is likely that they are presented in different positions and that the binding epitope is only accessible in certain orientations. The NDM-1 (+BAP) gave the largest absorbance signal at concentrations greater than 2.5 µg, with 2.5 µg being optimal. To minimise

differences in the orientation of the target molecule and possible blocking of the active site, the NDM-1 (+BAP) produced in AVB101 cells was used in all further assays.

In order to identify Affimer binders that are able to inhibit NDM-1, phage display screening should ideally be done against NDM-1 target protein that is in a conformationally active epitope. To confirm whether the modified and biotinylated NDM-1 (+BAP) was still functional, activity was assessed and compared to un-biotinylated NDM-1 and chemically biotinylated NDM-1 (NH-SS biotin) in a β-lactamase activity assay with nitrocefin as the substrate (Section 2.2.5.1) (Figure 6.10).

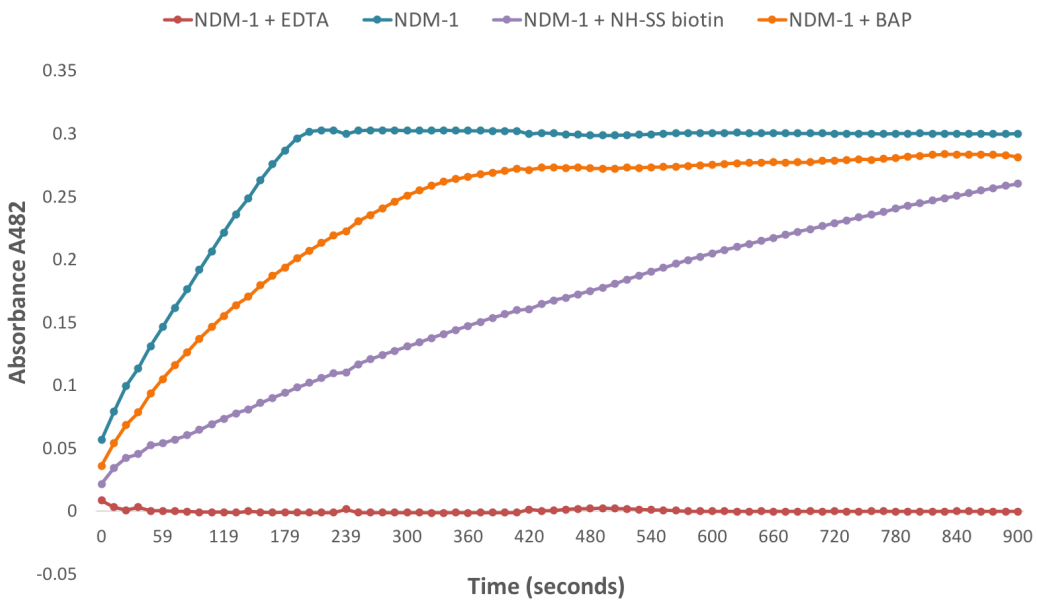

Figure 6.10: Rate of nitrocefin hydrolysis by NDM-1. NDM-1 activity was quantified by spectrophotometric measurement of nitrocefin hydrolysis at 482 nm and at 25 °C on a Tecan Spark microplate reader and readings for each well were taken every 12 secs for 15 min. Data was normalised to the EDTA control. The change in absorbance at 482 nm for un-biotinylated NDM-1 was recorded and compared to the change in absorbance for NDM-1 biotinylated via a BAP tag (NDM-1 + BAP) or chemical biotinylation (NDM-1 + NH-SS biotin).

Un-biotinylated NDM-1 showed the fastest rate of nitrocefin hydrolysis, with NDM-1 (+BAP) showing a slightly reduced rate of activity. NDM-1 (NH-SS biotin) showed the

largest decrease in the initial rate of activity, with a reduction in absorbance reading of approximately 75 % compared to the un-biotinylated NDM-1. NDM-1 (+BAP) was therefore taken forward as the target protein for subsequent phage display screens.

6.2.2.2 Phage display screening of library 1

Following the successful generation of library 1, immobilised NDM-1 (+BAP) was subjected to three rounds of phage display (Section 2.2.2.3) and 92 clones were selected at random from the final pan and checked for binding to NDM-1 by phage ELISA (Section 2.2.2.6) (Figure 6.11). Affimer 21 phage was produced alongside the 92 clones and included in the ELISA as a positive control. Of the 92 clones tested, 60 displayed binding to the target with no clones displaying non-specific binding to the control wells.

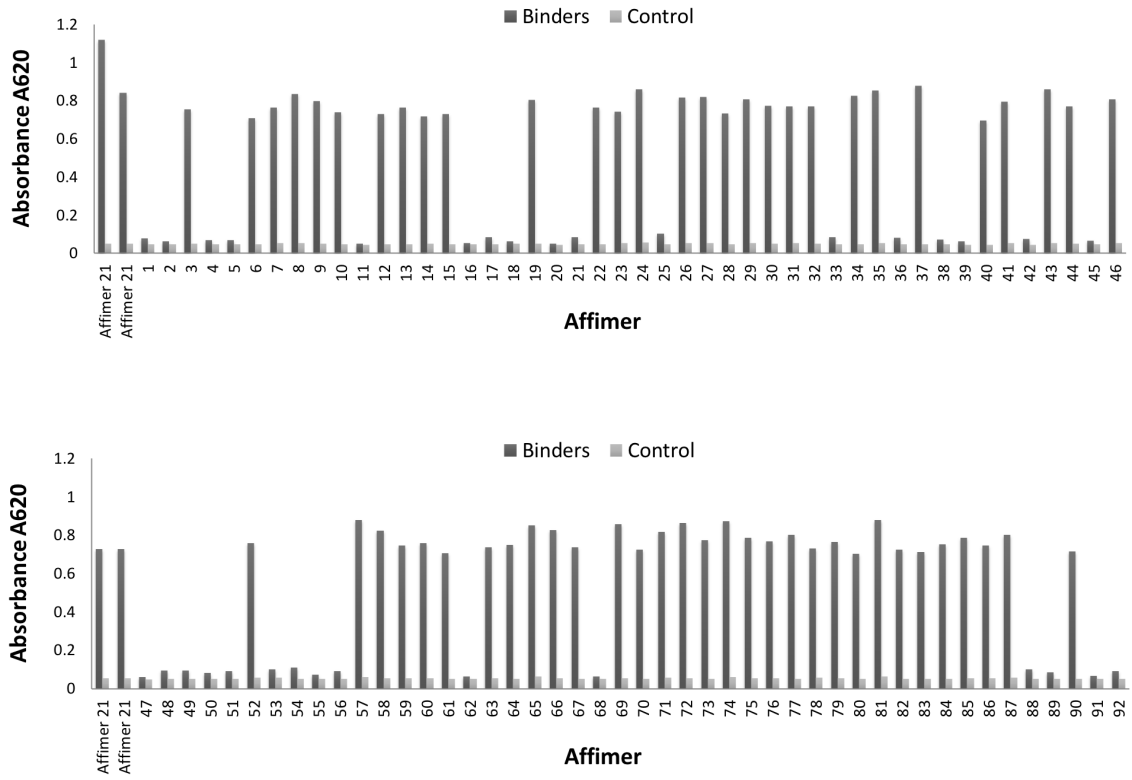

Figure 6.11: Phage ELISA results for Affimer reagents selected from library 1 against NDM-1 (+BAP). Following three rounds of phage display against NDM-1 (+BAP), 92 colonies were tested in a phage ELISA. Each colony represented one Affimer and was tested for binding against NDM-1 (+BAP) or an empty control well. Phage binding was detected with anti-Fd bacteriophage-HRP antibody and visualised on addition of TMB. Absorbance at 620nm was measured for each well.

The 60 clones that displayed binding to NDM-1 in the phage ELISA were grown up, DNA extracted and sequenced. Surprisingly, sequencing analysis revealed that all 60 clones were original Affimer 21 (Table 6.3).

Table 6.3: Variable region sequences for Affimer reagents selected against NDM-1 from library 1

Affimer	Variable region 1	Variable region 2	No. of sequencing appearances
21	GYKVWTPYG	THWDNGGLR	60

To check that the library had not been contaminated with Affimer 21, ER2738 cells were re-infected with library 1 and plated onto LB agar plates containing 100 µg/ml carbenicillin. Ten colonies were selected at random and sent for sequencing (Figure 6.12). None of these sequenced clones came back as Affimer 21.

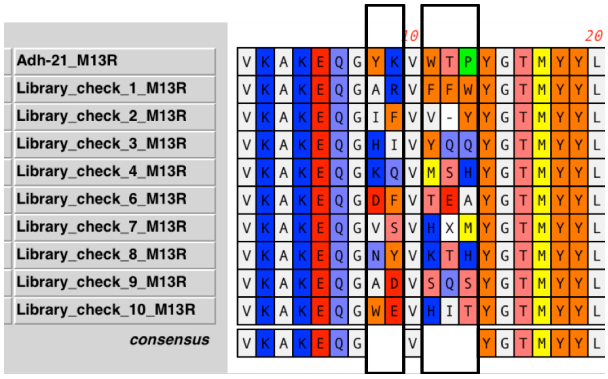

Figure 6.12: Sequencing results of ten library 1 clones. Analysis of variable region 1 confirmed that none of the clones were original Affimer 21. Alignment was made using MacVector 13.5.2.

It was hypothesised that increasing the stringency of the phage display screen might allow for the isolation of Affimer binders with higher affinity for NDM-1 than the original Affimer 21. The initial rate of reaction of an enzyme depends partly upon the affinity of the enzyme for its substrate. Similarly, the potency of an inhibitor depends upon its affinity for the enzyme and ability to slow the rate of reaction by blocking the interaction between the enzyme and its substrate. Therefore, increasing the stringency of the phage display screen to try to select for the highest affinity Affimers might also lead to more potent inhibitors of NDM-1.

The phage display screen was repeated with several adaptations to the original protocol to increase stringency (Section 2.2.2.5):

- shorter incubation of library with the target; to select for binders with the fastest on-rate. Incubation of the library with the target NDM-1 was reduced from the standard 1 hour to 3 minutes.
- longer incubation with more wash steps before eluting bound Affimers; to remove Affimers with weaker affinity from the selection process. Eight identical pans were set up and on each consecutive day the strips were washed 27x and one well was eluted.
- introduction of competition; addition of un-biotinylated NDM-1 to prevent any unbound phage from re-binding to the immobilised NDM1. After the daily 27x wash, fresh un-biotinylated NDM-1 was added to all remaining wells to capture binding reagents with a high off rate.
- an extra elution step; to ensure that the tightest bound Affimer binders are isolated from the screen. An additional trypsin elution step was performed following the low/high pH elutions and used to re-infect a separate aliquot of ER2728 cells

Following re-infection of ER2738 cells with eluted phage, the remaining cells were centrifuged and DNA extracted and sent for sequencing (Section 2.2.1.13). Overlapping peaks at variable region 1 confirmed that a mixed population of Affimer binders were present in the pool, rather than Affimer 21 sequence only (Figure 6.13).

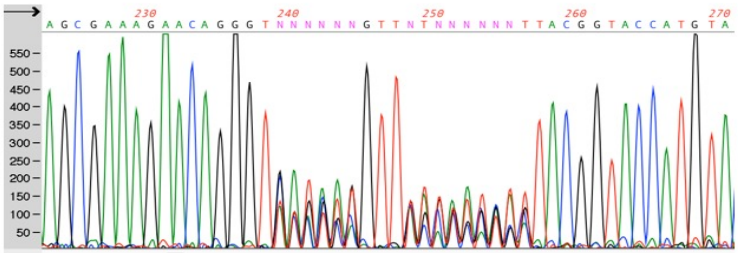

Figure 6.13: Sequencing trace of variable region 1 for eluted phage pool. ER2738 cells were re-infected with eluted phage and DNA extracted for sequencing. Overlapping peaks at variable region 1 confirmed that a mixed population of Affimer binders were present in the pool.

Following re-infection of ER2738 cells, dilutions were plated onto LB agar plates containing 100 µg/ml carbenicillin and grown overnight. Forty-five colonies were picked from each daily elution and tested in phage ELISAs (Section 2.2.2.6). Affimer 21 phage was included on each plate as a control. The phage ELISA for the final day of elutions (Day 8) is shown here as an example (Figure 6.14).

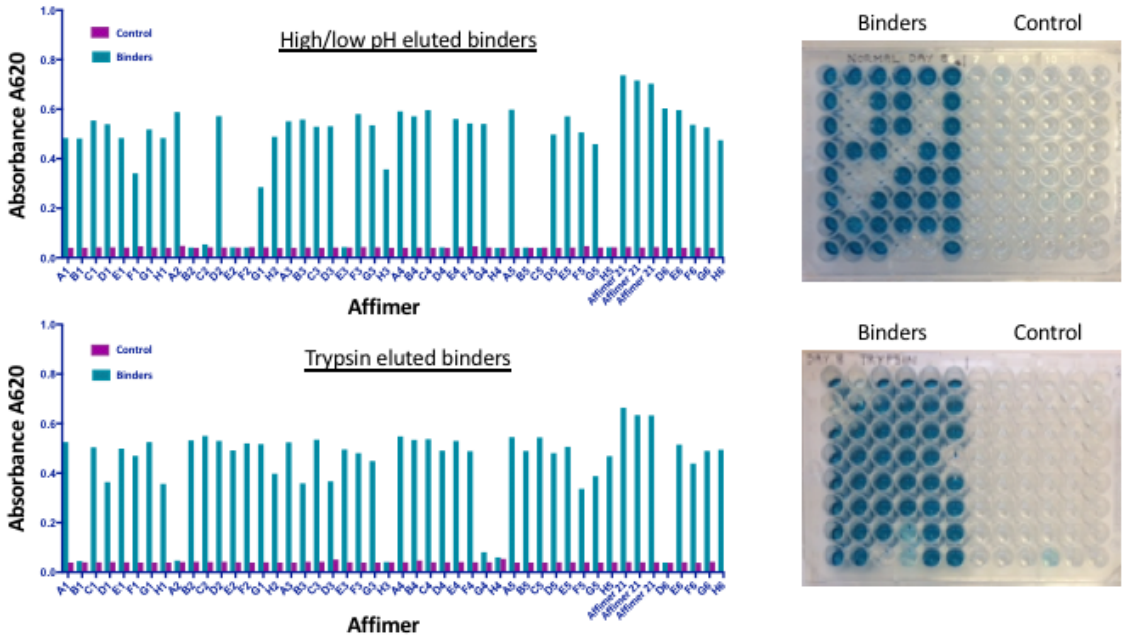

Figure 6.14: Phage ELISA results for Affimer binders selected from a competitive screen of library 1 against NDM-1 (+BAP). Following eight days of competitive screening, 45 colonies from the high/low pH elution and 45 colonies from the trypsin elution agar plates were tested in a phage ELISA. Each colony represented one Affimer and was tested for binding against NDM-1 (+BAP) or an empty control well. Affimer 21 phage was included in triplicate on each plate as a control. Phage binding was detected with anti-Fd bacteriophage-HRP antibody and visualised on addition of TMB. Absorbance at 620nm was measured for each well.

The clones that displayed binding to NDM-1 in the phage ELISAs for the 8 days of elutions were sequenced and 23 unique binders were identified (Table 6.4). The original Affimer 21 was isolated 8 times on day 1 but did not appear following the introduction of competition (unbiotinylated NDM-1). Variable region 1 of Affimer 22 contained an insertion of an extra residue between position 1.4 and 1.8.

Table 6.4: Variable region amino acid sequences for Affimers selected against NDM-1 from library 1 by competitive screening

Day	Clone	Variable region 1	Variable region 2	No. of sequencing appearances
1	21	**GYKVWTPYG**	**THWDNGGLR**	8
1	39	**G**EH**V**HQN**YG**	**THWDNGGLR**	1
2	1	**G**RR**V**VSK**YG**	**THWDNGGLR**	1
2	2	**G**VF**V**FVI**YG**	**THWDNGGLR**	1
2	3	**G**KH**V**KKT**YG**	**THWDNGGLR**	1
2	4	**G**PS**V**FLW**YG**	**THWDNGGLR**	1
2	5	**G**QN**V**VIY**YG**	**THWDNGGLR**	1
2	6	**G**KM**V**LVW**YG**	**THWDNGGLR**	1
2	7	**G**VA**V**QIH**YG**	**THWDNGGLR**	1
2	8	**G**NN**V**VWL**YG**	**THWDNGGLR**	1
3	9	**G**NY**V**IYI**YG**	**THWDNGGLR**	1
3	10	**G**NI**V**IYI**YG**	**THWDNGGLR**	2
3	12	**G**HD**V**VWV**YG**	**THWDNGGLR**	1
3	14	**G**QF**V**IMY**YG**	**THWDNGGLR**	1
4	15	**G**PI**V**WWI**YG**	**THWDNGGLR**	1
4	16	**GY**Y**V**RIT**YG**	**THWDNGGLR**	1
4	17	**G**AR**V**WKK**YG**	**THWDNGGLR**	1
5	18	**G**KF**V**IYL**YG**	**THWDNGGLR**	1
5	19	**G**VF**V**IRM**YG**	**THWDNGGLR**	1
6	20	**G**MK**V**VVM**YG**	**THWDNGGLR**	2
7	22	**G**GR**V**VMQI**YG**	**THWDNGGLR**	1
7	23	**G**WY**V**LRH**YG**	**THWDNGGLR**	1
8	47	**G**GD**V**SSG**YG**	**THWDNGGLR**	1
8	48	**G**FK**V**DNH**YG**	**THWDNGGLR**	1

*residues in bold indicate those that were conserved from the original Affimer 21 sequence

A heat map demonstrating the amino acid enrichment at each of the randomised positions was produced (Figure 6.15). Enrichment of an isoleucine or valine at position W1.5, a valine at T1.6 and an isoleucine at P1.7 could be observed, suggesting that a hydrophobic residue is preferentially included at positions 1.5, 1.6 and 1.7.

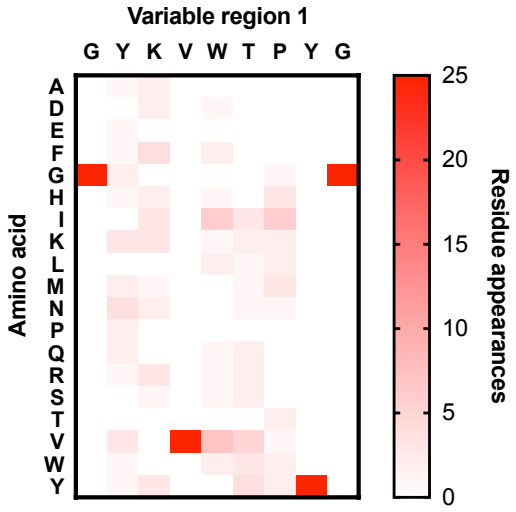

Figure 6.15: Heat map showing amino acid enrichment at the randomised positions of Affimer 21. The original residues for Affimer 21 are listed across the top. Dark red indicates high enrichment and white indicates no enrichment.

The 23 unique clones that showed positive binding to NDM-1 in the phage ELISA were taken forward for subcloning and expression independently of the PIII phage coat protein (Section 2.2.3) (Figure 6.16).

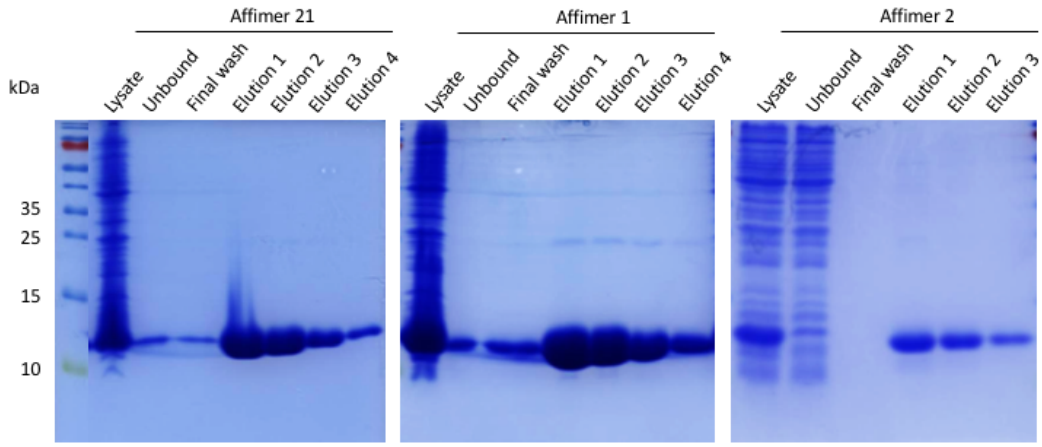

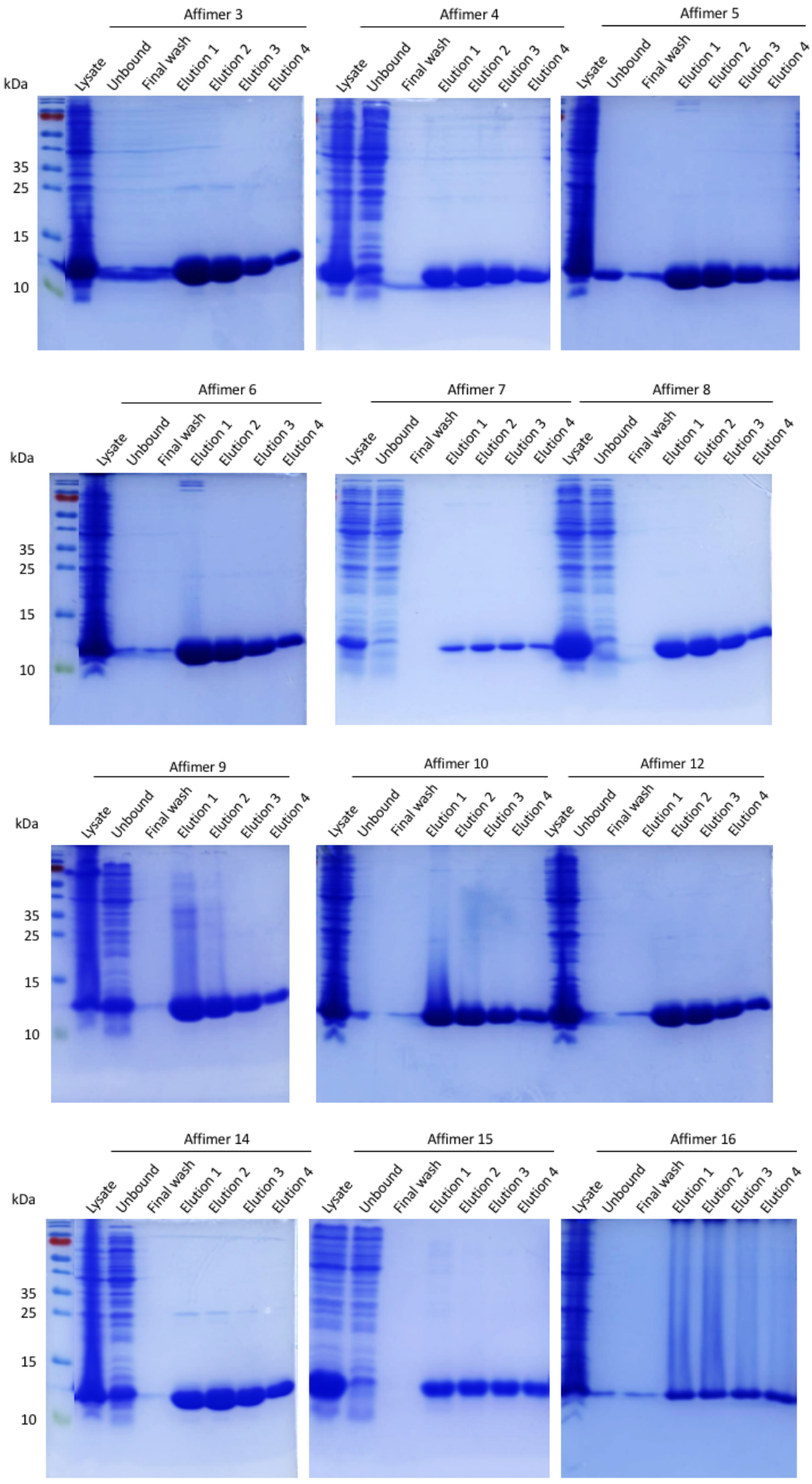
Affimer 3
Affimer 4
Affimer 5
Affimer 6
Affimer 7
Affimer 8
Affimer 9
Affimer 10
Affimer 12
Affimer 14
Affimer 15
Affimer 16
Lysate
Unbound
Final wash
Elution 1
Elution 2
Elution 3
Elution 4
kDa
35
25
15
10

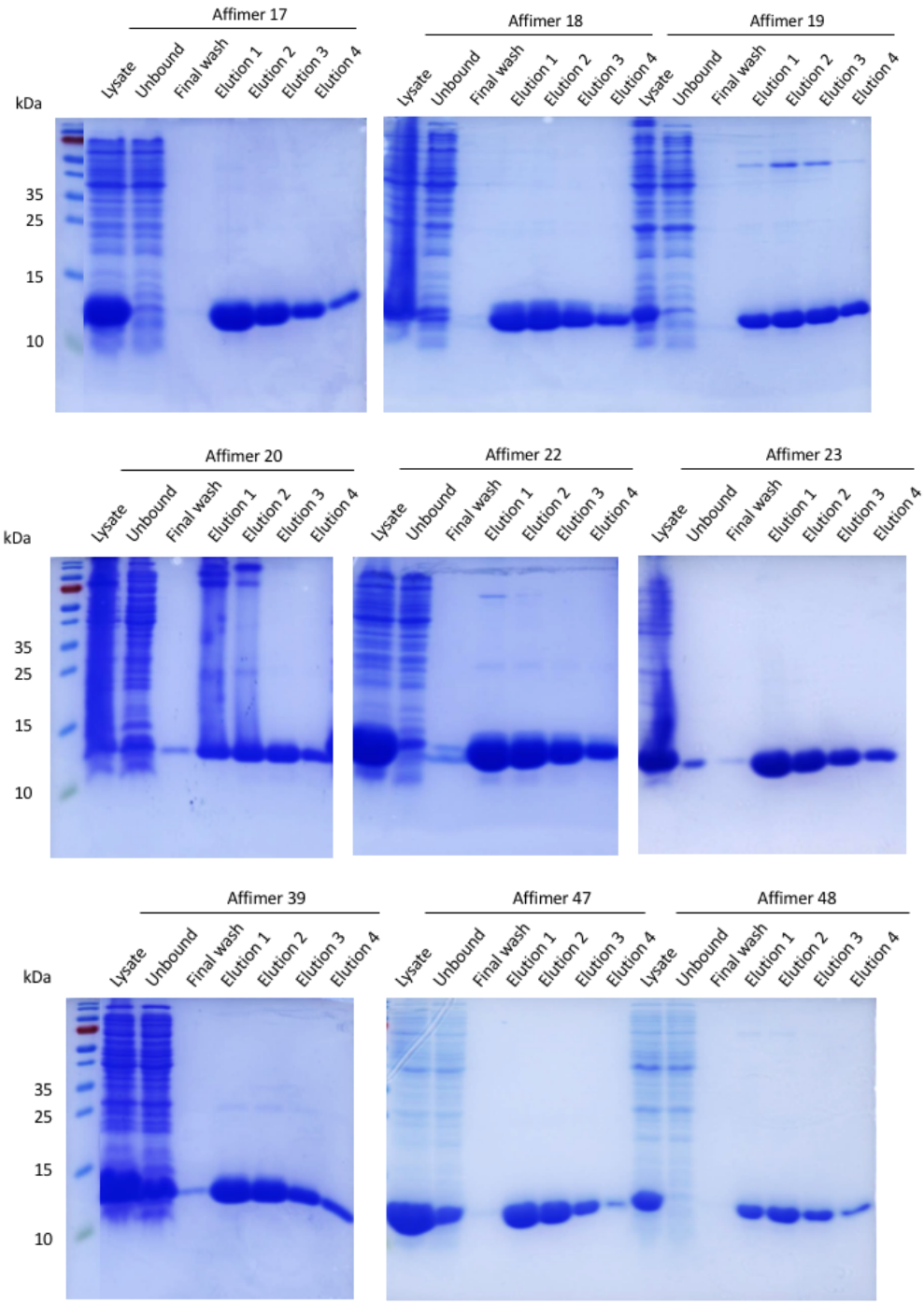

Figure 6.16: SDS-PAGE analysis of Affimer production and purification in BL21 Star™ (DE3) cells. Affimers isolated from library 1 were sub-cloned from the pBSTG-Aff phagemid vector into pET11a and produced in BL21 Star™ (DE3) cells. The proteins were purified from bacterial cell lysate using nickel ion affinity chromatography and separated by SDS-PAGE on a 15 % resolving gel and stained with Coomassie Blue to check purity. Affimers were visualised at ~12 kDa.

Purified Affimer proteins were then tested in β-Lactamase activity assays with nitrocefin as the substrate (Section 2.2.5.1), to determine whether they had any effect on NDM-1 enzyme activity (Figure 6.17). Reactions included 100 nM NDM-1, 10 μM clavulanic acid, 500 nM of Affimer and 65 μM nitrocefin and all Affimer isolates were normalised to the EDTA control. The EDTA negative control sequesters Zn^{2+} from the active site and renders NDM-1 inactive. Additionally, an NDM-1 only positive control containing no Affimer demonstrated the maximum rate of nitrocefin hydrolysis. Absorbance at 482 nm was plotted over time (s) to give an initial indication of trend (Figure 6.17a). After 3 replicate experiments, absorbance values measured during the first 250 seconds (during which the rates were constant) were converted to concentration in μM using Beer-Lambert's Law and then to rate in μM/s using linear regression analysis (Figure 6.17b).

a.

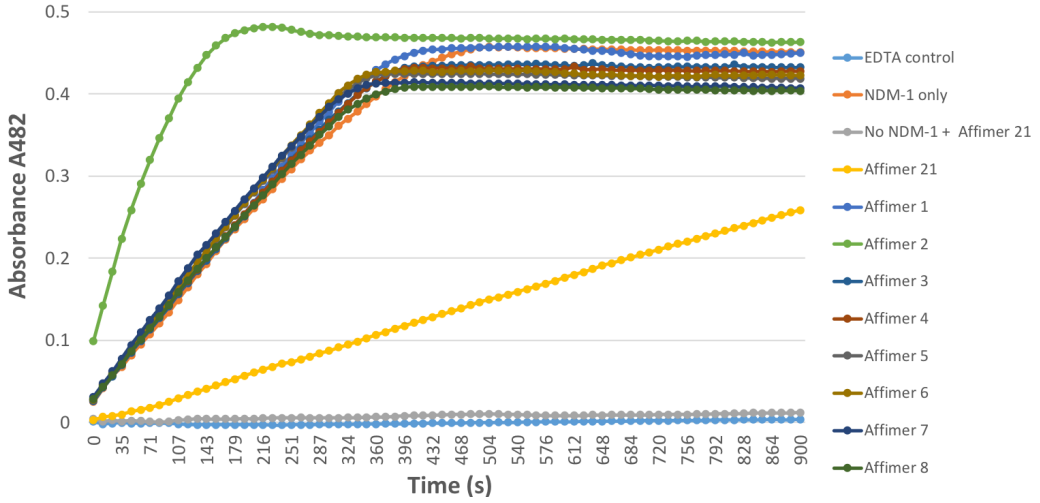
Absorbance A482
0.5
0.4
0.3
0.2
0.1
0
0 35 71 107 143 179 216 251 287 324 360 396 432 468 504 540 576 612 648 684 720 756 792 828 864 900
Time (s)
EDTA control
NDM-1 only
No NDM-1 + Affimer 21
Affimer 21
Affimer 1
Affimer 2
Affimer 3
Affimer 4
Affimer 5
Affimer 6
Affimer 7
Affimer 8

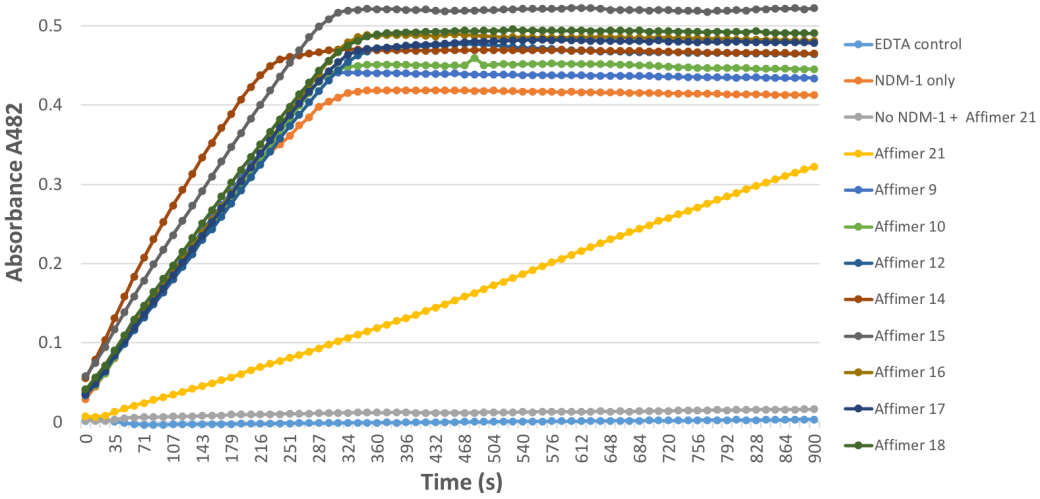
Absorbance A482
0.5
0.4
0.3
0.2
0.1
0
0 35 71 107 143 179 216 251 287 324 360 396 432 468 504 540 576 612 648 684 720 756 792 828 864 900
Time (s)
EDTA control
NDM-1 only
No NDM-1 + Affimer 21
Affimer 21
Affimer 9
Affimer 10
Affimer 12
Affimer 14
Affimer 15
Affimer 16
Affimer 17
Affimer 18

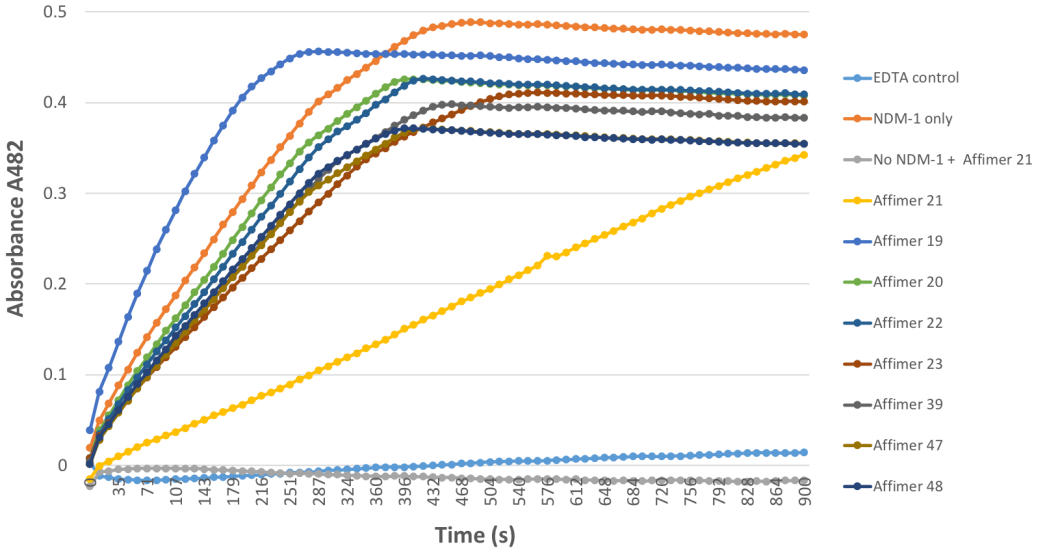
Absorbance A482
0.5
0.4
0.3
0.2
0.1
0
0 35 71 107 143 179 216 251 287 324 360 396 432 468 504 540 576 612 648 684 720 756 792 828 864 900
Time (s)
EDTA control
NDM-1 only
No NDM-1 + Affimer 21
Affimer 21
Affimer 19
Affimer 20
Affimer 22
Affimer 23
Affimer 39
Affimer 47
Affimer 48

b.

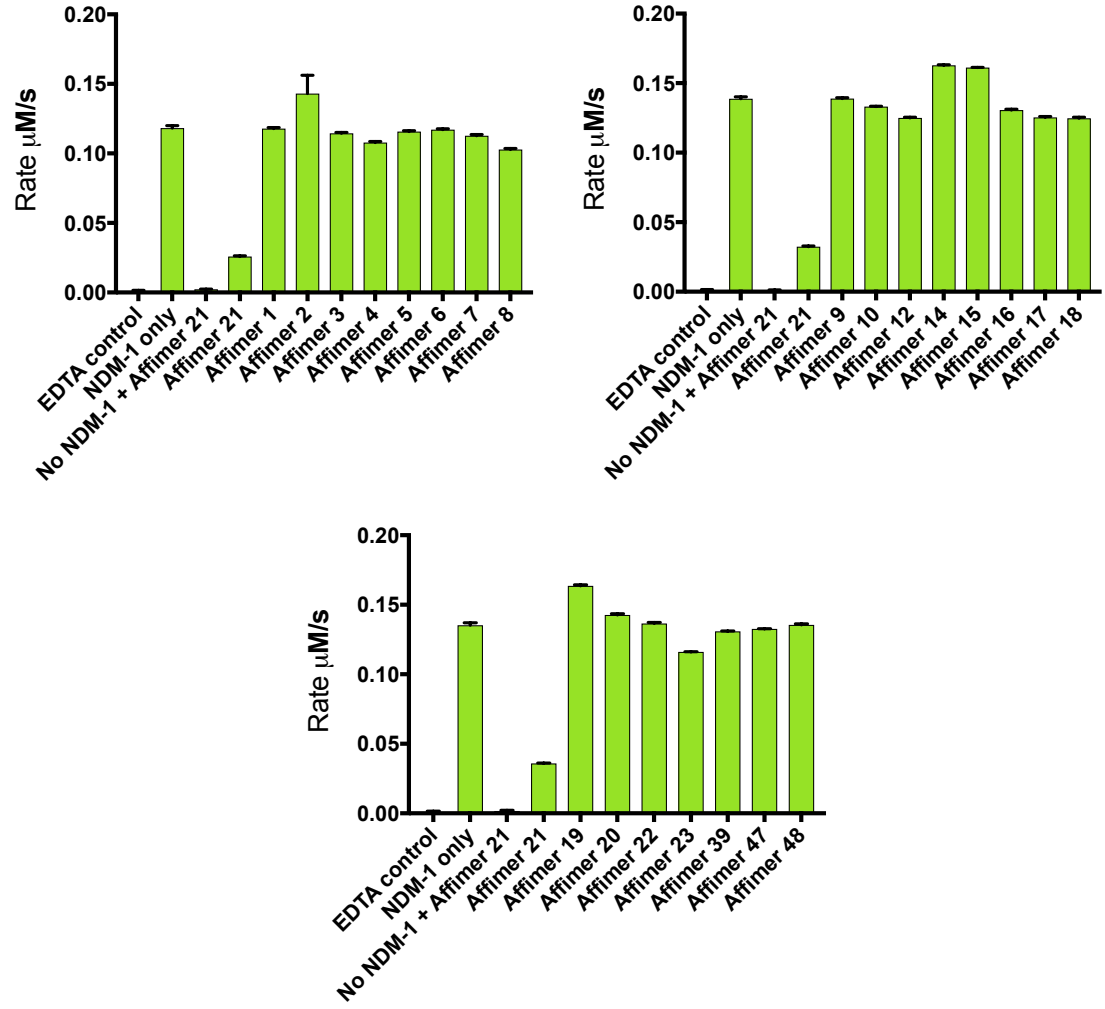

Figure 6.17: Effects of Affimer reagents on rate of nitrocefin hydrolysis by NDM-1. NDM-1 activity was quantified by spectrophotometric measurement of nitrocefin hydrolysis at 482 nm and at 25 °C on a Tecan Spark microplate reader and readings for each well were taken every 12 secs for 15 min. Data was normalised to the EDTA control. **(a)** The change in absorbance at 482 nm for NDM-1 only and upon addition of isolated Affimers was recorded **(b)** Activity of NDM-1 only or with 500 nM Affimer recorded as rate of nitrocefin hydrolysis (μM/s). Error bars represent standard errors from 3 replicate experiments.

Of the 23 Affimer reagents tested, none demonstrated higher inhibitory activity than Affimer 21. However, several of the Affimers appeared to increase NDM-1 activity. Affimer 2 increased activity of NDM-1 by 21 % when compared to that of the NDM-1 only control ($p < 0.05$, R^2 0.7218), Affimer 14 by 17.3 % ($p < 0.0001$, R^2 0.9956), Affimer 15 by 16.1 % ($p < 0.0001$, R^2 0.9954) and Affimer 19 by 20.9 % ($p < 0.0001$, R^2 0.9942).

6.2.3 Generation of library 2

For the second library, positions G1.1, V1.4, Y1.8 and G1.9 in variable region 1 of Affimer 21 were randomised. These residues had been shown via alanine scanning mutagenesis (Chapter 5) as not essential for inhibition of NDM-1 by Affimer 21. Since these 4 residues do not appear to contribute to the binding interaction, it was speculated that substitutions for other residues at these positions may improve affinity and inhibition. These 4 residues were therefore randomised as described previously for library 1, using codon-selected semi-trinucleotide cassette synthesis (excluding cysteines); and a new library was generated (Section 2.2.4). Primers to randomise the 4 residues were designed and then synthesized by Ella Biotech. Following the SOE PCR to join the two library fragments together, the primer P1 and primer P4 were used in a final reaction that incorporated five rounds of amplification to generate a final amplification product. DNA products were analysed by agarose gel electrophoresis (Figure 6.18).

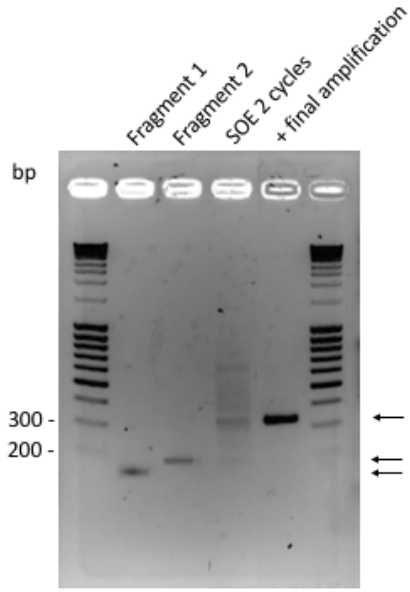

Figure 6.18: Construction of Library 2 insert DNA by splice overlap extension. Fragment 1 and 2, the SOE reaction and final amplification were analysed by agarose gel electrophoresis on a 2 % agarose gel. Following amplification of fragment 1 and 2, ten cycles of SOE PCR to join the two fragments was carried out followed by addition of 0.02 U/ul extra phusion DNA polymerase and a further ten cycles of SOE (SOE 2 cycles). Five rounds of amplification to generate a final amplification product using primer P1 and P4 was carried out. 5 µl of DNA was loaded for each.

After the library insert PCR product had been generated, it was digested using *NheI*-HF and *PstI*-HF restriction enzymes and ligated into a similarly digested pDHis vector. The pDHis vector was dephosphorylated to prevent re-ligation. Ligation reactions were set up at a 4:1 ratio of insert to vector using Roche T4 ligase, as this was shown to be most efficient during the generation of library 1. The resulting ligation products were transformed into *E. coli* XL1 Blue supercompetent cells and plated on LB agar plates supplemented with carbenicillin (Section). The following day, colonies were counted on each plate (Figure 6.19).

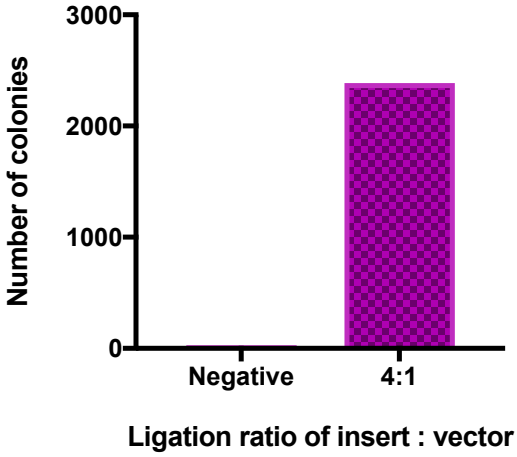

Figure 6.19: Number of colonies on ligation plates. A ligation reaction was set up at a molar concentration ratio of insert to vector of 4:1 using Roche T4 ligase. A negative control containing no insert DNA was also carried out to confirm full digestion and dephosphorylation of the vector.

There were very few colonies on the negative control plates which indicates that the vector was efficiently digested and dephosphorylated. Ten colonies selected at random from the ligation plates were grown up and DNA extracted for sequencing analysis using the pDHis-specific primer M13R (Table 6.5).

Table 6.5: Variable region amino acid sequences of 10 clones from Library 2

Affimer clone	Variable region 1	Variable region 2
1	V**YK**H**WTP**FQ	**THWDNGGLR**
2	H**YK**L**WTP**IK	**THWDNGGLR**
3	M**YK**Y**WTP**HP	**THWDNGGLR**
4	G**YK**P**WTP**IF	**THWDNGGLR**
5	P**YK**F**WTP**KH	**THWDNGGLR**
6	L**YK**S**WTP**YI	**THWDNGGLR**
7	H**YK**N**WTP**MY	**THWDNGGLR**
8	V**YK**G**WTP**AI	**THWDNGGLR**
9	I**YK**M**WTP**PE	**THWDNGGLR**
10	E**YK**A**WTP**AF	**THWDNGGLR**

* residues in bold indicate those that were conserved from the original Affimer 21 sequence

The sequencing results demonstrated a good variety of residues incorporated in the randomised positions. Subsequently, the ligation was electroporated into electrocompetent *E. coli* ER2738 cells (Section 2.2.1.12). Cell samples were plated out at a range of dilutions (1:10 - 1:100,000) onto agar plates containing carbenicillin to allow for estimation of the library size (Table 6.6). The 1:10 dilution plate contained too many colonies to accurately count and was therefore excluded.

Table 6.6: Estimation of library size from total infected cells

Dilution factor	µl plated	Average no. of colonies	Cells per µl	Total cells in 15 ml
1:100	10	1018	10180	1.53×10^8
1:1000	10	103	10300	1.55×10^8
1:10,000	10	12	12000	1.8×10^8
1:100,000	10	0	-	-

The mean library size was therefore estimated to be approximately 1.63 x 10^8. The maximum theoretical size of the library can be calculated as 19^4, or 1.3 x 10^5. The generated library was therefore estimated to give 1251x coverage of the possible combinations in the theoretical library. A further 96 colonies were randomly selected from the ligation plates and sequenced to check the diversity of amino acid incorporation in the 4 randomised positions (Figure 6.20).

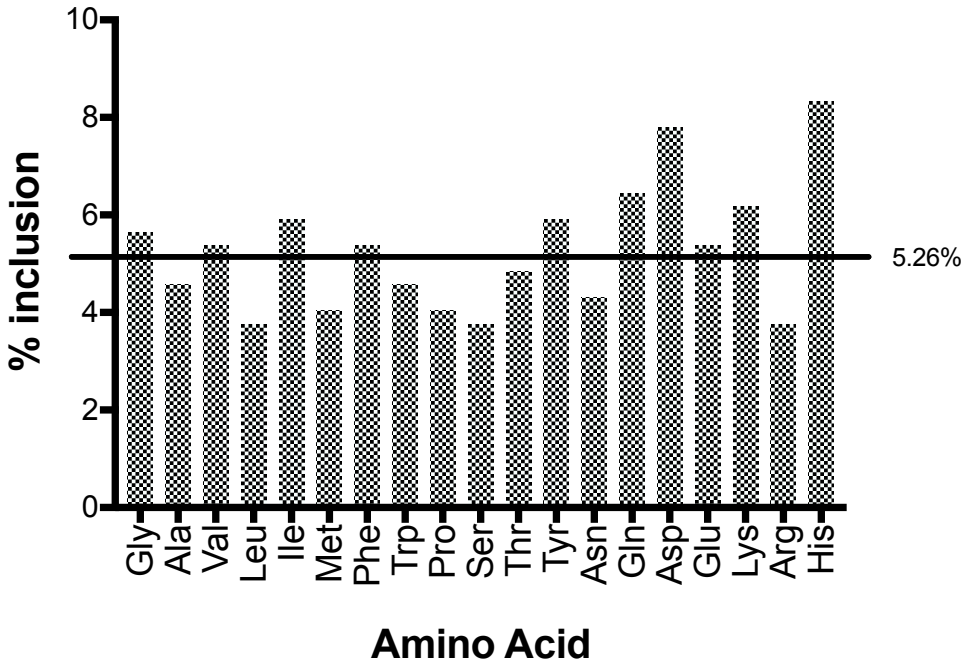

Figure 6.20: Inclusion rates (%) of amino acids in the 4 randomised positions of library 2. The theoretical inclusion rate for each of the 19 amino acids at any given randomised position was calculated to be 5.26 %.

The majority of amino acids are incorporated at close to the theoretical inclusion rate of 5.26 %. Histidines were again the most frequently observed residue. The phage titre of library 2 was estimated to be 9.1 x 10^{13} phage/ml via by spectrophotometric quantification (Section 2.2.4.2).

6.2.4 Isolation of Affimers against NDM-1 from Library 2

Immobilised NDM-1 (+BAP) was subjected to three rounds of competitive phage display (as was described for screening of library 1) using library 2 (Section 2.2.2.5). Eight identical pans were set up and on each consecutive day the strips were washed 27x and one well was eluted. Eluted phage from the high/low elution and trypsin elution were

combined. After the daily 27x wash, fresh un-biotinylated NDM-1 was added to all remaining wells to act as competition. Following re-infection of ER2738 cells, dilutions were plated onto LB agar plates containing 100 µg/ml carbenicillin and grown overnight. There were fewer colonies observed on the plates from day 1 and 2 compared to the number seen for library 1, therefore only 24 colonies were selected from each plate for testing for binding to NDM-1 in a phage ELISA (Section 2.2.2.6) (Figure 6.21). Affimer 21 phage was produced alongside the isolated clones and included in the ELISA as a positive control. Of the 48 clones tested, 6 displayed binding to the target with no clones displaying non-specific binding to the control wells. Day 3 Affimer binders were eluted and 24 colonies picked for testing in a phage ELISA but none demonstrated binding to NDM-1. Days 4-8 panning experiments were therefore not completed as it was thought unlikely that any further binders would be isolated.

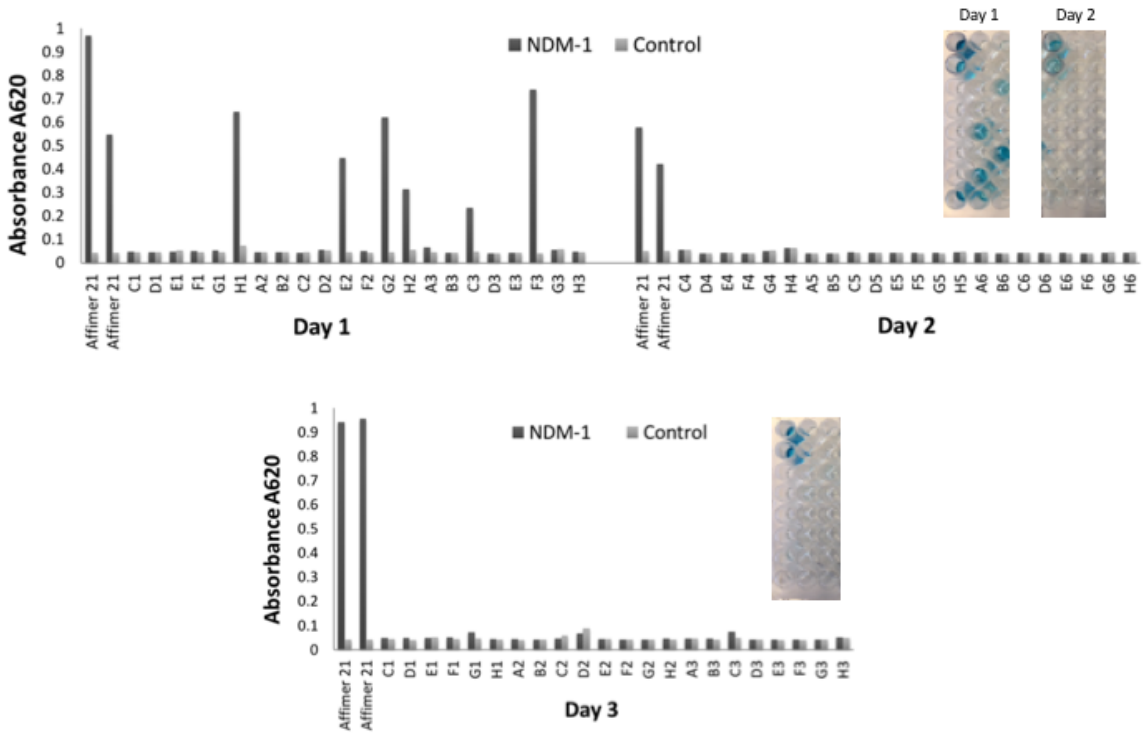

Figure 6.21: Phage ELISA results for Affimer binders selected from a competitive screen of library 2 against NDM-1 (+BAP). Following 3 days of competitive screening, 6 colonies were tested in a phage ELISA. Each colony represented one Affimer and was tested for binding against NDM-1 (+BAP) or an empty control well. Affimer 21 phage was included in duplicate on each plate as a control. Phage binding was detected with anti-Fd bacteriophage-HRP antibody and visualised on addition of TMB. Absorbance at 620nm was measured for each well.

The 6 clones that displayed binding to NDM-1 in the phage ELISAs were all isolated on day 1, before the introduction of competition via the addition of un-biotinylated NDM-1. These 6 clones were sequenced and 6 unique binders were identified (Table 6.7).

Table 6.7: Variable region sequences for Affimers selected for NDM-1 from library 2

Day	Clone	Variable region 1	Variable region 2	No. of sequencing appearances
1	C3	P**YK**I**WTP**YF	**THWDNGGLR**	1
1	F3	V**YK**V**WTP**HF	**THWDNGGLR**	1
1	E2	N**YK**V**WTP**LF	**THWDNGGLR**	1
1	H1	G**YK**H**WTP**YG	**THWDNGGLR**	1
1	H2	W**YK**I**WTP**DF	**THWDNGGLR**	1
1	G2	T**YK**I**WTP**MG	**THWDNGGLR**	1

*residues in bold indicate those that were conserved from the original Affimer 21 sequence

A heat map demonstrating the amino acid enrichment at each of the randomised positions was produced (Figure 6.22).

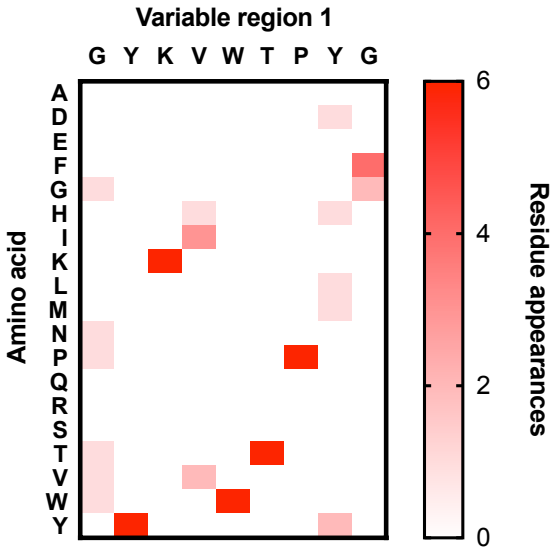

Figure 6.22: Heat map showing amino acid enrichment at the randomised positions of Affimer 21. The original residues for Affimer 21 are listed across the top. Dark red indicates high enrichment and white indicates no enrichment.

Enrichment of an isoleucine or valine at position V1.4 and a phenylalanine or glycine at G1.8 could be observed, suggesting that a hydrophobic residue is preferentially included at position 1.8. More data would be needed to confirm this as the sample size is small at only 6 clones. Interestingly, despite having little effect on inhibition of NDM-1, a number of residues were observed in the randomised positions from the original Affimer 21 sequence. This suggests that although these may not be essential for inhibition, they may still be involved in the binding interaction between Affimer and NDM-1.

The 6 isolated clones were taken forward for subcloning and expression independently of the PIII phage coat protein (Section 2.2.3) (Figure 6.23). Production and purification of proteins was carried out by Masters student Sam Cook, University of Leeds.

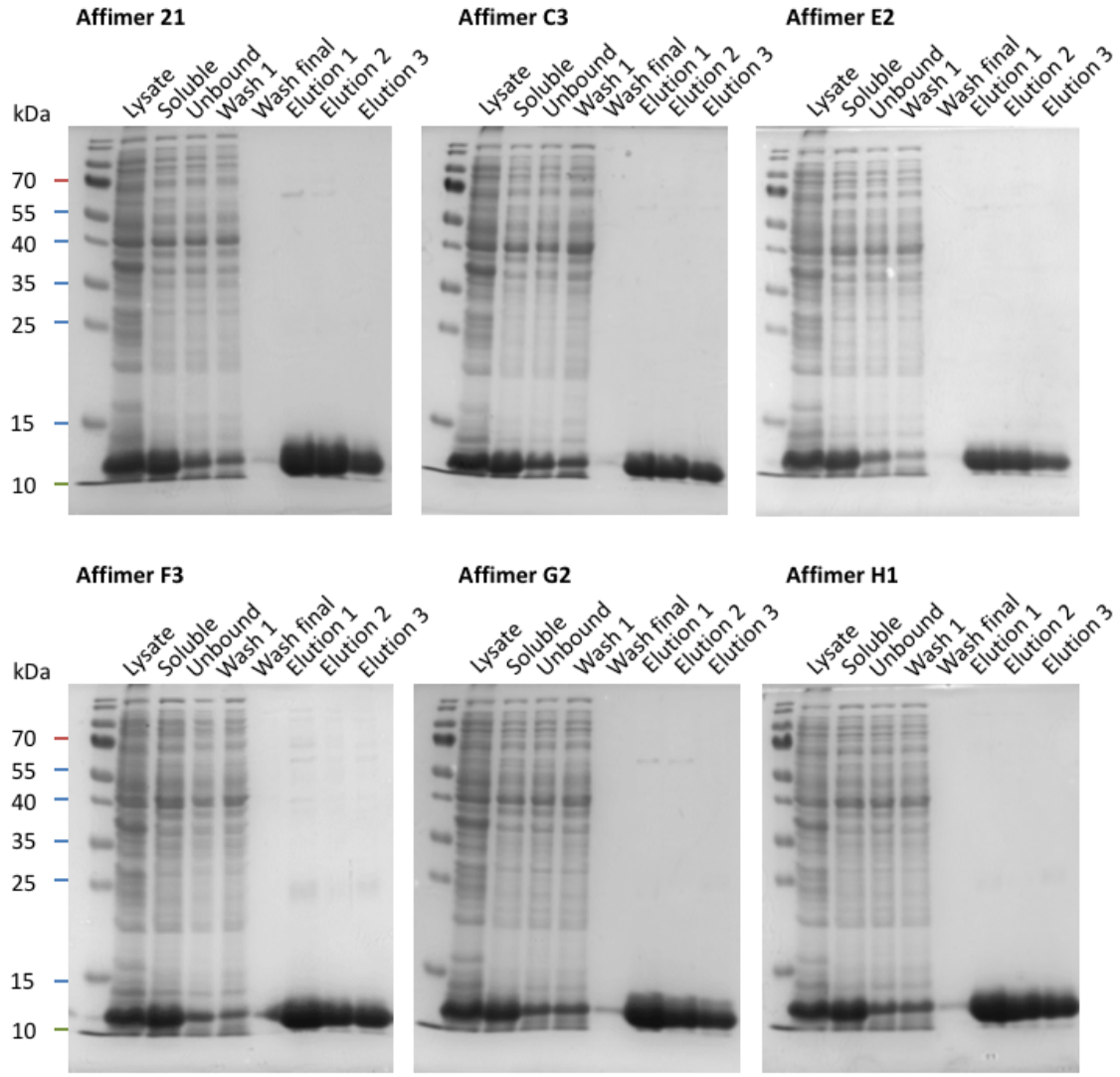

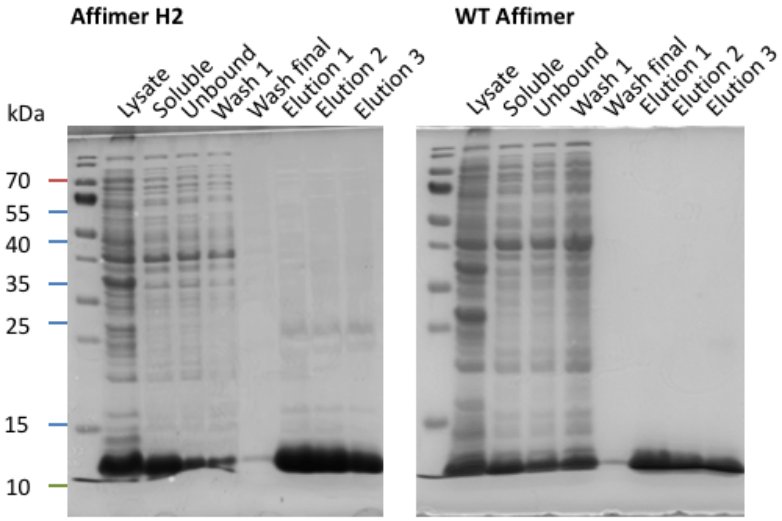

Figure 6.23: SDS-PAGE analysis of Affimer production and purification in BL21 Star™ (DE3) cells. Affimers isolated from library 2 were sub-cloned from the pBSTG-Aff phagemid vector into pET11a and produced in BL21 Star™ (DE3) cells. The proteins were purified from bacterial cell lysate using nickel ion affinity chromatography and separated by SDS-PAGE on a 15 % resolving gel and stained with Coomassie Blue to check purity. Affimers were visualised at ~12 kDa.

Purified Affimer proteins were then tested in β-Lactamase activity assays with nitrocefin as the substrate (Section 2.2.5.1), to determine whether they had any effect on NDM-1 enzyme activity (Figure 6.24). This assay was carried out by Masters student Sam Cook, University of Leeds. Reactions included 100 nM NDM-1, 10 μM clavulanic acid, 500 nM of Affimer and 65 μM nitrocefin and all Affimer isolates were normalised to the EDTA control. Absorbance at 482 nm was plotted over time (s) to give an initial indication of trend (Figure 6.24a). After 3 replicate experiments, absorbance values measured during the first 250 seconds (during which the rates were constant) were converted to concentration in μM using Beer-Lambert's Law and then to rate in μM/s using linear regression analysis (Figure 6.24b).

a.

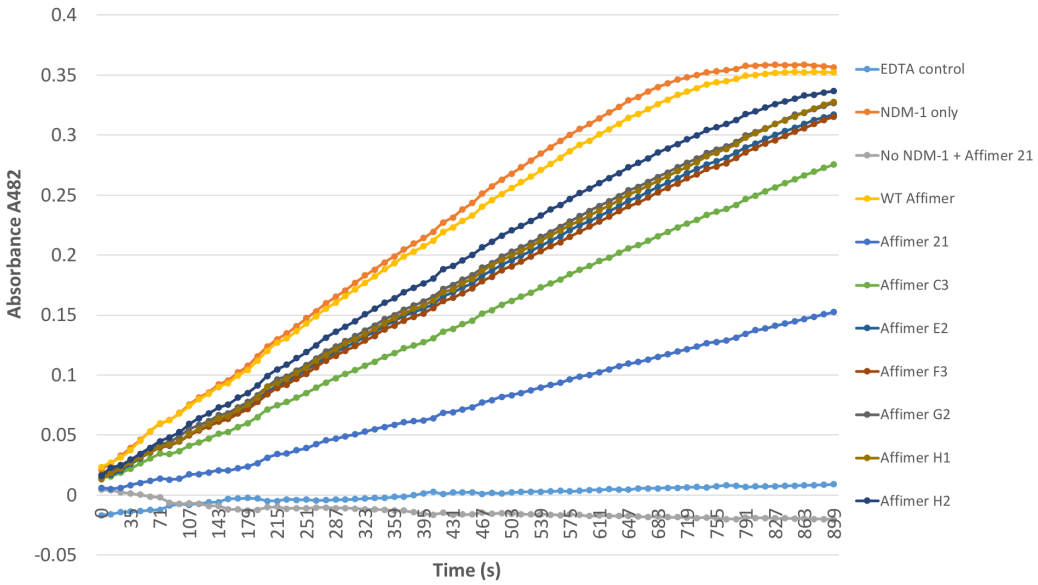

b.

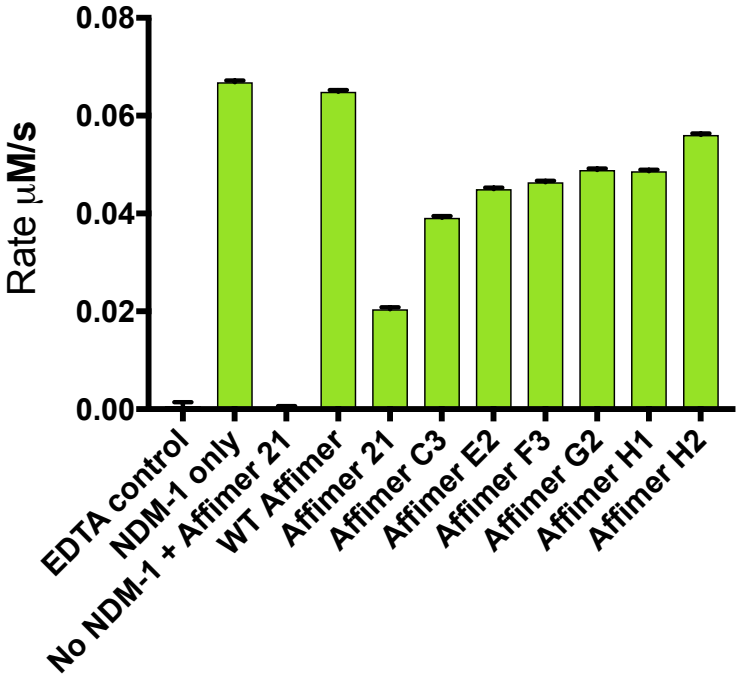

Figure 6.24: Effects of Affimer reagents on rate of nitrocefin hydrolysis by NDM-1. NDM-1 activity was quantified by spectrophotometric measurement of nitrocefin hydrolysis at 482 nm and at 25 °C on a Tecan Spark microplate reader and readings for each well were taken every 12 secs for 15 min. A wild type (WT) control was included containing the original scaffold variable regions to show that the Affimer scaffold itself has no effect on NDM-1 activity. Data was normalised to the EDTA control. **(a)** The change in absorbance at 482 nm for NDM-1 only and upon addition of isolated Affimers was recorded **(b)** Activity of NDM-1 only or with 500 nM Affimer recorded as rate of nitrocefin hydrolysis (μM/s). Error bars represent standard errors from 3 replicate experiments.

Of the 6 Affimer reagents tested, none demonstrated higher inhibitory activity than Affimer 21 (69 % $p < 0.0001$, R^2 0.9998). However, all of the Affimers appeared to demonstrate some inhibition, with Affimer C3 inhibiting activity of NDM-1 by 41 % when compared to that of the NDM-1 only control ($p < 0.0001$, R^2 0.9996). This is perhaps not surprising as the residues that are essential for inhibitory activity were maintained in this library.

6.3 Chapter summary and future work

Display technologies (e.g. yeast, ribosome, phage) are ideal for isolating highly specific binding reagents due to the ability to perform negative selections to remove non-specific binders. However, as mentioned previously, these naïve libraries often only sample a small proportion of the total potential library size. The size of the generated sub-libraries described in this chapter were 1.58×10^7 and 1.63×10^8, giving approximately 6.37x and 1251x coverage of the theoretical combinations of residues, respectively. This was a significant improvement on the coverage estimated for the naïve library, for which the library is 7.7×10^{12} times smaller than the theoretical size. It is expected that a high proportion of clones isolated from a sub-library will display binding to the target as the libraries often share high homology with an already-confirmed binder. Therefore, ideally all clones isolated from the sub-libraries would be tested for binding. However, the manual picking and testing of large numbers of clones using standard phage ELISA protocols is laborious and time consuming. Automated methods of picking and testing individual clones are available but require expensive robotic platforms. Methods to achieve high-throughput validation of isolated clones without the requirement of robotic platforms have begun to be explored by other researchers within the BSTG, University of Leeds.

Following a normal phage display panning protocol from which only Affimer 21 was isolated, the stringency of the phage display screens was increased through several adaptations to the protocol to select for the highest affinity binders. To remove Affimers with weaker affinity for the target, an 8-day washing protocol was implemented. A similar study to select for affinity matured anti-HER2 DARPins used a 25-day washing protocol during selection and reported improved binders with 3000x affinity increases (Zahnd et al, 2007). Additionally, the increased stringency screen of

the Affimer 21 sub-libraries included the introduction of competition to capture and remove binding reagents with a high off rate. Using a similar strategy, an improved affinity monobody targeted against the Lyn SH3 domain was selected from a sub-library. Non-biotinylated target protein was introduced during panning to compete away lower affinity clones and binders with 130-fold improvements in affinity were reported (Huang et al, 2016).

Increased stringency phage display screening of library 1 isolated 23 unique binders. Sequencing of these clones identified enrichment of various amino acids in the critical positions of variable region 1 of Affimer 21. Although three out of the four positions that were maintained from Affimer 21 were originally hydrophobic residues, the Affimers isolated from library 1 also seemed to be enriched at the randomised positions with further hydrophobic residues (Table 6.8).

Table 6.8: Amino acid groups for isolated Affimers from library 1

Affimer clone										Key
Original 21	**G**	**Y**	**K**	**V**	**W**	**T**	**P**	**Y**	**G**	HYDROPHOBIC
39	**G**	E	H	**V**	H	Q	N	**Y**	**G**	ACIDIC
1	**G**	R	R	**V**	V	S	K	**Y**	**G**	BASIC
2	**G**	V	F	**V**	F	V	I	**Y**	**G**	NEUTRAL
3	**G**	K	H	**V**	K	K	T	**Y**	**G**	
4	**G**	P	S	**V**	F	L	W	**Y**	**G**	
5	**G**	Q	N	**V**	V	I	Y	**Y**	**G**	
6	**G**	K	M	**V**	L	V	W	**Y**	**G**	
7	**G**	V	A	**V**	Q	I	H	**Y**	**G**	
8	**G**	N	N	**V**	V	W	L	**Y**	**G**	
9	**G**	N	Y	**V**	L	T	I	**Y**	**G**	
10	**G**	N	I	**V**	I	Y	I	**Y**	**G**	
12	**G**	H	D	**V**	V	W	V	**Y**	**G**	
14	**G**	Q	F	**V**	I	M	Y	**Y**	**G**	
15	**G**	P	I	**V**	W	W	I	**Y**	**G**	
16	**G**	Y	Y	**V**	R	I	T	**Y**	**G**	
17	**G**	A	R	**V**	W	K	K	**Y**	**G**	
18	**G**	K	F	**V**	I	Y	L	**Y**	**G**	
19	**G**	V	F	**V**	I	R	M	**Y**	**G**	
20	**G**	M	K	**V**	V	V	M	**Y**	**G**	
22	**G**	G	R	**V**	V	M	Q	I	**Y**	**G**
23	**G**	W	Y	**V**	L	R	H	**Y**	**G**	
47	**G**	G	D	**V**	S	S	G	**Y**	**G**	
48	**G**	F	K	**V**	D	N	H	**Y**	**G**	

*residues in bold indicate those that were conserved from the original Affimer 21 sequence

Table 6.8 reveals that both Affimer 21 and binders selected from library 1 are fairly hydrophobic in variable region 1. Interestingly, the published structure of the inhibitor L-captopril in complex with NDM-1 revealed that the hydrophobic face of L-captopril interacts with the flexible L3 loop of NDM-1 (King et al, 2012). Without protein structures of any of the Affimers in complex with NDM-1, any assumptions regarding the binding interactions are purely speculative. However, there is a possibility that the hydrophobic variable region 1 of these Affimer binders might also bind to the flexible L3 loop.

Interestingly, several of the Affimer reagents isolated from library 1 appear to increase NDM-1 activity. Affimers 2, 14, 15 and 19 demonstrated up to a 21 % increase in the rate of hydrolysis of nitrocefin. However, results for Affimer 2 were more variable and would need repeating to confirm. Three out of four of these binders show enrichment of a phenylalanine at position K1.3 and two binders also show a valine at Y1.2, suggesting that this combination may cause an activator modification. The Modified Hodge Test is a phenotypic method than can be used to test for presence of carbapenemase (Pasteran et al, 2016). Further investigation into these Affimer binders might be warranted in order to determine their potential for improving the sensitivity of NDM-1 detection assays such as these.

Only six Affimer binders were isolated from library 2. This was surprising as this library was based upon the randomising of residues that were thought to be non-critical for binding and it was therefore expected that there might be a greater variation in the residues tolerated at these positions in isolated binders. There was also much less variation in these positions than in binders isolated from library 1. In particular, enrichment of a valine or isoleucine at position V1.4 and a glycine or phenylanine at position G1.9 were observed (Table 6.9). This suggests that despite being non-critical for inhibition, these residues may play a part in the conformation of the binding region.

Table 6.9: Amino acid groups for isolated Affimers from library 2

Affimer clone										Key
Original 21	**G**	**Y**	**K**	**V**	**W**	**T**	**P**	**Y**	**G**	HYDROPHOBIC
C3	P	**Y**	**K**	I	**W**	**T**	**P**	Y	F	ACIDIC
F3	V	**Y**	**K**	V	**W**	**T**	**P**	H	F	BASIC
E2	N	**Y**	**K**	V	**W**	**T**	**P**	L	F	NEUTRAL
H1	G	**Y**	**K**	H	**W**	**T**	**P**	Y	G	
H2	W	**Y**	**K**	I	**W**	**T**	**P**	D	F	
G2	T	**Y**	**K**	I	**W**	**T**	**P**	M	G	

*residues in bold indicate those that were conserved from the original Affimer 21 sequence

However, despite demonstrating strong absorbance readings in the phage ELISA, indicating a good level of binding to NDM-1, none of the isolated binders from either library were able to match Affimer 21 for inhibiting NDM-1 activity. This suggests that either Affimer 21 already contains the optimal combination of residues for inhibition of NDM-1, or that the optimal combination of residues across the two variable regions was not achieved in these libraries. For example, a critical and non-critical residue might both need optimising to achieve the best possible binding and inhibition. Additionally, the affinity maturation of variable region 2 has not yet been explored. Another approach to affinity maturation might be to completely randomise one variable region whilst maintaining the original Affimer 21 residues in the other variable region. This strategy is currently being explored by Dr Christian Tiede, University of Leeds.

The Affimer reagents identified from the sub-libraries generated in this work did not demonstrate improved inhibition of NDM-1. However, as discussed previously, there are other strategies for affinity maturation that may still lead to the isolation of an improved Affimer. Protein structures to elucidate the mechanism of the interaction between NDM-1 and Affimer 21; and to confirm the roles of individual residues in the variable regions would be beneficial for determining the best strategy for affinity maturation.

Chapter 7

Discussion and future perspectives

7. Discussion and future perspectives

As the global spread and impact of multi-drug resistant infections increases, there has been a subsequent increase in the need for novel reagents that are able to detect and modulate metallo-β-lactamases (MBLs). The development of inhibitors that are able to reinstate sensitivity to previously ineffective antibiotics are particularly sought after. This work describes the identification of an Affimer reagent that is able to bind and modulate the activity of the metallo-β-lactamase NDM-1. Inhibition of NDM-1 in a dose dependent manner was confirmed by β-lactamase activity assays and cell based assays in clinical strains. Initial kinetic analysis suggested that Affimer 21 may be an allosteric inhibitor of NDM-1, although further investigation is required to confirm this. Attempts were made at obtaining a co-crystal structure to elucidate the binding mechanism but have so far been unsuccessful. Characterisation of the variable regions revealed that both variable regions of the Affimer are required for inhibition of NDM-1, and measurement of the functional effects of alanine substitutions on efficacy of NDM-1 inhibition revealed several residues in variable region 1 which are critical for inhibitory activity of the Affimer. This data was used to guide the generation of sub-libraries to select for improved inhibitors. However, despite stringent screening approaches, the original Affimer was established to be the most effective inhibitor, with an estimated IC_{50} of 0.37 μM. These preliminary data are promising for the use of Affimer 21 in a combination therapy, however certain biochemical and mechanistic details are yet to be elucidated.

7.1 Affimer 21 as an allosteric inhibitor of NDM-1

Therapeutics that function as inhibitors by binding directly to an enzymes active site constitute a significant proportion of the commercially available drugs that are in clinical use today (Grover, 2013). One advantage of this mechanism of action is that high affinity is often achievable. However, the ubiquitous prevalence of zinc ions in bacterial cells and the environment suggest that reactivation upon loss of the inhibitor might occur. Additionally, orthosteric inhibitors often result in adverse side effects as enzymes with similar functions often have conserved active sites. As an example, phosphatidylinositol (PI) analogues have been reported to inhibit Akt (protein kinase B), a cancer target in the PI3K pathway, by targeting its ATP catalytic domain (Lindsley

et al, 2005). Unfortunately, because of the similarity of the ATP pocket among other kinases, achieving target specificity has been extremely difficult and development during the clinical phase was therefore terminated (Lindsley et al, 2008). Targeting allosteric sites increases the specificity of inhibitors by binding to sites distant from the active site. Accordingly, novel allosteric Akt inhibitors that bind selectively between kinases of the same subclass have since been reported by researchers at Merck (Hirai et al, 2010).

Similarly, targeting the allosteric sites of MBLs may provide better specificity for inhibitors by binding away from the active site, helping the inhibitor to remain inactive towards similar human proteins. Therefore, there is a potential requirement for new tools and technologies to allow for the identification of novel allosteric inhibitors. Most reported inhibitors of NDM-1 are competitive, and there is currently only one report of a possible allosteric inhibitor. An azolylthioacetamide scaffold was shown to specifically inhibit NDM-1 with an IC_{50} of 0.17 µM and a Lineweaver-Burk plot indicated that the inhibitor was binding via an allosteric mechanism (Xiang et al, 2017). Artificial binding proteins such as Affimers may offer a platform for the selection of allosteric inhibitors. Affimers have previously been shown to inhibit protein function and interactions through allosteric mechanisms (Robinson et al, 2018). Attempts at inhibiting Fc gamma receptors (FcγRs) have been previously hampered by off-target effects involving homologous FcγR family members. In the study reported by Robinson et al, an Affimer reagent that is capable of specifically inhibiting FcγRIIIa but not closely related homologs was identified and shown to bind allosterically.

Kinetic analysis of Affimer 21 through the generation of Lineweaver-Burk plots suggests that Affimer 21 is an allosteric inhibitor of NDM-1. Non-antibody binding proteins often recognise binding ‘hot spots’ - small clusters of residues on the target protein that contribute significantly to the free energy of binding and are often more critical than large, diffuse interfaces (Modell et al, 2016). Therefore, it might be speculated that Affimer 21 is able to recognise a binding site on the target protein which is unrecognisable or inaccessible to other types of inhibitor. This would also indicate that the Affimer does not inhibit NDM-1 via zinc binding or chelating, potentially limiting off-target effects. Testing the efficacy of Affimer 21 against other metallo-β-lactamases

would further corroborate its specificity. Obtaining a crystal structure would provide a structural basis for better understanding and confirmation of the mode of inhibition. However, these early findings demonstrate the potential for generating highly specific inhibitors of protein-ligand interactions that bind unexplored sites, and suggest that further exploration into the feasibility of Affimer proteins as allosteric MBL inhibitors is warranted.

7.2 Affinity maturation of Affimer 21

Affinity maturation by mutagenesis followed by selection by surface display is one of the most frequently applied engineering processes during the development of antibody and novel biologic therapeutics. The underpinning theory behind affinity maturation is that the theoretical sequence space for a binding protein can only be sparsely sampled by the creation of a biological library of variants. As demonstrated, the naïve Affimer library has provided an NDM-1 inhibitory Affimer, but it was hypothesised that there might be better Affimer inhibitors that were not represented in the original library. As discussed in Chapter 6, the affinity maturation strategies so far trialled in this study did not yield an Affimer than was better than the original Affimer 21. However, not all possible strategies for the generation of sub-libraries were tested in the scope of this work and ongoing work is currently in progress to determine the best possible strategy for affinity maturation.

In this project, residues that were shown to be critical for binding and inhibition were randomised first in the generation of library 1. This is contradictory to most affinity maturation strategies in which the critical residues are normally maintained to maintain ligand binding, and substitution of non-critical residues is expected to yield an optimal sequence for enhancement of affinity (Ko et al, 2015). However, these methods do not explore the possibility that there may be better combinations of residues in these critical positions than the ones originally isolated, and that the best combination may not be represented in a naïve library. Despite this hypothesis, randomisation of the critical residues did not yield an improved inhibitor in this case. However, this strategy might still be successful for the affinity maturation of other binders and is worth further exploration.

In library 2, the non-critical residues were randomised. Isolated Affimers that bound to NDM-1 were limited to only six and there was less variation in these positions than in binders isolated from library 1. This suggests that despite being non-critical for inhibition, these residues may play a part in the conformation of the binding region. Randomisation of the non-critical residues has led to improved affinity for other novel biologics. A monobody that targets the Lyn Src Homology 3 (SH3) domain, a kinase associated with several cancers and autoimmune diseases, was subject to directed evolution and displayed a 130-fold increase in affinity (Huang et al, 2016). Alanine scanning identified critical residues and a secondary library was generated randomising the non-critical residues. The randomisation of non-critical binding residues and subsequent generation of a new sub-library for an Affimer that binds the TRPV1 ion channel has recently resulted in the selection of Affimer reagents with 200-fold improvements in affinity (unpublished data). Additionally, in Chapter 5, variable region 2 of Affimer 21 was shown to be less crucial than variable region 1, suggesting that affinity maturation of the less critical variable region might prove to be an improved strategy.

Investigation into the effects of affinity maturation of variable region 2 was not achieved within the scope of this study due to time constraints. However, it would be interesting to explore the effects of optimising this region through both randomisation and modification of the size of the variable region. This combination of diversifying loop length and recursive mutagenesis has been previously reported for the selection of improved affinity FN3 domain scaffolds (monobodies) (Hackel et al, 2008). In this study, improved monobodies were selected with both increases and reductions of up to three amino acids in the binding region lengths. Additionally, affinity maturation of an anti-HER2 DARPin has been previously used to obtain binders with picomolar affinity (Zahnd et al, 2007). Error-prone PCR was used to generate mutations leading to a 3000-fold increase in affinity. Interestingly, the highest affinity binders were gained from mutations to the framework of the DARPin, when compared to the wild-type scaffold. It might therefore be interesting to investigate the role of residues outside of the variable regions of the Affimer to determine whether changes in the framework scaffold are able to improve the binding interaction between Affimer 21 and NDM-1.

None of the isolated binders proved to be better inhibitors of NDM-1. This implies that either Affimer 21 already contains the optimal combination of residues for inhibition of NDM-1, or that the optimal combination of residues across the two variable regions was not achieved in these libraries. For example, a critical and non-critical residue might both need optimising to achieve the best possible binding and inhibition. In this case, a better approach might be to maintain variable region 1 whilst randomising variable region 2 and vice versa, to allow more detailed exploration of the contribution of each variable region and to improve the chance of attaining the optimal combination of residues. This strategy is currently being explored. However, a disadvantage to this strategy might be that as the number of residues randomised increases, the theoretical library size also increases and the likelihood of generating a library with good coverage decreases. Generating a library that both randomises and diversifies the size of the variable regions, as mentioned above, may therefore prove to be the most effectual.

7.3 Comparison to other NDM-1 inhibitors

The lowest reported IC_{50} value for an inhibitor of NDM-1 is currently 0.004 µM which was reported for a cyclic boronate. Additionally, the cyclic boronate VNRX-5133 (in phase I clinical trials) was reported as <0.1 µM (Venatorx, 2018). Currently, the cyclic boronates are probably the most promising class of inhibitors of β-lactamases. They have been proven to be effective against PBPs and serine and metallo-β-lactamases, as well as demonstrating high selectivity and little toxicity. Crystal structures of cyclic boronates in complex with the β-lactamases VIM-2, BcII and CTX-M-15 revealed that these molecules work by mimicking a common tetrahedral intermediate present in both classes of enzyme (Brem et al, 2016 and Cahill et al, 2017). The tetrahedral is formed alongside a Zn1-bound carboxylate during hydrolysis of β-lactams; when the hydroxide ion bridging the two zinc ions is used for nucleophilic attack. Protonation of this intermediate is required for product release. Tetrahedral intermediates occur in many enzyme catalysed reactions, making specificity a relevant issue when using this approach (Docquier et al, 2018). Further study is needed to determine any off-target effects. However, with the first cyclic boronate drug, tavaborole, clinically approved for the treatment of fungal infections (Elewski et al, 2015) and others in clinical development, some of these compounds seem to exhibit low toxicity, making them interesting for further investigation.

A derivative of 2,6-dipicolinic acid (DPA) also has a low reported IC_{50} of just 0.08 µM. DPA was discovered through fragment-based drug discovery in which a library of metal-binding pharmacophores was screened (Chen et al, 2017). DPA was shown to be a zinc chelator, but chemical modification of DPA lead to an improved compound with a different mechanism of inhibition. The improved compound acts as a metal-binding competitive inhibitor and inhibits several MBLs, including NDM-1, as well as showing 10-20 fold potentiation of imipenem in *Klebsiella* and *E. coli* clinical isolates. It would be interesting to test Affimer 21 in various strains of *Enterobacteriaceae* with different antibiotics to see how the MICs of Affimer 21 compare.

For almost all applications, an inhibitor must bind to its molecular target with a reasonable degree of affinity for it to be effective. Approximately 60 % of drug discovery projects fail in hit-to-lead because either the biological target was found to be not druggable, or the compound did not exhibit the required potency for a therapeutic (Cheng et al., 2007). Comparison of IC_{50} values for currently reported NDM-1 inhibitors indicates that IC_{50} values range from 4 nM to 23 µM (Table 7.1).

Table 7.1: Reported IC_{50} values of other NDM-1 inhibitors

Inhibitor class	Mechanism	Best IC_{50} (µM)	Reference
azolylthioacetamides	suspected allosteric	0.17	Xiang et al, 2017
VNRX-5133 (cyclic boronate)	competitive	<0.1	Venatorx, 2018
magnolol	competitive	6.47	Liu et al, 2018
1,2,4-triazole-3-thione	competitive	11	Sevaille et al, 2017
Mercaptoacetic acid thioesters	competitive	12.4	Liu et al, 2015
D-captopril	competitive	20.1	Brem et al, 2016
Aspergillomerase A	zinc chelator	4.0	King et al, 2014
Bismuth Bi(III)	irreversible metal displacement via Cys208	0.7	Wang et al, 2018
2,6-dipicolinic acid (DPA)	competitive	0.08	Chen et al, 2017
Cyclic boronate	competitive	0.004	Brem et al, 2016
Bisthiazolidines	competitive	23	Gonzalez et al, 2015
Rhodanine	zinc chelator	0.52	Brem et al, 2014

One advantage of phage display is that it allows for screening of diverse molecular targets to obtain high-potency binders suitable for development within a much faster timescale than that achievable for other compounds (Huang et al., 2012). For small molecules, inhibitors isolated by library screening are normally found with IC_{50}s in the 1 to 5 µM range. In this study, the IC_{50} of Affimer 21 was estimated as 0.37 µM. Comparison with the IC_{50} values of other inhibitors indicates that the IC_{50} value of 0.37 µM for Affimer 21 is within the lower range of those reported. As discussed in Chapter 4, repeating the assay with more Affimer concentrations will allow for a more widely spread IC_{50} curve and a more accurate IC_{50} value. Determining the spectrum of activity by testing Affimer 21 against other β-lactamases would allow more critical comparison to other reported inhibitors. It would also be beneficial to test the inhibitory potency of the Affimer against other β-lactam antibiotics. Despite this, the initial estimate of an IC_{50} value for Affimer 21 is encouraging.

There are currently only two reports of novel biologics that target MBLs. Although they do not target NDM-1, the reported IC_{50}s for the DNA aptamer that targets 5/B/6 and a nanobody against VIM-4 were 1.2 nM and 10 µM, respectively (Chapter 1). These studies are promising, and in addition to Affimer 21, demonstrate the potential of investigating novel biologics for the isolation and selection of highly specific inhibitors.

7.4 Continuation of the project and future applications

7.4.1 Structural characterisation

As has been mentioned previously, obtaining a crystal structure of the Affimer in complex with NDM-1 would be of great benefit for the expansion and improvement of this project. There are several published structures of NDM-1 in complex with antibiotic substrates, but only two in complex with other inhibitors; bismuth Bi(III) and l-captopril (Wang et al, 2018 and King et al, 2012). Confirmation of both the mode of inhibition and the residues involved in the interaction would have added important structural information to this project. Co-crystallisation of NDM-1 with Affimer 21 was attempted several times both by myself and in collaboration with the Oxford Protein Production Facility; however, this has so far been unsuccessful.

As mentioned in Chapter 4, an alignment of the amino acid sequences from published NDM-1 structures revealed that the majority of the proteins were truncated at the N-terminal, with most having a truncation of 10-20 residues compared to the full-length protein that was used in this study. Truncation of the N-terminal has been reported to improve solubility and level of expression of NDM-1 (Kim., 2011). The continuation of this project is currently focusing on obtaining a crystal structure of the enzyme-inhibitor complex, and crystallisation trials with similarly truncated NDM-1 protein are currently underway. Gaining insight into the binding of the Affimer reagent will also allow for comparison to other isolated NDM-1 inhibitors to determine any common mechanisms of inhibition or binding sites. There are several other published structures of Affimer binders in complex with various targets. These include the previously mentioned FcγRIIIa and SUMO-1 and 2; as well as ubiquitin binding Affimer reagents (Robinson et al., 2017, Hughes et al., 2018, Michel et al., 2017). These studies demonstrate how unexpected or unusual binding mechanisms can be revealed by establishing the protein structures of binder-target complexes.

As an example, the biophysical characterisation of bismuth Bi(III) in complex with NDM-1 revealed a novel mechanism of inhibition. One Bi(III) compound irreversibly inactivates the enzyme both *in vitro* and *in vivo* through replacement of Zn(II) via the critical residue of cysteine at the active site. Additionally, Bi(III) compounds are already clinically used drugs and have been shown to confer no resistance even after extended use (Wang et al, 2017). The previous co-crystallisation of Affimers with various targets has also revealed allosteric modes of inhibition and provided explanations for binding specificity (Robinson et al., 2018 and Michel et al., 2017). Co-crystallisation of NDM-1 and Affimer 21 would corroborate the kinetic data which suggests that Affimer 21 inhibits NDM-1 via an allosteric mechanism. An allosteric inhibitor would indicate high target specificity but might suggest that this particular Affimer would not be a broad-spectrum MBL inhibitor.

Structural information from a target-inhibitor complex can also be used as a lead structure for drug development and design of small molecules. An Affimer that binds to the ion channel TRPV1 was recently co-crystallised and data regarding important residues from both alanine scanning and the structure were used to design a

pharmacophore for the identification of small molecule compounds with similar shape (unpublished data). Results demonstrated that five of the compounds were able to inhibit the ion channel. Small molecules are often able to passively diffuse across cell membranes and are therefore much preferred for the development of therapeutics (Yang et al, 2015).

Additionally, Affimers that target p300 to disrupt the HIF-1α/p300 protein-protein interaction have been reported (Kyle et al., 2015). The HIF-1α/p300 interaction plays a key role in tumour metabolism and is associated with resistance to therapy and poor prognosis in cancer patients. Crystallisation of the Affimer in combination with molecular docking against the NMR structure of p300 allowed for characterisation of the binding interface. If future attempts at obtaining a co-crystal structure of NDM-1 and Affimer 21 are unsuccessful, it might be possible to crystallise the Affimer and carry out similar docking studies to elucidate the binding interaction.

7.4.2 Assessing the likelihood of development resistance

In any programme associated with developing novel reagents for treatment of multi-drug resistant pathogens, it is important to understand the potential for new resistance mechanisms to develop. Given bacterial propensity to evade selective pressures, potential resistance generation to Affimer 21 must be considered. In order to evaluate this, the likelihood of the development of escape mutations might be evaluated by treating NDM-1 expressing cells with antibiotic in combination with various concentrations of Affimer 21 and passaging for increasing periods of time (days to weeks) to identify whether any strains are able to escape Affimer inhibition by developing resistance.

Similar investigation into the mutational plasticity of NDM-1 has recently been reported. A recent study investigated the mutational plasticity of NDM-1 through the generation of randomised single codon mutation libraries combined with functional selection and deep sequencing (Sun et al, 2018). This approach identified a core set of residues which are essential for catalytic efficiency of NDM-1 against a range of antibiotics. The majority of these were in the active site. Additionally, several non-

essential residues were identified on the periphery of the active site in which mutations have little to no effect on NDM-1 function. A key finding from this study was the stringent sequencing constraints for carbapenem hydrolysis. This suggests that an inhibitor in combination with a carbapenem would be a good combination therapy as there are fewer options for mutations that will be tolerated whilst maintaining carbapenem hydrolysis, limiting the chance for resistance to develop.

7.4.3 Affimer inhibitors as therapeutics

As discussed in Chapter 1, there are currently no clinically approved inhibitors of metallo-β-lactamases available. For Affimer reagents to be utilised as therapeutics, an efficient system for intracellular delivery would need to be developed. This is more challenging for novel biologics than it is for small molecules due to their larger size and difficulty in permeating the cell membrane (Yang et al., 2015). It is especially difficult to target Gram-negative bacteria due to the additional barrier of the double-membrane cell envelope. However, with evidence to suggest that NDM-1 is localised to the periplasm or OMVs (King et al, 2011 and Gonzalez et al, 2016), it is likely that inhibitors would need to permeate only the outer membrane of pathogens to reach their target. Immunofluorescence microscopy of fluorescently labelled Affimer 21 might confirm the localisation of NDM-1 within bacterial cells. The Affimers are convenient for labelling purposes and have demonstrated their versatility in imaging applications (Chapter 3). This method might also allow for the use of Affimer 21 in diagnostic applications for detection of NDM-1.

Affimer 21 was shown to restore sensitivity to meropenem in a dose-dependent manner in a clinical strain of *Klebsiella pneumoniae* that carries the $bla_{\text{NDM-1}}$ gene, confirming that the Affimer is able to access NDM-1. Further testing in more NDM-1 expressing bacterial strains and with a larger range of antibiotics is recommended to confirm this finding. Given that the Affimer is approximately 12 kDa in size, independent passage through the membrane seems unlikely.

Several strategies to improve cell permeability have been developed. Over the past 18 years, there has been increasing interest in polymersomes as versatile carriers for drug delivery. Polymersomes (polymer vesicles) are a class of artificial vesicles that are

prepared from amphiphilic copolymers that can be used for encapsulation and delivery of a broad range of drugs (Rikken et al, 2016). They are especially interesting in that they can be functionalised to enable biocompatibility, permeability and triggered release. Nanocin^{TM} is a polymer vesicle that has been reformulated from a commercially available core polymer that is found in a range of over the counter pharmaceuticals. It is currently in Phase I/II human clinical trials and has been shown to enhance penetration of a range of molecular cargos (DNA, RNA, small molecules, proteins, peptides and natural products) into cells, tissues and microbes (Tecrea Ltd, 2017).

Researchers at Massachusetts Institute of Technology (MIT) have recently reported the development of porous silicone nanoparticles; an anti-infective nanoparticle that target the bacterial cell membrane and can be loaded with toxic peptide cargo (Kwon et al, 2017). The nanoparticles were used to treat Gram-negative *Pseudomonas aeruginosa* lung infections in mice and were shown to result in significant decreases in bacterial titres and to markedly improve survival. The nanoparticles also exhibited an improved safety profile compared to free peptides.

Cell-penetrating peptides (CPPs) have also been developed for the efficient and non-toxic delivery of a variety of cargoes and several examples are in clinical trials (Bashyal et al, 2016). Biologics can be conjugated to CPPs for cellular uptake by direct translocation and endocytosis. Although CPPs have mostly been investigated for targeting of mammalian cells, there is some research that reports their successful use for targeting bacterial pathogens. One CPP showed successful growth inhibition of several Gram-positive and Gram-negative bacteria and were shown to selectively permeabilise bacterial cell membranes without damaging mammalian cells (Nekhotiaeva et al, 2004). Additionally, a more recent study used CPPs to deliver gentamycin to intracellular bacteria, including *E. coli*, *S. enterica* and *S. flexneri* species (Gomarasca et al, 2017).

Despite developments in strategies for the intracellular delivery of proteins, the bacterial cell envelope remains a challenging barrier for any new biologic therapy. Furthermore, the possibility of immunogenetic effects need to be explored and overcome (Garcês et al, 2018). The formation of anti-drug antibodies (ADA) and

subsequent hypersensitivity to biologics is a potential risk. Both Type I and Type II Affimer scaffolds have shown low immunogenicity in an industry-standard in vitro immune cell assay (Avacta® Life Sciences, 2017). Immune responses in a T-cell activation/proliferation assay using human peripheral blood mononuclear cells was measured in 50 samples that had been treated with 50 µg/ml of Affimer for 7 days. Both scaffold types were shown to have a low immunogenic response which was comparable to that of the therapeutic antibody Avastin®. Despite these promising results that suggest Affimer reagents might be well tolerated in humans, and the development of new drug delivery reagents, there is still a lot of research and validation that is required before Affimer 21 might be considered as a potential therapeutic for the treatment of resistant infections.

7.5 Conclusions

Affimer binders show great potential for use as inhibitors of metallo-β-lactamases. Affimer 21 displays comparable IC_{50} values to other reported inhibitors and preliminary characterisation data indicates that it is well tolerated in mammalian cells. Arguably the most important feature of a successful MBL inhibitor is high specificity; a quality difficult to achieve due to the similarities in the active sites of metallo-β-lactamases. Although further work is required to confirm specificity and mechanism of binding, initial results suggest that Affimer 21 is an allosteric inhibitor, indicating that it may be highly specific for NDM-1, reducing the possibility of off-target effects. The ability to rapidly screen the Affimer library against multiple targets combined with their ease of manufacturing, suggest potential as a cost-effective method for the future generation of inhibitors against metallo-β-lactamases.

The information gained from alanine scanning of Affimer 21 combined with the β-lactamase activity assay data provides insight into which residues confer binding and inhibitory potential for NDM-1. With the future addition of structural data, this will help to inform the design of future specific reagents and inhibitors. It would be especially useful to confirm the localisation of NDM-1 and to elucidate the route of access for Affimer 21.

In most of the areas tested, Affimer 21 has shown comparable qualities to other reported NDM-1 inhibitors. As more robust delivery systems become available for intracellular targeting, the use of the Affimer in combination with antimicrobials could result in the re-potentiation of previously ineffective antibiotics. Further investigation into the use of Affimers as a platform for identifying novel inhibitors effective against metallo-β-lactamases could represent a useful tool in the ongoing battle against antibiotic resistant pathogens.

8. References

1. Abraham E P. and Chain E. 1940. An Enzyme from Bacteria able to Destroy Penicillin. *Nature*. 146 (837)
2. Ackerman S E., Currier N V., Bergen J M. and Cochran J R. 2014. Cystine-knot peptides: emerging tools for cancer imaging and therapy. *Expert Review of Proteomics*. 11 (5): p. 561-572
3. Agasti S S., Wang Y., Schueder F., Sukumar A., Jungmann R. and Yin P. 2017. DNA-barcoded labelling probes for highly multiplexed Exchange-PAINT imaging. *Chemical Science*. 8: p. 3080-3091
4. Ahmed U. and Saunders G. 2010. The Effect of NaCl Concentration on Protein Size Exclusion Chromatography. Application Note, *Agilent Technologies*.
5. Aissaoui S., Ouled-Haddar H., Sifour M., Beggah C. and Benhamada F. 2017. Biological Removal of the Mixed Pharmaceuticals: Diclofenac, Ibuprofen, and Sulfamethoxazole Using a Bacterial Consortium. *Iranian Journal of Biotechnology*. 15 (2): p. 135-142
6. Alifano P., Palumbo C., Pasanisi D. and Tala A. 2015. Rifampicin-resistance, rpoB polymorphism and RNA polymerase genetic engineering. 202: p. 60-77
7. Amin N., Liu A D., Ramer S., Aehle W., Meijer D., Metin M., Wong S., Gualfetti P. and Schellenberger V. 2004. Construction of stabilized proteins by combinatorial consensus mutagenesis. *Protein Engineering, Design and Selection*. 17 (11): p. 787-793
8. Aminov R I. 2010. A Brief History of the Antibiotic Era: Lessons Learned and Challenges for the Future. *Frontiers in Microbiology*. 1 (134)
9. Anderson E S. and Lewis M J. 1965. Drug resistance and its transfer in Salmonella typhimurium. *Nature*. 206: p. 579-583
10. Antibiotic Resistance UK. 2018. Causes of Antibiotic Resistance. [Online]. [Accessed 19 September 2018]. Available from: https://www.antibioticresearch.org.uk/causes-antibiotic-resistance/
11. Aoki N., Ishii Y., Tateda K., Saga T., Kimura S., Kikuchi Y., Kobayashi T., Tanabe Y., Tsukada H., Gejyo F. and Yamaguchi K. 2010. Efficacy of Calcium-EDTA as an Inhibitor for Metallo-β-Lactamase in a Mouse Model of *Pseudomonas aeruginosa* Pneumonia. *Antimicrobial Agents Chemotherapy*. 54 (11): p. 4582-4588

12. Atanosova K R. 2010. Interactions between porcine respiratory coronavirus and bacterial cell wall toxins in the lungs of pigs. [published dissertation].
13. Auld D S. 1988. *Methods in Enzymology.* Volume 158. Pages 110-114. San Diego: Academic Press.
14. Azadbakht A. and Derikvandi Z. 2018. Aptamer-based sensor for diclofenac quantification using carbon nanotubes and graphene oxide decorated with magnetic nanomaterials. *Journal of the Iranian Chemical Society*. 15 (3): p. 595-606
15. Azhar A., Ahmad E., Zia Q., Rauf M A., Owais M. and Ashraf G M. 2017. Recent advances in the development of novel protein scaffolds based therapeutics. *International Journal of Biological Macromolecules*. 102: p. 630-641
16. Bagge N., Schuster M., Hentzer M., Ciofu O., Givskov M., Greenberg E P. and Høiby N. 2004. *Pseudomonas aeruginosa* biofilms exposed to Imipenem exhibit changes in global gene expression and β-Lactamase and alginate production. *Antimicrobial Agents and Chemotherapy*. 48 (4): p. 1175-1187
17. Ball A P., Geddes A M., Davey P G., Farrell I D. and Brookes G R. 1980. Clavulanic Acid and Amoxycillin: A clinical, bacteriological and pharmacological study. *The Lancet*. 315 (8169): p. 620-623
18. Bandara A B., Zuo Z., Ramachandran S., Ritter A., Heflin J R. and Inzana T J. 2015. Detection of methicillin-resistant staphylococci by biosensor assay consisting of nanoscale films on optical fiber long-period gratings. *Biosensors and Bioelectronics*. 70 (0) p. 433-440
19. Barbas C F., Burton D R., Scott J K. and Silverman G J. 2001. *Phage Display: A Laboratory Manual*. New York: Cold Spring Harbor Laboratory Press.
20. Baroud M., Dandache I., Araj G F., Wakim R., Kanj S., Kanafani Z., Khairallah M., Sabra A., Shehab M., Dbaibo G. and Matar G M. 2013. Underlying mechanisms of carbapenem resistance in extended-spectrum β-lactamase-producing Klebsiella pneumoniae and Escherichia coli isolates at a tertiary care centre in Lebanon: role of OXA-48 and NDM-1 carbapenemases. *International Journal of Antimicrobial Agents*. 41 (1): p. 75-79
21. Batyuk A., Wu Y., Honegger A., Heberling M M. and Plückthun A. 2016. DARPin-Based Crystallization Chaperones Exploit Molecular Geometry as a

Screening Dimension in Protein Crystallography. *Journal of Molecular Biology*. 428 (8): p. 1574-1588

22. Bayshul S., Noh G., Keum T., Choi Y W. and Lee S. 2016. Cell penetrating peptides as an innovative approach for drug delivery; then, present and the future. *Journal of Pharmaceutical Investigation*. 46 (3): p. 205-220
23. Bebrone C. 2007. Metallo-β-lactamases (classification, activity, genetic organization, structure, zinc coordination) and their superfamily. *Biochemical Pharmacology*. 74 (12): p. 1686-1701
24. Bebrone C., Lassaux P., Vercheval L., Sohier J S., Jehaes A., Sauvage E. and Galleni M. 2010. Current Challenges in Antimicrobial Chemotherapy: Focus on β-Lactamase Inhibition. *Drugs*. 70 (6): p. 651-679
25. Bedford R., Tiede C., Hughes R., Curd A., McPherson M J., Peckham M. and Tomlinson D C. 2017. Alternative reagents to antibodies in imaging applications. *Biophysical Reviews*. 9 (4): p. 299-308
26. Betts M J. and Russell R B. 2003. Amino acid properties and consequences of substitutions: *Bioinformatics for Geneticists*. Hoboken: Wiley
27. Bhullar K., Waglechner N., Pawlowski A., Koteva K., Banks E D., Johnston M D., Barton H A. and Wright G D. 2012. Antibiotic Resistance Is Prevalent in an Isolated Cave Microbiome. *PLoS ONE*. 7 (4)
28. Binz H K., Stumpp M T., Forrer P., Amstutz P. and Pluckthun A. 2003. Designing repeat proteins: well-expressed, soluble and stable proteins from combinatorial libraries of consensus ankyrin repeat proteins. *Journal of Molecular Biology*. 332 (2): p. 489-503
29. Binz H K., Amstutz P. and Pluckthun A. 2005. Engineering novel binding proteins from nonimmunoglobulin domains. *Nature Biotechnology*. 23: p. 1257-1268
30. Bjarnsholt T. 2013. The role of bacterial biofilms in chronic infections. *Journal of Pathology, Microbiology and Immunology*. 121 (136); p. 1-58
31. Blair J M., Webber M A., Baylay A J., Ogbolu D O. and Piddock L J. 2015. Molecular mechanisms of antibiotic resistance. *Nature Reviews Microbiology*. 13: p. 42-51
32. Boehm A., Steiner S., Zaehringer F., Casanova A., Hamburger F., Ritz D., Keck W., Ackermann M., Schirmer T. and Jenal U. 2009. Second messenger

signalling governs Escherichia coli biofilm induction upon ribosomal stress. *Molecular Microbiology*. 72 (6): p. 1500-1516

33. Bonnefille B., Gomez E., Courant F., Escande A. and Fenet H. 2018. Diclofenac in the marine environment: A review of its occurrence and effects. *Marine Pollution Bulletin*. 131 (A): p. 496-506
34. Bonsor D A., Postel A., Pierce B G., Wang N., Zhu P., Buonpane R A., Weng Z., Kranz D M. and Sundberg E J. 2011. Molecular Basis of a Million-Fold Affinity Maturation Process in a Protein–Protein Interaction. *Journal of Molecular Biology*. 411: p. 321-328
35. Bosch F. and Rosich L. 2008. The Contributions of Paul Ehrlich to Pharmacology: A Tribute on the Occasion of the Centenary of His Nobel Prize. *Pharmacology.* 82 (3): p. 171-179
36. Both A., Huang J., Kaase M., Hezel J., Wertheimer D., Fenner I., Gunther T., Grundhoff A., Buttner H., Aepfelbacher M., Rohde H. and Hentschke M. 2016. First report of Escherichia coli co-producing NDM-1 and OXA-232. *Diagnostic Microbiology and Infectious Disease*. 86 (4): p. 437-438
37. Bradbury A. and Pluckthun A. 2015. Reproducibility: Standardize antibodies used in research. *Nature*. 518 (7537)
38. Brem J., van Berkel S S., Aik W., Rydzik A M., Avison M B., Pettinati I., Umland K-D., Kawamura A., Spencer J., Claridge T D W., McDonough M A. and Schofield C J. 2014. Rhodanine hydrolysis leads to potent thioenolate mediated metallo-β-lactamase inhibition. *Nature Chemistry*. 6: p. 1084-1090
39. Brem J., van Berkel S S., Zollman D., Lee S Y., Gileadi O., McHugh P J., Walsh T R., McDonough M A. and Schofield C J. 2016. Structural basis of metallo-β-lactamase inhibition by captopril stereoisomers. *Antimicrobial Agents Chemotherapy*. 60: p. 142-150
40. Brem J., Cain R., Cahill S., McDonough M A., Clifton I J., Jimenez-Castellanos J-C., Avison M B., Spencer J., Fishwick C W G. and Schofield C J. 2016b. Structural basis of metallo-β-lactamase, serine-β-lactamase and penicillin-binding protein inhibition by cyclic boronates. *Nature communications*. 7 (12406)
41. Brouwer J M., Lan P., Cowan A D., Bernardini J P., Birkinshaw R W., van Delft M F., Sleebs B E., Robin A Y., Wardak A., Tan I K., Reljic B., Lee E F., Fairlie W

D., Call M J., Smith B J., Dewson G., Lessene G., Colman P M. and Czabotar P E. 2017. Conversion of Bim-BH3 from Activator to Inhibitor of Bak through Structure-Based Design. *Molecular Cell*. 68 (4): p. 659-672

42. Bush K. and Bradford P A. 2016. β-Lactams and β-Lactamase Inhibitors: An Overview. *Cold Spring Harbor Perspectives in Medicine*. 6 (8)
43. Cahill S T., Cain R., Wang D Y., Lohans C T., Wareham D W., Oswin H P., Mohammed J., Spencer J., Fishwick C W., McDonough M A., Schofield C J. and Brem J. 2017. Cyclic Boronates Inhibit All Classes of β-Lactamases. *Antimicrobial Agents and Chemotherapy*. 61 (4)
44. Campos J C., da Silva M J., dos Santos P R., Barros E M., Pereira Mde O., Seco B M., Magagnin C M., Leiroz L K., de Oliveira T G., de Faria-Júnior C., Cerdeira L T., Barth A L., Sampaio S C., Zavascki A P., Poirel L. and Sampaio J L. 2015. Characterization of Tn3000, a Transposon Responsible for blaNDM-1 Dissemination among Enterobacteriaceae in Brazil, Nepal, Morocco, and India. *Antimicrobial Agents and Chemotherapy*. 59 (12): p. 7387-7395
45. Carpenter K J. 2000. Thomas Hughes Jukes (1906–1999). *The Journal of Nutrition*. 130 (6): p. 1521–1523
46. Castanheira M., Deshpande L M., Woosley L N., Serio A W., Krause K M. and Flamm R K. 2018. Activity of plazomicin compared with other aminoglycosides against isolates from European and adjacent countries, including Enterobacteriaceae molecularly characterized for aminoglycoside-modifying enzymes and other resistance mechanisms. *Journal of Antimicrobial Chemotherapy.* [Epub ahead of print]
47. Ceri H., Olson M E., Stremick C., Read R R., Morck D. and Buret A. 1999. The Calgary Biofilm Device: new technology for rapid determination of antibiotic susceptibilities of bacterial biofilms. *Journal of Clinical Microbiology*. 37 (6): p. 1771-1776
48. Ceylan Koydemir H., Kulah H., Ozgen C., Alp A. and Hascelik G. 2011. MEMS biosensors for detection of methicillin resistant Staphylococcus aureus. *Biosensors and Bioelectronics*. 29 (1): p.1-12
49. Chaibi E B., Sirot D., Paul G. and Labia R. 1999. Inhibitor-resistant TEM β-lactamases: phenotypic, genetic and biochemical characteristics. *Journal of Antimicrobial Chemotherapy*. 43 (4): p. 447–458

50. Chatterjee S., Mondal A., Mitra S. and Basu S. 2017. Acinetobacter baumannii transfers the blaNDM-1 gene via outer membrane vesicles. *Journal of Antimicrobial Chemotherapy*. 72 (8): p. 2201-2207

51. Chen A Y., Thomas P W., Stewart A C., Bergstrom A., Cheng Z., Miller C., Bethel C R., Marshall S H., Credille C V., Riley C L., Page R C., Bonomo R A., Crowder M W., Tierney D., Fast W. and Cohen S M. 2017. Dipicolinic Acid Derivatives as Inhibitors of New Delhi Metallo-β-lactamase-1. *Journal of Medicinal Chemistry*. 60 (17): p. 7267-7283

52. Chen Z Y., Hu Y T., Yang W S., He Y W., Feng J., Wang B., Zhao R M., Ding J P., Cao Z J., Li W X. and Wu Y L. 2012. Hg1, Novel Peptide Inhibitor Specific for Kv1.3 Channels from First Scorpion Kunitz-type Potassium Channel Toxin Family. *Journal of Biological Chemistry*. 287: p. 13813-13821

53. Cheng A C., Coleman R G., Smyth K T., Qing C., Soulard P., Caffrey D R., Salzberg A C. and Huang E S. 2007. Structure-based maximal affinity model predicts small-molecule druggability. *Nature Biotechnology*. 25: p. 71-75

54. Cheung L S., Shea D J., Nicholes N., Date A., Ostermeier M. and Konstantopoulos K. 2015. Characterization of Monobody Scaffold Interactions with Ligand via Force Spectroscopy and Steered Molecular Dynamics. *Scientific Reports*. 5 (8247)

55. Chiou J., Wan S., Chan K-F., So P-K., He D., Chan E W., Chan T H., Wong K-Y., Tao J. and Chen S. 2015. Ebselen as a potent covalent inhibitor of New Delhi metallo-β-lactamase (NDM-1). *Chemical Communications*. 51 (46): p. 9543-9546

56. Christopeit T., Albert A. and Leiros H-K S. 2016. Discovery of a novel covalent non-β-lactam inhibitor of the metallo-β-lactamase NDM-1. *Proteins and Proteomics*. 1834 (8): p. 1648-1659

57. Ciofu O., Beveridge T J., Kadurugamuwa J., Walther-Rasmussen J. and Hoiby N. 2000. Chromosomal β-lactamase is packaged into membrane vesicles and secreted from Pseudomonas aeruginosa. *Journal of Antimicrobial Chemotherapy*. 45 (1): p. 9-13

58. Clarks C. 2015. Antibiotic Pharmacology. [Online] [Accessed 20 September 2018] Available from: http://tmedweb.tulane.edu/pharmwiki/doku.php/antibiotic_pharmacology

59. Click E M. and Webster R E. 1998. The TolQRA Proteins Are Required for Membrane Insertion of the Major Capsid Protein of the Filamentous Phage f1 during Infection. *Journal of Bacteriology*. 180 (7): p. 1723-1728

60. Coleman K. 2011. Diazabicyclooctanes (DBOs): a potent new class of non-β-lactam β-lactamase inhibitors. *Current Opinion in Microbiology*. 14 (5): p. 550-555

61. Cox K., Devanarayan V., Kriauciunas A., Manetta J., Montrose C. and Sittampalam S. 2012. Immunoassay Methods. *Assay Guidance Manual*. [Online] [Accessed 19 September 2018] Available from: https://www.ncbi.nlm.nih.gov/books/NBK92434/

62. Crandon J L. and Nicolau D P. 2015. In Vivo Activities of Simulated Human Doses of Cefepime and Cefepime-AAI101 against Multidrug-Resistant Gram-Negative Enterobacteriaceae. *Antimicrobial Agents and Chemotherapy*. 59 (5): p. 2688-94

63. Crowder M W., Spencer J. and Vila A J. 2006. Metallo-β-lactamases: Novel Weaponry for Antibiotic Resistance in Bacteria. *Accounts of Chemical Research*. 39 (10): p. 721-728

64. Cunningham B C. and Wells J A. 1989. High-resolution epitope mapping of hGH-receptor interactions by alanine-scanning mutagenesis. *Science*. 244 (4908): p. 1081-1085

65. Cunningham B C. and Wells J A. 1993. Comparison of a Structural and a Functional Epitope. *Journal of Molecular Biol*ogy. 234: p. 554-563

66. D'Costa V M., et al. 2011. Antibiotic resistance is ancient. *Nature*. 477: p. 457-461

67. Davies J. 2006. Where have all the antibiotics gone? *Canadian Journal of Infectious Diseases and Medical Microbiology.* 17 (5): p. 287-290

68. Davies J., Spiegelman G B. and Yim G. 2006. The world of subinhibitory antibiotic concentrations. *Current Opinion in Microbiology*. 9 (5): p. 445-453

69. Demarest S J., Rogers J. and Hansen G. 2004. Optimization of the Antibody CH3 Domain by Residue Frequency Analysis of IgG Sequences. *Journal of Molecular Biology*. 335 (1): p. 41-48

70. Docquier J-D. and Mangani S. 2018. An update on β-lactamase inhibitor discovery and development. *Drug Resistance Updates*. 36: p. 13-29

71. Dolejska M., Villa L., Poirel L., Nordmann P. and Carattoli A. 2012. Complete sequencing of an IncHI1 plasmid encoding the carbapenemase NDM-1, the ArmA 16S RNA methylase and a resistance–nodulation–cell division/multidrug efflux pump. *Journal of Antimicrobial Chemotherapy*. 68 (1): p. 34-39

72. Dovers S. and Butler C. 2015. Population and environment: a global challenge. [Online] [Accessed 20 November 2018]. Available from: https://www.science.org.au/curious/earth-environment/population-environment

73. Dowd J E. and Riggs D S. 1965. A comparison of estimates of Michaelis–Menten kinetic constants from various linear transformations. *Journal of Biological Chemistry*. 240 (2): p. 863–869.

74. Du D., Wang-Kan X., Neuberger A., Van Veen H W., Pos K M., Piddock L J V. and Luisi B F. 2018. Multidrug efflux pumps: structure, function and regulation. *Nature Reviews Microbiology*. 16: p. 523-539

75. Durand-Réville T F., Guler S., Comita-Prevoir J., Chen B., Bifulco N., Huynh H., Lahiri S., Shapiro A B., McLeod S M., Carter N M., Moussa S H., Velez-Vega C., Olivier N B., McLaughlin R., Gao N., Thresher J., Palmer T., Andrews B., Giacobbe R A., Newman J V., Ehmann D E., de Jonge B., O'Donnell J., Mueller J P., Tommasi R A. and Miller A A. 2017. ETX2514 is a broad-spectrum β-lactamase inhibitor for the treatment of drug-resistant Gram-negative bacteria including Acinetobacter baumannii. *Nature Microbiology*. 30 (2)

76. Ehrlich P. 1877. Contributions to the knowledge of aniline dyeings and their use in the microscopic technique. *Archive for Microscopic Anatomy*. 13: 263-278

77. Ehrlich P. 1910. About the treatment of syphilis with dioxydiamidoarsenobenzene. *Clinico-therapeutic weekly*. 17: p. 1005-1018

78. Elewski B E., Aly R., Baldwin S L., Gonzalez Soto R F., Rich P., Weisfeld M., Wiltz H., Zane L T. and Pollak R. 2015. Efficacy and safety of tavaborole topical solution, 5%, a novel boron-based antifungal agent, for the treatment of toenail onychomycosis: Results from 2 randomized phase-III studies. *Journal of the American Academy of Dermatology*. 73 (1): p. 62-69

79. Ellington A D. and Szostak J W. 1990. In vitro selection of RNA molecules that bind specific ligands. *Nature*. 346 (6287): p. 818-822

80. Escapa C., Coimbra R N., Paniagua S., García A I. and Otero M. 2016. Comparative assessment of diclofenac removal from water by different microalgae strains. *Algal Research*. 18: p. 127-134

81. European Centre for Disease Prevention and Control (ECDC). 2017. Livestock-associated methicillin-resistant Staphylococcus aureus (LA-MRSA) among MRSA from humans across the EU/EEA, 2013: ECDC survey. [Online]. [Accessed 17 September 2018]. Available from: https://ecdc.europa.eu/en/news-events/livestock-associated-meticillin-resistant-staphylococcus-aureus-la-mrsa-among-mrsa

82. Falconer S B., Reid-Yu S A., King A M., Gerhke S S., Wang W., Britten J F., Coombes B K., Wright G D. and Brown E D. 2015. Zinc Chelation by a Small-Molecule Adjuvant Potentiates Meropenem Activity in Vivo against NDM-1-Producing Klebsiella pneumoniae. *ACS Infectious Diseases*. 1: p. 533-543

83. Feito, R., Valcarcel Y. and Catala M. 2012. Biomarker assessment of toxicity with miniaturised bioassays: diclofenac as a case study. *Ecotoxicology*. 21 (1): p. 289-296

84. Feng H., Ding J., Zhu D., Liu X., Xu X., Zhang Y., Zang S., Wang D-C. and Liu W. 2014. Structural and Mechanistic Insights into NDM-1 Catalyzed Hydrolysis of Cephalosporins. *Journal of the American Chemical Society.* 136: p. 14694−14697

85. Feng H., Liu X., Wang S., Fleming J., Wang D-C. and Liu W. 2017. The mechanism of NDM-1-catalyzed carbapenem hydrolysis is distinct from that of penicillin or cephalosporin hydrolysis. *Nature Communications*. 8 (1)

86. Ferrari B., Paxeus N., Giudice R L., Pollio A. and Garric J. 2003. Ecotoxicological impact of pharmaceuticals found in treated wastewaters: study of carbamazepine, clofibric acid, and diclofenac. *Ecotoxicology and Environmental Safety*. 55 (3): p. 359-370

87. Fishovitz J., Hermoso J A., Chang M. and Mobashery S. 2015. Penicillin-Binding Protein 2a of Methicillin-Resistant Staphylococcus aureus. *IUBMB Life*. 66 (8): p. 572-577

88. Fleetwood F., Klint S., Hanze M., Gunneriusson E., Frejd F Y., Stahl S. and Lofblom J. 2014. Simultaneous targeting of two ligand-binding sites on VEGFR2 using biparatopic Affibody molecules results in dramatically improved affinity. *Scientific Reports*. 4 (7518)

89. Fornasiero E F. and Opazo F. 2015. Super-resolution imaging for cell biologists. BioEssays. 37 (4): p. 436-451

90. Forsberg K J., Reyes A., Wang B., Selleck E M., Sommer M O. and Dantas G. 2012. The Shared Antibiotic Resistome of Soil Bacteria and Human Pathogens. *Science*. 337 (6098): p. 1107-1111

91. Forsström B., Axnas B B., Rockberg J., Danielsson H., Bohlin A. and Uhlen M. 2015. Dissecting Antibodies with Regards to Linear and Conformational Epitopes. *PLoS ONE*. 10 (3)

92. Fritsche T R., Castanheira M., Miller G H., Jones R N. and Armstrong E S. 2008. Detection of Methyltransferases Conferring High-Level Resistance to Aminoglycosides in Enterobacteriaceae from Europe, North America, and Latin America. *Antimicrobial Agents and Chemotherapy*. 52 (5): p. 1843-1845

93. Frolund Thomsen M C. and Nielsen M. 2012. Seq2Logo: a method for construction and visualization of amino acid binding motifs and sequence profiles including sequence weighting, pseudo counts and two-sided representation of amino acid enrichment and depletion. *Nucleic Acids Research*. 40 (W1): W281-W287

94. Garces S. and Demengeot J. 2018. The Immunogenicity of Biologic Therapies. *Current Problems in Dermatology*. 53: p. 37-48

95. Gebauer M. and Skerra A. 2009. Engineered protein scaffolds as next-generation antibody therapeutics. *Current Opinion in Chemical Biology*. 13 (3): p. 245-255

96. Gebauer M. and Skerra A. 2012. Anticalins small engineered binding proteins based on the lipocalin scaffold. *Methods in Enzymology*. 503: p. 157-188

97. Gehrlein M., Leying H., Cullmann W., Wendt S. and Opferkuch W. 1991. Imipenem resistance in Acinetobacter baumanii is due to altered penicillin-binding proteins. *Chemotherapy*. 37 (6): p. 405-412

98. Glotzbach B., Reinwarth M., Weber N., Fabritz S., Tomaszowski M., Fittler H., Christmann A., Avrutina O. and Kolmar H. 2013. Combinatorial Optimization

of Cystine-Knot Peptides towards High-Affinity Inhibitors of Human Matriptase-1. *PLoS One*

99. Gomarasca M., Martins T F C., Greune L., Hardwidge P R., Schmidt M A. and Rüter C. 2017. Bacterium-Derived Cell-Penetrating Peptides Deliver Gentamicin To Kill Intracellular Pathogens. *Antimicrobial Agents and Chemotherapy*. 61 (4)
100. Gomes de Castro M., Hobartner C. and Opazo F. 2017. Aptamers provide superior stainings of cellular receptors studied under super-resolution microscopy. *PLoSOne*. 12 (2)
101. Gonzalez L J., Bahr G., Nakashige T G., Nolan E M., Bonomo R A. and Vila A J. 2016. Membrane anchoring stabilizes and favors secretion of New Delhi metallo-β-lactamase. *Nature Chemical Biology*. 12: p. 516-522
102. Gonzalez M M., Kosmopoulou M., Mojica M F., Castillo V., Hinchliffe P., Pettinati I., Brem J., Schofield C J., Mahler G., Bonomo R A., Llarrull L I., Spencer J. and Vila A J. 2015. Bisthiazolidines: A Substrate-Mimicking Scaffold as an Inhibitor of the NDM-1 Carbapenemase. *ACS Infectious Diseases*. 1 (11): p. 544-554
103. Gould K. 2016. Antibiotics: from prehistory to the present day. *Journal of Antimicrobial Chemotherapy.* 71 (3): p. 572-575
104. Green N M. 1990. Avidin and streptavidin. *Methods in Enzymology.* Volume 184. Pages 51-67. San Diego: Academic Press.
105. Green V L., Verma A., Owens R J., Phillips S E. and Carr S B. 2011. Structure of New Delhi metallo-β-lactamase 1 (NDM-1). *Acta Crystallographica Section F*. 67 (10): p. 1160–1164
106. Grover A K. 2013. Use of Allosteric Targets in the Discovery of Safer Drugs. *Medical Principles and Practice*. 22 (5): p. 418-426
107. Guo Y., Wang J., Shui W., Zhou H., Zhang Y., Yang C., Lou Z. and Rao Z. 2011. A structural view of the antibiotic degradation enzyme NDM-1 from a superbug. *Protein Cell*. 2 (5): p. 384-394
108. Habib G, Lancellotti P, Antunes MJ, Bongiorni MG, Casalta JP, Del Zotti F, Dulgheru R., El Khoury G., Erba P A., Iung B., Miro J M., Mulder B J., Plonska-Gosciniak E., Price S., Roos-Hesselink J., Snygg-Martin U., Thuny F., Tornos Mas P., Vilacosta I. and Zamorano J L. 2015. 2015 ESC Guidelines for the

management of infective endocarditis: The Task Force for the Management of Infective Endocarditis of the European Society of Cardiology (ESC). Endorsed by: European Association for Cardio-Thoracic Surgery (EACTS), the European Association of Nuclear Medicine (EANM). *European Heart Journal*. 36 (44): p. 3075-3128

109. Hackel B J., Kapila A. and Wittrup K D. 2008. Picomolar affinity fibronectin domains engineered utilizing loop length diversity, recursive mutagenesis, and loop shuffling. *Journal of Molecular Biology*. 381 (5): p. 1238-1252
110. Hall C W. and Mah T F. 2017. Molecular mechanisms of biofilm-based antibiotic resistance and tolerance in pathogenic bacteria. *FEMS Microbiology Reviews*. 41 (3): p. 276-301
111. Hamers-Casterman C., Tarhouch T., Muyldermans S., Robinson G., Hammers C., Bajyana Songa E., Bendahman N. and Hammers R. 1993. Naturally occurring antibodies devoid of light chains. *Nature*. 363: p. 446-448
112. Hamilton S M., Alexander J A N., Choo E J., Basuino L., Da Costa T M., Severin A., Chung M., Aedo S., Strynadka N C J., Tomasz A., Chatterjee S S. and Chambers H F. 2017. High-Level Resistance of Staphylococcus aureus to β-Lactam Antibiotics Mediated by Penicillin-Binding Protein 4 (PBP4). *Antimicrobial Agents and Chemotherapy*
113. Hamrick J C., Chatwin C L., John K J., Pevear D C., Burns C J. and Xerri L. 2018. *The ability of broad-spectrum β-lactamase inhibitor VNRX-5133 to restore bactericidal activity of cefepime in Enterobacteriaceae and P. aeruginosa-expressing Ambler class A, B, C and D enzymes is demonstrated using time-kill kinetics*. [Online poster]. [Accessed 22 October 2018]. Available from: https://www.venatorx.com/wp-content/uploads/2018/04/ECCMID2018-P1545.pdf
114. Hedge P J. and Spratt B G. 1985. Resistance to β-lactam antibiotics by re-modelling the active site of an E. coli penicillin-binding protein. *Nature*. 318: p. 478-480
115. Hey T., Fiedler E., Rudolph R. and Fiedler M. 2005. Artificial, non-antibody binding proteins for pharmaceutical and industrial applications. *Trends in Biotechnology.* 23 (10): p.514-22

116. Hidalgo L., Hopkins K L., Gutierrez B., Ovejero C M., Shukla S., Douthwaite S., Prasad K N., Woodford N. and Gonzalez-Zorn B. 2013. Association of the novel aminoglycoside resistance determinant RmtF with NDM carbapenemase in Enterobacteriaceae isolated in India and the UK. *Journal of Antimicrobial Chemotherapy*. 68 (7): p. 1543-1550

117. Hirai H., Sootome, H., Nakatsuru Y., Miyama K., Taguchi S., Tsujioka K., Ueno Y., Hatch H., Mayumder P K., Pan B S. and Kotani H. 2010. MK-2206, an Allosteric Akt Inhibitor, Enhances Antitumor Efficacy by Standard Chemotherapeutic Agents or Molecular Targeted Drugs In vitro and In vivo. *Molecular Cancer Therapeutics*. 9 (7): p. 1956-1967

118. Hoerr V., Franz M., Pletz M W., Diab M., Niemann S., Faberf C., Doenst T., Schulze P C., Deinhardt-Emmer S. and Löffler B. 2018. S. aureus endocarditis: Clinical aspects and experimental approaches. *International Journal of Medical Microbiology*. 308 (6): p. 640-652

119. Holmes A H., Moore L S., Sundsfjord A., Steinbakk M., Regmi S., Karkey A., Guerin P J. and Piddock L J. 2015. Understanding the mechanisms and drivers of antimicrobial resistance. *The Lancet*. 387 (10014): p. 176-187

120. Hosse R J., Rothe A. and Power B E. 2006. A new generation of protein display scaffolds for molecular recognition. *Protein Science*. 15: p. 14-27

121. Hoyos-Nogues M., Gil F J. and Mas-Moruno C. 2018. Antimicrobial Peptides: Powerful Biorecognition Elements to Detect Bacteria in Biosensing Technologies. *Molecules*. 23 (7): p. 1683

122. Huang J X., Bishop-Hurley S L. and Cooper M A. 2012. Development of Anti-Infectives Using Phage Display: Biological Agents against Bacteria, Viruses, and Parasites. *Antimicrobial Agents and Chemotherapy*. 56 (9): p. 4569-4582

123. Huang R., Fang P, Hao Z. and Kay B K. 2016. Directed Evolution of a Highly Specific FN3 Monobody to the SH3 Domain of Human Lyn Tyrosine Kinase. *PLoS One*. 11 (1)

124. Huddleston J R. 2014. Horizontal gene transfer in the human gastrointestinal tract: potential spread of antibiotic resistance genes. *Infection and Drug Resistance*. 7: p. 167-176

125. Huebner M., Weber E., Niessner R., Boujday S. and Knopp D. 2015. Rapid analysis of diclofenac in freshwater and wastewater by a monoclonal

antibody-based highly sensitive ELISA. *Analytical and Bioanalytical Chemistry*. 407 (29): p. 8873-8882

126. Hughes J I., Baxter E W., Owen R L., Thomsen M., Tomlinson D C., Waterhouse M P., Win S J., Nettleship J E., Tiede C., Foster R J., Owens R J., Fishwick C W G., Harris S A., Goldman A., McPherson M J. and Morgan A W. 2018. Affimer proteins inhibit immune complex binding to FcγRIIIa with high specificity through competitive and allosteric modes of action. *PNAS*. 115 (1): p. 72-81
127. Hughes D J., Tiede C., Penswick N., Tang A A., Trinh C H., Mandal U., Zajac K Z., Gaule T., Howell G., Edwards T A., Duan J., Feyfant E., McPherson M J., Tomlinson D C. and Whitehouse A. 2017. Generation of specific inhibitors of SUMO-1- and SUMO-2/3-mediated protein-protein interactions using Affimer (Adhiron) technology. *Science Signalling*. 10 (505)
128. Jan A T. 2017. Outer Membrane Vesicles (OMVs) of Gram-negative Bacteria: A Perspective Update. *Frontiers in Microbiology*. 8
129. Janero D R. 2016. The reproducibility issue and preclinical academic drug discovery: educational and institutional initiatives fostering translation success. Expert Opinion on Drug Discovery. 11 (9): p. 835-842
130. Jeong K J., Mabry R. and Georgiou G. 2005. Avimers hold their own. *Nature Biotechnology*. 23: p. 1493-1494
131. Johnson A P. and Woodford N. 2013. Global spread of antibiotic resistance: the example of New Delhi metallo-b-lactamase (NDM)-mediated carbapenem resistance. *Journal of Medical Microbiology*. 62: p. 499-513
132. Jonsson A., Wållberg H., Herne N., Ståhl S. and Frejd F Y. 2009. Generation of tumour-necrosis-factor-alpha-specific affibody molecules capable of blocking receptor binding in vitro. *Biotechnology and Applied Biochemistry*. 54 (2): p. 93-103
133. Joshi P R., Acharya M., Kakshapati T., Leungtongkam U., Thummeepak R. and Sitthisak S. 2017. Co-existence of blaOXA-23 and blaNDM-1 genes of Acinetobacter baumannii isolated from Nepal: antimicrobial resistance and clinical significance. *Antimicrobial Resistance & Infection Control*. 6 (21)
134. Kannan N. and Neuwald A F. 2005. Did Protein Kinase Regulatory Mechanisms Evolve Through Elaboration of a Simple Structural Component? *Journal of Molecular Biology*. 351 (5): p. 956-972

135. Kaplan J B. 2011. Antibiotic-induced biofilm formation. *The International Journal of Artificial Organs*. 34 (9): p. 737-751

136. Kapmaz M., Erdem F., Abulaila A., Yeniaras E., Oncul O. and Aktas Z. 2016. First detection of NDM-1 with CTX-M-9, TEM, SHV and rmtC in Escherichia coli ST471 carrying IncI2, A/C and Y plasmids from clinical isolates in Turkey. *Journal of Global Antimicrobial Resistance*. (7): p. 152-153

137. Karsisiotis A I., Damblon C F. and Roberts G C K. 2014. A variety of roles for versatile zinc in metallo-β-lactamases. *Metallomics*. 6 (1181)

138. Kayushin A L., Korosteleva M D., Miroshnikov A I., Kosch W., Zubov D. and Piel N. 1996. A Convenient Approach to the Synthesis of Trinucleotide Phosphoramidites-Synthons for the Generation of Oligonucleotide/peptide Libraries. *Nucleic Acids Research.* 24 (19): p. 3748–3755.

139. Khan A U., Maryam L. and Zarrilli R. 2017. Structure, Genetics and Worldwide Spread of New Delhi Metallo-β-lactamase (NDM): a threat to public health. *BMC Microbiology*. 17 (101)

140. Kim S K., Sims C L., Wozniak S E., Drude S H., Whitson D. and Shaw R W. 2009. Antibiotic Resistance in Bacteria: Novel Metalloenzyme Inhibitors. *Chemical Biology and Drug Design*. 74: p. 343-348

141. Kim S W., Park S B., Im S P., Lee J S., Jung J W., Gong T W., Lazarte J M S., Kim J., Seo J S., Kim J H., Song J W., Jung H S., Kim G J., Lee Y J., Lim S K., and Jung T S. 2018. Outer membrane vesicles from β-lactam-resistant Escherichia coli enable the survival of β-lactam-susceptible E. coli in the presence of β-lactam antibiotics. *Nature Scientific Reports*. 8 (5402)

142. Kim Y., Cunningham M A., Mire J., Tesar C, Sacchettini J. and Joachimiak A. 2013. NDM-1, the ultimate promiscuous enzyme: substrate recognition and catalytic mechanism. *FASEB*. 27 (5): p. 1917-1927

143. Kim Y., Tesar C., Mire J., Jedrzejczak R., Binkowski A., Babnigg G., Sacchettini J and Joachimiak A. 2011. Structure of Apo and Monometalated Forms of NDM-1 - A Highly Potent Carbapenem-Hydrolyzing Metallo-β-Lactamase. *PLoS One*. 6 (9)

144. King A M., Reid-Yu S A., Wang W., King D T., De Pascale G., Strynadka N C., Walsh T R., Coombes B K. and Wright G D. 2014. Aspergillomarasmine A

overcomes metallo-β-lactamase antibiotic resistance. *Nature*. 510: p. 503-506

145. King D. and Strynadka N. 2011. Crystal structure of New Delhi metallo-β-lactamase reveals molecular basis for antibiotic resistance. *Protein Science*. 20 (9): p. 1484-1491
146. King D T., Worrall L J., Gruninger R. and Strynadka N C. 2012. New Delhi Metallo-β-Lactamase: Structural Insights into β-Lactam Recognition and Inhibition. *Journal of the American Chemical Society*. 134 (28): p. 11362-11365
147. Kirby A E., Garner K. and Levin B R. 2012. The Relative Contributions of Physical Structure and Cell Density to the Antibiotic Susceptibility of Bacteria in Biofilms. *Antimicrobial Agents and Chemotherapy*. 56 (6): p. 2967-2975
148. Klein A., Hank S., Raulf A., Joest E F., Tissen F., Heilemann M., Wieneke R. and Tampe R. 2018. Live-cell labeling of endogenous proteins with nanometer precision by transduced nanobodies. *Chemical Science*. 9: p. 7835-7842
149. Klingler F M., Wichelhaus T A., Frank D., Cuesta-Bernal J., El-Delik J., Muller H F., Sjuts H., Gottig S., Koenigs A., Pos K M., Pogoryelov D. and Proschak E. 2015. Approved Drugs Containing Thiols as Inhibitors of Metallo-βlactamases: Strategy To Combat Multidrug-Resistant Bacteria. *Journal of Medicinal Chemistry*. 58: p. 3626-3630
150. Knight S., Collins M. and Takeuchi Y. 2013. Insertional Mutagenesis by Retroviral Vectors: Current Concepts and Methods of Analysis. *Current Gene Therapy*. 13: p. 211-227
151. Ko B-K., Choi S., Cui L G., Lee Y H., Hwang I S., Kim K T., Shim H. and Lee J S. 2015. Affinity Maturation of Monoclonal Antibody 1E11 by Targeted Randomization in CDR3 Regions Optimizes Therapeutic Antibody Targeting of HER2-Positive Gastric Cancer. *PLoS One*.
152. Kong K F., Schneper L. and Mathee K. 2011. Beta-lactam Antibiotics: From Antibiosis to Resistance and Bacteriology. *APMIS*. 118 (1): p. 1-36
153. Koutsoumpeli E., Tiede C., Murray J., Tang A., Bon R S., Tomlinson D C. and Johnson S. 2017. Antibody Mimetics for the Detection of Small Organic Compounds Using a Quartz Crystal Microbalance. 89 (5): p. 3051-3058

154. Krauss I R., Merlino A., Vergara A. and Sica F. 2013. An Overview of Biological Macromolecule Crystallization. *International Journal of Molecular Sciences*. 14: p. 11643-11691

155. Kruse H. and Sorum H. 1994. Transfer of Multiple Drug Resistance Plasmids between Bacteria of Diverse Origins in Natural Microenvironments. *Applied and Environmental Microbiology*. 60 (11): p. 4015-4021

156. Kubala M H., Kovtun O., Alexandrov K. and Collins B M. 2010. Structural and thermodynamic analysis of the GFP:GFP-nanobody complex. Protein Science. 19 (12): p.2389-2401

157. Kumarasinghe I R. and Woster P M. 2018. Cyclic peptide inhibitors of lysine-specific demethylase 1 with improved potency identified by alanine scanning mutagenesis. *European Journal of Medicinal Chemistry.* 148: p. 210-220

158. Kummer L., Parizek P., Rube P., Millgramm B., Prinz A., Mittl P R., Kaufholz M., Zimmermann B., Herberg F W. and Plückthun A. 2012. Structural and functional analysis of phosphorylation-specific binders of the kinase ERK from designed ankyrin repeat protein libraries. *PNAS*. 109 (34): p. 2248-2257

159. Kwon E J., Skalak M., Bertucci A., Braun G., Ricci F., Ruoslahti E., Sailor M J. and Bhatia S N. 2018. Porous Silicon Nanoparticle Delivery of Tandem Peptide Anti-infectives for the Treatment of P. aeruginosa Lung Infections. *Advanced Materials*. 29 (35)

160. Kyle H .F, Wickson K F., Stott J., Burslem G M., Breeze A L., Tiede C., Tomlinson D C., Warriner S L., Nelson A., Wilson A J. and Edwards T A. 2015. Exploration of the HIF-1α/p300 interface using peptide and Adhiron phage display technologies. *Molecular Biosystems*. 11 (10): p. 2738-2749

161. Kyle S. 2018. Affimer Proteins:Theranostics of the Future? *Trends in Biochemical Sciences*. 43 (4): p. 230-232

162. Labrou N E. 2010. Random Mutagenesis Methods for In Vitro Directed Enzyme Evolution. *Current Protein and Peptide Science*. 11: p. 91-100

163. Laureti L., Matic I. and Gutierrez A. 2013. Bacterial Responses and Genome Instability Induced by Subinhibitory Concentrations of Antibiotics. *Antibiotics*. 2 (1): p. 100-114

164. Lehmann M., Loch C., Middendorf A., Studer D., Lassen S F., Pasamontes L., van Loom A P G M. and Wyss M. 2002. The consensus concept for

thermostability engineering of proteins: further proof of concept. *Protein Engineering*. 15 (5): p. 403-411

165. Levasseur P., Girard A M., Miossec C., Pace J. and Coleman K. 2015. In vitro antibacterial activity of the ceftazidime-avibactam combination against enterobacteriaceae, including strains with well-characterized β-lactamases. *Antimicrobial Agents and Chemotherapy*. 59 (4)
166. Li J S., Sexton D J., Mick N., Nettles R., Fowler V G Jr., Ryan T., Bashore T. and Corey G R. 2000. Proposed modifications to the Duke criteria for the diagnosis of infective endocarditis.
167. Lindsley C W., Barnett S F., Layton M E. and Bilodeau M T. 2008. The PI3K/Akt pathway: recent progress in the development of ATP-competitive and allosteric Akt kinase inhibitors. *Current Cancer Drug Targets*. 8: p. 7-18
168. Lindsley C W., Zhao Z., Leister W H., Robinson R G., Barnett S F., Defeo-Jones D., Jones R E., Hartman G D., Huff J R., Huber H E. and Duggan M E. 2005. Allosteric Akt (PKB) inhibitors: discovery and SAR of isozyme selective inhibitors. *Bioorganic & Medicinal Chemistry Letters*. 15 (3): p. 761-764
169. Lineweaver, H. and Burk D. 1934. The Determination of Enzyme Dissociation Constants. *Journal of the American Chemical Society.* 56 (3): p. 658-666
170. Lipovsek D. 2011. Adnectins: engineered target-binding protein therapeutics. *Protein Engineering, Design and Selection*. 24 (1-2): p. 3-9
171. Lise S., Archambeau C., Pontil M. and Jones D T. 2009. Prediction of hot spot residues at protein-protein interfaces by combining machine learning and energy-based methods. *BMC Bioinformatics*. 10 (365)
172. Lisitsyn N., Chernyi A., Nikitina I., Karpov V. and Beresten S. 2014. Methods of protein immunoanalysis. *Journal of Molecular Biology*. 48 (5): p. 624-633
173. Liu S., Zhou Y., Niu X., Wang T., Li J., Liu Z., Wang J., Tang S., Wang Y. and Deng Z. 2018. Magnolol restores the activity of meropenem against NDM-1-producing Escherichia coli by inhibiting the activity of metallo-beta-lactamase. *Cell Death Discovery*. 4 (28)
174. Liu X-L., Shi Y., Kang J S., Oelschlaeger P. and Yang K W. 2015. Amino acid thioester derivatives: a highly promising scaffold for the development of metallo-β-lactamase L1 inhibitors. *ACS Medicinal Chemistry*. 6: p. 660-664

175. Livermore D M., Mushtaq S., Warner M., Vickers A. and Woodford N. 2017. In vitro activity of cefepime/zidebactam (WCK 5222) against Gram-negative bacteria. *Journal of Antimicrobial Chemotherapy*. 72 (5): p. 1373–1385

176. Lomovskaya O., Sun D., Rubio-Aparicio D., Nelson K., Tsivkovski R., Griffith D C. and Dudley M N. 2017. Vaborbactam: Spectrum of Beta-Lactamase Inhibition and Impact of Resistance Mechanisms on Activity in Enterobacteriaceae. *Antimicrobial Agents and Chemotherapy*. 61 (11)

177. Lopata A., Hughes R., Tiede C., Heissler S M., Sellers J R., Knight P J., Tomlinson D C. and Peckham M. 2018. Affimer proteins for F-actin: novel affinity reagents that label F-actin in live and fixed cells. *Scientific Reports*. 8 (1)

178. Lorian, V. 2005. *Antibiotics in Laboratory Medicine*, (5th edition) Lippincott Williams & Wilkins.

179. Makena A., Brem J., Pfeffer I., Geffen R E., Wilkins S E., Tarhonskaya H., Phee L M., Wareham D W. and Schofield C J. 2015. Biochemical characterization of New Delhi metallo-β-lactamase variants reveals differences in protein stability. *Journal of Antimicrobial Chemotherapy*. 70 (2): p. 463–469.

180. Maldonado R F., Sa-Correia I. and Valvano M A. 2016. Lipopolysaccharide modification in Gram-negative bacteria during chronic infection. *FEMS Microbiology Reviews*. 40 (4): p. 480-493

181. Martin H L., Bedford R., Heseltine S J., Tang AA., Haza K J., Rao A, McPherson M J. and Tomlinson D C. 2018. Non-immunoglobulin scaffold proteins: Precision tools for studying protein-protein interactions in cancer. *New Biotechnology*

182. Masi M. and Pages J-M. 2013. Structure, Function and Regulation of Outer Membrane Proteins Involved in Drug Transport in Enterobactericeae: the OmpF/C – TolC Case. *The Open Microbiology Journal*. 7: p. 22-33

183. Matsuura A., Okumura H., Asakura R., Ashizawa N., Takahashi M., Kobayashi F., Ashikawa N. and Arai K. 1993. Pharmacological Profiles of Aspergillomarasmines as Endothelin Converting Enzyme Inhibitors. *The Japanese Journal of Pharmacology*. 63 (2): p. 187-193

184. McCall K A., Huang C. and Fierke C A. 2000. Function and Mechanism of Zinc Metalloenzymes. *The Journal of Nutrition*. 130 (5): p. 1437-1446

185. McGeary R P., Tan D T. and Schenk G. 2017. Progress toward inhibitors of metallo-β-lactamases. *Future Medicinal Chemistry*. 9 (7): p. 673-691

186. McPherson A. and Gavira J A. 2014. Introduction to protein crystallization. *Acta Crystallographica Section F.* 70 (1): p. 2-20

187. Meini M R., Llarrull L I. and Vila A J. 2015. Overcoming differences: The catalytic mechanism of metallo-beta-lactamases. *FEBS Letters*. 589 (22): p. 3419-32.

188. Mendonca N., Manageiro V., Robin F., Jose Salgado M., Ferreira E., Canica M. and Bonnet R. 2007. The Lys234Arg Substitution in the Enzyme SHV-72 Is a Determinant for Resistance to Clavulanic Acid Inhibition. *Antimicrobial Agents and Chemotherapy*. 52 (5)

189. Michael C A., Dominey-Howes D. and Labbate M. 2014. The Antimicrobial Resistance Crisis: Causes, Consequences, and Management. *Frontiers in Public Health*. 2 (145)

190. Michel M A., Swatek K N., Hospenthal M K. and Komander D. 2017. Ubiquitin Linkage-Specific Affimers Reveal Insights into K6-Linked Ubiquitin Signaling. *Molecular Cell*. 68 (1): p. 233-246

191. Mirani Z A. and Jamil N. 2011. Effect of sub-lethal doses of vancomycin and oxacillin on biofilm formation by vancomycin intermediate resistant Staphylococcus aureus. *Journal of Basic Microbiology*. 51: p. 191-195

192. Moerner W.E. 2012. Microscopy beyond the diffraction limit using actively controlled single molecules. *Journal of Microscopy*. 246 (3): p. 213-220

193. Mojica M F., Bonomo R A. and Fast W. 2017. B1-Metallo-beta-Lactamases: Where do we stand? *Current Drug Targets*. 17 (9): p. 1029-1050

194. Monogue M L., Giovagnoli S., Bissantz C., Zampaloni C. and Nicolau D P. 2018. In Vivo Efficacy of Meropenem with a Novel Non-β-Lactam–β-Lactamase Inhibitor, Nacubactam, against Gram-Negative Organisms Exhibiting Various Resistance Mechanisms in a Murine Complicated Urinary Tract Infection Model. *Antimicrobial Agents and Chemotherapy*. 62 (9)

195. Morrison K L. and Weiss G A. 2001. Combinatorial alanine-scanning. *Current Opinions in Chemical Biology*. 5 (3): p. 302-307

196. Mross K., Richly H., Fischer R., Scharr D., Buchert M., Stern A., Gille H., Audoly L P. and Scheulen M E. 2013. *PLoS One*. 8 (12)

197. Munita J M. and Arias C L. 2016. Mechanism of Antibiotic Resistance. *Microbiology Spectrum*. 4 (2)

198. Munoz-Price L.S., Poirel L., Bonomo R A., Schwaber M J., Daikos G L., Cormican M., Cornaglia G., Garau J., Gniadkowski M., Hayden M K., Kumarasamy K., Livermore D M., Maya J J., Nordmann P., Patel J B., Paterson D L., Pitout J., Villegas M V., Wang H., Woodford N. and Quinn J P. 2013. Clinical epidemiology of the global expansion of Klebsiella pneumoniae carbapenemases. *Lancet Infectious Diseases*. 13(9): p. 785-96.

199. Nakashima R., Sakurai K., Yamasaki S., Nishino K. and Yamaguchi A. 2011. Structures of the multidrug exporter AcrB reveal a proximal multisite drug-binding pocket. *Nature*. 480: p. 565-569

200. National Institute of Allergy and Infectious Diseases. 2016. Gram-negative Bacteria. [ONLINE] Available at: https://www.niaid.nih.gov/research/gram-negative-bacteria. [Accessed 15 August 2018].

201. Nature Biotechnology. 2018. Wanted: a reward for antibiotic development. [Online]. [Accessed 19 September 2018]. 36 (555) Available from: https://www.nature.com/articles/nbt.4193

202. Needham B D. and Trent M S. 2013. Fortifying the barrier: the impact of lipid A remodelling on bacterial pathogenesis. *Nature Reviews Microbiology*. 11: p. 467-481

203. Nekhotiaeva N., Elmquist A., Rajarao G K., Hällbrink M., Langel U. and Good L. 2004. Cell entry and antimicrobial properties of eukaryotic cell-penetrating peptides. *FASEB*. 18 (2): p. 394-396

204. New York Times Archives. 1945. PENICILLIN'S FINDER ASSAYS ITS FUTURE. *New York Times*. 26 June. p.21

205. Neylon C. 2004. Chemical and biochemical strategies for the randomization of protein encoding DNA sequences: library construction methods for directed evolution. *Nucleic Acids Research*. 32 (4): p. 1448-1459

206. NICE. 2018. CO-AMOXICLAV. [Online]. [Accessed 21 October 2018]. Available from: https://bnf.nice.org.uk/drug/co-amoxiclav.html#prescribingAndDispensingInformations

207. Nobel Media. *The Nobel Prize in Physiology or Medicine 1945*. [Online]. [Accessed 16 Nov 2018]. Available from: https://www.nobelprize.org/prizes/medicine/1945/summary/

208. Nord K., Gunneriusson E., Ringdahl J., Stahl S., Uhlen M. and Nygren PA. 1997. Binding proteins selected from combinatorial libraries of an alpha-helical bacterial receptor domain. *Nature Biotechnology*. 15: p. 772-777

209. Norris A L. and Serpersu E H. 2013. Ligand promiscuity through the eyes of the aminoglycoside N3 acetyltransferase IIa. *Protein Science*. 22 (7): p. 916-928

210. Oaks J L., Gilbert M., Virani M Z., Watson R T., Meteyer C U., Rideout B A., Shivaprasad H L., Ahmed S., Chaudhry M J I., Arshad M., Mahmood S., Ali A. and Khan A A. 2004. Diclofenac residues as the cause of vulture population decline in Pakistan. *Nature*. 427(6975): p.630-633

211. O'Callaghan C H., Morris A., Kirby S. M. and Shingler A H. 1972. Novel Method for Detection of β-Lactamases by Using a Chromogenic Cephalosporin Substrate. *Antimicrobial Agents and Chemotherapy*, 1 (4), 283–288.

212. O'Neill J. 2014. Antimicrobial Resistance: Tackling a crisis for the health and wealth of nations. Review on Antimicrobial Resistance

213. Opazo F., Levy M., Byrom M., Schäfer C., Geisler C., Groemer T W., Ellington A D. and Rizzoli S O. 2012. Aptamers as potential tools for super-resolution microscopy. *Nature Methods*. 9: p. 938-939

214. Oulton R L., Kohn T. and Cwiertny D M. Pharmaceuticals and personal care products in effluent matrices: A survey of transformation and removal during wastewater treatment and implications for wastewater management. 2010. *Journal of Environmental Monitoring*. 12 (11): p. 1956-1978

215. Palzkill T. 2013. Metallo β-lactamase structure and function. *Antimicrobial Therapeutics Reviews.* 1277 (1): p. 91-104

216. Papagiannitsis C C., Malli E., Florou Z., Sarrou S., Hrabak J., Mantzarlis K., Zakynthinos E. and Petinaki E. 2017. Emergence of sequence type 11 Klebsiella pneumoniae coproducing NDM-1 and VIM-1 metallo-β-lactamases in a Greek hospital. *Diagnostic Microbiology and Infectious Disease*. 87 (3): p. 295-297

217. Pasteran F., Gonzalez L J., Albornoz E., Bahr G., Vila A J. and Corso A. 2016. Triton Hodge Test: Improved Protocol for Modified Hodge Test for Enhanced Detection of NDM and Other Carbapenemase Producers. *Journal of Clinical Microbiology*. 54: p. 640-649

218. Payne D J., Hueso-Rodríguez J A., Boyd H., Concha N O., Janson C A., Gilpin M., Bateson J H., Cheever C., Niconovich N L., Pearson S., Rittenhouse S., Tew D., Díez E., Pérez P., De La Fuente J., Rees M. and Rivera-Sagredo A. 2002. Identification of a series of tricyclic natural products as potent broad-spectrum inhibitors of metallo-beta-lactamases. *Antimicrobial Agents and Chemotherapy*. 46 (6): p. 1880-1886

219. Peleg A Y. and Hooper D C. 2010. Hospital-Acquired Infections Due to Gram-Negative Bacteria. *The New England Journal of Medicine.* 362 (19): p. 1804-1813

220. Petersen T N., Brunak S., von Heijne G. and Nielson H. 2011. SignalP 4.0: discriminating signal peptides from transmembrane regions. *Nature Methods*. (8): p. 785-786

221. Petti L M., Talbert-Slagle K., Hochstrasser M L. and DiMaio D. 2013. A single amino acid substitution converts a transmembrane protein activator of the platelet-derived growth factor β receptor into an inhibitor. *Journal of Biological Chemistry*. 288 (38): p. 27273-27286

222. Piddock L J V. 2006. Clinically Relevant Chromosomally Encoded Multidrug Resistance Efflux Pumps in Bacteria. *Clinical Microbiology Reviews*. 19 (2): p. 382-402

223. Pieris Pharmaceuticals Inc. 2018.[Online]. [Accessed 26 December 2018]. Available from: https://www.pieris.com/anticalin-technology/overview

224. Poirel L., Dortet L., Bernabeu S. and Nordmann P. 2011. Genetic Features of blaNDM-1 Positive Enterobacteriaceae. *Antimicrobial Agents and Chemotherapy*. 55 (11): p. 5403-5407

225. Porebski B T., Nickson A A., Hoke D E., Hunter M R., Zhu L., McGowan S., Webb G I. and Buckle A M. 2015. Structural and dynamic properties that govern the stability of an engineered fibronectin type III domain. *Protein Engineering, Design and Selection*. 28 (3): p. 67-78

226. Poulou A., Voulgari E., Vrioni G., Koumaki V., Xidopoulos G., Chatzipantazi V., Markou F. and Tsakris A. 2013. Outbreak Caused by an Ertapenem-Resistant, CTX-M-15-Producing Klebsiella pneumoniae Sequence Type 101 Clone Carrying an OmpK36 Porin Variant. *Journal of Clinical Microbiology*. 51 (10): p. 3176-3182

227. Rahbarnia L., Farajnia S., Babaei H., Majidi J., Veisi K., Ahmadzadeh V. and Akbari B. 2017. Evolution of phage display technology: from discovery to application. *Journal of Drug Targeting*. 25 (3)

228. Rahman M., Prasad K N., Pathak A., Pati B K., Singh A., Ovejero C M., Ahmad S. and Gonzalez-Zorn B. 2015. RmtC and RmtF 16S rRNA Methyltransferase in NDM-1–Producing Pseudomonas aeruginosa. *Emerging Infectious Diseases*. 21 (11): p. 2059-2062

229. Rakonjac J., Bennett N J., Spagnuolo J., Gagic D. and Russel M. 2011. Filamentous bacteriophage: biology, phage display and nanotechnology applications. *Current Issues in Molecular Biology*. 13 (2): p. 51-76

230. Rau S., Hilbig U. and Gauglitz G. 2014. Label-free optical biosensor for detection and quantification of the non-steroidal anti-inflammatory drug diclofenac in milk without any sample pre-treatment. *Analytical and Bioanalytical Chemistry*. 406 (14): p. 3377-3386

231. Read A F. and Woods R J. 2014. Antibiotic resistance management. *Evolution, Medicine & Public Health*. 1 (147)

232. Reading C. and Cole M. 1977. Clavulanic Acid: a Beta-Lactamase-Inhibiting Beta-Lactam from Streptomyces clavuligerus. *Antimicrobial Agents and Chemotherapy*. 11 (5): p. 852-857

233. Redshaw C H., Stahl-Timmins W M., Fleming L E., Davidson I. and Depledge M H. 2013. Potential changes in disease patterns and pharmaceutical use in response to climate change. *Journal of Toxicology and Environmental Health*. 16 (5): p. 285-320

234. Reimer A., Maffenbeier V., Dubey M., Sentchilo V., Tavares D., Gil MH., Beggah S. and van der Meer J R. 2017. Complete alanine scanning of the Escherichia coli RbsB ribose binding protein reveals residues important for chemoreceptor signaling and periplasmic abundance. *Scientific Reports*. 7 (8245)

235. Rhee E G., Rizk M L., Calder N., Nefliu M., Warrington S J., Schwartz M S., Mangin E., Boundy K., Bhagunde P., Colon-Gonzalez F., Jumes P., Liu Y. and Butterton J R. 2018. Pharmacokinetics, Safety, and Tolerability of Single and Multiple Doses of Relebactam, a β-Lactamase Inhibitor, in Combination with Imipenem and Cilastatin in Healthy Participants. *Antimicrobial Agents and Chemotherapy*. 62 (9)

236. Ries J., Kaplan C., Platonova E., Eghlidi H. and Ewers H. 2012. A simple, versatile method for GFP-based super-resolution microscopy via nanobodies. *Nature Methods*. 9: p. 582-584

237. Rigobello E S., Di Bernardo Dantas A., Di Bernardo L. and Vieira E M. 2013. Removal of diclofenac by conventional drinking water treatment processes and granular activated carbon filtration. *Chemosphere*. 92 (2): p. 184-191

238. Rikken R S M., Engelkamp H., Nolte R J M., Maan J C., van Hest, J C M., Wilson D A. and Christianen P C M. 2016. Shaping polymersomes into predictable morphologies via out-of-equilibrium self-assembly. *Nature Communications*. 7 (12606)

239. Robinson J I., Baxter E W., Owen R L., Thomsen M., Tomlinson D C., Waterhouse M P., Win S J., Nettleship J E., Tiede C., Foster R J., Owens R J., Fishwick C W G., Harris S A., Goldman A., McPherson M J. and Morgan A W. 2018. Affimer proteins inhibit immune complex binding to FcγRIIIa with high specificity through competitive and allosteric modes of action. *PNAS*. 115 (1): p. 72-81

240. Rodriguez E A., Campbell R E., Lin J Y., Lin M Z., Miyawaki A., Palmer A E., Shu X., Zhang J. and Tsien R Y. 2017. The Growing and Glowing Toolbox of Fluorescent and Photoactive Proteins. *Trends in Biochemical Science*. 42 (2): p. 111-129

241. Rossmann M., Greive S., Moschetti T., Dinan M. and Hyvonen M. 2017. Development of a multipurpose scaffold for the display of peptide loops. *Protein Engineering, Design and Selection*. 30 (6): p. 419-430

242. Rossolini G M., Arena F., Pecile P. and Pollini S. 2014. Update on the antibiotic resistance crisis. *Current Opinion in Pharmacology.* 18: p. 56-60

243. Rothbauer U., Zolghadr K., Tillib S., Nowak D., Schermelleh L., Gahl A., Backmann N., Conrath K., Muyldermans S., Cardoso M C. & Leonhardt H.

2006. Targeting and tracing antigens in live cells with fluorescent nanobodies. *Nature Methods*. 3: p. 887-889

244. Rothbauer U., Zolghadr K., Muyldermans S., Schepers A., Cardoso MC. and Leonhardt H. 2008. A versatile nanotrap for biochemical and functional studies with fluorescent fusion proteins. *Molecular & Cellular Proteomics*. 2008. 7 (2): p.282-289
245. Rothe C. and Skerra A. 2018. Anticalin® Proteins as Therapeutic Agents in Human Diseases. *BioDrugs*. 32 (3): p. 233-243
246. Rotondo, C.M. and Wright G D. 2017. Inhibitors of metallo-β-lactamases. *Current Opinion in Microbiology.* 39: p. 96-105
247. Rumbo C., Fernandez-Moreira E., Merino M., Poza M., Mendez J A., Soares N C., Mosquera A., Chaves F. and Bou G. 2011. Horizontal Transfer of the OXA-24 Carbapenemase Gene via Outer Membrane Vesicles: a New Mechanism of Dissemination of Carbapenem Resistance Genes in Acinetobacter baumannii. *Antimicrobial Agents and Chemotherapy*. 55 (7): p. 3084-3090
248. Sader H S., Flamm R K. and Jones R N. 2013. Antimicrobial Activity of Ceftaroline-Avibactam Tested against Clinical Isolates Collected from U.S. Medical Centers in 2010-2011. *Antimicrobial Agents and Chemotherapy*. 57 (4)
249. Sader H S., Mendes R E., Pfaller M A., Shortridge D., Flamm R K. and Castanheira M. 2018. Antimicrobial Activities of Aztreonam-Avibactam and Comparator Agents against Contemporary (2016) Clinical Enterobacteriaceae Isolates. *Antimicrobial Agents and Chemotherapy*. 62 (1)
250. Sader H S., Rhomberg P R., Flamm R K., Jones R N. and Castanheira M. 2017. WCK 5222 (cefepime/zidebactam) antimicrobial activity tested against Gram-negative organisms producing clinically relevant β-lactamases. *Journal of Antimicrobial Chemotherapy*. 72 (6): p. 1696-1703
251. Sambrook J. and Green M R. 1989. *Molecular Cloning, A Laboratory Manual.* 4th ed. New York: Cold Spring Harbor Laboratory Press.
252. Schadow K H., Simpson W A. and Christensen G D. 1988. Characteristics of Adherence to Plastic Tissue Culture Plates of Coagulase-Negative Staphylococci Exposed to Subinhibitory Concentrations of Antimicrobial Agents. *The Journal of Infectious Diseases*. 157 (1): p. 71-77

253. Schatz P J. 1993. Use of peptide libraries to map the substrate specificity of a peptide-modifying enzyme: a 13 residue consensus peptide specifies biotinylation in Escherichia coli. *Nature Biotechnology*. 11 (10): p. 1138-1143

254. Scheifner A. and Skerra A. 2015. The menagerie of human lipocalins: a natural protein scaffold for molecular recognition of physiological compounds. *Accounts of Chemical Research*. 48 (4): p. 976-985

255. Schomer R A., Park H., Barkei J J. and Thomas M G. 2018. Alanine Scanning of YbdZ, an MbtH-like Protein, Reveals Essential Residues for Functional Interactions with Its Nonribosomal Peptide Synthetase Partner EntF. *Biochemistry*. 57 (28): p. 4125-4134

256. Schlichthaerle T., Eklund A S., Schueder F., Strauss M T., Tiede C., Curd A., Ries J., Peckham M., Tomlinson D C. and Jungmann R. 2018. Site-specific labelling of Affimers for DNA-PAINT microscopy. *Angewandte Chemie International Edition*. 57 (34): p. 11060-11063

257. Schwechheimer C. and Kuehn M J. 2015. Outer-membrane vesicles from Gram-negative bacteria: biogenesis and functions. *Nature Reviews*. 13: p. 605-619

258. Sevaille L., Gavara L., Bebrone C., De Luca F., Nauton L., Achard M., Mercuri P., Tanfoni S., Borgianni L., Guyon C., Lonjon P., Turan-Zitouni G., Dzieciolowski J., Becker K., Bénard L., Condon C., Maillard L., Martinez J., Frère J M., Dideberg O., Galleni M., Docquier J D. and Hernandez J F. 2017. 1,2,4-Triazole-3-thione Compounds as Inhibitors of Dizinc Metallo-β-lactamases. *ChemMedChem*. 12 (12): p. 972-985

259. Sharma R., Deacon S E., Nowak D., George S E., Szymonik M P., Tang AA., Tomlinson D C., Davies A G., McPherson M J. and Wälti C. 2016. Label-free electrochemical impedance biosensor to detect human interleukin-8 in serum with sub-pg/ml sensitivity. *Biosensors and Bioelectronics*. 80: 607-613

260. Sherrard L J., Tunney M M. and Elborn J S. 2014. Antimicrobial resistance in the respiratory microbiota of people with cystic fibrosis. *The Lancet*. 384 (9944): p. 703-713

261. Shim H. 2015. Synthetic approach to the generation of antibody diversity. *BMB Reports*. 49 (9): p. 489-494

262. Shrivastava A. and Gupta V. 2011. Methods for the determination of limit of detection and limit of quantitation of the analytical methods. *Chronicles of Young Scientists*. 2 (1): p. 21

263. Shui B., Ozer A., Zipfel W., Sahu N., Singh A., Lis J T., Shi H. and Kotlikoff M I. 2012. RNA aptamers that functionally interact with green fluorescent protein and its derivatives. *Nucleic Acids Research*. 40 (5): p. e39

264. Sidhu S S. 2001. Engineering M13 for phage display. *Biomolecular Engineering*. 18 (2): p. 57-63

265. Singh J., Petter R C., Baillie T A. and Whitty A. 2011. The resurgence of covalent drugs. *Nature Reviews Drug Discovery*. 10: p. 307-317

266. Skerra A. and Schmidt S R. 2015. Engineered protein scaffolds: have they lived up to expectations? *Pharmaceutical bioprocessing*. 3: p. 383-386

267. Skrlec K., Strukelj B. and Berlec A. 2015. Non-immunoglobulin scaffolds: a focus on their targets. *Trends in Biotechnology*. 33 (7): p. 408-418

268. Smeal S W., Schmitt M A., Pereira R R., Prasad A. and Fisk J D. 2017. Simulation of the M13 life cycle I: Assembly of a genetically-structured deterministic chemical kinetic simulation. *Virology*. 500: p. 259-274

269. Sohier J S., Laurent C., Chevigne A., Pardon E., Srinivasan V., Werery U., Lassaux P., Steyaert J. and Galleni M. 2013. Allosteric inhibition of VIM metallo-β-lactamases by a camelid nanobody. *Biochemical Journal*. 450: p. 477-486

270. Somboro A M., Sekyere J O., Amoako D G., Essack S Y. and Bester L A. 2018. Diversity and Proliferation of Metallo-β-Lactamases: a Clarion Call for Clinically Effective Metallo-β-Lactamase Inhibitors. *Applied and Environmental Microbiology*. 84 (18)

271. Somboro A M., Tiwari D., Bester L A., Parboosing R., Chonco L., Kruger H G., Arvidsson P I., Govender T., Naicker T. and Essack S Y. 2015. NOTA: a potent metallo-β-lactamase inhibitor. *Journal of Antimicrobial Chemotherapy*. 70 (5): p. 1594-1596

272. Sorbera M., Chung E., Ho C W. and Marzella N. 2014. Ceftolozane/Tazobactam: A New Option in the Treatment of Complicated Gram-Negative Infections. *Pharmacy and Therapeutics*. 39 (12): p. 828-832

273. Soto S M. 2013. Role of efflux pumps in the antibiotic resistance of bacteria embedded in a biofilm. *Virulence*. 4 (3): p. 223-229

274. Spanogiannopoulos P., Waglechner N., Koteva K. and Wright G D. 2014. A rifamycin inactivating phosphotransferase family shared by environmental and pathogenic bacteria. *PNAS*. 111 (19): p. 7102-7107

275. Sriramulu D. 2013. Evolution and Impact of Bacterial Drug Resistance in the Context of Cystic Fibrosis Disease and Nosocomial Settings. *Microbiology Insights*. 6 (6): p. 29-36

276. Sun J., Deng Z. and Yan A. 2014. Bacterial multidrug efflux pumps: Mechanisms, physiology and pharmacological exploitations. *Biochemical and Biophysical Research Communications*. 453 (2): p. 254-267

277. Sun S., Selmer M. and Andersson D I. 2014. Resistance to β-Lactam Antibiotics Conferred by Point Mutations in Penicillin-Binding Proteins PBP3, PBP4 and PBP6 in Salmonella enterica. *PLoS One*. 9 (5)

278. Sun Z., Hu L., Sankaran B., Prasad B V V. and T. Palzkill. Differential active site requirements for NDM-1 β-lactamase hydrolysis of carbapenem versus penicillin and cephalosporin antibiotics. *Nature Communications*. 9 (4524)

279. Takakusagi Y., Takakusagi K., Sugawara F. and Sakaguchi K. 2010. Use of phage display technology for the determination of the targets for small-molecule therapeutics. *Expert Opinions in Drug Discovery*. 5 (4): p. 361-389

280. Tang A A., Tiede C., Hughes D J., McPherson M J. and Tomlinson D C. 2017. Isolation of isoform-specific binding proteins (Affimers) by phage display using negative selection. *Science Signalling*. 10 (505)

281. Tanner W D., Atkinson R M., Goel R K., Toleman M A., Benson L S., Porucznik C A. and VanDerslice J A. 2017. Horizontal transfer of the bla_{NDM-1} gene to Pseudomonas aeruginosa and Acinetobacter baumannii in biofilms. *FEMS Microbiology Letters*. 364 (8)

282. Tawil N., Mouawad F., Levesque S., Sacher E., Mandeville R. and Meunier M. 2013. The differential detection of methicillin-resistant, methicillin-susceptible and borderline oxacillin-resistant Staphylococcus aureus by surface plasmon resonance. *Biosensors and Bioelectronics*. 49 p.334-40

283. Tecrea Ltd. 2015. A new tool for drug development. [Online]. [Accessed 26 December 2018]. Available from: http://www.tecrea.com/drug-formulation/nanocin/

284. Terwisscha van Scheltinga A G., Lub-de Hooge M N., Hinner M J., Verheijen R B., Allersdorfer A., Hülsmeyer M., Nagengast W B., Schröder C P., Kosterink J G., de Vries E G., Audoly L. and Olwill S A. 2014. In vivo visualization of MET tumor expression and anticalin biodistribution with the MET-specific anticalin 89Zr-PRS-110 PET tracer. *The Journal of Nuclear Medicine*. 55 (4): p. 665-671

285. Thakur P K., Kumar J., Ray D., Anjum F. and Hassan I. 2013. Search of potential inhibitor against New Delhi metallo-beta-lactamase 1 from a series of antibacterial natural compounds. *Journal of Natural Science, Biology and Medicine*. 4 (1): p. 51-56

286. The UniProt Consortium. 2017. UniProt: the universal protein knowledgebase. *Nucleic Acids Research*. 45 (1): p. 15-169

287. Thie H V., Dübel S., Hust M. and Schirrmann T. 2008. Affinity Maturation by Phage Display. *Methods in Molecular Biology™*. p. 309-322

288. Thomas P W., Cammarata M., Brodbelt J S. and Fast W. 2014. Covalent Inhibition of New Delhi Metallo-β-Lactamase-1 (NDM-1) by Cefaclor. *ChemBioChem*. 15 (17): p. 2541-2548

289. Thuny F., Grisoli D., Collart F., Habib G. and Raoult D. 2012. Management of infective endocarditis: challenges and perspectives. *The Lancet*. 379 (9819): p. 965-975

290. Tiller K E. and Tessier P M. 2015. Advances in Antibody Design. *Annual Review of Biomedical Engineerin*g. 17: p. 191-216

291. Tiede C., Tang A A., Deacon S E., Mandal U., Nettleship J E., Owen R L., George S E., Harrison D J., Owens R J., Tomlinson D C. and McPherson M J. 2014. Adhiron: a stable and versatile peptide display scaffold for molecular recognition applications. *Protein Engineering, Design and Selection*. 27 (5): p. 145-55.

292. Tiede C., Bedford R., Heseltine S J., Smith G., Wijetunga I., Ross R., AlQallaf D., Roberts A P., Balls A., Curd A., Hughes R E., Martin H., Needham S R., Zanetti-Domingues L C., Sadigh Y., Peacock T P., Tang A A., Gibson N., Kyle H., Platt G W., Ingram N., Taylor T., Coletta L P., Manfield I., Knowles M., Bell S., Esteves

F., Maqbool A., Prasad R K., Drinkhill M., Bon R S., Patel V., Goodchild S A., Martin-Fernandez M., Owens R J., Nettleship J E., Webb M E., Harrison M., Lippiat J D., Ponnambalam S., Peckham M., Smith A., Ferrigno P K., Johnson M., McPherson M J. and Tomlinson D C. 2017. Affimer proteins are versatile and renewable affinity reagents. *Elife*. 6.

293. Toleman M A., Spencer J., Jones L. and Walsh T R. 2012. blaNDM-1 Is a Chimera Likely Constructed in Acinetobacter baumannii. *Antimicrobial Agents and Chemotherapy*. 56 (5): p. 2773-2776

294. Tran D N., Tran H H., Matsui M., Suzuki M., Suzuki S., Shibiyama K., Pham T D., Van Phuong T T., Dang D A., Trinh H S., Loan C T., Nga L T V., van Doorn H R. and Wertheim H F L. 2017. Emergence of New Delhi metallo-beta-lactamase 1 and other carbapenemases-producing Acinetobacter calcoaceticus-baumannii complex among patients in hospitals in Ha Noi, Vietnam. European *Journal of Clinical Microbiology and Infectious Diseases*. 36 (2): p. 219-225

295. Turek D., Van Simaeys D., Johnson J., Ocsoy I. and Tan W. 2013. Molecular recognition of live methicillin-resistant staphylococcus aureus cells using DNA aptamers. *World Journal of Translational Medicine*. 2 (3): p. 67-74

296. United Nations. 2018. World Urbanization Prospects: The 2018 Revision. [Accessed 21 Nov 2018]. Available from: https://population.un.org/wup/Publications/Files/WUP2018-KeyFacts.pdf

297. Van Dorst B., Mehta J., Rouah-Martin E., Blust R. and Robbens J. 2012. Phage display as a method for discovering cellular targets of small molecules. *Methods*. 58 (1): p. 56-61

298. VenatoRx Pharmaceuticals. 2018. *VenatoRx Pharmaceuticals to Present in vitro, in vivo and Phase I Data for Cefepime/VNRX-5133 at IDWeek 2018*. [Press release]. [Accessed 21 Oct 2018]. Available from: https://www.venatorx.com/press-releases/venatorx-pharmaceuticals-to-present-in-vitro-in-vivo-and-phase-i-data-for-cefepimevnrx-5133-at-idweek-2018/

299. Ventola C L. 2015. The Antibiotic Resistance Crisis Part 1: Causes and Threats. *Pharmacy and Therapeutics*. 40 (4): p. 277-283

300. Vieno N. and Sillanpaa M. 2014. Fate of diclofenac in municipal wastewater treatment plant — A review. *Environment International*. 69: p. 28-39

301. Virnekas B., Ge L., Plückthun A., Schneider K C., Wellnhofer G. and Moroney S E. 1994. Trinucleotide phosphoramidites: ideal reagents for the synthesis of mixed oligonucleotides for random mutagenesis. *Nucleic Acids Research*. 22 (25): p. 5600-5607

302. Voets G M., Fluit A C., Scharringa J., Schapendonk C., van den Munckhof T., Leverstein-van Hall M A. and Stuart J C. 2013. Identical plasmid AmpC beta-lactamase genes and plasmid types in E. coli isolates from patients and poultry meat in the Netherlands. *International Journal of Food Microbiology*. 167 (3): p. 359-362

303. Walsh F. BBC, 2013. *Antibiotics resistance 'as big a risk as terrorism' - medical chief*. [ONLINE] Available at: https://www.bbc.co.uk/news/health-21737844. [Accessed 16 August 2018].

304. Wang J. and Wang S. 2016. Removal of pharmaceuticals and personal care products (PPCPs) from wastewater: A review. Journal of Environmental Management. 182: p. 620-640

305. Wang R., Lai T-P., Gao P., Zhang H., Ho P-L., Woo P C-Y., Ma G., Kao R Y-T., Li H. and Sun H. 2018. Bismuth antimicrobial drugs serve as broad-spectrum metallo-β-lactamase inhibitors. *Nature Communications*. 9 (439)

306. Wark K L. and Hudson P J. 2006. Latest technologies for the enhancement of antibody affinity. *Advanced Drug Delivery Reviews*. 58 (5-6): p. 657-670

307. Weigert M G., Lanka E. and Garen A. 1965. Amino acid substitutions resulting from suppression of nonsense mutations. II. Glutamine insertion by the Su-2 gene; tyrosine insertion by the Su-3 gene. *Journal of Molecular Biology*. 14 (2): p. 522-527

308. Weiss G A., Watanabe C K., Zhong A., Goddard A. and Sidhu S S. 2000. Rapid mapping of protein functional epitopes by combinatorial alanine scanning. *PNAS*. 97 (16)

309. Weiss W J., Pulse M E., Nguyen P., Valtierra D., Pevear D C., Burns C J. and Xerri L. 2018. *Efficacy of cefepime / VNRX-5133, a novel broad-spectrum β-lactamase inhibitor (BS-BLI), in a murine bacteremia infection model with carbapenem-resistant Enterobacteriaceae (CREs)*. [Online poster]. [Accessed 22 October 2018]. Available from: https://www.venatorx.com/wp-content/uploads/2018/04/ECCMID2018-P1538.pdf

310. Willyard C. 2017. The drug-resistant bacteria that pose the greatest health threats. *Nature News*. 543 (7643)

311. Wise R. and Piddock L JV. 2018. The Urgent Need: Regenerating Antibacterial Drug Discovery Development. *British Society of Antimicrobial Chemotherapy (BSAC)*. http://antibiotic-action.com/wp-content/uploads/2011/07/TUN-Report.pdf [Accessed 13 August 2018]

312. Woodman R., Yeh J T H., Laurenson S. and Ko Ferrigno P. 2005. Design and Validation of a Neutral Protein Scaffold for the Presentation of Peptide Aptamers. *Journal of Molecular Biology*. 352: p. 1118-1133

313. World Bank Group. 2017. Drug-Resistant Infections: A Threat to Our Economic Future.

314. World Health Organisation. 2016. *Antibiotic Resistance: Fact Sheet*. World Health Organization, Geneva Switzerland.

315. World Health Organization. 2017. *Global priority list of antibiotic-resistant bacteria to guide research, discovery, and development of new antibiotics*. World Health Organization, Geneva Switzerland.

316. Wozniak A., Villagra N A., Undabarrena A., Gallardo N., Keller N., Moraga M., Roman J C., Mora G C. and Garcia P. 2012. Porin alterations present in non-carbapenemase-producing Enterobacteriaceae with high and intermediate levels of carbapenem resistance in Chile. *Journal of Medical Microbiology*. 61 (9): p. 1270-1279

317. Xiang Y., Chang Y-N., Ge Y., Kang J S., Zhang Y-L., Liu X-L., Oelschlaeger P. and Yang K-W. 2017. Azolylthioacetamides as a potent scaffold for the development of metallo-β-lactamase inhibitors. *Bioorganic & Medicinal Chemistry Letters*. 27 (23): p. 5225-5229

318. Xie C., Tiede C., Zhang X., Wang C., Li Z., Xu X., McPherson M J., Tomlinson D C. and Xu W. 2017. Development of an Affimer-antibody combined immunological diagnosis kit for glypican-3. *Scientific Reports*. 7 (9608)

319. Xie L., Dou Y., Zhou K., Chen Y., Han L., Guo X. and Sun J. 2017. Coexistence of blaOXA-48 and truncated blaNDM-1 on different plasmids in a Klebsiella penumoniae isolate in China. *Frontiers in Microbiology*. 8 (133)

320. Yang H., Cai W., Xu L., Lv X., Qiao Y., Li P., Wu H., Yang Y., Zhang L. and Duan Y. 2015. Nanobubble-Affibody: Novel ultrasound contrast agents for targeted molecular ultrasound imaging of tumor. *Biomaterials*. 37: p. 279-288

321. Yang N. and Hinner M J. 2015. Getting Across the Cell Membrane: An Overview for Small Molecules, Peptides, and Proteins. *Methods in Molecular Biology*. 1266: p. 29-53

322. Yang S K., Kang J S., Oelschlaeger P. and Yang K W. 2015. Azolylthioacetamide: A highly promising scaffold for the development of metallo-β-lactamase inhibitors. *ACS Medicinal Chemistry Letters*. 6 (4): p. 455-460

323. Yilmaz B. and Ciltas U. 2015. Determination of diclofenac in pharmaceutical preparations by voltammetry and gas chromatography methods. *Journal of Pharmaceutical Analysis*. 5 (3): p. 153-160

324. Yong D., Toleman M A., Giske C G., Cho H S., Sundman K., Lee K. and Walsh T R. 2009. Characterization of a New Metallo-β-Lactamase Gene, blaNDM-1, and a Novel Erythromycin Esterase Gene Carried on a Unique Genetic Structure in Klebsiella pneumoniae Sequence Type 14 from India. *Antimicrobial Agents and Chemotherapy*. 53 (12): p. 5046-5054

325. Zahnd C., Wyler E., Schwenk J M., Steiner D., Lawrence M C., McKern N M., Pecorari F., Ward C W., Joos T O and Pluckthun A. 2007. A Designed Ankyrin Repeat Protein Evolved to Picomolar Affinity to Her2. *Journal of Molecular Biology*. 369 (4): p. 1015-1028

326. Zgurskaya H I., Lopez C A. and Gnanakaran S. 2015. Permeability Barrier of Gram-Negative Cell Envelopes and Approaches To Bypass It. *ACS Infectious Diseases*. 1 (11): p. 512-522

327. Zhai L., Zhang Y L., Kang J S., Oelschlaeger P., Xiao L., Nie S S. and Yang K W. 2016. Triazolylthioacetamide: a valid scaffold for the development of New Delhi metallo-βlactamase-1 (NDM-1) inhibitors. *ACS Medicinal Chemistry Letters*. 7 (4): p. 413-417

328. Zhang H. and Hao Q. 2011. Crystal structure of NDM-1 reveals a common β-lactam hydrolysis mechanism. *FASEB*. 25 (8)

329. Zhang H., Ma G., Zhu Y., Zeng L., Ahmad A., Wang C., Pang B., Fang H., Zhao L. and Hao Q. 2018. Active site conformational fluctuations promote the

enzymatic activity of NDM-1. *Antimicrobial Agents and Chemotherapy*. [Epub ahead of print]

330. Zhang L., Wang J-C., Hou L., Cao P-R., Wu L., Zhang Q-S., Yang H-Y., Zang Y., Ding J-P. and Li J. 2015. Functional Role of Histidine in the Conserved His-x-Asp Motif in the Catalytic Core of Protein Kinases. *Nature Scientific Reports*. 5 (10115)
331. Zheng B., Dong H., Xu H., Lv J., Zhang J., Jiang X., Du Y., Xiao Y and Li L. 2016. Coexistence of MCR-1 and NDM-1 in Clinical Escherichia coli Isolates. *Clinical Infectious Diseases*. 63 (10): p. 1393-1395
332. Zhurauski P., Arya S K., Jolly P., Tiede C., Tomlinson D C., Ko Ferrigno P. and Estrela P. 2018. Sensitive and selective Affimer-functionalised interdigitated electrode-based capacitive biosensor for Her4 protein tumour biomarker detection. *Biosensors and Bioelectronics*. 108: p. 1-8